Lecture Notes in Electrical Engineering 625

Papia Ray
Monalisa Biswal *Editors*

Microgrid: Operation, Control, Monitoring and Protection

Springer

Lecture Notes in Electrical Engineering

Volume 625

The book series *Lecture Notes in Electrical Engineering* (LNEE) publishes the latest developments in Electrical Engineering - quickly, informally and in high quality. While original research reported in proceedings and monographs has traditionally formed the core of LNEE, we also encourage authors to submit books devoted to supporting student education and professional training in the various fields and applications areas of electrical engineering. The series cover classical and emerging topics concerning:

- Communication Engineering, Information Theory and Networks
- Electronics Engineering and Microelectronics
- Signal, Image and Speech Processing
- Wireless and Mobile Communication
- Circuits and Systems
- Energy Systems, Power Electronics and Electrical Machines
- Electro-optical Engineering
- Instrumentation Engineering
- Avionics Engineering
- Control Systems
- Internet-of-Things and Cybersecurity
- Biomedical Devices, MEMS and NEMS

For general information about this book series, comments or suggestions, please contact leontina.dicecco@springer.com.

To submit a proposal or request further information, please contact the Publishing Editor in your country:

China

Jasmine Dou, Associate Editor (jasmine.dou@springer.com)

India, Japan, Rest of Asia

Swati Meherishi, Executive Editor (Swati.Meherishi@springer.com)

Southeast Asia, Australia, New Zealand

Ramesh Nath Premnath, Editor (ramesh.premnath@springernature.com)

USA, Canada:

Michael Luby, Senior Editor (michael.luby@springer.com)

All other Countries:

Leontina Di Cecco, Senior Editor (leontina.dicecco@springer.com)

**** Indexing: The books of this series are submitted to ISI Proceedings, EI-Compendex, SCOPUS, MetaPress, Web of Science and Springerlink ****

More information about this series at http://www.springer.com/series/7818

Papia Ray · Monalisa Biswal
Editors

Microgrid: Operation, Control, Monitoring and Protection

Springer

Editors
Papia Ray
Department of Electrical Engineering
Veer Surendra Sai University of Technology
Sambalpur, Odisha, India

Monalisa Biswal
Department of Electrical Engineering
National Institute of Technology, Raipur
Raipur, Chhattisgarh, India

ISSN 1876-1100 ISSN 1876-1119 (electronic)
Lecture Notes in Electrical Engineering
ISBN 978-981-15-1780-8 ISBN 978-981-15-1781-5 (eBook)
https://doi.org/10.1007/978-981-15-1781-5

This Springer imprint is published by the registered company Springer Nature Singapore Pte Ltd.
The registered company address is: 152 Beach Road, #21-01/04 Gateway East, Singapore 189721, Singapore

Preface

Over the past few decades, the electric power industry continues to play a major role in the welfare, progress and technological development of the country. With conventional power systems struggling to meet the consumers' increasing demand for electric power, renewable energy resources are being installed to mitigate the energy shortfall. The concept of Microgrid is to integrate multiple renewable energy sources as well as conventional sources, energy storage devices and loads into the electric power system.

Further in the power system, only electric grid refers to a network of transmission lines, substations, transformers and more that deliver electricity from the power plant to the user end. The electric grid is considered to be an engineering prodigy in handling so many generating units, high megawatts of generating capacity and several miles of transmission lines. However, in recent scenario the electricity disruption like a blackout is very common not only in India but in advanced countries like USA. A grid will be more efficient when more resiliencies are added to the existing electric power system and makes it better prepared to address diffident unavoidable emergencies and natural calamities. Therefore, if these extra powerful features are added to the existing grid, then it becomes a smart grid. A combination of microgrid is a smart grid.

A microgrid is a low-voltage small-scale power grid (on distribution side) with distributed generation (DG), storage devices and controllable loads. Microgrids can operate independently called the islanded (autonomous) mode of operation or in conjunction with the main grid called the grid-connected mode of operation. Microgrids offer several advantages and benefits including increased reliability, improved energy efficiency and resiliency, cost reduction, reduction in transmission losses, CO_2 emission reduction and other environmental benefits. However, they also introduce several major challenges regarding the monitoring, operation, control and protection which are also subjects of research. Furthermore, each mode of

operation (grid connected or islanded) requires unique control and protection schemes. The major issues and potential solutions in microgrid protection and control include:

- **Bidirectional power flows**: The power flow in a conventional distribution system is unidirectional, i.e., from the substation to the loads. Integration of distributed generations (DGs) on the distribution side of the grid can cause reverse power flow. As a result, the conventional protection coordination schemes are no longer valid.
- **Short-circuit capacity**: In the case of inverter-based DGs, the fault current is limited. Hence, the conventional overcurrent relay cannot sense the fault.
- **Stability issues**: Local oscillations may arise as a result of the interaction of the control system of microgenerators. Hence, small-signal stability analysis and transient stability analysis are required to ensure proper operation in a microgrid.
- **Low inertia**: In a conventional power system, the bulk power is generated at power plants and hence they have high inertia. Microgrids on the other hand, have dispersed generation and sizes of the DGs are very small. Consequently, they have a low inertia characteristic, especially for inverter-based DGs. Low inertia can result in severe frequency deviations in the islanded mode of operation. Hence, a special control mechanism is required.
- **Intermittent output**: Microgrids with renewable energy resources (photovoltaic or wind) as distributed generation are intermittent in their power output. Hence, coordination between DGs and storage devices is essential.
- **Protection coordination issues**: In a microgrid, there is always a need of smooth transition from islanding to the grid-connected state and overcurrent relay with proper coordination fulfills this requirement. During fault or islanding condition, the current flows bidirectional in the microgrid and becomes many times the rated current as a result of which the protection scheme gets disturbed. So, in order to gain the same protection scheme for both islanded and grid-connected mode of the microgrid, proper coordination is required, and it becomes a challenging issue for power system engineers.

The above-mentioned major challenges and many more with various monitoring, operation, control and protection techniques to handle those issues are discussed in this book.

This book is organized into 11 chapters. This book covers diverse fields to satisfy engineers, researchers and personnel of power and control industry. The main topics which are covered in this book are various aspects related to monitoring, protection, control and operation of microgrid. Introduction of this book deals with the basic concept of microgrid and their different challenging issues with adequate solutions in the power and control sector.

Chapter "Microgrid System" provides holistic learning of microgrid system as well as barriers in its implementation. Also, the different aspects of the deployment of microgrids such as its architecture, mode of operations, control strategies, monitoring methods, protection schemes and energy management strategies are categorically explained. In chapter "Optimal Day-Ahead Renewable Power

Generation Scheduling of Hybrid Electrical Power System," day-ahead renewable power forecasting and optimal generation scheduling of microgrid are discussed. Further in this chapter, new optimal generation scheduling problem is solved in a hybrid power system by considering trade-off between system operating cost and risk level and best-fit schedules are provided by optimizing the real-time and day-ahead deviation costs. In chapter "Performance of Control Algorithms in Wind-Based Distributed Generation System with Power Quality Features: A Review," performance review of control algorithms is discussed in wind-based distributed power generation system for power quality improvement. Further in this chapter, the control algorithms are selected based on their faster dynamics, less steady-state error and stable operation. Chapter "Modern Control Methods for Adaptive Droop Coefficients Design" proposes "fuzzy logic and model reference-based control methods " of microgrid for the adaptive p-ω droop and q-v droop coefficients design so that the issues in frequency and voltage deviations and the limitations of the state-of-the-art design methods can be eliminated. Chapter "Design of Linear and Nonlinear Controllers for a Grid-Connected PV System for Constant Voltage Applications" presents the design of linear and nonlinear controllers for a grid-connected photovoltaic (PV) system. Further in this chapter, discussion on the performance of various controllers like proportional integral (PI), sliding mode and H-infinity for a grid-connected photovoltaic (PV) system more specifically the conversion stage is carried out, and tracking performance and robustness of these controllers are verified with varying inputs and loads. In chapter "Protection Challenges with Microgrid," all the protection-related issues like islanding detection, fault detection and classification, relay coordination, etc. with AC/DC microgrid are highlighted with the existing solutions. Chapter "Hybrid Event Classification Scheme for Converter-Based DG with Improved Power Quality" proposes a new method to detect and differentiate between islanding and fault events in microgrids with embedded converter-based distributed generation. Further in this chapter, the proposed scheme is based on an alert signal (generated using several features) and a parameter called superimposed impedance (SI) that has never been used for such application. The results obtained in this chapter from the off-line and real-time simulations show that the scheme is accurate for different islanding, fault and other events and successfully classifies different events. In chapter "Intelligent Relay Coordination Method for Microgrid," protection coordination of a typical microgrid with distributed energy sources is discussed. In this chapter, a smart grid-based fault current limiter (FCL) has been proposed which suppresses the fault currents to the level such that proper protection coordination is possible. Further in this chapter, three configurations of the microgrid are considered, i.e., grid connected, islanded and dual. From the simulation results of this chapter, it is observed that the optimized FCL is able to co-ordinate properly the protective devices for different configurations of microgrid. Chapter "Energy Management System of a Microgrid using Particle Swarm Optimization (PSO) and Communication System" focuses on optimizing the behavior of energy management system (EMS) of a microgrid such that it can operate in a safe and reliable manner to match the demanded load with the available energy sources. In chapter

"Uninterrupted Power Supply to Microgrid," energy storage system (ESS) and its application in the uninterruptible power supply system to provide resilience and stability to the microgrid are discussed. This chapter also signifies the use of line adaptive reclosing scheme which optimizes the use of ESS providing improved efficiency and savings in cost. Chapter "Mitigation of Power System Blackout with Microgrid System" talks about the causes of protection system failure and blackouts. In this chapter, an intelligent load shedding and adaptive defense plan for islanding in the integrated power system are presented to mitigate the power system blackout and to obtain a perfect load match situation.

Unlike many other books, this book does not direct the reader to the manufacturer's documentation, but instead, it tends to gather detailed information for both better understanding and comparison. Also, in this book the diverse fields of research interest have been covered comprehensively, and new concepts in research fields have been discussed. Further, this book also presents some practical case studies for the utility personnel. The primary reason for writing this book is to provide knowledge about recent research activities in the field of microgrid system. The individual chapters are different from most technical publications. They are basically journal-type chapters but are not textbook in nature. Furthermore, they are intended to be overviews providing ready access to needed information while at the same time providing sufficient references to more in-depth coverage of the topic.

This is a book intended for researchers, utility engineers and advanced teaching in the fields of power and control engineering.

Happy Reading!

Sambalpur, India Papia Ray
Raipur, India Monalisa Biswal

About This Book

Due to the growing awareness of the harmful impact of conventional fossil fuels and advancements in renewable energy technologies, microgrid has grown in popularity. This book highlights the different aspects of the deployment of microgrids such as its architecture, mode of operations, control strategies, monitoring methods, protection schemes and energy management strategies. This book basically emphasizes the need and merits of the adoption of microgrid systems while also discussing the barriers in its implementation. The coverage of this book is within the four major topics, i.e., operation, control, monitoring and protection of microgrid. The objective of this book is to provide awareness to the readers with the right advanced skills, vision and knowledge to lead in teams involved in the operation, control, monitoring and protection of the microgrid. This book is not only helpful for readers who are new to the world of microgrid energy systems but also provides essential information to the experts in this field. The content of this book is organized into eleven chapters. The chapters are written primarily for the power and control researchers and utility personnel who are seeking factual information, and secondarily for the professional from other engineering disciplines who want an overview of the entire field or specific information on one aspect of it. The individual chapters are different from most technical publications and are of journal type but not textbook in nature. Further, the chapters in this book are intended to be overviews providing ready access to needed information while at the same time providing sufficient references to more in-depth coverage of the topic. Unlike many other books, this book does not direct the reader to the manufacturer's documentation, but instead, it tends to gather detailed information for both better understanding and comparison.

Contents

Editors and Contributors

About the Editors

Dr. Papia Ray is an Associate Professor at the Department of Electrical Engineering, Veer Surendra Sai University of Technology, Odisha, India. She completed her Ph.D. in the area of power system engineering at the Indian Institute of Technology, Delhi. Her current research area includes Power system protection, Power quality, Wide area measurement systems and application of soft computing techniques in power system protection. She is a senior member of IEEE, Life Member of Indian Society for Technical Education and Member of Institution of Engineer's India.She has published numerous papers in various international journals and conferences. She is the recipient of Young Scientist Award from DST-2015.

Dr. Monalisa Biswal an Assistant Professor at the Department of Electrical Engineering, National Institute of Technology, Raipur, India. She completed her Ph.D. at Sambalpur University. Her research interests include power system protection, smart grid protection, wide area protection, FACTS devices, adaptive relaying, and signal processing application to power system relaying. She is a member of IEEE and the Institution of Engineers, and a life member of the Odisha Bigyan Academy and ISTE. She has published numerous papers in various journals and conferences. She is also an active reviewer for several reputed journals and conferences. She is the recipient of Young Scientist Award from DST-2015, and Chhattisgarh Council of Science and Technoloy-2017. She won the POSOCO Power System Award in 2013 for her Ph.D. work.

Contributors

Mohammad Y. Ali University of Ontario Institute of Technology (UOIT), Oshawa, ON, Canada

Sabha Raj Arya Department of Electrical Engineering, Sardar Vallabhbhai National Institute of Technology, Surat, India

Ravikumar Bhimasingu Department of Electrical Engineering, Indian Institute of Technology Hyderabad (IITH), Sangareddy, Telangana, India

Monalisa Biswal Department of Electrical Engineering, National Institute of Technology Raipur, Raipur, Chhattisgarh, India

Pinku Das Department of Electrical Engineering, National Institute of Technology Raipur, Raipur, Chhattisgarh, India

Shubham Ghore Department of Electrical Engineering, National Institute of Technology Raipur, Raipur, Chhattisgarh, India

Ashutosh K. Giri Department of Electrical Engineering, Sardar Vallabhbhai National Institute of Technology, Surat, India

Om Hari Gupta Department of Electrical Engineering, National Institute of Technology Jamshedpur, Jamshedpur, Jharkhand, India

Faizan Khan University of Ontario Institute of Technology (UOIT), Oshawa, ON, Canada

Abhishek Kumar College of Electrical Engineering, Zhejiang University, Hangzhou, People's Republic of China

Ding Lei School of Electrical Engineering, Shandong University, Jinan, People's Republic of China

Rakesh Maurya Department of Electrical Engineering, Sardar Vallabhbhai National Institute of Technology, Surat, India

Nand K. Meena School of Engineering and Applied Science, Aston University, Birmingham, UK

Nivedita Pati Department of Electrical Engineering, Silicon Institute of Technology, Bhubaneswar, Odisha, India

Y. V. Pavan Kumar School of Electronics Engineering, Vellore Institute of Technology-Andhra Pradesh (VIT-AP) University, Amaravati, Andhra Pradesh, India

Papia Ray Department of Electrical Engineering, Veer Surendra Sai University of Technology, Burla, Odisha, India

Surender Reddy Salkuti Department of Railroad Electrical Systems, Woosong University, Daejeon, Republic of Korea

Arvind R. Singh School of Electrical Engineering, Shandong University, Jinan, People's Republic of China

Ranjay Singh Department of EECE, University of Pretoria, Pretoria, South Africa

Vijay K. Sood Department of Electrical, Computer and Software Engineering, Ontario Tech University, Oshawa, ON, Canada;
University of Ontario Institute of Technology (UOIT), Oshawa, ON, Canada

Nibedita Swain Department of Electrical Engineering, Silicon Institute of Technology, Bhubaneswar, Odisha, India

Manoj Tripathy Department of Electrical Engineering, Indian Institute of Technology Roorkee, Roorkee, Uttarakhand, India

Kasimala Venkatanagaraju Department of Electrical Engineering, National Institute of Technology Raipur, Raipur, Chhattisgarh, India

Microgrid System

Arvind R. Singh, Ding Lei, Abhishek Kumar, Ranjay Singh and Nand K. Meena

Abstract Due to the growing awareness of the harmful impact of conventional fossil fuels and advancements in renewable energy technologies, microgrid has grown in popularity. This chapter aims to provide holistic learning of the microgrid system. This chapter is not only helpful for readers who are new to the world microgrid energy systems but also provide essential information to experts of this field. The chapter highlights the need and merits of adoption of microgrid systems while also highlighting the barriers in its implementation. The chapter also provides the various methods of categorization of microgrid while also emphasizing critical points of multiple categories. The different aspect of the deployment of microgrids, such as its architecture, mode of operations, control strategies, monitoring methods, protection schemes, and energy management strategies are categorically explained. The fundamental requirement of the protection system and its functions are described to provide the overview of protection schemes used in the microgrid in this chapter. Various protection schemes will be discussed in the other following chapter giving more emphasis on new protection strategies.

Keywords Active distribution · Passive distribution · Central controller · Control system · Protection · Differential protection · Relaying · Microgrid · Renewable energy sources

A. R. Singh (✉) · D. Lei
School of Electrical Engineering, Shandong University, Jinan, People's Republic of China
e-mail: arvindsinghwce@sdu.edu.cn

D. Lei
e-mail: dinglei@sdu.edu.cn

A. Kumar
College of Electrical Engineering, Zhejiang University, Hangzhou, People's Republic of China

R. Singh
Department of EECE, University of Pretoria, Pretoria, South Africa
e-mail: ranjaysingh.c@gmail.com

N. K. Meena
School of Engineering and Applied Science, Aston University, Birmingham, UK
e-mail: nkmeena@ieee.org

P. Ray and M. Biswal (eds.), *Microgrid: Operation, Control, Monitoring and Protection*,
Lecture Notes in Electrical Engineering 625,
https://doi.org/10.1007/978-981-15-1781-5_1

Nomenclature

BSS	Battery Storage System
CCMS	Central Control and Management System
DCS	Current Protection
DIR	Directional Impedance Relay
DNO	Distribution Network Operator
DPS	Differential Protection Scheme
EMS	Energy Management System
ESS	Energy Storage System
f	Frequency
HMI	Human-Machine Interface
LAN	Local Area Network
MPPT	Maximum Power Point Tracking
OCR	Overcurrent Relay
P	Active Power
PCC	Point of Common Coupling
PCS	Protection and Coordination System
PI	Proportional Integral
PV	Photovoltaic
Q	Reactive Power
REC	Renewable Energy Controller
RES	Renewable Energy Source
SCADA	Supervisory Control and Data Acquisition
SOs	System Operators
V	Voltage
VSC	Voltage Source Converter
VSI	Voltage Source Inverter
WAN	Wide Area Networks

1 Introduction

1.1 General Overview

The energy demand has increased due to industrial development, population increase, and other issues in recent years. Energy crisis due to the increased demand is considered a significant problem in the world. Due to an imbalance in the electricity supply market and generation of electrical energy along with faults in the system leads to a large number of outages and blackouts in the grid all around the world which impact on the economy as well as social life [1]. Conventional power grids and generation power station are not able to meet the increasing energy demands.

Also, the rising fuel cost, environmental pollution is considered as another disadvantage of the traditional power generation plants. Because of these several problems forced the governments and other private agencies all over the world to increase the penetration of Renewable Energy Source (RES) in the power grid to meet the rising energy demands. The wind and solar is most reliable of all other RES and considered as the primary source of electricity generation in many countries. The low power generation capacity of RES has motivated to combine different types of electricity generating to form more sustainable microgrid. Microgrid has more power generation capacity and reliability, supplying local loads as well as possible integration with the conventional grid [2]. Nowadays, with an increase in RES penetration and technological development of efficient solar panel, wind power generation technology, the microgrid is one of the prominent solutions to the problem of depleting fossil fuel resources in traditional power generation. Power generation from fossil fuels having several environmental issues and low energy generation efficiency. RES is a potential solution to the problems of meeting load demand, reducing dependency on depleting fossil fuels, reducing carbon emission thus reducing pollution and other environmental benefits as well as human health benefits [3].

A microgrid is a single structure composed of RES, loads, Energy Storage System (ESS), control system or central controller and protection system. Based on power generation and load nature of power consumption, the microgrid is either AC or DC forming load grid to connect loads, RES generators, battery energy storage system and possible interface with local utility network via the bi-directional converter system. The AC microgrid is more or less similar to the conventional AC power network, and research in this area has advanced comprehensively. In recent times, the advantage of DC microgrid gained the attention of the study due to its benefits and fewer conversion losses to deliver DC power using a cable system. Moreover, DC transmission system is inherently efficient, no skin effect and have fewer transmission losses. With the research and development in the area of the microgrid, it has three categories as DC microgrid, AC microgrid, and hybrid microgrid architecture. The microgrid has three layers in its structure, namely distribution layer, central control layer and individual RES control layer. Microgrid has two operation mode, which is a grid-connected mode and islanded mode of operation. Microgrid has several control modes; some best control modes are master-slave control mode, peer-to-peer mode, combined mode, inverter control mode, etc. This chapter is more focused on establishing the fundamentals of microgrid and an overview of its challenges.

1.2 Classification of Microgrid

Microgrids are classified based on its generation capacity, type of installation and load, structure and connection to the grid. Table 1 show the classification of the microgrid based on its installed capacity. Based on installation and load the microgrid caters, it is classified as military grade microgrid, campus microgrid, community microgrid, Island microgrid, and remote microgrid. Based on the nature of supply

Table 1 Generation capacity based microgrid classification

Capacity (MW)	Type
<2	Simple microgrid
2–5	Corporate microgrid
5–20	Feeder microgrid
>20	Substation microgrid

system microgrid adopts and the common bus it makes inside the structure, the microgrid is classified into three types, which are shown in Fig. 1 Each unit is in Fig. 1 of the microgrid structure has a power controller (maximum power point tracking), a circuit breaker to disconnect in even of severe disturbances and appropriate communication protocols. In remote type microgrid, the AC structure is very suitable to supply local load while for Universities or organizations (campus microgrid) DC type microgrid is more ideal for heating purposes and military and corporate microgrid; the hybrid structure is more preferred to maintain the reliability, minimization of losses and supply DC loads. Based on the connection to the grid, the microgrid is classified as large grid-connected microgrid and small grid-connected microgrid. Some other general classification can also be done based on the number of supply phases, voltage levels, etc.

Technological, environmental and social advantages of microgrid make it highly preferable for supplying power in the remote/rural area, independent organization and also to the national grid. However, to accomplish a stable, reliable and secure microgrid grid operation, numerous technical, regulatory, social and economic issues should be addressed before making microgrid a conventional [3]. Some areas that would require more attention are irregular and weather-dependent power generation from RESs, low energy harvesting, and efficiency, lack of suitable standards and grid connection code for the microgrid. The research on these issues is taken up by leading engineering and research organization/institute across the globe by conducting extensive real-time and off-line microgrid technology research.

1.3 Advantages of Microgrid in Power Distribution Network

Microgrid development and integration in the utility is hopeful for the traditional power distribution network and have the following advantages:

1. **Environmental benefits**: in comparison to conventional power generation (thermal-coal based), microgrid based on renewables have a lesser and negligible impact on the environment [4]. The energy harvested from renewables helps to reduce greenhouse gas emission, pollution reduction, particulate matters and harmful gases reduction in air, improvement in air quality, no waste production. The carbon and greenhouse gas emission is contributing to global temperature rise, and widespread deployment of the microgrid will help in the reduction of

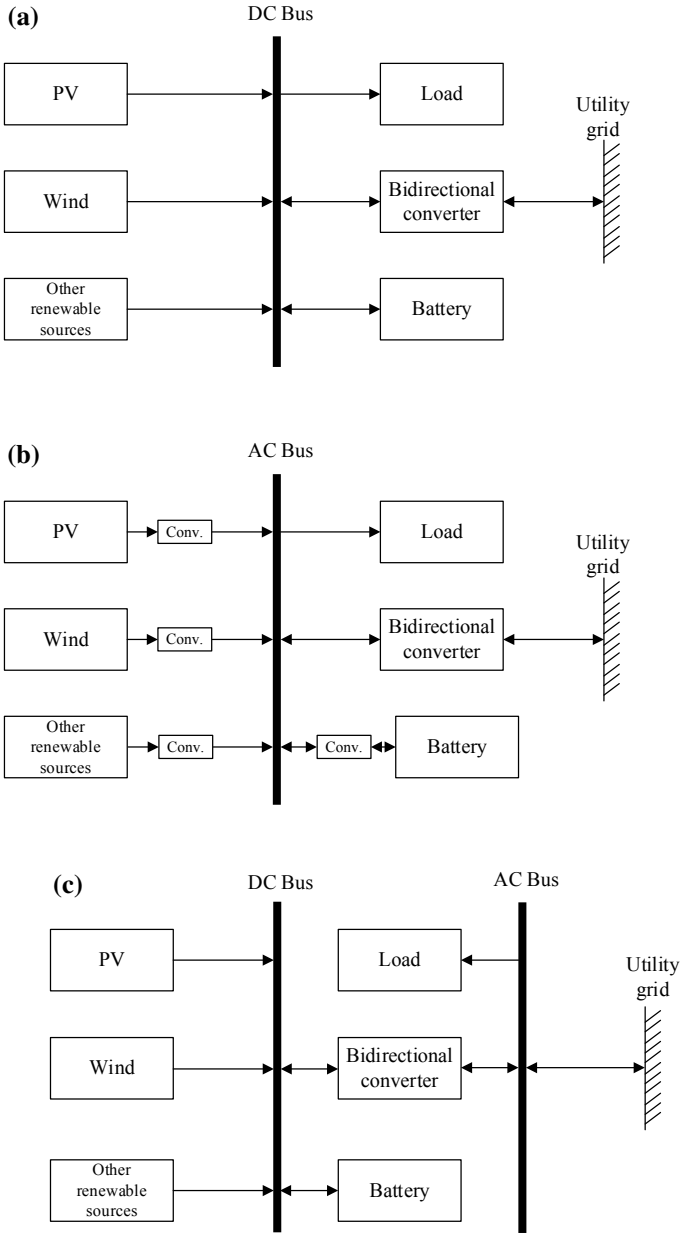

Fig. 1 Microgrid classification based on structure **a** DC microgrid, **b** AC microgrid, **c** AC/DC Hybrid microgrid

global temperature [5]. RES based microgrid has significant environmental benefits, and with currently available technology, it is feasible to deploy microgrid to save earth's environment for a future generation [6].

2. **Operational benefits**: microgrid is installed at the load, and it reduces the utility transmission and distribution losses hence save the energy wastage. It improves voltage profile providing local reactive power support. Improves reliability to supply critical loads and therefore helps in maintaining continuity of power supply. Reduction in investment for transmission and distribution network expansions. Microgrid supply surplus power to utility and helps in power system stability improvement. Microgrid participates in ancillary services to improve overall system security.
3. **Power quality benefits**: enhancement in power quality of supply due to decentralization, a better balance between generation and load demand, reduction in power outages from utility-side, system downtime reduction and improves restoration of the power system.
4. **Human development index benefits**: energy access to all helps in the improvement in human development indexes such as [7–11] (a) energy access for clean cooking and lighting purpose can immensely improve the household air quality and thus providing a better healthy condition to women and children which can lead to a significant reduction in premature deaths (b) the energy needs for the medical and health sectors specifically in developing economies is sure to rise individually for having better-equipped hospitals and storage units for vaccines (c) access to modern, economic and reliable energy services can undoubtedly improve the women's wellbeing and could also provide them with new economic opportunities (d) girls with better electricity access in rural areas are more likely to complete their school education by the age of 18, and also self-employed women with better electricity access are expected to generate more income as compared to ones without access [7] (e) proper access to energy in the agriculture sector in a rural developing area where animal and human power acts as a primary energy source for farming purposes, the yield, and productive uses can be improved significantly (f) reliable and economical electricity access can help entrepreneurs to start and grow business enterprises which can provide services to the sectors and communities that add towards economic development and well-being (g) better energy access helps in reducing poverty and income opportunities which also improves gender equality in developing nations (h) better energy access can help in avoiding the high levels of food losses with better processing and storage units and thereby reducing hunger and poverty (i) helps to achieve development goals and support expanding economy in developing nations providing surplus energy generation.

1.4 Challenges in Microgrid Project Development

The microgrid energy system based on RES has been entirely transformed from a simple system to a more complex system due to the inclusion of multiple benchmarks, stakeholders, and disagreeing aims [4–11]. Moreover, to achieve widespread integration of RESs in the present electrical energy system scenario thoughtful consideration should be given in planning and execution considering economic, technical, social, environmental as well as institutional hurdles [12]. The next significant barriers/hurdles remain in the successful deployment, and implementation of renewable microgrids for rural electrification in developing nations are:

1.4.1 Socio-Cultural

Social factors play a crucial role in electrification projects in developing areas. Public acceptance is one of the significant barriers to the successful implementation of energy projects. The participation and view of local communities help in deciding possible energy alternative for their needs. The chances of failure occur whenever the people views are ignored, which make them feel isolated and sometimes endangered by it. In the majority of cases, lack of public acceptance has direct implications on microgrid projects based on renewables which also results to higher upfront cost, delays due to frequent protests against the plans and sometimes termination of the energy projects. Other social factors are closely interconnected to community acceptance, which are more of traditional and cultural traits, health, economic benefits from projects, etc. Many times due to lack of awareness and primary energy education, community populace do not want to use the advanced energy services often thinking it as an economic burden to their livelihood and thereby opposing the microgrid projects in developing nations.

1.4.2 Economic

Microgrid electrification projects based on renewables requires a higher upfront capital cost investment, which in turns leads to a higher cost of generation as compared to the energy projects based on the conventional energy sources. The one closely related factor connected to the higher capital cost of renewable energy-based projects is not giving thoughtful consideration towards the selection and development of microgrids based on least-cost energy resource first. Some other financial obstacles include the absence of sufficient long-term funding prospects, which in turn can support the products for renewables. There is often a case of a disparity between the term of supporting funds and the cash flow of the microgrid projects. Moreover, financial security and return on investments in energy projects based on the renewables are also questionable. Market constraints such as inconsistency and uneven pricing of renewable products, information irregularities, misrepresentation in power market,

indigenous underdeveloped renewable industrial chain, etc. and trade barriers such as imposing heavy import duty taxes which makes the renewable products quite expensive adds up to the economic obstacles.

1.4.3 Environmental

Zoning regulations and environmental features (harsh climatic condition and tougher geographical terrain) can hinder the deployment of microgrid project in specific areas. Land requirements and its acquisition are also one of the significant obstacles for microgrids based on the wind, hydropower, solar photovoltaics, etc. Other renewable sources such as hydro have adverse effects on the aquatic life and sometimes real threat to damaging the biodiversity spot of many endangered species [13]. Also, other closely related issues are the risk of the flash flood in case of hydropower, noise pollution in case of wind power, water contamination, soil erosion, and deforestation during site development for the installation and construction phase of microgrid projects.

1.4.4 Institutional

Institutional organization of the energy sector in the majority of developing economies is government owned which has all the authority and responsibility for generation, transmission, and distribution with scaled-down trust between state and central federal government structure divided into several bodies. Majority of times disarray and insufficient coordination including a lack of authority which certainly creates an unstable economic environment which significantly increases the risk and sometimes reduces the investments thus causing significant obstacles in the deployment of microgrid projects. Lack of dedicated institution, policies, and planning guidelines related to renewables. The absence of clearly defined roles, complicated and inconsistent licensing procedure. Difficulty in obtaining prime land with complicated, slow, lengthy and opaque project clearances process.

1.4.5 Technical

Technical issues include inadequate technology and lack of necessary infrastructure to support the deployment of microgrids. Inability to integrate the renewable energy technologies into the existing power system and lack of proper physical facilities for local transmission and distribution networks, equipment's and services are few of significant barriers to the development of microgrid projects in developing countries. Controlled grid connection is another apprehension, predominantly for distributed technologies and in cases of a vertically integrated power sector. Lack of skilled local human capital force for operating and maintaining the energy projects are additional issues being encountered in developing nations.

2 Passive and Active Distribution

Electrical power network is in the era of power transition from passive stable distribution network of unidirectional power flow to an active distribution network of bidirectional power flow. An electrical system without RES units is passive as power is supplied from the utility grid and customers are connected with unidirectional power flow from generation to the load. The distribution network becomes active once RES units are added in the current distribution network, which leads to bidirectional power flow in the system. To support this transition in the distribution network, more emphasis should be given for the development of sustainable electrical distribution network in the developing nations while developed nations should address the technical and economic challenges associated with this transition. It requires to integrate flexible, supervisory and intelligent control incorporating a smart system. To harvest clean, renewable energy, active distribution network employs future technologies to progress towards smart-grid/microgrid. Several countries departments of science and technologies and technical reports from institutes indicate that development of active intelligent distribution network has gained momentum. The factors which are in favour of advancement of such distribution networks are (i) customer demand of highly reliable power supply distribution (ii) nations commitment for carbon emission reduction by 50% till 2050 (iii) policies design to accommodate RESs (iv) better network asset utilization and management by network operators with replacement of inefficient old equipment's, etc.

Microgrid requires superior network management and control to achieve the stable, secure, optimal operation and mode switchover without violating grid regulation and system constraint. Active network management of microgrid needs Central Control and Management System (CCMS), Renewable Energy Controller (REC), Energy Management System (EMS), Protection and Coordination System (PCS). REC look after the local control functions of RES for optimal power generation. PCS corresponds to microgrid faults and main grid faults to ensure the correct protection of microgrid with adaption to change in the fault current due to change in the microgrid operation mode from grid-connected to standalone mode. CCMS performs the overall operation and control functions of the microgrid. The primary role of CCMS is to maintain reliability by power-frequency control, power quality, voltage regulation by reactive power control, economic load dispatch, generation scheduling, and grid power (buy/sell) management. All the controllers are designed to operate in an autonomous mode with an option for manual interventions at any time required. Application of discussed controllers will provide active distribution network dispatch with microgrid for secure and economical operation in the grid-connected or standalone mode of operation. Several issues need extensive research in the area of microgrid management system design in a real sense to make it intelligent for active distribution network development.

3 DC, AC and Hybrid Microgrid System

This section discusses the various advantages of microgrid based on the type of its supply to the load.

3.1 DC Microgrid System

As shown in Fig. 1a, the PV, wind, other renewable sources, battery, and the load is connected to DC bus with appropriate individual converter system. The DC bus is connected with the utility grid with bi-direction DC-AC converter for power exchange for maintaining the power balance. The advantage of DC microgrid are as follows:

1. Higher energy efficiency and reduced energy conversion losses with the reduction in the used-on converters.
2. Easier RES integration, control, and coordination as control solely based on DC voltage.
3. More efficient supply to the load.
4. RES generation and load fluctuations are easily managed using a battery to supply deficient power.
5. Optimal operation of rotating renewable generators with the elimination of the need for synchronization.
6. Easier to damp circulating current between RES.
7. Grid integration is easier.

Most of the load work on AC and requirement of inverters to convert the DC supply to AC is its only disadvantage. Also, in DC microgrid distribution system, the voltage drops in a subsequent part of the network, and at the far end of the network the voltage level is low, hence requires intermediate voltage boost in case of medium to vast DC microgrid distribution network.

3.2 AC Microgrid

The utility grid is connected to the AC microgrid via AC bus, and it controls the connection and disconnection using a circuit breaker depending on the system condition. Figure 1b shows AC microgrid structure in which PV, wind, other renewable sources, and the battery is connected with the suitable converter to the AC bus and load is directly connected without any power electronics interface. The AC microgrid is preferable considering the facts that almost all the electrical load works on AC supply system and most dominant in the research and development. The advantage AC microgrid is that it directly connects with the utility grid without any bi-directional converter. The disadvantage is that it requires a sophisticated control system and operation and management is difficult.

3.3 Hybrid Microgrid

The hybrid microgrid consists of AC as well as DC bus in microgrid structure, as shown in Fig. 1c. The AC bus directly connects to the utility grid without any converter and supply power to loads. The DC bus connects PV, wind, other renewable sources, and battery directly and can supply power to DC loads if any. The power exchange between AC bus and DC bus occurs using a bi-directional converter to provide power to AC loads, store cheap utility power in batteries and perform various grid support functions like ancillary support, grid voltage support, etc. The hybrid microgrid has advantages of DC as well as AC microgrid, which overcomes the disadvantage of both structures.

4 Operation and Control of Microgrid

4.1 Microgrid Operation Modes

Microgrid operates in two modes, which is grid-connected mode and Islanded mode. The grid-connected mode is divided into two operating modes as power-mismatched operation and power-matched operation as per power exchange between microgrid and utility grid [14]. In the power-mismatched mode of operation active power ($\Delta P \neq 0$) and reactive power ($\Delta Q \neq 0$) are not equal to zero and current flows between microgrid and utility grid. If $\Delta P > 0$, the power flows from network to microgrid to cater the load demand as power generation from RES is insufficient and if $\Delta P < 0$, the energy flows from microgrid to the system after meeting load demand as power generation from RES is surplus. In the power-matched operation mode, active ($\Delta P = 0$) and reactive ($\Delta Q = 0$) is balanced which means that generated power from RES meets the load demand and no power exchange between microgrid and grid occurs. Hence this mode is most economical microgrid operation mode. Similarly, reactive power is excessive if $\Delta Q < 0$ and deficient if $\Delta Q > 0$, this variation in reactive power is categorized under power mismatch.

4.1.1 Grid-Connected Mode of Operation

In this mode of operation, the microgrid is connected with utility at Point of Common Coupling (PCC) to exchange power with the distribution network. The microgrid can transfer its mode using connection/disconnection controls as:

1. When microgrid is operational and connected with utility via PCC, it can be disconnected from utility by gird disconnection control; when not connected with utility, it can be connected by grid connection control.

2. In grid disconnection control, microgrid stop working in grid-connected mode and switch to Islanded mode while in grid connection control, microgrid stop working in Islanded mode and switch to the grid-connected mode of operation.
3. When microgrid is operating in grid-connected or Islanded mode, it can stop working using shut control.

4.1.2 Islanded Mode of Operation

In this mode of operation, the microgrid is disconnected from the utility due to grid-faults or scheduled disconnection operation. The RESs, Battery Storage System (BSS), other renewable sources and load work independently with individual control functions [15]. The electricity generated in this mode might not be sufficient all the time to cater to the load demand, and hence, it is necessary to prioritize the critical loads. In an Islanded mode of operation is carried by shedding unimportant load during inadequate availability of electrical energy in microgrid using load-shedding control to ensure the uninterrupted electricity supply [16].

4.2 Microgrid Control Modes

Microgrid works mostly in three commonly used control modes: master-slave combined control mode and peer-to-peer. The selection of microgrid control mode depends on its size and capacity; for example, small microgrid mostly works in master-slave control mode [17]. Apart from these overall control modes, inverter controls are also used which are namely: active-reactive (P-Q) power control, Voltage-frequency (V-f) control, droop control, etc. some of these microgrid controls are discussed in following sections to understand its functions [18].

4.2.1 Master-Slave Control Mode

In this control mode, the different RESs are controlled with varying tasks of control and methods. One or group of RES act as a master and other RESs are act as a slave. In an Islanded mode of operation, the master RES works in V-f control mode and act as a reference for other slaves RESs similar to a slack bus. In grid-connected operation mode, all RESs work in P-Q control mode and PCC is act as a reference for power flow. The master RES regulates voltage and frequency subjected to load fluctuations, and hence, power generation should be controllable with fast control response. Master control mode has some disadvantages as:

1. Master RES working in V-f control has its output voltage constant. The only way to increase the generated power output is to control its current production. Also, to respond to the instantaneous load fluctuations, master RES should have

enough adjustable generation capacity analogues to spinning reserve capacity of conventional generators.
2. The master RES governs the coordination and control of all other RESs in microgrid system if it fails the complete system will collapse.
3. This control mode needs highly accurate and time-bound islanding detection. Since islanding detection is complemented by time-delay and error, without a sound communication system, it is likely to fail; thus, not performing the functions of control strategies.

To support the fast transfer of control functions, the following combination of RESs should be used as a master RES as:

– PV + Wind.
– BSS + Other stable and easily controlled renewable sources such as fuel cell or micro-turbines, etc.
– PV + BSS or PV + BSS + fuel cell.

The third combination of RESs is more advantageous than first two as it can efficiently use the BSS for quick charge and discharge functions and ability of RES to work in Islanded operation mode of a microgrid for an extended duration. The BSS can provide power support immediately when microgrid switches from grid-connected mode to Islanded mode of operation; hence, effectively damp the significant voltage and frequency fluctuations. With increasing research in this area and use of other renewable generators to efficiently support the microgrid operation, the several different combinations are available on scientific literature [7–11].

4.2.2 Peer-to-Peer Control Mode

This control mode strategy is based on the idea of 'plug-and-play,' which is mostly used on power electronic technologies. In this control mode, all RESs are equal and no master-slave RES combination in the microgrid system. Each RES participates in active and reactive power regulation with pre-set of control functions to maintain the voltage and frequency stability in microgrid [2]. Each RES uses droop control in this control mode of the microgrid. In peer-to-peer control mode, all RESs under droop control work to regulate voltage and frequency in Islanded mode of microgrid operation. When load fluctuations occur, the changes in the voltage and frequency automatically distributed between RESs based on droop factor. RESs adjust its output frequency and voltage amplitude to achieve a new steady state of microgrid with appropriate distribution of output power generation. The droop control permits automatic load fluctuation distribution between RESs thus the voltage and frequency of microgrid also changes accordingly; hence, this control mode is essentially a proportional control. The droop control functions of RESs remains unchanged in both grid-connected and Islanded mode of microgrid operation and enable a smooth transition between two modes. In grid-connected mode, the droop control permits RESs independent control based on voltage and frequency at PCC, which makes voltage

and frequency regulation easily achievable. This does not require the need of communication system for RES, which helps in the flexible and smooth deployment of the microgrid. This control mode is simple, flexible, reliable and easily deployable with little compromise of microgrid stability in terms of voltage and frequency.

4.2.3 Combined Control Mode

As the name suggests, the combined control mode is a combination of advantages peer-to-peer control mode and master-slave overcoming disadvantages of both modes. The microgrid may have multiple RESs or group of RESs (for example, PV farm, wind farm, etc.) with the randomness of power generation profile or easily controllable other renewable sources. Control functions of RESs vary for different types of RESs, and the single control mode is not sufficient to meet the operational requirements of microgrid [3]. Considering dispersive aspects of RESs and loads in the microgrid needs different types of control modes. Hence, both the control modes can work in combination to achieve the stable, reliable and smooth operation of the microgrid.

4.3 Inverter Control Modes

RES integrated with the converter in the microgrid to operate either in parallel with utility in grid-connected mode or independently in Islanded mode. In the grid-connected mode of operation, RES requires to control the generated active and reactive output power to maintain the load-demand balance in the microgrid. The overall electricity generation capacity of the microgrid is small as compared to utility, and it regulates the rated voltage and frequency of in microgrid; hence the converters (specifically inverters) works in *P*-*Q* control [19]. In an Islanded mode of microgrid operation, one RES or group of RESs considered as a reference/slack bus to maintain the rated voltage and frequency and work in *V*-*f* control mode or droop control mode. These methods will be discussed in the following sections to understand the control concept.

4.3.1 *P*-*Q* Control

In this mode of control, the primary control function of the inverter is to control the generated active and reactive power of RES. RES inverter generates an active and reactive power based on pre-set power reference based on the power control algorithm. RES with small generation capability can be integrated into the utility on constant power generation control, and grid manages the voltage and frequency regulation [2]. In such a scenario, RES only supplies or absorbs power and do not contribute to the regulation of voltage and frequency. Grid voltage oriented decoupled

control algorithm is the basis of *P-Q* control, in its inner-loop looks after the output current control and the outer-loop adopts output power control. The mathematical model of *P-Q* control of inverter output voltage in *dq* reference is given as:

$$v_d = \mathrm{R}i_d + L\frac{\mathrm{d}i_d}{\mathrm{d}t} - \omega L i_q + u_d \tag{1}$$

$$v_q = \mathrm{R}i_q + L\frac{\mathrm{d}i_q}{\mathrm{d}t} - \omega L i_d + u_q \tag{2}$$

Where u_d and u_q are inverter terminal voltage, $\omega L i_d$ and $\omega L i_q$ are cross-coupling terms which get eliminated in feedforward compensation by subsequent control. The Proportional Integral (PI) control is used in the outer power control loop, which is expressed as:

$$i_{d\mathrm{ref}} = (P_{\mathrm{ref}} - P)\left\{k_p + \frac{k_i}{s}\right\} \tag{3}$$

$$i_{q\mathrm{ref}} = (Q_{\mathrm{ref}} - Q)\left\{k_p + \frac{k_i}{s}\right\} \tag{4}$$

Where P_{ref} and Q_{ref} are active and reactive power reference, $i_{d\mathrm{ref}}$ and $i_{q\mathrm{ref}}$ is *d*-axis and *q*-axis current reference, k_p and k_i is proportional and integral gains, respectively. When grid voltage u is constant, the active power output is equivalent to *d*-axis current $i_{d,}$ and reactive power output is proportional to *q*-axis current i_q. The transfer function of voltage (v_{d1}/v_{q1}) and current (i_d/i_q) is first-order lag, which means same axis currents can control the *d*-axis and *q*-axis voltages. Considering this as the basis for the inner-loop current controller and applying PI control, the mathematical model is given as:

$$v_{d1} = (i_{d\mathrm{ref}} - i_d)\left\{k_p + \frac{k_i}{s}\right\} \tag{5}$$

$$v_{q1} = \left(i_{q\mathrm{ref}} - i_q\right)\left\{k_p + \frac{k_i}{s}\right\} \tag{6}$$

By adding cross-compensating terms to achieve the decoupling current control, the effect of grid voltage and *d-q* axis cross-coupling can be eliminated. Three phase inverter gating pulses are obtained using inverse park transformation and inverter output voltage by using sinusoidal pulse-width modulation in *P-Q* control [2]. Figure 2 shows the microgrid *P-Q* control schematic.

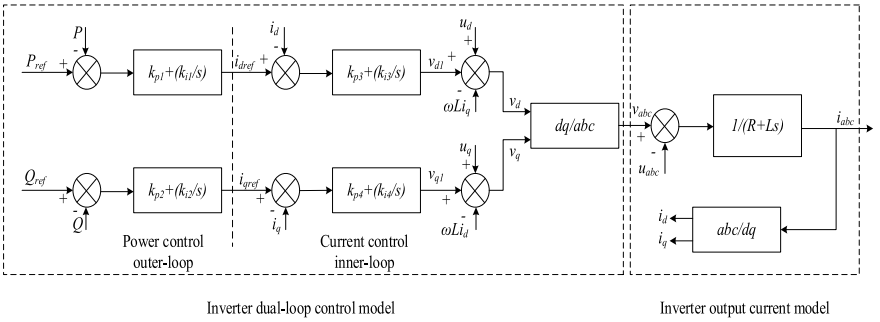

Fig. 2 Microgrid *P-Q* control

4.3.2 V-f Control

In *V-f* control, the output of inverter voltage and frequency is constant to enable RES operation in slave mode and critical loads when the microgrid is disconnected from the utility. It is necessary to curtail load in Islanded mode of operation considering the low generation capacity of the microgrid to maintain the continuity of power supply to critical loads. Hence, this control must be able to respond and detect load switching. To keep the constant output, based on feedback from the inverter, the AC side voltage is regulated and the dual-control scheme is adopted with voltage control in outer-loop and current control in inner-loop [20]. The function of voltage control in outer-loop is to maintain output voltage constant and current control in inner-loop to accelerate the fast response against load fluctuations or disturbances. In *V-f* control mechanism, the current control in the inner loop has wide bandwidth in the inverter control which increases the speed of dynamic response of inverter dynamic response ability and adaptability for non-linear load disturbances with reduced harmonic distortion in output voltage. This control has a high dynamic response and steady-state accuracy because it makes the best usage of system status information. In terms of decoupling and control functions, the *V-f* control is similar to *P-Q* control. Figure 3 show the microgrid *V-f* control schematic, the reference voltages U^*_{1dd} and U^*_{1dq} and measured voltages U_{1dd} and U_{1dq} adopted in this for voltage control outer-loop and current control inner-loop are specified [21].

4.3.3 Droop Control

The droop control method is based on power converters parallel-connection technology. This control algorithm is implemented by mimicking the droop characteristics of traditional generational connected to the utility. The voltage and frequency output of Voltage Source Inverter (VSI) or Voltage Source Converter (VSC) is controlled according to variation of the power output. The microgrid operating in Islanded mode with multiple RES inverters connected in parallel, individual inverters active

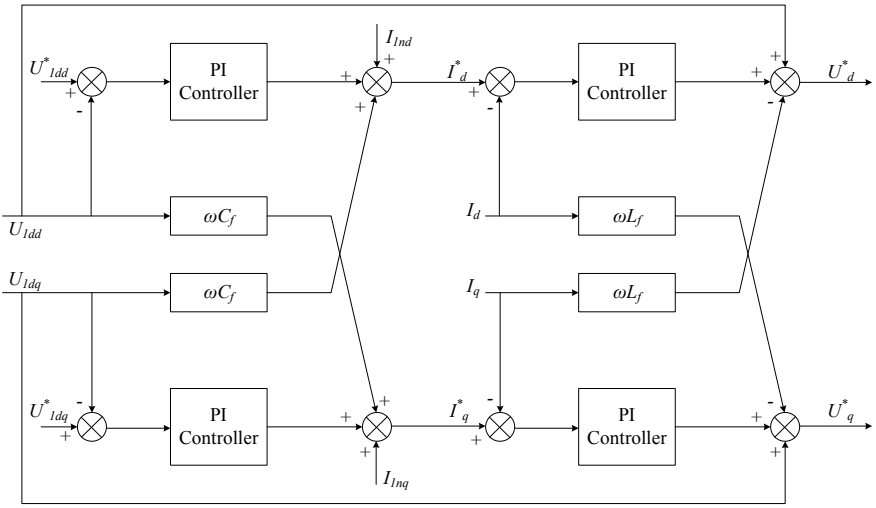

Fig. 3 Microgrid *V-f* control

and reactive power equation is expressed as:

$$P_n = \frac{VV_n}{X_n}\delta_n \quad Q_n = \frac{VV_n - V^2}{X_n} \tag{7}$$

Where V is the voltage at inverter point of connection, V_n is the output voltage of the inverter, δ_n is an angle between V and V_n and X_n is output impedance (reactance) inverter. From Eq. (7) it is evident that active inverter power mainly depends on the angular difference (δ_n) between the voltage at the point of connection (or PCC) and inverter output voltage while reactive power primarily on voltage magnitude. By controlling the output frequency, the inverter phase can be controlled, and the voltage can be directly controlled with appropriate triggering strategy. The frequency of the inverter is given as:

$$f_n = \frac{\omega_n}{2\pi} = \frac{\mathrm{d}\delta_n}{\mathrm{d}t} \tag{8}$$

From Eqs. (7) and (8). it is evident that inverter output voltage regulates its reactive power output and frequency regulates its active power. The inverse droop control strategy is to control its active and reactive power outputs based on measured grid voltage magnitude and frequency by calculating the predefined droop control characteristics [2]. The inverter output voltage is regulated by measured active power; hence, this control mode is inverse droop control. Figure 4 show the microgrid droop control characteristics for active and reactive power.

The RES inverters can use any of these discussed control methods, and output can be controlled using local measurement data to achieve smooth and reliable operation

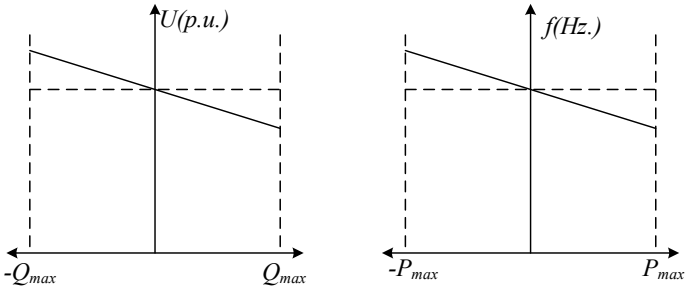

Fig. 4 Microgrid droop control characteristics

of the microgrid. The control methods discussed in this chapter is elementary in understanding to make the basis of operation and control concept of the microgrid.

4.4 Operation and Management

A microgrid is operated and managed using various controllers such as RES, CCMS, EMS, and PCS, which work to coordinate and manage several essential functions for smooth and reliable operation. The detail functions of these controllers are discussed as follows:

4.4.1 Renewable Energy Controller

REC primary function is to autonomously control the flow of power and voltage profile of load response to contingency and load transitions. Here 'autonomously' suggests without any communications or control command from the CCMS. REC also participates in generation scheduling, load management, and demand-side management by controlling the BSS or other storage devices. Furthermore, REC must ensure that each RES quickly picks up its generation to provide power to its load in Islanded mode and automatically reconnect to the grid to work in coordination with CCMS. The most crucial aspect of REC is its fast response for the locally measured voltages and currents regardless of the information from the other RECs. This functionality enables RES to work as plug-and-play devices, which also helps of new RES at any point in the microgrid without compromising the protection and control of newly added RES generation. Another vital function of REC is that it does not communicate other RECs in the microgrid independently and it never supersede the CCMS control commands.

4.4.2 Central Control and Management System

CCMS is the primary controller in the microgrid and regarded as the brain of a microgrid. CCMS executes all commands for operation, management, and control of microgrid through RECs and other controllers. The main functions of CCMS are (i) it maintains the rated voltage and frequency at all load points through power-frequency and voltage controls (ii) it keeps the power balance in the microgrid (iii) optimized energy generation and load dispatch (iv) load management through load shedding (v) monitoring and data storage (vi) supervisory controls. CCMS mostly designed to work autonomously but it can be switched to manual control whenever it's required. It also manages the functions of EMS and settings of PCS depending on system configuration changes. Some vital role of CCMS in grid-connected mode are (a) system monitoring and diagnostic by collecting information from RESs (b) state estimation of overall microgrid and RESs (c) security assessment (d) monitoring of economic RESs generation scheduling (e) monitoring and controlling of active and reactive generation from RESs (f) ensuring the grid synchronization to enable power exchange. Essential functions of CCMS in Islanded mode are (a) maintaining voltage and frequency by initializing optimized active and reactive power control from RES generators (b) initializing efficient and optimum load shedding or load curtailment algorithms (c) management of BSS for optimum utilization and maintaining power balance within limit (d) executing connection and disconnection with utility.

4.4.3 Energy Management System

EMS provides the reference of active power, reactive power, voltage and frequency for REC of each RES. To achieve the function of calculation of various reference parameters, EMS uses state-of-art communication system protocols and embedded algorithms based on Fuzzy, artificial intelligence, or other novel computational mathematical morphology [20]. The setpoint is calculated based on operation, management and control requirements of the microgrid. The essential functions of EMS are (a) RES able to meet the load demand with customer satisfaction (b) microgrid able to meet the operational guideline set by grid satisfactorily (c) optimization of RES generation to meet guidelines of green-house-gas and CO_2 emission reduction (d) optimization of renewable energy fraction of generation (e) maintaining the higher efficiency of RES generation.

4.4.4 Protection and Coordination System

PCS primary function in a microgrid is to ensure protection against faults within the microgrid and main grid operating in grid-connected and Islanded mode. The protection scheme should be adaptive and under the control of CCMS to change the relay settings as per the scenarios in the microgrid. Relays threshold detection and coordination settings should correspond to change in the current fault level.

To achieve this, the strong backbone of a communication system is needed which facilitate communication between CCMS, PCS, and REC. When a fault is detected in the utility side, PCS straightway issues the command to PCC circuit-breaker to disconnect and switches microgrid operation to Islanded mode to maintain the supply the critical loads. For utility faults, PCS allows fault-ride-through following the grid code in the grid-connected mode for a stipulated time in case of temporary fault conditions before issuing a command for the disconnection. For faults within the microgrid, the PCS disconnects the faulted section of the microgrid to keep good part stable and smooth operation. Under-frequency and undervoltage relays are used concerning bus voltage for RES protection in case of severe faults in the microgrid. PCS also governs the resynchronization of microgrid with utility and initiates the switchover from Islanded to the grid-connected mode by issuing circuit breaker commands. More details of protection schemes and coordination algorithms will be discussed in the book chapter in further information in various chapters. The protection philosophy is different for microgrid in comparison to conventional power transmission or distribution system due to (a) bidirectional power flows between generators and loads in the radial microgrid system (b) microgrid distribution system is active because of RES and (c) the short-circuit level of microgrid is not constant, and it changes significantly depending on mode or operation as well as a number of RESs active in the system.

5 Monitoring and Protection of Microgrid

5.1 Monitoring of Microgrid

The success of microgrid operation, control, and management functioning as an active distribution network depends on the cost-effective and efficient communication system. The Supervisory Control And Data Acquisition (SCADA) is preferable along with Distribution Network Operator (DNO) to achieve these function in the microgrid system. The increased penetration of RES generation the network connection becoming more complex day-by-day due to constraints of thermal limit, voltage limit, wired connection complications, etc. These constraints are creating unwanted hurdles in the future incorporation of RES generation, which demands the active distribution network system and cost-effective solutions to overcome these challenges. In a conventional distribution system, SCADA is mainly available voltage level 6.6–11 kV and higher voltages network with high-bandwidth local area and wide area networks (LAN and WAN). SCADA function varies from several tasks such as data acquisition, remote switching, alarm indication, data processing, emergency control, demand-side management, human-machine interface (HMI), etc. SCADA system is very secure and robust in terms of security and functioning. SCADA uses a combination of communication circuits such as pilot cables, standard copper cable, optical

fiber, mobile telecommunication, radio. The optical fiber-based communication circuit is the fastest and most reliable in comparison of others, but in rural areas, the copper cable-based communication circuit is used due to cost constraints. DNOs is similar to System Operators (SOs) in the power system, and it operates in urban as well as rural networks. DNOs uses several remote terminal units for a variety of functions such as switch change time tagging and alarms with 1 ms accuracy, relay connections, programmable logic sequence and digital outputs with pulse duration. Therefore, the active distribution network management control centers should be located at strategic sub-stations instead of remote location which host DNOs with the SCADA system. Microgrid system has typically two types of SCADA systems as a centralized and decentralized system.

5.1.1 Centralized System

The SCADA has some crucial functions which need to be controlled centrally, e.g., load scheduling, load switching, load management and implementation of load curtailment. However, the main challenge is the appropriate communication infrastructure for reliable data information and control command transmission. High voltage substations have real-time units installed, but microgrid connects to low voltage substations which might not have installed real-time units and appropriate communication system. It will lead to slow switch status detection, which in turn, slow the SCADA system to operate its functions. Centralized system with information of network diagram, switch operation and sequencing details, historical components database, hardware maintenance schedule, skilled and experienced personnel, switch control sequence, etc., will be helpful to implement intelligent switch control algorithm for microgrid operation and smooth control. Moreover, the centralized system needs costly communication system to provide efficient services if it lacks that it will have slow SCADA response, which might lead to the risk of single point system failure.

5.1.2 Decentralized System

The decentralized system has widespread small SCADA system installed at various substations located in urban and remote areas. It is more advantageous for single DNOs to control the number of small SCADA system which can provide efficient management and control. The dispersed SCADA system requires dedicated support and communication workstations. The decentralized system has the advantage of low-cost communication system, better switch change response, cost-effective logic controllers, etc. However, it might suffer from high upfront investment cost, suitable maintenance facility, field visit and complexity in the integration of dispersed SCADAs with a central SCADA system. With the advancement in technology, the implementation and operation of such a system may become cost-effective and feasible in a few years. The aim of this section to introduce DNO and SCADA system

with the type of control architecture, there are numerous components, functions, and modules, which plays a significant role in monitoring. However, more detail discerption and its functioning can be found in scientific literature as well as in textbooks and not elaborated in this chapter.

5.2 Protection of Microgrid

Microgrid operating under reasonable condition should work in grid-connected mode and the case of any fault or disturbance it must dis-connect from utility and work in Islanded mode. Microgrid with RESs, BSS and other renewable sources is capable of catering load demand and if not, it may initiate optimize load shedding control algorithm to supply critical loads. The primary function of the protection system in the microgrid to provide stable and smooth operation of a microgrid during a contingency. The protection system determines under what conditions microgrid should be disconnected from the utility, which section of microgrid under faulted condition should be isolated and how to provide coordinated protection. The elements of the protection system feature and performance of microgrid is not similar to the distribution system due to inverter-based RES the operating characteristics are not the same due to (a) inverter operating characteristics are not consistent (b) different RES inverter has its unique design and not uniform (c) RES inverter design depends on system requirement and operational conditions. The protection system of microgrid design is very complex and require prior research to understand the dynamics of microgrid operation for grid-connected and Islanded mode. This section will put forward basic microgrid protection concept and issues.

5.2.1 Microgrid Protection Functions

Microgrid protection system has to work in both grid-connected and Islanded mode. In grid-connected mode, the multiple RES, BSS, and other renewable energy sources influence the fault current, other electrical parameters significantly; hence, traditional protection schemes fail to detect and locate the faults. In Islanded mode, the inverter protection functions may force to disconnect the RES and inverter operation of forced RES disconnection need to be blocked by the protection system. Before the introduction of the microgrid in the mainstream, the RESs integrating with the utility was not working independently, and utility protection system was under tremendous stress to maintain the operation of RES. The accurate and reliable protection scheme is a crucial aspect for microgrid control and operation, which is highly complicated in implementation. Based on current scientific literature and research, microgrid protection is the main area of research and development technology. The microgrid protection schemes mainly perform functions as (a) Fast RES disconnection from utility network in the event of a fault on the utility side (following the newly introduced fault-ride-through grid conditions) does not affect the utility distribution

network protection. The generation capacity of a microgrid is not significant as compared to the ability of utility and disconnection of RES will not affect the power imbalance significantly. (b) Prevention of unwanted disruption of microgrid from the utility which will create momentary power instability in utility and may trigger other protection systems to bring network in stable operating condition. (c) Disconnection operation from the utility in reasonable working condition for scheduled maintenance. (d) Re-connected or resynchronization of microgrid with the utility for enabling power exchange. (e) RES protection and coordination with other protection systems.

5.2.2 Microgrid Protection Schemes

A. Differential Protection

The issues in the protection of microgrid due to the integration with the utility is mitigated using Differential Protection Scheme (DPS), which is installed at PCC. DPS acts as primary protection and is installed at PCC to protect microgrid from utility-side disturbances in grid-connected mode and severe faults in Islanded mode. DPS works on Kirchhoff node current law and its best scheme for the protection of microgrid utility installed at PCC. The DPS pickup setting and percentage differential setting forms AND gate to detect and isolate fault conditions. DPS is highly sensitive, accurate and straightforward to implement for the protection of microgrid having multiple RES. Research and development in this area also persisted, and DPS with advanced computational methods and in combination with machine-learning has been reported in several scientific works of literature with better accuracy and detection sensitivity. DPS is highly reliable and dependable protection scheme, and the only disadvantage is the high cost. In the following chapters, the other protection schemes will be discussed in detail.

B. Backup Protection

DPS circuit breaker failure is not common, but to protect it, neighboring circuit breaker operates to isolate the fault if it fails to perform. Backup protection is provided using overcurrent relay (OCR) with specific time-delay setting. In the event of DPS failure due to certain circumstances and central DPS goes offline, OCR performs primary protection to prevent complete protection system loss from service. OCR also severe as backup protection for internal faults of the transformer and internal microgrid faults to avoid excess current flow from RES. The utility-side protection scheme such as distance protection serves as backup protection of PCC with time delay setting. With the application of wide area monitoring system penetration in distribution and microgrid for advanced control and management, the advanced backup protection schemes based on negative sequence, rate of change of impedance and other important system parameters are reported and available in the scientific literature. New Islanding schemes based on advanced measurement technology with highly fast and accurate detection of stable and unstable microgrid

operating conditions are reported in the scientific research and will be discussed in following chapters.

C. Directional Protection

The other very important protection scheme for the microgrid is Directional Current Protection (DCS). The microgrid is considered as an active distribution network, and power flows in bi-direction due to multiple RES installed. DCS which plays a significant role in the detection of reverse power flow and helps to maintain the stable microgrid operation. During severe faults within the microgrids network, depending on the fault location and sections, the current contributed from other sources may increase the current fault level and damage the pieces of equipment. DCS helps to divide the microgrid network into small-small parts by detecting reverse power flow and help to prevent harm to the costly equipment's. Directional Impedance Relay (DIR) acts as a primary protection scheme in the microgrid distribution system to locate and isolate the fault. DCS and DIR work in coordination to detect, isolate the faulted section and protect the RES generators from excessive current flow damage. In the event of a fault at PCC and failure of the PCC protection system, DCS can also provide backup protection and initiate the microgrid disconnection with specific time-delay settings.

References

1. Bansal R (ed) (2017) Handbook of distributed generation: electric power technologies, economics and environmental impact. Springer
2. Li F, Li R, Zhou F (2015) Microgrid technology and engineering application. Elsevier, pp 11–27
3. Chowdhury S, Chowdhury SP, Crossley P (2009) Microgrids and active distribution networks. IET Renew Ser 6:1–12
4. Kumar A, Singh A, Deng Y et al (2019) Integrated assessment of a sustainable microgrid for a remote village in hilly region. Energy Convers Manag 180:442–472. https://doi.org/10.1016/j.enconman.2018.10.084
5. Kumar A, Singh A, Deng Y et al (2018) Multiyear load growth based techno-financial evaluation of a microgrid for an academic institution. IEEE Access 6:37533–37555. https://doi.org/10.1109/access.2018.2849411
6. Kumar A, Singh A, Deng Y et al (2018) A novel methodological framework for the design of sustainable rural microgrid for developing nations. IEEE Access 6:24925–24951. https://doi.org/10.1109/access.2018.2832460
7. Kumar A, Sah B, Singh A et al (2017) A review of multi criteria decision making (MCDM) towards sustainable renewable energy development. Renew Sustain Energy Rev 69:596–609. https://doi.org/10.1016/j.rser.2016.11.191
8. Singh R, Bansal R (2018) Review of HRESs based on storage options, system architecture and optimisation criteria and methodologies. IET Renew Power Gener 12:747–760. https://doi.org/10.1049/iet-rpg.2017.0603
9. Singh R, Bansal R (2019) Optimization of an autonomous hybrid renewable energy system using reformed electric system cascade analysis. IEEE Trans Ind Inform 15:399–409. https://doi.org/10.1109/tii.2018.2867626

10. Singh R, Bansal R, Singh A, Naidoo R (2018) Multi-objective optimization of hybrid renewable energy system using reformed electric system cascade analysis for islanding and grid connected modes of operation. IEEE Access 6:47332–47354. https://doi.org/10.1109/access.2018.2867276
11. Singh R, Bansal R, Singh A (2018) Optimization of an isolated photo-voltaic generating unit with battery energy storage system using electric system cascade analysis. Electr Power Syst Res 164:188–200. https://doi.org/10.1016/j.epsr.2018.08.005
12. Al Mamun K, Amanullah MTO (2018) Smart energy grid design for island countries. Springer
13. Merritt NR, Chakraborty C, Bajpai P (2015) A control strategy for islanded operation of a voltage source converter (VSC) based distributed resource unit under unbalanced conditions. In: 2015 IEEE 13th international conference on industrial informatics (INDIN), IEEE, 1550–1555 July
14. Saha S, Roy T, Mahmud M et al (2018) Sensor fault and cyber attack resilient operation of DC microgrids. Int J Electr Power Energy Syst 99:540–554. https://doi.org/10.1016/j.ijepes.2018.01.007
15. Gaztanaga H, Etxeberria-Otadui I, Bacha S, Roye D (2006) Real-time analysis of the control structure and management functions of a hybrid microgrid system. In: IECON 2006-32nd annual conference on IEEE industrial electronics, IEEE, 5137–5142 Nov
16. Yongbiao Y, Weiliang L, Jie S, Kun H, Lu C, Li H (2012) The wide-area measurement technology application in micro grid. In: 2012 China international conference on electricity distribution, IEEE, 1–5 Sep
17. Kaletsanos A, Xepapas F, Xepapas S, Manias SN (2003) Nonlinear control technique for three-phase boost AC/DC power converter. In: IEEE 34th annual conference on power electronics specialist, 2003. PESC'03, vol 3. IEEE, 1080–1085 June
18. Sarkar T, Dan A, Ghosh S et al (2017) Interfacing solar PV power plant with rural distribution grid: challenges and possible solutions. Int J Sustain Energy 37:999–1018. https://doi.org/10.1080/14786451.2017.1414051
19. Patrao I, Figueres E, Garcerá G, González-Medina R (2015) Microgrid architectures for low voltage distributed generation. Renew Sustain Energy Rev 43:415–424. https://doi.org/10.1016/j.rser.2014.11.054
20. Guo Z, Li S, Zheng Y (2018) Feedback linearization based distributed model predictive control for secondary control of islanded microgrid. Asian J Control. https://doi.org/10.1002/asjc.1906
21. Ambia M, Al-Durra A, Caruana C, Muyeen SM (2012) Islanding operation of hybrid micro-grid system with power management control scheme. In: Proceedings of the IASTED international conference on power and energy systems, EuroPES, 26–33 2012

Optimal Day-Ahead Renewable Power Generation Scheduling of Hybrid Electrical Power System

Surender Reddy Salkuti

Abstract In this chapter, new optimal generation scheduling problem is solved in a hybrid power system by considering trade-off between system operating cost and risk level and provides best-fit schedules by optimizing the real-time and day-ahead deviation costs. The hybrid system considered in this work consists of wind, solar photovoltaic (PV), and conventional thermal generators. In this chapter, a set of batteries is considered for storing the energy. The intermittency of these renewable energy resources (RERs) creates imbalances between generation and load demand as the renewable power output cannot be known with certainty for the next few hours. Therefore, to handle uncertainties involved in these RERs, the optimal scheduling strategies are required to adapt to these requirements. The imbalance between generation and load demand is due to the forecast errors, and they need additional generation capacity (i.e., ancillary service) to handle this issue. In proposed approach, uncertainties in renewable power generations are handled by using anticipated real-time deviation bids, i.e., by considering the spinning reserves in the system. In this work, the spinning reserve offers from thermal units are considered. The intermittent nature of wind power is represented by Weibull distribution function and the solar PV power by bimodal distribution function. The proposed problem is solved by using multi-objective-based non-dominated sorting genetic algorithm-II (NSGA-II).

Keywords Renewable energy · Solar PV power · Wind power · Uncertainty · Weibull distribution · System operating cost · System risk level · Reserves · Multi-objective optimization

Nomenclature

Doubly fed induction generators	DFIGs
Energy storage systems	ESSs
National renewable energy laboratory	NREL

S. R. Salkuti (✉)
Department of Railroad Electrical Systems, Woosong University, Daejeon, Republic of Korea
e-mail: surender@wsu.ac.kr

P. Ray and M. Biswal (eds.), *Microgrid: Operation, Control, Monitoring and Protection*,
Lecture Notes in Electrical Engineering 625,
https://doi.org/10.1007/978-981-15-1781-5_2

Non-dominated sorting genetic algorithm-II	NSGA-II
Pareto archived evolution strategy	PAES
Photo voltaic	PV
Probability density function	PDF
Renewable energy resources	RERs
Spinning reserves	SRs
Strength Pareto evolutionary algorithm	SPEA
System operator	SO
Total operating cost	TOC
Ultra-high voltage	UHV
Wind energy generators	WEGs

1 Introduction

A wide installation of RERs into power system has been promoted during last decades. Increased development and deployment of green/renewable energy technologies rank among the top priorities of many countries. The search for the development and utilization of RERs has coincidentally, aligned the interests of both industrialized and developing nations. The industrialized countries need to satisfy increases in power demand without increasing their dependence on foreign importation of oil and extra degradation of the environment. The developing countries see renewable energy as a way of meeting increasing power demands and extending electricity usage to disperse population with reduced stress on national electric network and also to take benefit of carbon credit. This alignment of interests will spur economic growth because any successful technology developed in one part of the world can easily be deployed in any other part of the world. This will also require the developments of standards and quality that is acceptable to the international community. The power output from wind and solar PV generators is uncertain, and hence, new energy storage technologies are required to overcome the difficulties posed by these characteristics. Increasing concerns about energy security, climate change, and diminishing the reserves of fossil fuels around the world are leading the increased interest in generation, distribution, and management of renewable power. However, the intermittent nature of RERs is a challenging problem to address. In particular, spinning reserves are coupled with RERs to mitigate the impact of uncertain behavior [1].

The role of wind and solar PV powers cannot be ignored, as they become significant in modern power systems because of their increased penetration level. The increased penetration levels of RERs have brought new challenges to system operation, such as system reliability, power quality, stability, planning, operation, and maintenance. [2]. As mentioned earlier, because of increasing environmental concerns, the RERs, such as solar PV and wind power sources, are gaining popularity. But they are weather dependent. Studies show that climate change will have adverse

effects on the environment; hence, the RERs are important to maintain the carbon footprint at a low value [3]. However, these RERs are intermittent in nature. The intermittency of these sources can be handled by maintaining the additional reserves into the system. As the RERs are intermittent in nature, after certain penetration levels of RERs, the performance of power system may deteriorate. Therefore, there is a requirement to determine optimal penetration levels of RERs into the system. The reliability of RERs can be ensured by additional strategies such as resource forecasting, control strategies, demand side management, hydro generation coordination, new market designs, and storage systems. [4].

The solution of optimal generation scheduling problem determines the optimal set-point values throughout the system such that a specified objective is met by satisfying the various network constraints, including generator voltage and line-flow limits [5]. Getting to high shares of renewables in electricity and/or the energy system more broadly will involve the electrification of other sectors. This will change the role of the electricity system within high share renewable energy systems, and it is important to understand what sectors and to which extent should be electrified [6]. There is a great need for careful analyses of economic and technologic questions to address practical implementation issues based on the state-of-the-art knowledge in power engineering and other disciplines [7].

The process of deregulation has introduced several new interesting research topics in electrical power system and energy management areas. One of the most fascinating issues among them is the integration of RERs into the existing power network. The optimal operation and planning of the resources in smart grids bring up new challenges and opportunities for decision makers. To keep the system secure, determination of optimal distribution and locations of SRs is required. In a deregulated market environment, there is a requirement for the optimal scheduling of both energy and SRs. As there is a strong coupling between energy and spinning reserves, simultaneous optimization of these provides more secure and economic solutions [8]. Nowadays, the heuristic optimization has undergone significant developments. By using various new approaches for improved search exploitation and exploration, the modern heuristic optimization tools have demonstrated a great promise for solving the practical problems with high mathematical complexity [9]. Renewable energy with ESSs can increase reliability of power supply and increases the flexibility of power systems operation.

An optimal operation of hybrid electrical power system integrating wind energy generators and concentrated solar power with an electric heater is proposed in Ref. [10]. A multi-objective-based optimal scheduling problem incorporating the uncertainty and optimizing operating cost, emission, and reliability simultaneously is presented in Ref. [11]. A day-ahead optimum generation scheduling of joint power and heat units with ESSs incorporating the security constraints is solved in Ref. [12]. Reference [13] proposes an optimal generation scheduling of a thermal-solar PV-wind hybrid electrical power system considering the energy produced is transmitted to long distance loads using UHV transmission lines. An optimal scheduling method of an exemplar multi-energy system comprising battery energy storage systems, combined cycle power plants, RERs, boilers, thermal energy storage systems, electric

loads, and thermal loads, is presented in Ref. [14]. Reference [15] proposes a statistical scheduling method for the economic dispatch and energy reserves problem. A new mathematical approach for optimal generation scheduling of wind and pumped storage for 25–48 h ahead is described in Ref. [16].

From the above literature review, it is clear that with the increasing penetration levels of renewable power in electrical power systems, the fluctuation of these RERs has great influence on the optimal generation scheduling and operation of power system with RERs. Studies on the optimization of utilization of RERs usually consider both the planning mode and the operational mode of the power system network. This chapter focuses on operational mode of network. The aim of proposed optimal day-ahead generation scheduling is to find a best-compromised solution by optimizing total operating cost and system risk levels simultaneously by incorporating thermal, solar PV, and wind generators simultaneously, over a scheduling period by satisfying various inequality and equality constraints. The aim of this chapter is to propose a novel approach, which is able to schedule a hybrid power system containing conventional and renewable energy generation while ensuring power system security. With the combination of RERs, i.e., wind, solar PV powers, and battery storage, the non-dispatchable nature of RERs becomes dispatchable. Contributions of this work are listed below:

- A multi-objective-based generation scheduling problem is proposed in this chapter by considering two (i.e., multiple) conflicting objectives (total operating cost and the system risk level) considering stochastic characteristics of renewable energy.
- The proposed approach incorporates reactive power capability of synchronous generating units, DFIGs, and solar PV units in optimum generation scheduling problem.
- Uncertainties involved in solar PV and wind energy generations are handled by using anticipated real-time deviation bids considering spinning reserves.
- Multi-objective-based non-dominated sorting genetic algorithm-II (NSGA-II) is used to get the best-compromised solution for the proposed optimal scheduling problem.
- The uncertainties in wind and solar PV powers are represented by Weibull and bimodal distribution functions.
- The performance of proposed optimal scheduling has been tested on standard IEEE 30 bus system.

The remainder of this chapter is organized as follows: Sect. 2.2 describes the modeling of uncertainty of wind and solar PV energy systems. The problem formulation of proposed optimum scheduling of hybrid power system by considering two objective functions (total operating cost and system risk level) is presented in Sect. 3. The description of multi-objective-based NSGA-II technique is presented in Sect. 4. Simulation results and analysis are presented in Sect. 5. Section 6 summarizes the major contributions with concluding remarks.

2 Uncertainty Handling of Wind and Solar PV Energy Generators

2.1 Wind Power Distribution

To determine power output of WEG, it is required to know the profile of wind speed at a particular location. In this chapter, Weibull PDF is used to present the variation of wind speed (v). Here, the wind speed (v) is modeled by using the Weibull PDF, and it is represented by [17],

$$f_v(v) = \left(\frac{k}{c}\right) * \left(\frac{v}{c}\right)^{(k-1)} \exp\left[-\left(\frac{v}{c}\right)^k\right] \quad 0 < v < \infty \tag{1}$$

The cumulative distribution function of wind power probability function is expressed as,

$$F_v(v) = f_v(v \le v_x) = \int_0^{v_x} f_v(v)\mathrm{dv} = 1 - \exp\left[-\left(\frac{v_x}{c}\right)^k\right] \tag{2}$$

The Weibull distribution parameters, i.e., scale factor (c) and shape factor (k), should be greater than zero. The advantages of Weibull distribution are a two-parameter distribution, depending only on c and k. Normally, c is varied from 1 to 3 and k is in the range from 5 to 25. From the values of scale and shape parameters, one can easily estimate the mean and standard deviation of PDF curve. The mean of Weibull PDF can be expressed using,

$$E(V) = c * \Gamma\left(1 + k^{-1}\right) = \frac{c}{k} * \Gamma\left(\frac{1}{k}\right) \tag{3}$$

Variance is expressed as,

$$\mathrm{var}(V) = E\left(V^2\right) - E^2(V) = \frac{c^2}{k}\left[2\Gamma\left(\frac{2}{k}\right) - \frac{1}{k}\left[\Gamma\left(\frac{1}{k}\right)^2\right]\right] \tag{4}$$

Here, $\Gamma(x)$ is gamma function. It can be expressed using,

$$\Gamma(\alpha) = \int_0^{\infty} \mathrm{e}^{-\mathrm{t}} * t^{\alpha-1}\mathrm{dt} \tag{5}$$

If α positive integer, then the above equation becomes,

$$\Gamma(\alpha) = (\alpha - 1) \tag{6}$$

After the wind speed (v) is represented by a random variable, then the power output from WEG is also expressed as a random variable using the random variable transformation principle. Power output of the WEG (p) is classified into three ranges: (i) below cut-in wind speed (v_i), the WEG will not produce any power. This is due to the fact that there are some friction losses in wind turbine; (ii) wind speed (v) between the cut-in speeds to rated speed (v_r), then the wind power will increase linearly, and this range is termed as continuous range; and (iii) finally, when the wind speed (v) is increased above rated speed (v_r) and below cut-out speed (v_o), then it will produce rated wind power, and it is the discrete probability distribution function. In the similar lines, above cut-out speed (v_o) and below cut-in speed it will not produce any power. This is also termed as discrete range. The power output from the WEG for a specified wind speed (v) is represented by [18],

$$p = \begin{cases} p = 0 & \text{for } v < v_i \text{ and } v > v_o \\ p = p_r * \frac{(v - v_i)}{(v_r - v_i)} & \text{for } v_i \le v \le v_r \\ p = p_r & \text{for } v_r \le v \le v_o \end{cases} \tag{7}$$

By using the linear variable transformation, the power output in the continuous range takes the form,

$$p = p_r * \frac{(v - v_i)}{(v_r - v_i)} = \frac{p_r}{(v_r - v_i)} * (v) - \frac{(v_i)}{(v_r - v_i)} \quad \text{for } v_i \le v \le v_r \tag{8}$$

Then, the Weibull PDF is expressed as,

$$f_p(p) = \frac{k(v_r - v_i)}{c^k * p_r}\left[v_i + \frac{p}{p_r}(v_r - v_i)^{k-1}\right] \exp\left[-\left[\frac{v_i + \frac{p}{p_r}(v_r - v_i)}{c}\right]^k\right] \tag{9}$$

The above probability distribution is only valid for continuous probability. From Eq. 7, it can be observed that there are two discrete probability events occur when there is no wind power and rated power outputs. The probability of event at ($P = 0$) is expressed as,

$$\begin{aligned} P_r(P = 0) &= P_r(V < v_i) + P_r(V \ge v_o) = F_V(v_i) + (1 - F_V(v_o)) \\ &= 1 - e\left(-\left(\frac{v_i}{c}\right)^k\right) + e\left(-\left(\frac{v_o}{c}\right)^k\right) \end{aligned} \tag{10}$$

The probability of event at ($P = P_r$) is expressed as [18],

$$\begin{aligned} P_r(P = P_r) &= P_r(v_r < V < v_o) = F_V(v_o) - F_V(v_r) \\ &= e\left(-\left(\frac{v_r}{c}\right)^k\right) + e\left(-\left(\frac{v_o}{c}\right)^k\right) \end{aligned} \tag{11}$$

From the above Eqs. (9)–(11), it can be observed that it is a mixed probability function with continuous and discrete power outputs.

2.2 *Uncertainty Modeling and Power Output of Solar PV Energy System*

For solving optimal scheduling problem, electrical companies are concerned in hourly availability of solar photovoltaic power data. The hourly data is needed to simulate performance of solar PV energy system. Actual size of battery energy storage system will depend on the desired amount of peak shaving. Figure 1 shows solar PV energy system along with the battery ESS [19].

Amount of power output from solar PV module (P_S) depends on power output from the solar PV cell (P_{PV}), spillage power (P_U), and battery energy storage (P_B). This can be expressed using [19],

$$P_S = P_{PV}(G) + P_B - P_U \tag{12}$$

In this work, it is considered that there is no spillage power from solar PV energy system. Power obtained from solar PV system can be controlled by using power tracking control method, or it is charged into storage batteries. Therefore, the upper level of penetration of solar PV power into the system is expressed using,

$$|P_S| \leq P_S^{\max} \tag{13}$$

where $P_S^{\max}$ (MW) is maximum penetration level of solar PV power generation. P_S can be positive or negative. Positive P_S represents power flow from solar PV unit to power grid. The maximum discharge and charge capacity levels of storage battery are expressed as,

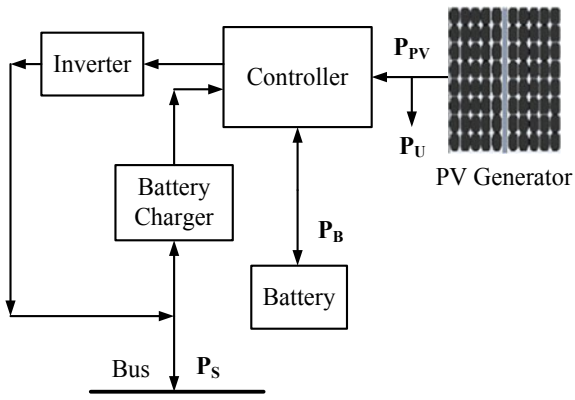

Fig. 1 Solar photovoltaic system along with an integrated battery energy storage

$$P_{\mathrm{B,disch}}^{\max} \leq P_{\mathrm{B}} \leq P_{\mathrm{B,ch}}^{\max} \tag{14}$$

P_{B} is negative for charging and positive for discharging. $P_{\mathrm{B,disch}}^{\max}$ and $P_{\mathrm{B,ch}}^{\max}$ are the aggregated discharging (positive) and charging (negative) power limits of all batteries. The solar PV power generation during the interval 'Δt' can be expressed using [20],

$$P_{\mathrm{S}} = P_{\mathrm{PV}}(G) + \frac{(C_{\mathrm{init}} - C)V_{\mathrm{B}}}{\eta_{\mathrm{B}}\Delta t} - P_{\mathrm{U}} \tag{15}$$

where C_{init} is initial state of charge (SoC), C final SoC of battery, η_{B} is efficiency of battery during charging period (75%), V_{B} is battery voltage, and $P_{\mathrm{PV}}(G)$ is solar irradiation to power output from the solar photovoltaic cell [19], and it can be represented using,

$$P_{\mathrm{PV}}(G) = \begin{cases} P_{\mathrm{S}}^{\max}\left(\frac{G^2}{G_{\mathrm{std}}R_{\mathrm{c}}}\right) & \text{for } 0 < G < R_{\mathrm{c}} \\ P_{\mathrm{S}}^{\max}\left(\frac{G}{G_{\mathrm{std}}}\right) & \text{for } G > R_{\mathrm{c}} \end{cases} \tag{16}$$

where G is solar irradiation forecast, G_{std} is standard solar irradiation, which is 1000 W/m^2. R_{c} is certain solar irradiation; in this work, it is set as 150 W/m^2, and $P_{\mathrm{S}}^{\max}$ is the rated equivalent power output of solar PV module.

From Eq. 16, it can be seen that $P_{\mathrm{PV}}(G)$ mainly depends on solar irradiance. At a particular location, the distribution of hourly irradiance follows a bimodal probability distribution function, and it is modeled using two unimodal distribution functions. These are modeled using the Log-normal, Weibull, and Beta PDFs. Here, Weibull PDF is considered, and it can be represented by [20],

$$\begin{aligned} f_G(G) = {} & \omega\left(\frac{k_1}{c_1}\right)\left(\frac{G}{c_1}\right)^{k_1-1}\exp\left[-\left(\frac{G}{c_1}\right)^{k_1}\right] \\ & + (1-\omega)\left(\frac{k_2}{c_2}\right)\left(\frac{G}{c_2}\right)^{k_2-1}\exp\left[-\left(\frac{G}{c_2}\right)^{k_2}\right] \quad 0 < G < \infty \end{aligned} \tag{17}$$

where ω is weight parameter ($0 < \omega < 1$). k_1, k_2, c_1, and c_2 are shape and scale factors, respectively.

3 Problem Formulation: Optimal Scheduling of Hybrid Power System

Renewable power generation plays a major role in modern power system, and its penetration has been increasing in recent years. During the last decade and in the

coming days, the solar PV and wind energy are set to play a significant growth rate across the globe. However, wind and solar PV powers introduce additional uncertainties in transaction. The intermittency of these renewable sources affects the system operation. Therefore, the system operator takes a decision by compromising the system operating cost and risk level. This uncertainty emphasizes the system operation and may involve additional cost of electricity due to power imbalance. Hence, every participant in the electricity market will be interested in reducing this imbalance cost as much as possible. Aiming at these difficulties, a reasonable trade-off between the system operational cost and risk level is required. Therefore, the objective of this chapter is to include the wind and solar PV powers in the optimum scheduling problem to handle both economical and risk issues simultaneously. The schematic diagram of proposed optimal scheduling approach for hybrid power system is depicted in Fig. 2.

Here, different factors involved in the intermittency of solar PV and wind powers are evaluated. Solar PV and wind power forecasting error variation in under- and over-estimation of power production are performed in a detailed manner. Wind power output varies based on wind speed, and the wind speed profile which closely follows Weibull distribution. Solar PV power output depends on solar irradiance, and then the hourly irradiance follows a bimodal distribution. The two objectives presented in this chapter, i.e., simultaneous optimization of system operating cost and risk level, are optimized by using multi-objective-based NSGA-II algorithm. The proposed optimal operation strategy is implemented on six-unit system with solar PV and wind units situated at various buses in the system. The solution of proposed optimum scheduling approach indicates the amount of reserve requirement to handle the wind and solar

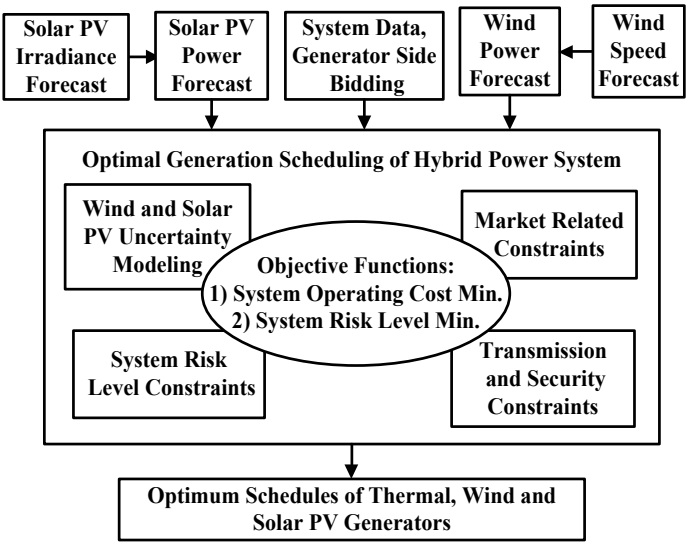

Fig. 2 Schematic diagram of optimal scheduling approach for hybrid power system

PV uncertainties by minimizing system operating cost. Formulation of two objective functions is described next:

3.1 Objective 1: Total Operating Cost (TOC) Minimization

Integration of renewable power into electricity markets can be based on the policy that renewable power is schedulable or not. In this chapter, it is considered that the renewable power is schedulable. Here, the total operating cost (TOC) is considered as an objective function, and it can be expressed using, minimize,

$$\mathrm{TOC} = \sum_{i=1}^{N_G}\left[C_{Gi}(P_{Gi}) + C_{SRi}(P_{SRi}) + C_{Dev,i}\left(\widetilde{P_{Dev,i}}\right)\right] + \sum_{j=1}^{N_W} C_{Wj}\left(P_{Wj}\right) + \sum_{k=1}^{N_S} C_{Sk}(P_{Sk}) \tag{18}$$

The terms in the above Eq. 18 are described next:
First term represents the cost of thermal units, and it can be expressed using,

$$C_{Gi}(P_{Gi}) = a_i + b_i P_{Gi} + c_i P_{Gi}^2 \tag{19}$$

Second term is spinning reserve (SR) cost of thermal energy units, and it can be represented by,

$$C_{SRi}(P_{SRi}) = d_i + e_i P_{SRi} \tag{20}$$

Third term is deviation cost to account the uncertainties of solar PV and wind power costs. Deviation power is the difference between the scheduled and actual wind and solar PV powers. This cost is represented by [21],

$$C_{Dev,i}\left(\widetilde{P_{Dev,i}}\right) = a_i' + b_i'\left(\widetilde{P_{Dev,i}}\right) + c_i'\left(\widetilde{P_{Dev,i}}\right)^2 \tag{21}$$

where $\widetilde{P_{Dev,i}}$ is uncertain deviation power from thermal energy generator. Fourth term is cost of WEGs, and it can be expressed as,

$$C_{Wj}\left(P_{Wj}\right) = x_j P_{Wj} \tag{22}$$

Fifth term is cost of solar PV generators, and it can be represented by,

$$C_{Sk}(P_{Sk}) = y_k P_{sk} \tag{23}$$

3.2 Objective 2: System Risk Level Minimization

In most of the electricity markets, the policy is that all the available renewable power has to absorb into the system. If this increased renewable power penetration exceeds a certain level in the system, then the system faces the security problems. As mentioned earlier, in this chapter, it is considered that renewable power is schedulable/dispatchable similar to thermal generators. Therefore, the system operator determines the lower and upper bounds of renewable power (solar PV and wind powers). In this chapter, fuzzy-based method is used to express the penetration levels of wind and solar PV powers. Figure 3 depicts the linear fuzzy membership function of system security level [8].

A fuzzy membership function with linear characteristics for the renewable power penetration (μ) is used to represent system security level, and it is represented by using [8],

$$\mu = \begin{cases} 1 & \text{if } P_{\mathrm{R}} \le P_{\mathrm{R}}^{\min} \\ \left(\frac{P_{\mathrm{R}}^{\max} - P_{\mathrm{R}}}{P_{\mathrm{R}}^{\max} - P_{\mathrm{R}}^{\min}} \right) & \text{if } P_{\mathrm{R}}^{\min} < P_{\mathrm{R}} < P_{\mathrm{R}}^{\max} \\ 0 & \text{if } P_{\mathrm{R}} \ge P_{\mathrm{R}}^{\max} \end{cases} \tag{24}$$

where $P_{\mathrm{R}}^{\min}$ and $P_{\mathrm{R}}^{\max}$ are minimum and maximum limits of renewable power generations. The above equation represents that if $P_{\mathrm{R}} \le P_{\mathrm{R}}^{\min}$, then it can be said that system is secure, whereas if $P_{\mathrm{R}} \ge P_{\mathrm{R}}^{\max}$, then the system is unsecure. This equation also depicts that larger the value of system security level (μ), more is system security. Then, the objective of system risk level (R) minimization is defined by,

$$R = \frac{1}{\mu} \tag{25}$$

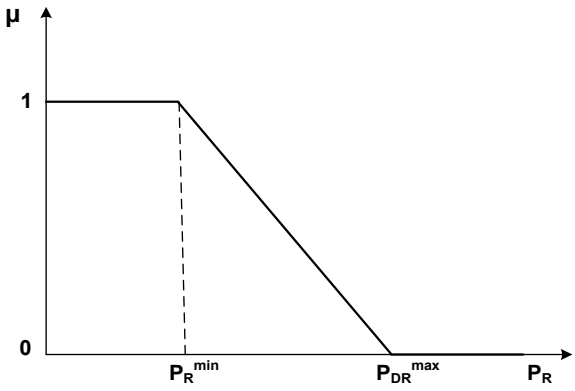

Fig. 3 Linear fuzzy membership function of system security level

The above objective functions are optimized subjected to various constraints, and they are expressed next:

3.3 Equality Constraints

3.3.1 Power Balance Constraints

These are active and reactive power balance equations, and they are represented by,

$$P_{\mathrm{Gi}} - P_{\mathrm{Di}} = V_i \sum_{j=1}^{n} \left[V_j \left(G_{ij} \cos\left(\delta_i - \delta_j\right) + B_{ij} \sin\left(\delta_i - \delta_j\right) \right) \right] \tag{26}$$

$$Q_{\mathrm{Gi}} - Q_{\mathrm{Di}} = V_i \sum_{j=1}^{n} \left[V_j \left(G_{ij} \sin\left(\delta_i - \delta_j\right) - B_{ij} \cos\left(\delta_i - \delta_j\right) \right) \right] \tag{27}$$

where $i = 1,2,3, \ldots, n$. B_{ij} and G_{ij} are transfer susceptance and conductance between bus i and bus j. P_{Di} and Q_{Di} are active and reactive power load demands of ith demand.

3.3.2 Total Spinning Reserve Requirement Constraints

Here, it is considered that amount of SRs that are required ($\mathrm{TSR_{req}}$) is calculated based on the outage of online conventional thermal generator with highest capacity and uncertainties due to wind and solar PV power forecasts. Hence, the total amount of SRs required ($\mathrm{TSR_{req}}$) is calculated using [8],

$$\mathrm{TSR_{req}} = P_{\mathrm{G}}^{\mathrm{largest}} + \sum_{j=1}^{N_{\mathrm{W}}} \left(P_{\mathrm{Wj}} - P_{\mathrm{Wj,av}} \right) + \sum_{k=1}^{N_{\mathrm{S}}} \left(P_{\mathrm{Sk}} - P_{\mathrm{Sk,av}} \right) \tag{28}$$

The total amount of SRs required ($\mathrm{TSR_{req}}$) has been provided by online thermal energy generators. Therefore,

$$\sum_{i=1}^{N_{\mathrm{G}}} P_{\mathrm{SRi}} = \mathrm{TSR_{req}} \tag{29}$$

3.4 Inequality Constraints

3.4.1 Generator Power Constraints

Power output limits of thermal generators is limited by [22],

$$\max\left[P_{\mathrm{Gi}}^{\min}, P_{\mathrm{Gi}}^{0} - RR_{\mathrm{Gi}}^{\mathrm{down}}\right] \leq P_{\mathrm{Gi}} \leq \min\left[P_{\mathrm{Gi}}^{\max}, P_{\mathrm{Gi}}^{0} + RR_{\mathrm{Gi}}^{\mathrm{up}}\right] \tag{30}$$

where $RR_{\mathrm{Gi}}^{\mathrm{down}}$ and $RR_{\mathrm{Gi}}^{\mathrm{up}}$ are ramp down and up bounds of thermal units. The power outputs of wind energy generators (WEGs) and the solar PV generators are limited by,

$$0 \leq P_{\mathrm{Wj}} \leq P_{\mathrm{Wj}}^{\max} \tag{31}$$

$$P_{\mathrm{Sk}} \leq P_{\mathrm{Sk}}^{\max} \tag{32}$$

where $P_{\mathrm{Wj}}^{\max}$ and $P_{\mathrm{Sk}}^{\max}$ are the maximum active power generation of WEGs and solar PV generators. The reactive power limits of these generators are limited by,

$$Q_{\mathrm{Gi}}^{\min} \leq Q_{\mathrm{Gi}} \leq Q_{\mathrm{Gi}}^{\max} \quad i \in (N_{\mathrm{G}} + N_{\mathrm{W}} + N_{\mathrm{S}}) \tag{33}$$

3.4.2 Generator Spinning Reserve Constraints

The spinning reserves of thermal generators are limited by,

$$0 \leq P_{\mathrm{SRi}} \leq \min\left(RR_{\mathrm{Gi}}^{\mathrm{up}}, P_{\mathrm{SRi}}^{\max}\right) \tag{34}$$

where $P_{\mathrm{SRi}}^{\max}$ is the maximum available spinning reserve capacity of ith thermal generator, and it can be calculated as

$$P_{\mathrm{SRi}}^{\max} = \left(P_{\mathrm{Gi}}^{\max} - P_{\mathrm{Gi}}\right) \tag{35}$$

3.4.3 Generator Voltage Constraints

The voltage magnitudes of generators are limited by,

$$V_{\mathrm{Gi}}^{\min} \leq V_{\mathrm{Gi}} \leq V_{\mathrm{Gi}}^{\max} \quad i \in (N_{\mathrm{G}} + N_{\mathrm{W}} + N_{\mathrm{S}}) \tag{36}$$

3.4.4 Reactive Power Capability Limits of Synchronous Generator

Reactive power capability of synchronous generator is restricted by field and armature currents. The armature current results in active power loss, i.e., I^2R loss, and energy associated with this power loss has to be removed to limit temperature of conductor. Hence, MVA rating is given by [18],

$$P^2 + Q^2 \leq V_t I_a \tag{37}$$

Field heating limit is due to the heat resulting from the field circuit; hence, the field current introduces a second limit on operation of generator. It is given by,

$$P^2 + \left(Q + \frac{V_t^2}{X_s}\right)^2 \leq \left(\frac{V_t E_{af}}{X_s}\right)^2 \tag{38}$$

The combined effect of armature and field limits (i.e., Eqs. 37 and 38) will give reactive power capability limits of the synchronous generator.

3.4.5 Reactive Power Capability Limits of DFIG

The reactive power generation of wind-driven generator model, i.e., DFIG can be controlled by rotor current. The capability limit of reactive power injected by DFIG is expressed using [8],

$$Q_s \geq -\frac{v_t^2}{\omega_s(L_s + L_m)} - \frac{L_m v_t}{(L_s + L_m)}\sqrt{I_r^{\max^2} - \left[\frac{P_s(L_s + L_m)}{v_t L_m}\right]^2} \tag{39}$$

$$Q_s \leq -\frac{v_t^2}{\omega_s(L_s + L_m)} + \frac{L_m v_t}{(L_s + L_m)}\sqrt{I_r^{\max^2} - \left[\frac{P_s(L_s + L_m)}{v_t L_m}\right]^2} \tag{40}$$

3.4.6 Reactive Power Capability Limits of Solar PV Generator

Solar PV inverter injects a maximum current I_i, and it imposes the limit on active and reactive powers, which can be injected by solar PV unit through a solar PV inverter. This can be expressed as,

$$P^2 + Q^2 = \left(V_g I_i\right)^2 \tag{41}$$

The maximum PV inverter voltage V_i imposes the restriction on inverter voltage. This voltage imposes an additional capacity limit of active and reactive powers, and it is expressed using [23],

$$P^2 + \left(Q + \frac{V_g^2}{X}\right)^2 = \left(\frac{V_g V_i}{X}\right)^2 \tag{42}$$

3.4.7 Security Constraints

The system security level (μ) is limited by [24],

$$0 \leq \mu \leq 1 \tag{43}$$

Load bus voltage magnitudes, transformer taps, and line flows are limited by [25, 26],

$$V_{\mathrm{Di}}^{\min} \leq V_{\mathrm{Di}} \leq V_{\mathrm{Di}}^{\max} \tag{44}$$

$$T_i^{\min} \leq T_i \leq T_i^{\max} \tag{45}$$

$$\left|S_{ij}\right| \leq S_{ij}^{\max} \tag{46}$$

where V_{Di} is the ith load bus voltage magnitude, T_i is the transformer tap settings, and S_{ij} is line flow in a transmission line between buses i and j.

4 Non-dominated Sorting Genetic Algorithm-II (NSGA-II) Algorithm

NSGA-II algorithm is a widely used and reliable multi-objective optimization (MOO) technique with several real-world applications. Fast non-dominated sorting approach, fast crowded distance estimation approach, and a simple crowded comparison operator are three special characteristics of NSGA-II algorithm. It generates offspring using a specific type of mutation and crossover and then selects the population of next generation using the non-dominated sorting and crowding distance comparison. The NSGA-II technique performs better compared to other MOO algorithms, such as Pareto Archived Evolution Strategy (PAES) and Strength Pareto Evolutionary Algorithm (SPEA) algorithms in terms of determining a diverse set of solutions [27]. The NSGA-II algorithm is composed of two principal parts: preservation of the solution's diversity part and a fast non-dominated sorting solution part. The detailed flow chart of NSGA-II algorithm is depicted in Fig. 4.

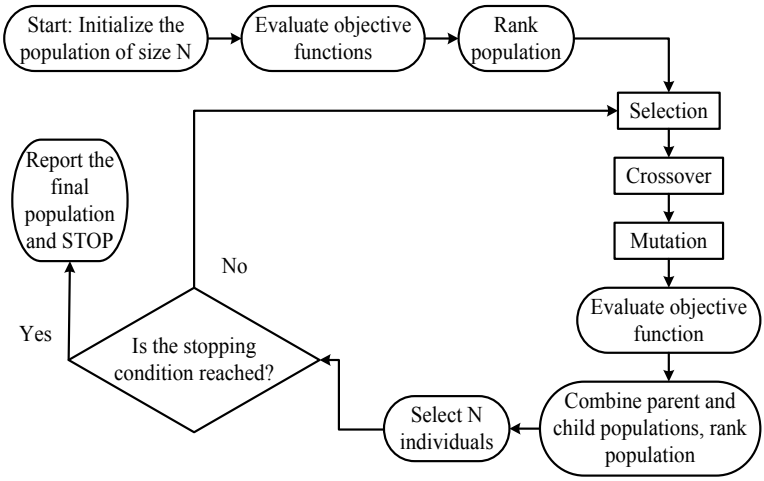

Fig. 4 Flow chart of NSGA-II technique

5 Simulation Results and Discussion

IEEE 30 bus test system [28] is used to ascertain the utility of proposed optimal generation scheduling methodology. This system has six generating units; among them, four are selected to be thermal energy units which are positioned at buses 1, 2, 5, and 8, and two are selected to be the RERs. Among these two RERs, one is considered as the wind farm situated at bus 11, and another one is a solar PV plant with battery ESS located at bus number 13. However, in practice, each wind and solar PV unit can be represented by an aggregated model of wind farm with several wind-driven DFIGs and solar PV plant consisting of several solar PV generators. Here, it is assumed that all the wind turbines and solar PV generating units are considered to be identical. In this test system, the total system active and reactive load demands are 283.4 MW and 126.2 MVAr. Here, it is assumed that the renewable power is assumed to be schedulable and the demand is inelastic to price. It is considered that the SO purchases the power from wind and solar PV units. In this test system, the thermal generator on bus number 2 is selected as largest thermal generator, even though capacity of thermal generator on bus number 1 is highest. This is due to the fact that in case the generator on bus number 1 is being out, then the total system load cannot be met by all other generating units in the electrical power system.

For the case studies, the maximum penetration limit of wind plant is considered to be 45 MW, and forecasted wind velocity is assumed to be 10 m/s. For a particular forecast of wind speed (v), the amount of power output from WEG is determined by Eq. 7. Hence, the maximum power output from wind farm is 35 MW, i.e., this value can go anywhere from 0 to 35 MW. In this chapter, cut-in (v_i), rated (v_r), and cut-out (v_o) wind speeds are assumed to be 3, 12, and 30 m/s.

In this chapter, it is considered that the maximum penetration limit of solar PV generator is 70 MW. Here, it is considered that the forecasted solar insolation is 500 W/m^2. For a particular forecast of solar irradiation, the power output from the solar PV module is determined by using Eq. 16. Hence, the solar photovoltaic power output ($P_{PV}(G)$) is 35 MW. Bimodal distribution with Weibull PDF is utilized to depict uncertain nature of solar power output. Lower and upper bounds of SoC of battery energy storage are selected as 10 KVh and 20 KVh, respectively. The state of charge (SoC) of battery at a particular operating time is considered to be 10 KAh. Considered efficiencies of inverter and battery are 95% and 75%, respectively.

The levels of uncertainties of solar and wind power forecasts depend on historical data and their corresponding probability analysis. For the case studies considered in this chapter, ±three uncertainties in solar and wind plants are considered based on historical solar irradiation and wind speed information obtained from the National Renewable Energy Laboratory (NREL) Web site [29]. The optimization programs related to all the case studies are coded in MATLAB, and they are implemented on a personal computer—Core2 Quad with 8 GB of RAM. In this chapter, two studies are formulated, and they are:

- Study 1: Optimal scheduling without considering uncertainties in RERs.
- Study 2: Optimal scheduling considering uncertainties in RERs.

5.1 Study 1: Optimal Scheduling Without Considering Uncertainties in RERs

As mentioned earlier, in this study 1, the objective of TOC minimization is considered as a single objective optimization without considering forecast uncertainties in wind and solar power generations. Normally, the cost of renewable power generation is less than the thermal generation. Here, they tend to schedule their maximum power outputs. But, due to the security concerns, the optimal scheduling problem can curtail their power outputs. Table 1 depicts scheduled optimum power outputs, amount of SRs and objective function value for study 1. As this study doesn't consider any forecast uncertainties in wind and solar power generations, the total amount of SRs required (TSR_{req}) is equal to the largest online thermal power generation ($P_G^{largest}$). In this study, total operating cost (TOC) optimization minimization (i.e., Eq. 18) is optimized without considering the deviation/adjustment cost term. This TOC minimization function consists of costs due to conventional thermal units, WEGs, solar PV units, and the SR cost of thermal energy generators.

The scheduled optimal power outputs of wind plant and solar PV unit placed at bus 11 and bus 13, respectively, are 34.4604 and 34.7650 MW. From obtained scheduled power outputs, it can be observed that they are very close to their maximum power limits. Here, the total amount of spinning reserves (SRs) needed (TSR_{req}) is equal to 51.1528 MW (scheduled power of generator located at bus number 2, i.e., largest

Table 1 Scheduled optimal power generations, SRs, and objective function values for TOC minimization objective without considering uncertainties

Scheduled optimal power outputs		Scheduled spinning reserves	
P_{G1}(MW)	119.2120	P_{SR1}(MW)	10.9207
P_{G2}(MW)	**51.1528**	P_{SR2}(MW)	19.5628
P_{G5}(MW)	28.0589	P_{SR5}(MW)	4.6212
P_{G8}(MW)	26.0531	P_{SR8}(MW)	18.0481
P_{W11}(MW)	34.4604		
P_{S13}(MW)	34.7650		
Cost of thermal, solar PV, and wind power outputs ($/h)		969.0863	
Spinning reserve cost of thermal generators ($/h)		246.2597	
Total operating cost (TOC) ($/h)		1215.346	
Total amount of SRs required (MW)		51.1528	

The bold letters indicate the objective function values

online thermal power output). Here, the obtained optimum TOC is 1215.346 $/h, which is sum of thermal, solar PV, and wind power cost of 969.0863 $/h and SRs cost of 246.2597 $/h.

5.2 Study 2: Optimal Scheduling Considering Uncertainties in RERs

In study 2, three different cases are simulated, and they are:

- Case 1: Single objective optimization considering total operating cost (TOC) minimization.
- Case 2: Single objective optimization considering system risk level minimization.
- Case 3: Multi-objective optimization considering total operating cost (TOC) and system risk level minimization as objective functions.

Here, the cases 1 and 2 are solved as single objective optimization problems, and they are solved by using the genetic algorithm (GA), whereas the case 3 is a MOO problem, and it is solved by using the NSGA-II approach. Table 2 depicts objective function values, scheduled optimal power outputs, and SRs values for study 2—cases 1, 2, and 3. In this study 2, ±three uncertainties in wind and solar PV power forecasts are considered.

Table 2 Optimal scheduled power generations, SRs, and objective function values for study 2: cases 1, 2, and 3

Scheduled optimum power outputs and SRs	Case 1: TOC minimization	Case 2: risk level minimization	Case 3: both TOC and risk level minimizations
P_{G1}(MW)	106.7150	165.3720	151.2385
P_{G2}(MW)	**50.6349**	**35.6309**	**38.0622**
P_{G5}(MW)	44.0567	25.1153	29.1080
P_{G8}(MW)	26.4128	19.1272	18.8227
P_{W11}(MW)	33.5055	25.0641	28.6601
P_{S13}(MW)	30.2380	23.2105	27.0085
P_{SR1}(MW)	23.1263	21.3155	20.5210
P_{SR2}(MW)	18.8901	14.0617	16.1528
P_{SR5}(MW)	16.5220	13.3092	15.7426
P_{SR8}(MW)	10.5136	8.5068	10.8357
Cost of thermal, wind, and solar PV power generations ($/h)	961.6354	1074.8631	1014.8151
Spinning reserve (SR) cost of thermal generators ($/h)	301.0541	285.2910	295.2453
Mean deviation cost ($/h)	241.2410	236.2011	240.2259
Total operating cost ($/h)	**1503.9305**	**1596.3552**	**1550.2863**
		0.3621	0.2388
System risk level (R)	**9.5877**	**2.7617**	**4.1876**
Total amount of SRs required (MW)	69.0520	57.1932	63.2251

The bold letters indicate the objective function values

5.2.1 Study 2—Case 1

Here, the total operating cost (TOC) minimization is optimized as a single objective optimization problem, and the TOC equation, i.e., Eq. 18, consists of all the terms in that equation. As mentioned earlier, ±three uncertainties in solar PV and wind power forecasts are considered in real time. Table 2 presents the optimum objective function values, scheduled power outputs, and SRs for study 2—case 1. After solving proposed optimal scheduling problem, obtained optimum power outputs from wind and solar units situated at bus 11 and bus 13 are 33.5055 and 30.2380 MW. In this case, total amount of SRs required (TSR_{req}) is equal to the largest online thermal power output and amount of spinning reserves needed due to uncertainties involved

in wind and solar PV power forecasts, and its value is equal to 69.0520 MW. Here, the obtained optimum TOC is 1503.9305 $/h, which includes the thermal, solar, and wind power costs of 961.6354 $/h, spinning reserve cost of 301.0541 $/h, and mean deviation cost of 241.2410$/h.

Here, the system security level (μ) is calculated by using Eq. 24, and its obtained value is 0.1043, and system risk level (R) is determined by using Eq. 25, and its obtained value is 9.5877. From simulation results obtained in this case, it can be concluded that the obtained TOC is optimum, but the system risk level (R) has been deviated from the optimum value.

5.2.2 Study 2—Case 2

In this case, the system risk level (R) minimization is selected as an independent objective to be optimized considering ±three forecast uncertainties in solar and wind power outputs. The obtained scheduled optimal power outputs of thermal generators and RERs, spinning reserves, and optimum objective function values are depicted in Table 2. The obtained scheduled optimal solar and wind power outputs for this case are 13.3092 MW and 8.5068 MW, respectively. Here, the obtained optimum system risk level is 2.7617, but the TOC has been deviated from optimum, and its value is 1596.3552 $/h, which is higher compared to the TOC obtained in study 2—case 1.

From the results obtained from cases 1 and 2, it can be concluded that when only TOC minimization objective is optimized independently, then the system risk level has been deviated from optimum value, whereas when only system risk level is optimized independently, then TOC minimization objective has been deviated from optimum value. Therefore, there is a pressing need for obtaining best-compromised solution by using multi-objective optimization algorithm.

5.2.3 Study 2—Case 3

In this case, both the objectives (TOC and system risk level minimizations) are optimized simultaneously by using multi-objective-based NSGA-II algorithm. The obtained optimum objective function values, scheduled optimum power outputs of thermal generators and RERs, and SR values for this study 2—case 3 are also presented in Table 2. Figure 5 shows the scheduled power generations of thermal energy generators, solar PV and wind generating units, and number of scheduled SRs for study 2—cases 1, 2, and 3.

The multi-objective-based NSGA-II technique has been used to find Pareto optimal front of considered two conflicting objective functions. Figure 6 depicts Pareto optimal front of TOC and system risk level minimizations for study 2—case 3. In this work, fuzzy min-max methodology [30] is utilized to determine best-compromised solution. The best-compromised solution has TOC of 1550.2863 $/h and the system risk level (R) of 4.1876.

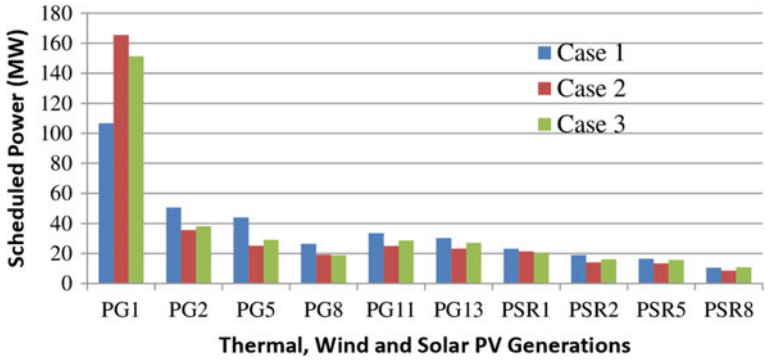

Fig. 5 Scheduled optimum power outputs and spinning reserves for study 2—cases 1, 2, and 3

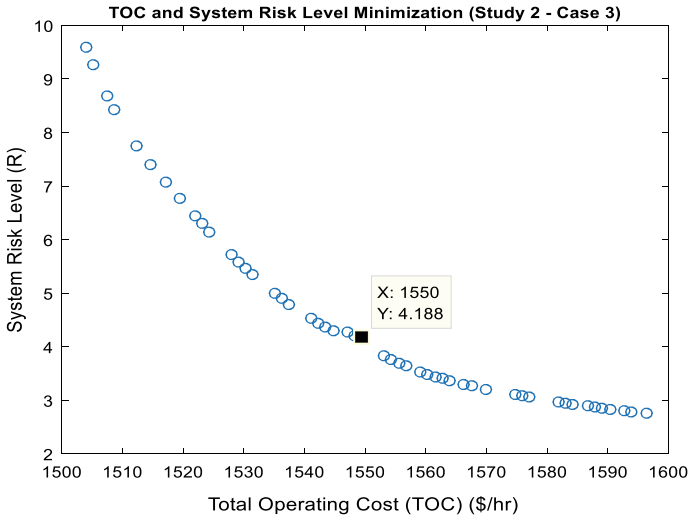

Fig. 6 Pareto optimal front of total operating cost (TOC) and the system risk level minimizations for study 2—case 3

From the above simulation results, it is clear that by incorporating solar PV and wind power forecasts, there is an increase in total operating cost and system risk level. By introducing RERs into the system, there is an increasing the reserve requirement.

6 Conclusion

A new optimal generation scheduling approach is proposed in this chapter by considering the impact of solar PV and wind power forecast uncertainties. The impact

of wind and solar PV power volatility on the optimum scheduling problem in the hybrid electrical power system is considered. The proposed approach includes spinning reserve (SR) offers from the thermal energy generators. Two conflicting objectives were proposed in this chapter, i.e., total operating cost (TOC) minimization and system risk level minimization. Multi-objective-based NSGA-II algorithm has been applied on these objectives to obtain best-compromised solution for proposed optimal scheduling problem. The uncertainties in wind power are expressed by Weibull probability distribution function and solar PV power by bimodal distribution function. From the simulation results, it can be observed that total operating cost and system risk level has increased with an increase in uncertainty levels. And also, the increase in uncertainty level leads to rise in total reserves requirement. The effectiveness of proposed optimal scheduling methodology has been tested on IEEE 30 bus system.

References

1. Yi W, Zhang Y, Zhao Z, Huang Y (2018) Multiobjective robust scheduling for smart distribution grids: considering renewable energy and demand response uncertainty. IEEE Access 6:45715–45724. https://doi.org/10.1109/access.2018.2865598
2. Wu H, Shahidehpour M, Alabdulwahab A, Abusorrah A (2015) Demand response exchange in the stochastic day-ahead scheduling with variable renewable generation. IEEE Trans Sustain Energy 6:516–525. https://doi.org/10.1109/tste.2015.2390639
3. Wu Y, Lau V, Tsang D et al (2014) Optimal energy scheduling for residential smart grid with centralized renewable energy source. IEEE Syst J 8:562–576. https://doi.org/10.1109/jsyst.2013.2261001
4. Yi J, Lyons P, Davison P et al (2016) Robust scheduling scheme for energy storage to facilitate high penetration of renewables. IEEE Trans Sustain Energy 7:797–807. https://doi.org/10.1109/tste.2015.2498622
5. Zhang Y, Gatsis N, Giannakis G (2013) Robust energy management for microgrids with high-penetration renewables. IEEE Trans Sustain Energy 4:944–953. https://doi.org/10.1109/tste.2013.2255135
6. Liu Y, Li Y, Gooi H et al (2019) Distributed robust energy management of a multimicrogrid system in the real-time energy market. IEEE Trans Sustain Energy 10:396–406. https://doi.org/10.1109/tste.2017.2779827
7. Li T, Dong M (2018) Real-time residential-side joint energy storage management and load scheduling with renewable integration. IEEE Trans Smart Grid 9:283–298. https://doi.org/10.1109/tsg.2016.2550500
8. Reddy S, Bijwe P, Abhyankar A (2015) Joint energy and spinning reserve market clearing incorporating wind power and load forecast uncertainties. IEEE Syst J 9:152–164. https://doi.org/10.1109/jsyst.2013.2272236
9. Singh S, Singh M, Kaushik S (2016) Optimal power scheduling of renewable energy systems in microgrids using distributed energy storage system. IET Renew Power Gener 10:1328–1339. https://doi.org/10.1049/iet-rpg.2015.0552
10. Yang Y, Guo S, Liu Q, Li R (2019) Day-ahead scheduling for a new wind-csp hybrid system. Energy Procedia 158:6254–6259. https://doi.org/10.1016/j.egypro.2019.01.461
11. Salkuti S (2019) Day-ahead thermal and renewable power generation scheduling considering uncertainty. Renewable Energy 131:956–965. https://doi.org/10.1016/j.renene.2018.07.106

12. Kia M, Nazar M, Sepasian M et al (2017) Optimal day ahead scheduling of combined heat and power units with electrical and thermal storage considering security constraint of power system. Energy 120:241–252. https://doi.org/10.1016/j.energy.2016.11.079
13. Yuan T, Ma T, Sun Y et al (2017) Game-based generation scheduling optimization for power plants considering long-distance consumption of wind-solar-thermal hybrid systems. Energies 10:1260. https://doi.org/10.3390/en10091260
14. Krishnan A, Sampath L, Eddy F et al (2018) Multi-energy scheduling using a hybrid systems approach. IFAC-PapersOnLine 51:229–234. https://doi.org/10.1016/j.ifacol.2018.08.039
15. Gu Y, Jiang H, Zhang Y, Gao DW (2014) Statistical scheduling of economic dispatch and energy reserves of hybrid power systems with high renewable energy penetration. In: 2014 48th Asilomar Conference on Signals, Systems and Computers, Pacific Grove, CA, 2014, p 530–534
16. Jurasz J, Kies A (2018) Day-ahead probabilistic model for scheduling the operation of a wind pumped-storage hybrid power station: overcoming forecasting errors to ensure reliability of supply to the grid. Sustainability 10:1989. https://doi.org/10.3390/su10061989
17. Reddy S, Bijwe P, Abhyankar A (2015) Optimum day-ahead clearing of energy and reserve markets with wind power generation using anticipated real-time adjustment costs. Int J Electr Power Energy Syst 71:242–253. https://doi.org/10.1016/j.ijepes.2015.03.002
18. Hetzer J, Yu D, Bhattarai K (2008) An economic dispatch model incorporating wind power. IEEE Trans Energy Convers 23:603–611. https://doi.org/10.1109/tec.2007.914171
19. Reddy S (2017) Optimal scheduling of thermal-wind-solar power system with storage. Renew Energy 101:1357–1368. https://doi.org/10.1016/j.renene.2016.10.022
20. Reddy S (2016) Optimal power flow with renewable energy resources including storage. Electr Eng 99:685–695. https://doi.org/10.1007/s00202-016-0402-5
21. Surender Reddy S, Bijwe P, Abhyankar A (2015) Optimal posturing in day-ahead market clearing for uncertainties considering anticipated real-time adjustment costs. IEEE Syst J 9:177–190. https://doi.org/10.1109/jsyst.2013.2265664
22. Surender Reddy S, Bijwe P, Abhyankar A (2013) Multi-objective market clearing of electrical energy, spinning reserves and emission for wind-thermal power system. Int J Electr Power Energy Syst 53:782–794. https://doi.org/10.1016/j.ijepes.2013.05.050
23. Albarracín R, Alonso M (2013) Photovoltaic reactive power limits. In: 12th International Conference on Environment and Electrical Engineering, Wroclaw, 5–8 May 2013, p 13-18
24. Wang L, Singh C (2008) Balancing risk and cost in fuzzy economic dispatch including wind power penetration based on particle swarm optimization. Electr Power Syst Res 78:1361–1368. https://doi.org/10.1016/j.epsr.2007.12.005
25. Augustine N, Suresh S, Moghe P, Sheikh K (2012) Economic dispatch for a microgrid considering renewable energy cost functions. In: IEEE PES Innovative Smart Grid Technologies (ISGT), Washington, DC, p 1–7
26. Reddy K, Meikandasivam S (2018) Smart Distribution Network with Integration of Stochastic Renewable Energy Sources and Plug-in Electric Vehicles: Challenges and Issues. J Green Eng 8:431–474. https://doi.org/10.13052/jge1904-4720.841
27. Yusoff Y, Ngadiman M, Zain A (2011) Overview of NSGA-II for optimizing machining process parameters. Procedia Eng 15:3978–3983. https://doi.org/10.1016/j.proeng.2011.08.745
28. Available. [Online]: https://labs.ece.uw.edu/pstca/pf30/pg_tca30bus.htm
29. Wind and solar data sets (2014) NREL solar radiation research laboratory, Washington, DC, USA, [Online]. Available: http://www.nrel.gov/midc/srrl_bms/
30. Kothari D, Dhillon J (2012) Power system optimization. PHI Learning Private Ltd., New Delhi

Performance of Control Algorithms in Wind-Based Distributed Generation System with Power Quality Features: A Review

Ashutosh K. Giri, Sabha Raj Arya, Rakesh Maurya and Papia Ray

Abstract This work introduces the performance review regarding control algorithms implemented in wind-based distributed generation system for improving the system's power quality. The system is comprised of three-phase self-excited induction generator, nonlinear load and voltage source converter. The nonlinear load is directly fed by the generator in off-grid operation. Due to this, the operation of the generator suffers as a whole means the voltage and frequency variation takes place according to variation in the load. Moreover, the power quality problems such as harmonics in the supply current, poor power factor, load unbalance and neutral current at the supply side are prominent. Therefore, the voltage source converter is used along with load to mitigate the power quality problems as well as voltage and frequency fluctuations. For frequency control, the input terminal of the converter uses a battery storage system. The converter operation is dependent on the dynamical performance of the control algorithm used for fundamental current extraction followed by reference current generation. Hence, authors have presented performance review of some control algorithms such as Lorentzian adaptive filter (LAF), momentum LMS, VCO-less PLL, adaptive vectorial filter (AVF) and nonlinear adaptive Volterra filter (NAVF) for reference current generation followed by gate pulses for converter for power quality features of the system. The control algorithms are selected based on their faster dynamics, less steady-state error and stable operation. The simulation and experimental performance of each have been carried out, and comparative analysis is provided.

A. K. Giri · S. R. Arya (✉) · R. Maurya
Department of Electrical Engineering, Sardar Vallabhbhai National Institute of Technology, Surat 395007, India
e-mail: sabharaj79@gmail.com

A. K. Giri
e-mail: ashu_ee2002@rediffmail.com

R. Maurya
e-mail: rmaurya@eed.svnit.ac.in

P. Ray
Department of Electrical Engineering,
Veer Surendra Sai University of Technology, Burla, Odisha, India
e-mail: papia_ray@yahoo.co.in

P. Ray and M. Biswal (eds.), *Microgrid: Operation, Control, Monitoring and Protection*,
Lecture Notes in Electrical Engineering 625,
https://doi.org/10.1007/978-981-15-1781-5_3

Keywords Power quality · Wind energy · LAF · AVF · Power factor · Voltage regulation

List of symbols

AVF	Adaptive vectorial filter
DPG	Distributed power generation
FRRLS	Fast robust recursive least-squares
IRPT	Instantaneous reactive power theory
LMS	Least mean square
NLMS	Normalized least mean square
PLL	Phase-locked loop
SRFT	Synchronous reference frame theory
SAPF	Shunt active power filter
SEIG	Self-excited induction generator
SD	Steepest descent
VSC	Voltage source converter

1 Introduction

The unconventional energy resources such as solar, wind, biomass, ocean/tidal wave and hydro are seen as a promising option to reduce the carbon dioxide emissions [1]. The limited natural resources of fossil fuels force us to shift our focus to utilize the natural resources for electricity generation. The oil and coal availability as per some estimates remains only for 40 years and 130 years, respectively [2]. Therefore, the use of nonconventional energy sources has gained immense importance in new millennium. The wind energy and solar energy especially in offshore coastal region are abundant in nature [3]. Solar and wind energy as sustainable sources experiences a huge growth worldwide [4]. Nevertheless, for powering the load centres in remote locations like hill stations, remote places and islands, the power supply from grid is quite expensive because it requires long transmission lines [5]. Therefore, distributed power generation (DPG) is emerging nowadays at these places. Transmission lines are not required in this kind of power generation [6]. Generally, single-phase loads are more common among the middle-class family living at remote places [7]. The wind-powered single-phase induction generator based on self-excitation is placed nearer to the load locations for feeding electricity [8]. Induction generators require very less maintenance, robust in construction and are cost-effective as compared to traditional generators [9]. Therefore, it is selected for DPGS. The presence of harmonic current at supply side along with reactive power control is the basic power quality under nonlinear load and needed to resolve [10]. Power quality problem was

addressed in a better manner with a come up in power electronics converter. The VSC is used across the loading condition for mitigating the harmonics source current and reactive power compensation. The more attention is given in this work to control the voltage source converter. The control strategy of the mentioned device determines the overall performance of the induction generator. The control algorithms are the key to generate the reference current for voltage source converter that is used as a multi-function power electronics device for the control of distributed power generation system. Therefore, authors have carried out an exhaustive review related to the applicability and feasibility of various control methods in the system under study. It is provided as below. The usefulness of shunt active filter is dependent on the patterns of gate pulse generation and the control technique used for the estimation of reference currents and generation of switching pulses. Control algorithms based on time domain are explained in the literature for reference current extraction. There are two popularly known algorithms named instantaneous reactive power theory (IRPT) [10] which is based on a conversion from three phases to two phases and synchronous reference frame theory (SRFT) [10] that utilizes stationary frame to rotating frame conversion. The selective harmonics elimination scheme is provided in [11]. Several other control algorithms have been mentioned in the literature like model-based controller [12] for H-bridge multilevel converter, linear feedback control [13], symmetrical component theory [14], backpropagation control algorithm [15] which is based on the feedforward training of the input signal, feedback feedforward proportional–integral (PI)-type learning [16], frequency adaptive control [17], one cycle control for active harmonic filter [18], non-iterative optimized algorithm [19] and composite observer-based [20] algorithm, which is based on continuous composite observer of districted load currents. The aforesaid control algorithms carrying a lot of computational burden, many tuning constants etc. and hence slow responsive under load dynamics. These algorithms are useful in specific application. When fast dynamical changes occur in voltage/current amplitude or frequency, response of these algorithms becomes slow or sometimes fails due to non-adaptive nature of amplitude. Yazdani et al. [21] presented a control approach based on a real-time decomposition of sequence components in synchronized and standalone the distributed power generation system. Subsequent versions were presented in [22, 23] more accurately for estimating the amplitude of the fundamental, frequency and in phase as well as quadrature components of load current. In these techniques, the phase-locked loop is not required for parameter estimation. Adaptive neural filter is implemented for harmonic cancellation of current in single-phase system [24]. Authors in [25] have presented soft computing-based shunt active power filter (SAPF); apart from this, Widrow-Hoff weight updating algorithm is used for current harmonics cancellation. The application of some of these control algorithms is reported in distributed power system. In the references [26, 27], comparative analysis for power quality issues in four-wire system is presented. Chilipi et al. [28] proposed different kinds of voltage and frequency control in which voltage is controlled by reactive power compensation through VSC and frequency control is done by operating induction motor connected with water pumps based on DTC drive

control. Kasal and Singh [29] have suggested various configuration schemes of electronic load controllers for frequency and voltage control of SEIG. For this system, extracting a time-varying signal (non-stationary) on real-time basis is an important task. This has improved the power quality. In [30, 31], generator design with FEM is presented. Jabri et al. [32] have presented the selection of capacitance for the excitation of generator. Murthy et al. [33] have investigated the excitation capacitance requirement under different conditions of the self-excited induction generator. In the available texts, ample number of techniques based on frequency domain, transformation and time domain is proposed [34–58]. Rajgopal et al. [35] have implemented instantaneous reactive power theory for regulating the voltage source converter with the load in distributed power generation system. References [36–38] have presented power quality issues and their solution in standalone distributed power generation system. The classical and adaptive type control strategies are adopted to solve the power quality issues. Yazdani et al. [39] have presented notch filter approach for the extraction of harmonic/reactive current and decomposition of harmonics. The application of PQ theory is limited only to non-distorted supply waveform. Mojiri [40] has suggested some modification in PQ theory by adding a three-phase sinusoidal waveform generator. Yin et al. [41] have done technical assessment by considering the robustness for the operation non-ideal supply, control signal conditioning, uneven load currents, etc. Blaabjerg et al. [42] have presented the review of an adaptive anti-aliasing filter. Mishra et al. [43] have proposed control strategies for compensation of load with the help of symmetrical component theory under various levels of supply voltages, and electronic load controller is presented for voltage and frequency control of SEIG. Ghartemani et al. [44] have addressed the series of control based on PLL for the performance of VSC. It is extensively implemented in three-phase system. VSC has been operated in ZVR mode and PFC mode. Arya and Singh [45] have presented a leaky LMS control algorithms for the implementation of VSC in three-phase distribution system. Due to the presence of leakage term in the weight update equation, convergence becomes faster and control is more stable. Sinnaka [46] has proposed a method based on PLL structure for estimating frequency and amplitude of variable frequency input. Guo et al. [47] presented a PLL-based multiple-complex coefficient filter. Its special characteristic is that it can extract positive- and negative-sequence elements from the unfiltered grid voltage precisely and speedily. Arabloue et al. [48] have presented gradient-descent total least-squares (GD-TLS) algorithm for extracting the fundamental component of load current. Shuai et al. [49] have proposed distinct control method of injection-type hybrid power filter. Bhattacharya et al. [50] have presented different schemes of shunt compensation. It can be utilized in reactive power control and harmonics removal in three-phase or single-phase system. Suresh et al. [51] have addressed fuzzy logic-based controller for filters. Chang et al. [52] have presented a survey for the prime solutions in ILC (iterative learning control). There are the most accepted emerging four design techniques which have been discussed. The trouble in robustness, learning fleeting manners, stability and performance was also discussed. Douglas et al. [53] have proposed a new control topology that is learning-based method for tracking control with high performance.

It is helpful in tracking the parameters in high-speed variation. This control is implemented for three-phase distribution system. Vazquez et al. [54] have presented the adaptive vectorial filter (AVF). The AVF approach is used for active power filtering such as mitigation of supply current harmonics of single-phase induction generator that is supplying to linear/nonlinear load powered by wind turbine. In [55], control strategy for BESS is reported for wind power application.

In [56], authors have reported the method for upgrading the LMS filter parameter partially. Authors in [57] have given a customized version of the two-step least mean square (LMS)-type adaptive algorithm. Authors in [58] have presented a novel normalized least mean square (NLMS) algorithm with robust formulation. In this algorithm, filter parameter is dynamically updated which is fixed in the conventional NLMS algorithms. It is a computationally efficient and robust updating scheme which is derived by exploiting the gradient descent algorithms. Das et al. [59, 60] have proposed different methods from conventional block least mean square (LMS) algorithms those use both cross-correlation and convolution machines. References [61, 62] presented a fast robust recursive least-squares (FRRLS) algorithm based on a newly introduced structure for manipulating robust adaptive filters. The paper [63] had given control algorithm which is derived by optimizing a cost function related to a time-dependent constraint. Adaptive linear sinusoidal tracer control [64] is presented in three-phase distribution system. In this letter [65], a novel least mean square (LMS) algorithm based on the squared Euclidean norm minimization is proposed for filtering in the adaptive noise cancellation (ANC) problem. In reference [66], a new adaptive algorithm, named LLMS, is proposed, where two least mean square (LMS) sections are connected in series. The authors [67] have discussed the technique of steepest descent (SD) and least mean square (LMS) algorithms which is useful to linear detection. There are other control algorithms reported in the references [68–75] for adaptive filtering for nonlinear system. The variable step Griffith's LMS algorithm [74] is used to run VSC in the proposed system for harmonics elimination from the supply mains. Moreover, it is also performing the reactive power control with zero voltage regulation distributed generation based in single-phase induction generator [75]. It is also used to restrain the outcome of observation noise experienced from sensors. With the gradual development of power electronic converters in the last two decades, this problem has been reduced up to certain extent. These converters are basically used for the solution of power quality-related problems [76]. Moreover, converter operation is reliant on the methods for its control. Several adaptive control algorithms have been invented for online applications like system identifications, noise deletion and channel evaluation [77]. Among these, the accepted algorithms related to least mean square (LMS) algorithm and its various versions are developed by optimizing $l2$ norm of error signals; therefore, they yield fast convergence [78]. Though, their performance deteriorates enormously in impulsive conditions which may occur naturally when atmospheric conditions like wind changes suddenly. In [79], fast convergence rate of the APA and the effectiveness of the APSA against impulsive conditions are obtained using robust adaptive filters. The sign algorithm (SA) [80, 81] that is extracted from absolute error value of the cost function gives high performance against the impulsive noise. In [82–84], a

group of shrinkage adaptive filters, known as shrinkage LMS (SHLMS), a shrinkage NLMS (SHNLMS) algorithm and shrinkage AP (SHAP) algorithm, has been proposed. In [85], the polynomial-type filter is proposed for noise cancellation. In [86], the proposed cost function can answer to the changes instantaneously in the statistical profiles. Broadly, the suggested algorithm achieves smaller time error and takes more gradual steps. In case the error becomes larger due to a difference in statistical profile, the algorithm can make a response without delay by taking slightly steeper steps. In [87–89], power quality application of few algorithms is addressed. Sharma et al. [89] have tested the power balance theory in three-phase system successfully. This control is classical one and more suitable when mechanical input is impulse free. In [90], practical method having only two control loops for voltage regulation of induction generator is presented. It is simple, novel and each with only one PI regulator. In [91–94], a variable mixing factor-based CSS-APSA control algorithm to achieve an effective tracking capability is proposed. The accepted algorithms related to least mean square (LMS) algorithm and its various versions are developed by optimizing L_2 norm of generated error signals; therefore, they could have faster convergence [95]. In [96], a nonlinear adaptive Volterra filter is presented for fundamental extraction of only active component in power factor correction mode. The limitation of this filter is that it only detects up to 7th harmonic component in the load current. Sharma et al. [97] have proposed the wind diesel hybrid combination of distributed generation by connecting permanent magnet-based generator. This type of small generator requires special design and not economic after certain ratings. In [98, 99], the application of few algorithms is implemented in the area of power quality. In [98], affine-type projection algorithms have been used for improving the power quality of wind diesel hybrid system. This algorithm is very tedious and requires a lot of computational memory. Hardware implementation of this kind of algorithm may not be an easy task in more complex system. Chittora et al. [99] have proposed the modified Gauss Newton recursive algorithms in solving the power quality problems. This control has been implemented with grid-connected load where the number of variables in Jacobian matrix is less due to constant bus voltage angle. If this control would have to implement in isolated induction generator with varying frequency and voltage, the number of variables in Jacobian matrix would be more and system would be difficult to implement. In references [100, 101], the different adaptive type control logics have been addressed. In [100], Roy et al. have discussed simple logic to get easily implemented in power quality area. Its mathematical analyses like stability and convergence criteria, etc., are given in [101]. Power quality issues have been again addressed in [102]. In reference [102], power quality issues have been resolved by considering the regulated input of diesel engine that is working as a prime mover. It is assumed that frequency and speed of prime mover will not be change. The adaptive notch filter-built control mechanism is used for improvement in power quality features. The PLL-based synchronization methods are widely accepted and most conventional [17, 103–119]. In [103], an improved predictive deadbeat sensor-less vector control is developed towards a greater performance. In [104], experimental-based all-digital phase-locked loop (ADPLL) is used for estimating the phase angle and frequency based on zero-voltage crossing for adding the converters to grid.

In [105, 106], a PLL circuit is designed for implementation in the control circuit of power conditioner. In [107], three advanced PLL-based synchronization methods are presented. The decoupled double synchronous reference frame PLL (DDSRF PLL), the dual second-order generalized integrator PLL (DSOGI PLL) and the enhanced three-phase PLL. Reference [108] to solve the phase angle error problem by the selective harmonics elimination (SHE) method has been proposed. The key individuality of [109] is that the digital oscillator is implemented to compute the trigonometric functions. Reference [110] presented the dynamic behaviour of the closed-loop PLL system and investigated in both continuous and discrete-time domains. Further the optimization method is considered for the second-order PLL system. In [111], it is explored that the optimization of settling time is impossible for a phase disturbance without making the PLL response slower to frequency fluctuations. The tuning techniques which may give non-optimum values and not considered low-gain features [112, 113]. For extraction purpose, the SRF-PLL [114, 115] has been extensively used due to its robust behaviour and simplicity. For solving phase angle issue, several techniques have been proposed [17, 116–119], which are observed as follows. The first approach to get rid of the calculation of trigonometric functions in the PLL implementation with VCO. It can be observed that the estimated frequency signals contain a harmonics content that creates a large variable error. To avoid these problems in the PLL output, an moving average filter (MAF) before the PI controller and selective harmonic mitigation (SHM) with square wave instead of the simple square wave is recommended in [116]. The consequential PLL structure is known as the SHE-PLL. This PLL has suffered from the two major problems. For overcoming these limitations, PLL with high-grade performance VCO is suggested in [117, 118]. But on the other hand, nonlinearities appeared in the computed sin (θ) and cos (θ) caused by the saturations. The total harmonic distortion (THD) of these sine and cosine unit vectors is inversely proportional to the sampling frequency. Authors of this chapter have decided to implement the technique known as VCO-less PLL by looking advantages and disadvantages above [119]. Usually, it is called as synchronization method better known as VCO-less PLL based on the frequency-locked loop due to its mathematical equivalency with SRF-PLL under certain circumstances. The effective utilization of VSC is dependent on the nature of gate pulses generated from the control logic [120–124]. The plenty amount of information on different control algorithms are given in the references [22, 52, 124–130]. The utmost task of following control mechanisms is to provide voltage synchronization at the PCC in any operating conditions. Numerous techniques can be used to synchronize the VSC with the PCC voltage. Generally, the phase-locked loop (PLL)-based circuit is the most effective [124, 125]. Other frequency estimation methods like complex coefficient band-pass filters for extraction of the positive-/negative-sequence frequency harmonics are proposed in [130]. In reference [131, 132], the application neural network-based control algorithm is proposed. Dong et al. [133] worked for harmonics elimination from the supply current using the four-leg converter topology. Rahmani et al. [134] have proposed the basic nonlinear control techniques for the voltage source converter working as an active filter to suppress the current harmonics. In [135], the partially decoupled Volterra filter based on Volterra series which is

nonlinear in nature is proposed. In reference [136–138], adaptive LMS second-order Volterra filter (SOVF) and its variants are applied for the steady-state performance of the nonlinear system.

The above control algorithms are mostly classical in nature except addaline control algorithm which is working on the principle of least mean square (LMS) method. The main drawbacks of classical control algorithm are slow response and more steady-state error under random input or output variations like uncertainty in wind velocity or changing loads. Moreover, the use of low pass filter and its sensitivity towards the selection of cut-off frequency is added disadvantage. The distortion of voltage will lead to inaccurate result, limiting their further application. The limitation of Addaline control algorithm is its fixed learning rate; due to this, the convergence is not faster. Therefore, authors in this review work worked on the implementation of few adaptive control algorithms for power quality features which looks more suitable options in situations like wind-based system.

2 Design of Wind-Based Distributed Generation System

A wind turbine rotating vertically is coupled with three-phase SEIG which is shown in Fig. 1. This system feeds the nonlinear load. The three-phase capacitor bank is used for nominal voltage generation across the terminal of the generator. This capacitor

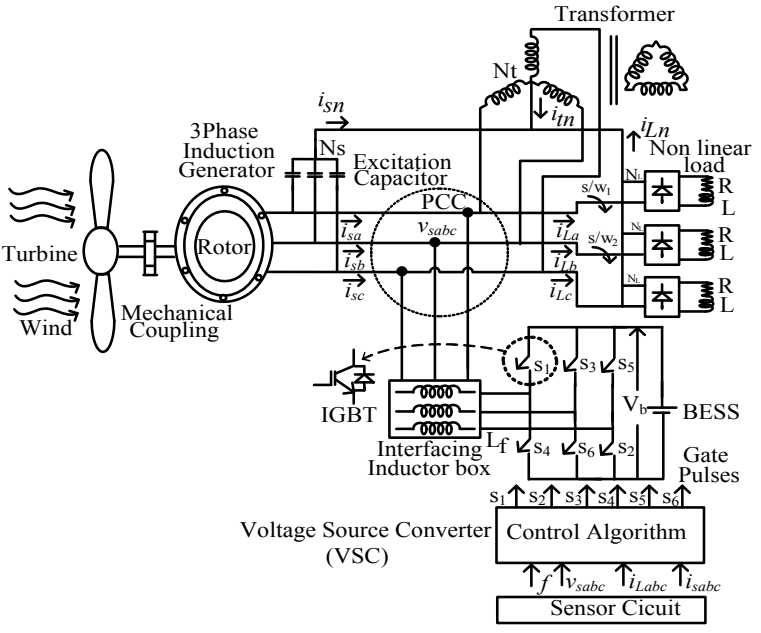

Fig. 1 System configuration of four-wire wind-based distributed power generation system

bank also feeds the supports for the excitation of self-excited induction generator at the initial stage. For harmonic compensation and reactive power compensation of the nonlinear load current, a voltage source converter (VSC) is placed across the load at the PCC. The battery energy storage fed VSC is made of six IGBT arranged on three-phase bridge configurations. The three-phase interfacing inductor (L_f) box is connected for interfacing the VSC to the point of common coupling and filtering the ripple of harmonic current.

Authors have worked on distributed generation system based on generator employed in it. The **t**hree-phase SEIG is employed in distributed power generation system. Sometimes, load such as fan or florescent lamp requires single-phase supply from the standalone generator while to run pumps, flour mills and other similar small-scale domestic appliances at remote places require the three-phase supply. In our system, the sole objective is to provide power from the wind-based standalone distributed generation with improved power quality. Therefore, this subsection presents the design and configuration for each system in detail as under.

2.1 Wind Turbine Design [1]

In this work, for SEIG, the wind turbine is working as a prime mover, therefore making rating selection to be more significant. For energy conversion, the available wind power depends on wind velocity (V_W), power coefficient (C_P) and area of the turbine blade (A). The real power output can be presented by the below-mentioned equation

$$P_m = C_P\left(\frac{1}{2}\rho A V_W^3\right) = \frac{1}{2}\rho\pi R^2 V_W^3 C_P(\lambda, \beta) \tag{1}$$

where V_W, R and ρ are the wind speed (m/s), radius of blade (m) and the air density (kg/m^3), respectively. The tip speed ratio is defined and given as,

$$\lambda = \frac{\omega_R R}{V_W} \tag{2}$$

where V_W and ω_R are the speed of wind in m/s and angular velocity in rad/s, respectively. The ω_R can be calculated using Eq. (3)

$$\omega_R = \frac{2\pi n}{60} \tag{3}$$

The rating of three-phase power of the generator is 3.7 kW (5 hp), and efficiency is 85%.

The required mechanical input for generator: 3700/.85 = 4352 W.

Generally, 10% mechanical loss occurs in gearboxes, etc.; hence, requirement from the turbine output = 4352 + 4352*10/100 = 4787 W. From Eq. (1), R is equal to 1.81 m.

2.2 Selection of Excitation Capacitor [1, 34–36, 88, 94]

The leading volt-ampere reactive (VAR) is drawn by the induction generator for its excitation to build the nominal terminal voltage at no load. The selection of terminal capacitors is decided according to the type and nature of consumer loads to be connected on distributed power generation system. When generator is running in standalone mode, this reactive power is supplied by using star-connected capacitor bank at generator terminal. The design method given in [1] is adopted to get the required value of capacitive reactance (X_c) for maintaining rated terminal voltage with rated active loading. The capacitive nature reactive power values for three phases are obtained using the reactance value X_c (i.e. 13.225 Ω) and are given by Eq. (4).

$$Q = 3V^2/X_c \tag{4}$$

The 4-kVAR star-connected capacitive bank is selected for a 3.7-kW, SEIG system.

2.3 Rating of Battery Energy Storage System [38]

A battery is used to store the power during the power mismatch between generator and load [88 and 94]. For providing proper storage backup, the battery size must be selected. The nearest optimum capacity of battery voltage must be considered at 400 V that is very close or greater to calculated value of V_{dc} as 376 V. Therefore, battery storage capacity of 2.8 kWh is used in this prototype.

2.4 Switch (IGBT/Diode) Rating Used in Three-Phase VSC

The average value of current rating of the IGBT/diode switch used in VSC and dump load circuit is calculated by the ratio of active power delivered and the RMS value of the terminal voltage. The current at the source side of nonlinear load is computed as,

$$i_{ac} = \frac{P_r}{\sqrt{3}\times V_r} = \frac{3700}{\sqrt{3}\times 240} = 9\,\text{A} \tag{5}$$

In case of three-leg rectifier (uncontrol), the distortion factor (DF) is almost equal to 0.83 [10]. It has been noticed during the hardware validation that the crest factor (CF) of the three-leg diode bridge rectifier almost equal to 1.6. Hence, the peak value of rated ac current is computed below as,

$$\begin{aligned} i_{\text{peak}} &= \frac{i_{\text{ac}} \times \text{CF}}{\text{DF}} \\ &= 9.0 \times 1.6/0.83 \\ &= 17.34\,\text{A}. \end{aligned} \tag{6}$$

The voltage rating of IGBT and diode bridge is decided by the peak value of 20% transient over voltage of the ac terminal voltage. This is formulated as below.

$$V_{\text{dc}} = \sqrt{2}(V_{\text{t}} + 0.2V_{\text{t}}) = 1.414 \times 1.2 \times 240 = 407\,\text{V}$$

In our experimental set-up, the current rating and voltage rating of IGBT NGTG50N60FWG are 50 A and 600 V, respectively. Moreover, these IGBT is provided in embedded VSC module having 5 kVA capacity and made by semicron Pvt. Ltd. The remaining design parameters can be seen from Appendix.

3 Control Algorithms

A standalone four-wire system is applicable to supply single-phase loads as well as three-wire loads simultaneously at remote locations. A large pool of load demand can be met by installing relatively larger capacity of wind energy-based SEIG using four-wire system. The major challenges are to maintain voltage and frequency at reference value despite the variations at the input or load side. Moreover, harmonics reduction in the supply current, neutral current compensation and reactive power control is also required for reliable supply. Therefore, voltage source converter (VSC) is required to achieve the reliable operation of the system. The VSC operation is basically governed by the control algorithm used to obtain the modulating signal. The main characteristics of these selected algorithms are their ability to respond with accuracy under dynamical conditions. In this work, authors are mainly focused on the implementation of five different adaptive type control algorithms for the reference current extraction which is further used for the gate pulse generation to operate the voltage source converter used for the mitigation of power quality problems. The control algorithms used for said purpose are namely Lorentzian adaptive filter (LAF) [73], momentum least mean square (MLMS) [100], VCO-less PLL [118] control technique, adaptive vectorial filter (AVF) [54] and nonlinear Volterra filter (NAVF)-based control algorithm [134–138] which are implemented. The mathematical modelling, simulation analysis and hardware implementation are carried out in detail.

3.1 *Features of Selected Control Algorithms for Power Quality Improvement [54, 73, 100, 118]*

In this research work, there are five adaptive control algorithms selected for implementation in the proposed system. The selection of these controls is based on some special features which are discussed below for each of the selected controls.

(i) The implementation of Lorentzian adaptive filter (LAF)-based control algorithm in the voltage and frequency controls of distributed power generation system is done due to continuous nature/norm. Moreover, its stronger stability in impulsive condition is an added advantage. The Lorentzian norm does not penalize heavily for large deviations. The mathematical modelling of the control algorithm is presented in Eqs. (7) and (8), where the dependency of current weight (w_{pa}) on gain factor g_i (n) is shown in Eq. (7). The gain factor is inversely dependent and adaptive to the error square, and it is represented by Eq. (8).

$$w_{\text{pa}}(n+1) = w_{\text{pa}}(n) + \mu u_{\text{pa}}^{T} g_i(n)(i_{\text{La}}(n) - w_{\text{pa}}(n)u_{\text{pa}}(n)) \tag{7}$$

$$g_n(i) = \frac{\gamma^2}{\gamma^2 + e_{w(n)}^2(n-i)} \tag{8}$$

(ii) The implementation of MLMS-based adaptive control algorithm in the voltage and frequency controls of distributed generation system is done due to the presence of scaling factor. It is effectively convergent with required rate. Moreover, it reveals stronger stability in impulsive environment. The mathematical modelling of MLMS is shown in Eq. (9) where the additional momentum term is utilized for faster convergence.

$$w(n+1) = w(n) + 2\lambda u_n^{T}(d_n - w(n)u_n(n)) + \varepsilon\{w(n) - w(n-1)\} \tag{9}$$

(iii) **VCO-less PLL**-based control algorithm is used to control the voltage and frequency by properly switching the VSC. Moreover, power quality features of the generator such as harmonic compensation, mitigation of distortions, load balancing and reactive power control can also be obtained by this controlled operation. This control algorithm is selected for extraction of fundamental component of input current.

(iv) **AVF-FLL**-based control algorithm has been implemented for extracting only fundamental frequency components from input. In other similar approaches, the tuning of loop gain is time taking and its value affects the steady-state error as well as component of bandwidth of the filter. This results the estimation of reference source current for gate pulse generation of voltage source converter.

(v) **NAVF-based control algorithm** works on the truncated Volterra series of second order. It is nonlinear second-order Volterra filtering. Generally, nonlinear

less strong memory systems are illustrated by a number of set kernels. The nonlinear input–output operation of the system is characterized by the same.

4 Simulation Performance

A Simulink model is designed and developed for three-phase induction generator and four-wire configurations. The LAF, M-LMS, VCO less, adaptive vectorial filter and NAVF control algorithm have been applied. The VSC is designed and controlled for power quality issues. The simulated system parameters are given in Tables 1, 2 and 3. Figures 3, 4, 5, 6, 7, 8, 9, 10, 11, 12, 13, 14 and 15 depict the simulation results, and significant points are discussed in the subsequent sections below.

4.1 Simulation Performance of LAF-Based Control Algorithm

The entire block diagram is displayed in Fig. 2a, b. It reveals the simulation study

Table 1 Wind turbine simulation data

Nominal mechanical output power	4.5 kW
Base power of the mechanical generator	3.8/0.9 kW
Base wind speed	12 m/s
Maximum power at level of base wind speed	1 pu
Base-level rotational speed	0.9 pu
Pitch angle	0°

Table 2 Three-phase SEIG simulation data

Rated power (P)	3.73 kW
Rated voltage (V_{L-L})	240 V
Frequency (f)	50 Hz
No. of poles (p)	4
Stator resistance (R_s)	0.3939 Ω
Stator inductance (L_s)	0.002002 Ω
rotor resistance (R_r)	0.4791 Ω
Rotor inductance (L_r)	0.00252 Ω
Mutual inductance (L_r)	0.07669 Ω
Inertia	0.305
Friction factor	0.0197
Initial conditions	[1, 0, 0.2, 0.2, 0.2, 0, 0, 0]

Table 3 Three star-delta transformer and load data used in simulation

	Nominal power	2.4 VA
Transformer data	Frequency	50 Hz
	Primary winding voltage (V_1)	140 V
	Primary winding resistance (r_1)	0.0098 Ω
	Primary winding inductance (L_1)	0.0012478 H
	Secondary winding voltage (V_2)	240 V
	Secondary winding resistance (r_1)	0.0288 Ω
	Secondary winding inductance (L_1)	0.003667 H
	Magnetizing resistance (R_m)	2450 Ω
	Magnetizing reactance (L_m)	7.7986 H
Load data	Resistance (R_L)	30 Ω
	Inductance (L_L)	100 mH

of the proposed LAF control in the application of standalone four-wire system that employ the three-phase SEIG as a generation unit. The block diagram presents the connection of generator, load and voltage source converter (VSC). The three-phase star-delta transformer is also connected at the receiving end for neutral current compensation. For controlling the operation of this system as well as for power quality features, LAF control algorithm is implemented.

4.1.1 Control Signal Generation Using LAF Control Algorithm

The simulation performance for the generation of control signals and for reference current (i_s^*) extraction has been carried out, and the results are displayed in Fig. 3. The process of current error calculation and weight extraction has been observed. The load transient is introduced by opening the phase '*a*' at time (*t*) equal to 7.5 s. The variation in the quantities such as load current (i_{Labc}), unit voltage templates (u_{pa}), current error (i_{er}), active and reactive weights (w_{pa}, w_{qa}), average weights (w_{pav}, w_{qav}), terminal voltage (v_t), frequency (f), etc., are observed. The reference current for gate pulse generation is extracted using LAF which is dependent on weight extraction of load current. From the diagram, it is evident that the sinusoidal reference current (i_s*) is obtained despite the nonlinear load current.

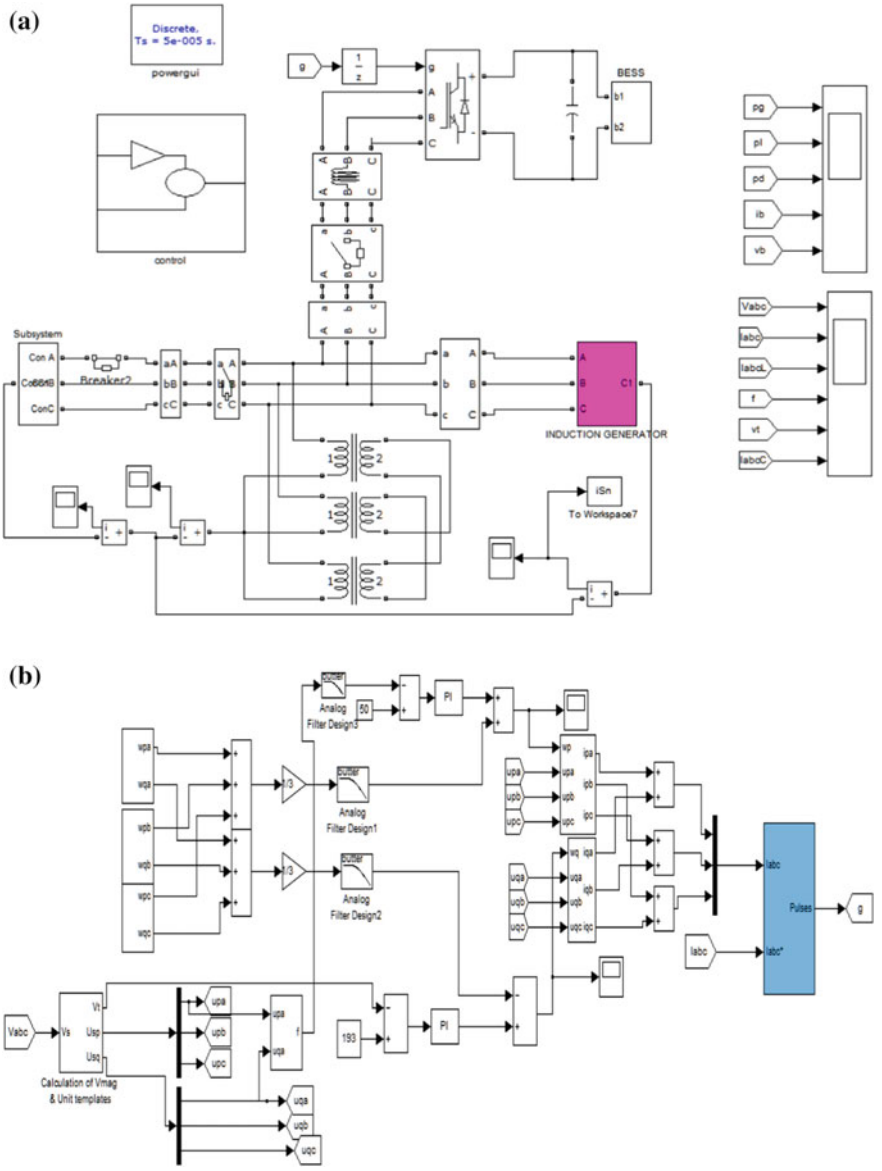

Fig. 2 Simulation block diagram **a** Power circuit diagram **b** Voltage and frequency estimation followed by gate pulse generation

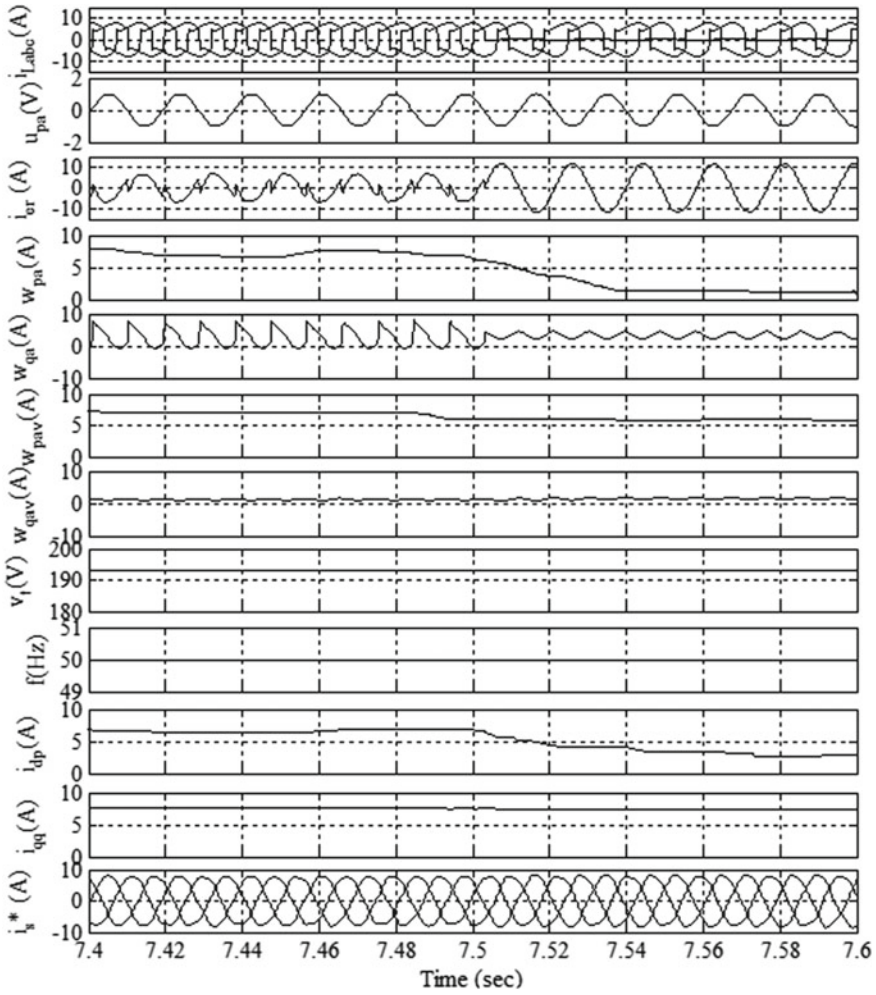

Fig. 3 Generation of control signals using LAF

4.1.2 Performance of DG System with Consumer-Type Linear Load

The simulation performance of the proposed system with LAF control algorithm under variable load condition and fixed wind speed is displayed in Fig. 4. The simulation circuit parameters are provided in Appendix. The load transient is introduced at time (t) equal to 7.5 s for dynamics. Though load current in phase 'a' is removed and unbalance is created at the load end, source current remains balanced and almost purely sinusoidal. This indicates the effective control provided by LAF control algorithm. The effect of neutral current compensation is also presented. Unless and until load current is not disturbed, the neutral current in the source (i_{Sn}), load (i_{Ln}) and

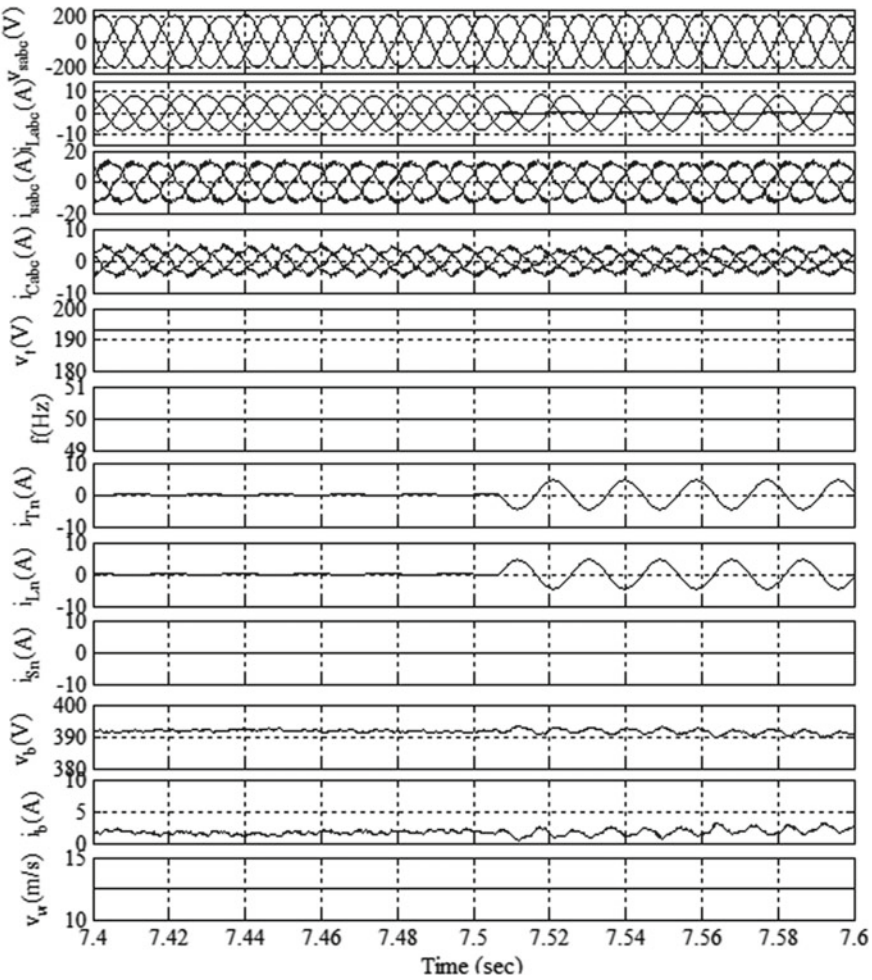

Fig. 4 Performance of DG system under output power variations and fixed wind speed in linear load

transformer (i_{Tn}) is almost zero. The moment when transient in the load current appears at time (t) equal to 7.5 s, neutral wire current in the transformer and load are in phase opposition; therefore, neutral current in the source becomes zero. In addition to it, during load disturbance battery energy storage system (BESS) also reacts according to the requirement of the system. When load is removed in one phase, battery current (i_{b}) is increased for excess energy storage. Throughout the operation, wind speed is taken constantly at 12.5 m/s. Frequency (f) and magnitude of PCC voltage (v_t) are observed constant during the course of operation.

4.1.3 Performance of DG with Fixed Linear Load and Variable Wind Speed

The proposed system is tested with variable speed and fixed linear load by performing simulation. The main objective of this study is to discussed power quality feature of the system. The transient in the wind speed is created at (t equal to 7.5 s), and results are observed. These results are presented in Fig. 5. It is clear from the software results that when wind speed increased from the level 12.5 to 14.5 m/s, the generated current also increased. This results in the increased charging current towards battery due to fixed load and increased generation. In this case, neutral current compensation from

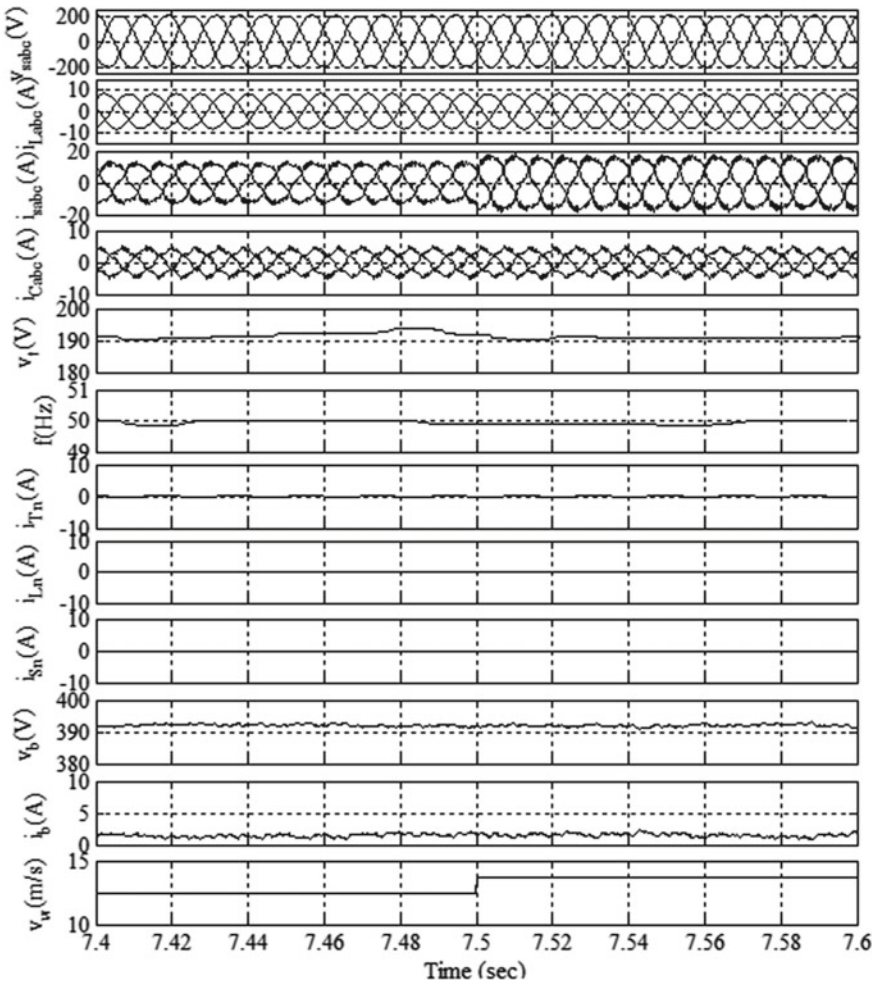

Fig. 5 Dynamics of DG system under variable wind speed in linear load

the transformer is zero due to balanced load current. Voltage and frequency remain constant even before or after the wind speed changes; this indicates the controlled operation of voltage source converter whose switches are operated using the LAF control algorithm.

4.2 Simulation Performance of MLMS-Based Control Algorithm

The simulation work of MLMS control algorithm for power conditioning features in distributed generation system has been carried out in various operating conditions as discussed below.

4.2.1 Performance of DG System with Variable Linear Load

The simulation performance of said DG system under variable loading condition and with fixed wind speed is carried out, and results are displayed in Fig. 6. The quantities under observation were supply voltage (v_{sabc}), source current (i_{sabc}), compensator current (i_{cabc}), load current (i_{Labc}), terminal voltage (v_t), wind speed (v_W), frequency (f), load neutral current (i_{Ln}), transformer neutral current (i_{Tn}), source neutral current (i_{sn}), battery voltage (v_b) and battery current (i_b). Under linear loading condition of 10 A current of 0.70 pf, the value of compensator current is low as compared to nonlinear load. The reason behind it is that no harmonics mitigation is required. The supply current is always balanced either under balanced load or unbalanced load. For checking the battery dynamics in the system, transient is introduced at the moment (t) equal to 7.5 s. The moment when one phase is open circuited for reducing the load up to 33%, without any change in the generation, battery starts charging with the difference of current between load and generator. Similarly, the transformer employed to neutralize the zero-sequence current in the source neutral wire will be supplying neutral current only under the condition of load unbalance. It is evident from the simulation results shown.

4.2.2 Dynamic Performance of DG System with Linear Load Under Wind Speed Variations

The simulation study of proposed system is carried out with variable wind speed and constant load. The similar quantities are observed for power quality improvement and voltage and frequency control as in the previous case. In this case, wind velocity is changed from 12.5 to 14.5 m/s at the moment (t equal to 7.5 s) for introducing the dynamics in the system. The dynamic response of the MLMS control is evaluated and presented in Fig. 7. From the results, it is evident that voltage and frequency

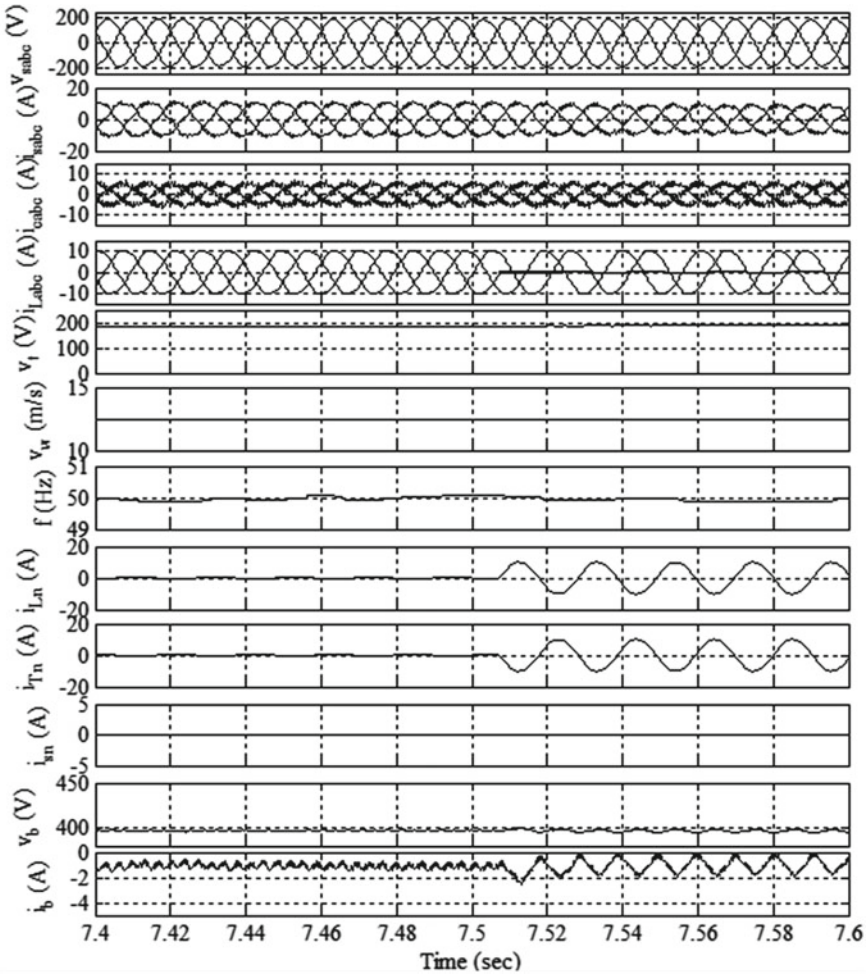

Fig. 6 Dynamics of DPGS under linear load variations with fixed wind speed

remain unchanged before or after the wind speed changes. Moreover, power quality issues are also solved means that voltage and current are purely sinusoidal. Due to balanced load throughout the course of operation, neutral current compensation is not required, and therefore, no current is flowing through the transformer as seen in the results. The response of battery energy storage system is also studied and presented. It is understandable from the results that when wind speed is increased the current flow from the generator which is also increased. Therefore, the current difference of load and generator has flown towards battery for energy storage purpose. The simulation results are satisfactory as shown in Fig. 7.

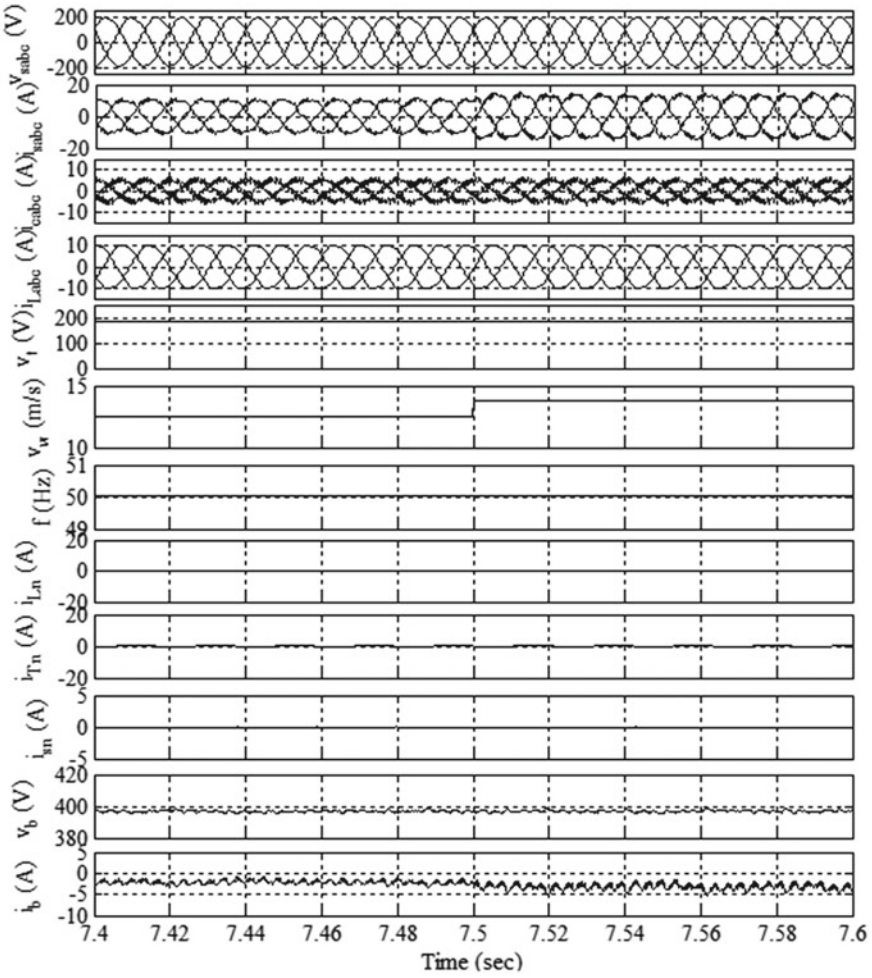

Fig. 7 Dynamics of DPGS under linear load with wind speed variations

4.3 Simulation Study of VCO-less PLL-Based Control Algorithm

The MATLAB simulation for VCO-less PLL control is performed, and results are presented in following subsections. The simulation is arranged in various parts such as the generation of control signals, system dynamics with variable wind speed under linear/nonlinear load and system dynamics under variable linear/nonlinear load with constant wind speed. The descriptions for each of the cases are here as follows.

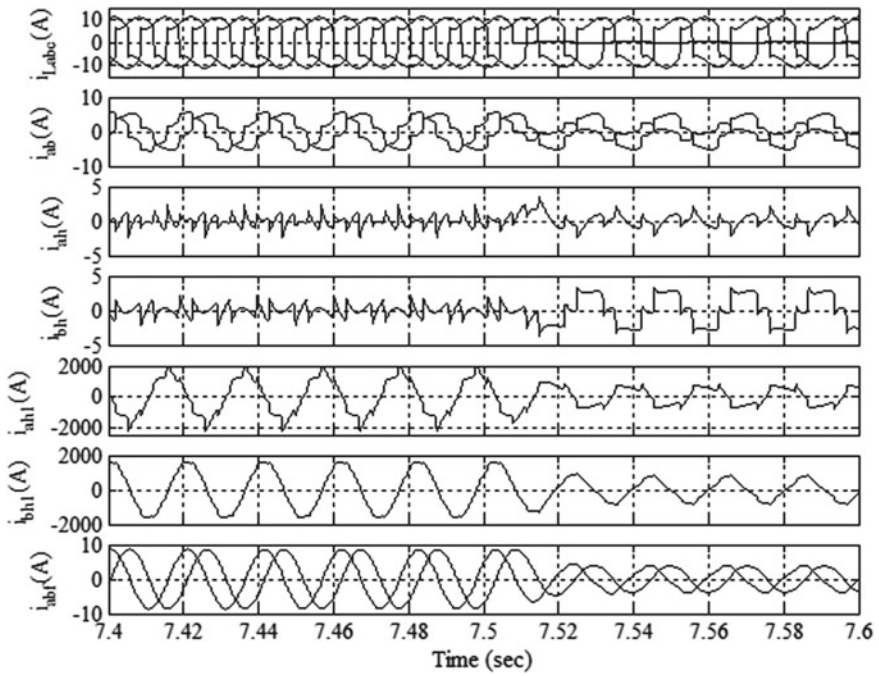

Fig. 8 Control signal generation by VCO-less control algorithm

4.3.1 Generation of Control Signal Using VCO-less PLL Control Algorithm

The intermediate stages of control algorithms are required to generate the reference current for current controller. These signals are presented in Fig. 8. In the VCO-less PLL control algorithm, *abc* to α_β conversion is required at very first stage. Therefore, α_β component of load current (i_{ab}) is generated from the three-phase nonlinear load current fed to control algorithm as an input signal. In the second stage, harmonics component (i_{ah}, i_{bh}) of α_β component of load is extracted by subtracting the fundamental component. Finally, fundamental active and reactive components (i_{abf}) are extracted from the load current. It is evident from the result that the fundamental component is sinusoidal despite the nonlinear load current. This current is used for gate pulse generation.

4.3.2 Dynamic Performance with Constant Wind Speed and Variable Linear Load

The performance of self-excited induction generator is evaluated under the linear load dynamics with constant wind speed consideration. The load transient is created

by opening phase '*a*' at the moment (*t*) equal to 7.5 s. Despite the load imbalance, the source current is balanced in each phase. The voltage magnitude at PCC remains the same irrespective of loading condition. Unless and until load current is almost balanced in each and every phase, the neutral current compensation is not required from the transformer connected at PCC. However, when one-phase load current is removed, the load neutral current is compensated by the transformer as shown in Fig. 9. The transformer current and load neutral current are in phase opposition; therefore, the neutral wire current from the generator side becomes zero. From the diagram, it is evident that the battery current is increased when load is reduced by almost 33% by removing one phase. Battery voltage remains constant throughout the course of operation.

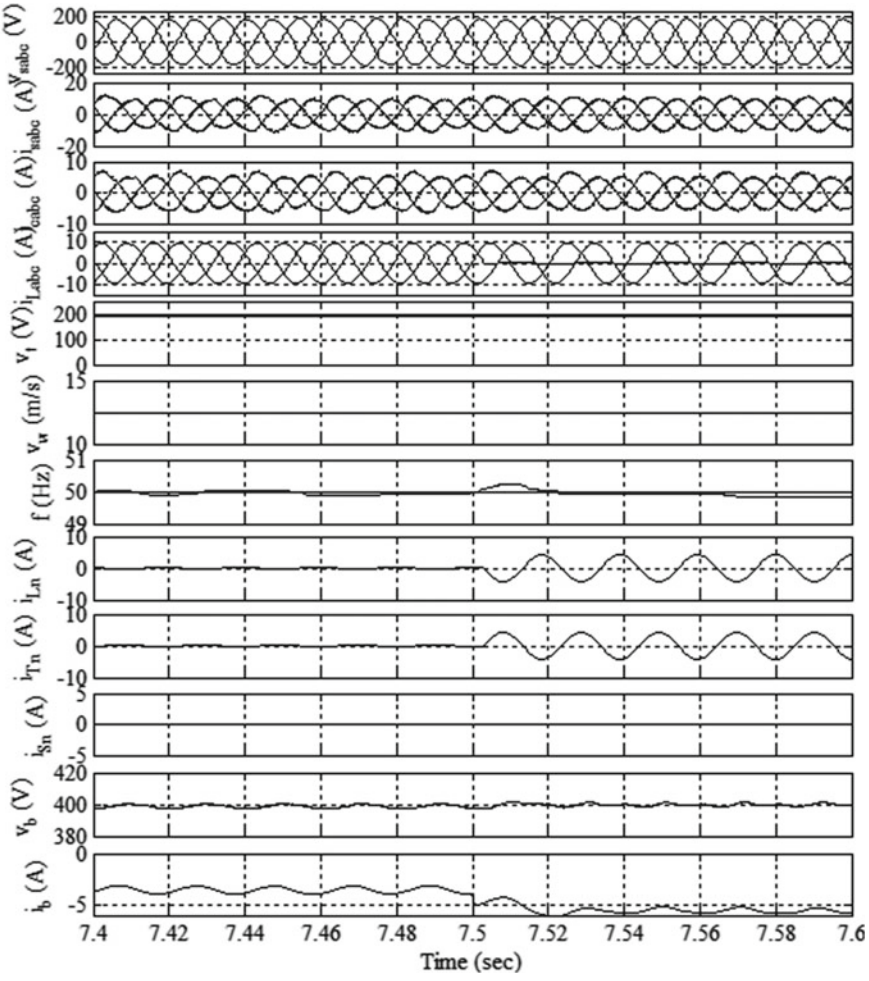

Fig. 9 Dynamics of DPGS under linear load variations with fixed wind speed

4.3.3 Dynamic Performance with Variable Wind Speed and Constant Linear Load

The performance of self-excited induction generator is evaluated under the constant linear load with wind speed dynamics consideration. The wind speed is increased from 12 m/s to 14.5 m/s for introducing the wind dynamics at the moment time (t) equal to 7.5 s. The load is balanced in this case; therefore, neutral current compensation is not required any time. The moment when wind speed is increased by keeping the same load, the source current is increased at the generator terminal due to increased power flow with regulated voltage supply. Hence, surplus power started flowing towards battery system. The voltage magnitude at PCC remains the same irrespective of wind velocity condition. Unless and until load current is almost balanced in each and every phase, the neutral current compensation is not required from the transformer connected at PCC. These effects are shown in Fig. 10.

4.4 Simulation Study of Adaptive Vectorial Filter (AVF)-Based Control Algorithm

The simulation performance of distributed generation system is studied using the AVF-based control algorithm. The process of reference current generation is followed by dynamic response under nonlinear load variations which are discussed in detail as below.

4.4.1 Control Signal Generation by AVF Control Algorithm for VSC

The procedure of reference current generation by AVF control algorithm has been discussed in detail in the previous section. Here, the simulation performance of control algorithm for generation of reference source current and intermediate signals required to estimate the same has been shown in Fig. 11a. The observed signals are three-phase load current (i_{Labc}), α_β transform component (i_{ab}) of load current, adaptive parameter (k_f), frequency adaptive coefficient (ω), current error (i_{e}), amplification of current error ($i_{\mathrm{e}}{*}\omega{*}k_f$), fundamental component of load current on α_β transform axis (i_{abf}), current component from the frequency control loop (i_{dp}) and current component from the voltage control loop (i_{qq}). The dynamics in the load current is introduced at time (t) equal to 7.5 s, and the variation in the fundamental load current is observed. When load is removed on phase 'a', the fundamental current is also reduced, and it reduces the source current. By observing the results, it is seen that the fundamental component of load current is purely sinusoidal despite the nonlinearity in the load current. The fundamental extraction was main objective of this control. It should not have much delayed zero crossing with reference to zero

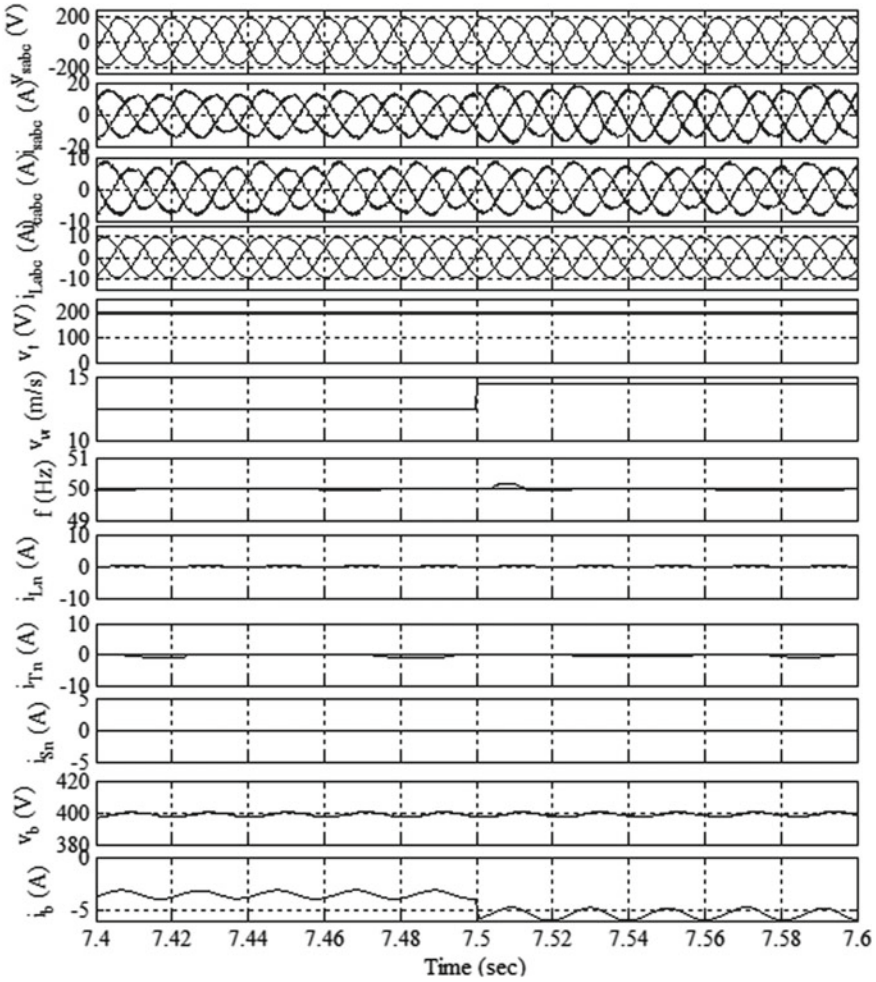

Fig. 10 Dynamics of DPGS under linear load with variable wind speed

crossings of load current. The required response is obtained from the AVF-based control algorithm.

4.4.2 Dynamic Performance of DPGS by AVF Control Algorithm Under Variable Nonlinear Load

The dynamic performance of distributed power generation system comprising three-phase self -excited induction generator feeding nonlinear load is carried out using AVF-based control. This algorithm was operating the VSC to solve power quality issues at point of common coupling. This performance was done under variable

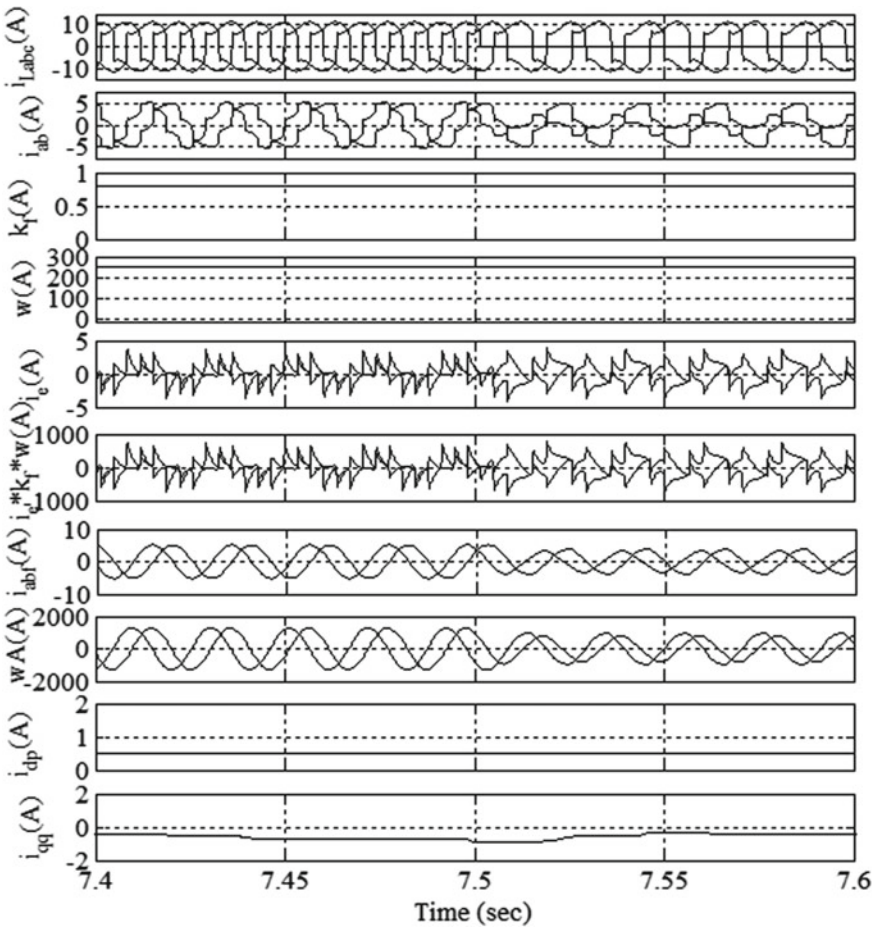

Fig. 11 **a** Control signal generation at various stages of AVF

nonlinear load with fixed wind speed, and results are discussed in Fig. 11b. The load dynamics is introduced at the moment time 't' which is equal to 7.5 s by making the load current in phase 'a' zero. The observed results are source voltage (v_{sabc}), source current (i_{sabc}), load current (i_{Labc}), compensator current (i_{Cabc}), terminal voltage (v_t), battery voltage (v_b), frequency (f), battery current (i_b), load neutral current (i_{Ln}), transformer neutral current (i_{Tn}), source neutral current (i_{Sn}) and wind speed (v_W). From the results, it is clear from the voltage source waveform (v_{sabc}) that the magnitude of voltage and frequency are constant at PCC despite the load dynamics in the system. The neutral wire current of the load is fully compensated by the neutral current of transformer, and therefore, neutral current in the source is almost zero. The dynamic response of battery energy storage unit is also observed. The battery current is increased to store surplus power under less loading condition

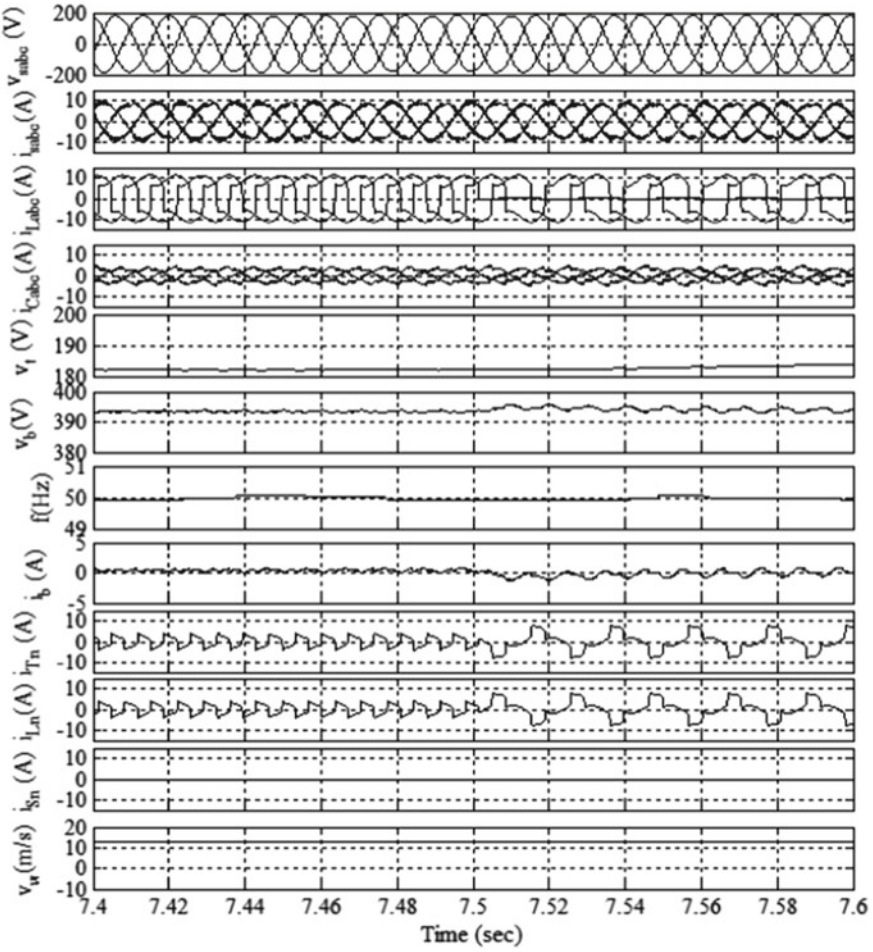

Fig. 11 **b** Performance of distributed power generation system under variable wind speed and fixed load

with same mechanical input to the generator. In this case, wind speed was fixed at the 12.0 m/s. The overall simulation results are found satisfactory.

4.4.3 Dynamic Performance of DPGS by AVF Control Algorithm Under Variable Wind Velocity

The dynamic performance of distributed generation system by AVF control algorithm under variable input to the generator is shown in Fig. 12a. In this case, load is fixed and nonlinear in nature. The observed results are source voltage (v_{sabc}), source current (i_{sabc}), load current (i_{Labc}), compensator current (i_{Cabc}), terminal voltage (v_t), battery

voltage (v_b), frequency (f), battery current (i_b), load neutral current (i_{Ln}), transformer neutral current (i_{Tn}), source neutral current (i_{Sn}) and wind speed (v_W). The wind velocity is changed from 12 m/s to 13.5 m/s at the moment time (t) which is equal to 7.5 s, and variations in other quantities are observed. Due to controlled action of VSC which is operated by AVF control algorithm, the no change is noticed in the magnitude of voltage and frequency at PCC. Due to increased mechanical input to the generator by the increased wind velocity, the output power is raised. Because the magnitude of voltage is kept constant by the AVF control algorithm therefore source current is also increased to raise the power output. The neutral current is compensated separately using the star-delta transformer at the PCC. The battery dynamics are also noticed and found satisfactory. The steady-state results are also observed and are shown in Fig. 12b. The total harmonics distortion (THD) values for source voltage (v_s), source current (i_s) and load current (i_L) are recorded. It is clear from the results that the THD value in source current is less than 5% as prescribed by IEEE standards 519. While the THD value in the load current is 29.5%. The source voltage THD is also well below the prescribed limit of IEEE standards.

4.5 Simulation Study of Nonlinear Adaptive Volterra Filter (NAVF)-Based Control Algorithm

The simulation performance of distributed generation system comprising wind turbine, three-phase self-excited induction generator, nonlinear load and voltage source converter operated by NAVF-based control algorithm is carried out and discussed in the following subsections.

4.5.1 Control Signal Generation by NAVF Control Algorithm for VSC

The process of reference current generation and intermediate signals required to estimate it is shown in Fig. 13. The developed control algorithm is nonlinear in nature, and it requires the multiple frequency in-phase and quadrature templates to remove the harmonics from the load current. The load dynamics is introduced at t equal to 7.5 s to the see the dynamic response of the system which is controlled by NAVF. The observed results are source voltage (v_{sabc}), in-phase unit templates (u_{sp}), quadrature unit templates (u_{sq}), load current (i_{Labc}), multiple harmonic in-phase and quadrature templates vector (v_k), active and reactive weights (w1 and w2), current component from the frequency control loop (i_{dp}) and current component from the voltage control loop (i_{qq}) and reference source current (i^*_{sabc}). In this control algorithm, multiple harmonics templates are estimated from the fundamental unit voltage templates as described in the above section of NAVF control algorithm. The zoom version is shown separately for more clarity of the reader. The variations in the intermediate signals under load dynamics are shown in Fig. 13. From the results, it is clear that the

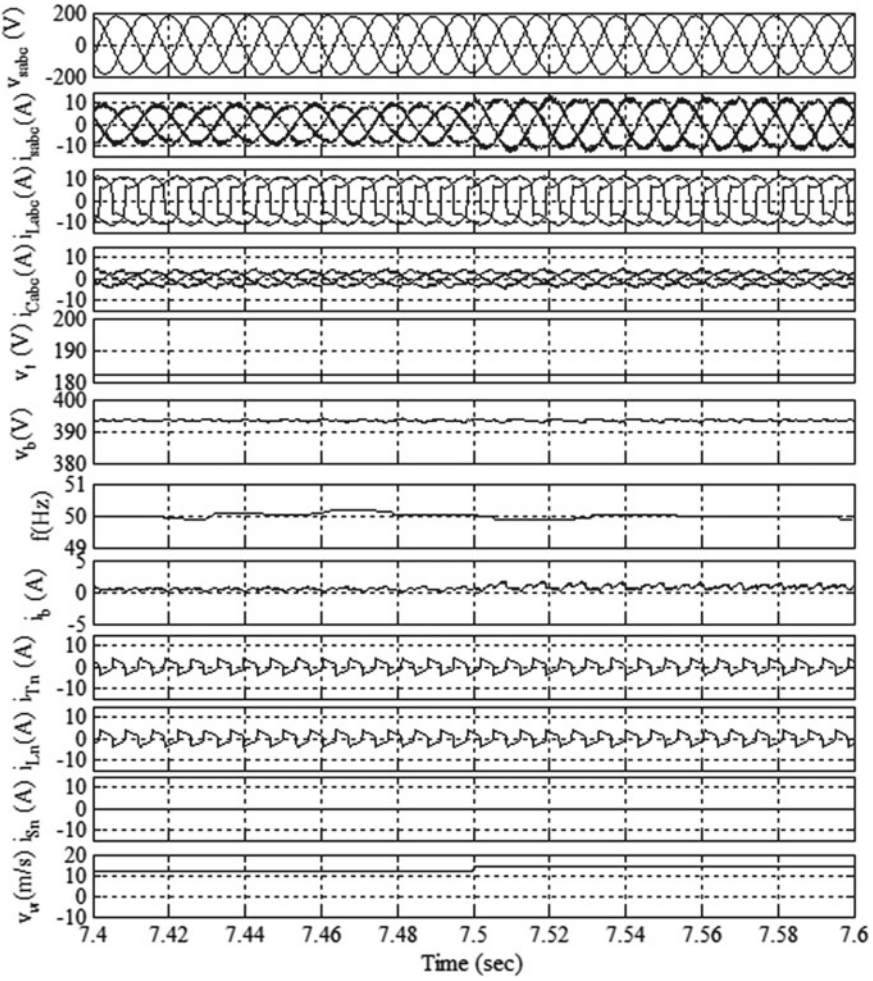

Fig. 12 **a** Distributed power generation system performance under variable wind speed and fixed load

control algorithm responded well by estimating the stable value of active and reactive weight of load current which is useful for the estimation of reference current.

4.5.2 Dynamic Performance of DPGS by NAVF Control Algorithm Under Variable Nonlinear Load

The dynamic performance of wind-based distributed power generation system (DGPS) is evaluated using the NAVF control algorithm under variable loading conditions, and waveforms are shown in Fig. 14. The system parameters which were

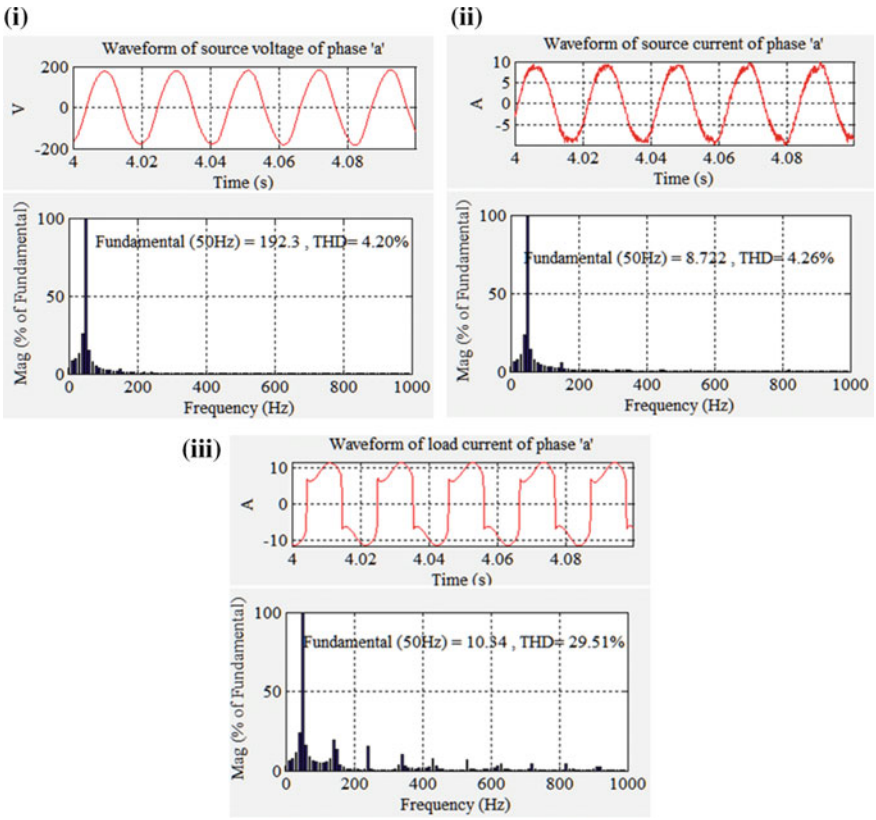

Fig. 12 **b** Harmonics spectrum (i) THD in source voltage (ii) THD in source current (iii) THD in load current

under observation are source voltage (v_{sabc}), source current (i_{sabc}), load current (i_{Labc}), compensator current (i_{Cabc}), terminal voltage (v_t), battery voltage (v_b), frequency (f), battery current (i_b), load neutral current (i_{Ln}), transformer neutral current (i_{Tn}), source neutral current (i_{Sn}) and wind speed (v_W). The wind velocity is assumed at constant value of 12 m/s during entire course of action. Due to rectifier-fed RL load, the load current is nonlinear. It is noticed that the source current becomes sinusoidal due to the compensating current supplied by the voltage source converter. The nature of compensating current is dependent on the NAVF control algorithm. The proposed control algorithm has made the proper compensation of load harmonics; therefore, source current becomes almost purely sinusoidal. From the waveforms of supply voltage, it is clear that the magnitude and frequency are almost constant due to effective functioning of voltage and frequency control loop of algorithm applied in place. The dynamics of battery energy storage system is observed for real power balance in network. The neutral current compensation is also achieved with the help of star-delta

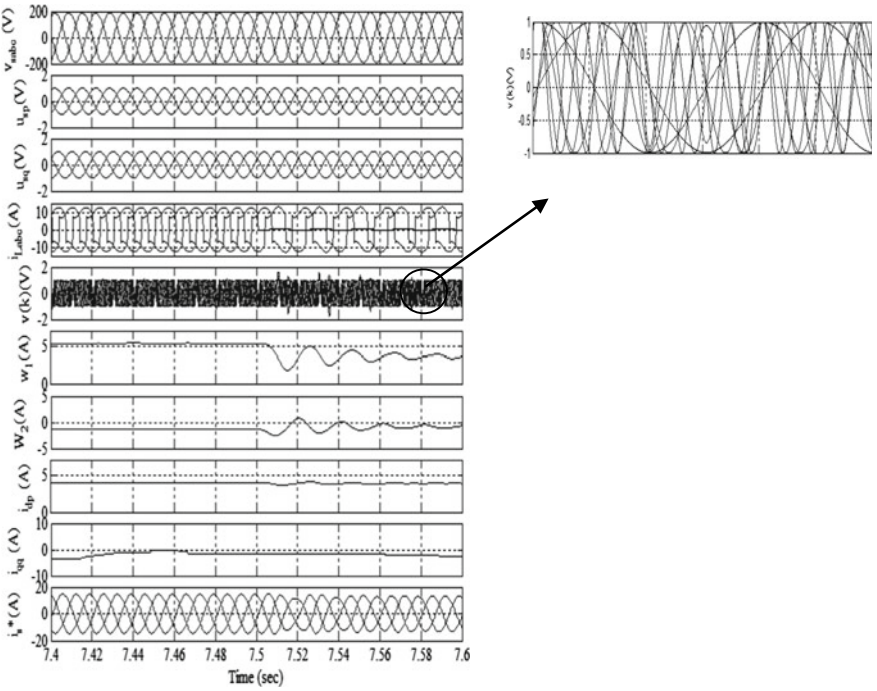

Fig. 13 Generation of control signal by NAVF control algorithm

transformer that cancels the neutral current of the load. All the targeted objectives are met, and control algorithm has performed satisfactorily.

4.5.3 Dynamic Performance of DPGS by NAVF Control Algorithm Under Variable Wind Velocity

The system is simulated under dynamic wind conditions with proposed control algorithm running in the controller, and results are shown in Fig. 15a. Again, the similar parameters at point of common coupling are observed. The observation parameters are source voltage (v_{sabc}), source current (i_{sabc}), load current (i_{Labc}), compensator current (i_{Cabc}), terminal voltage (v_t), battery voltage (v_b), frequency (f), battery current (i_b), load neutral current (i_{Ln}), transformer neutral current (i_{Tn}), source neutral current (i_{Sn}) and wind speed (v_W). For creating dynamics in the system, the wind speed is increased in one step from 12 m/s to 13.5 m/s at the moment 't' which is equal to 7.5 s. Due to increased wind speed at the turbine, the generated power is increased. However, voltage magnitude at PCC is controlled and kept at the constant value; hence, source current is increased. The other parameters are fully controlled under the wind dynamics. Under steady-state condition, the system is simulated with nonlinear load

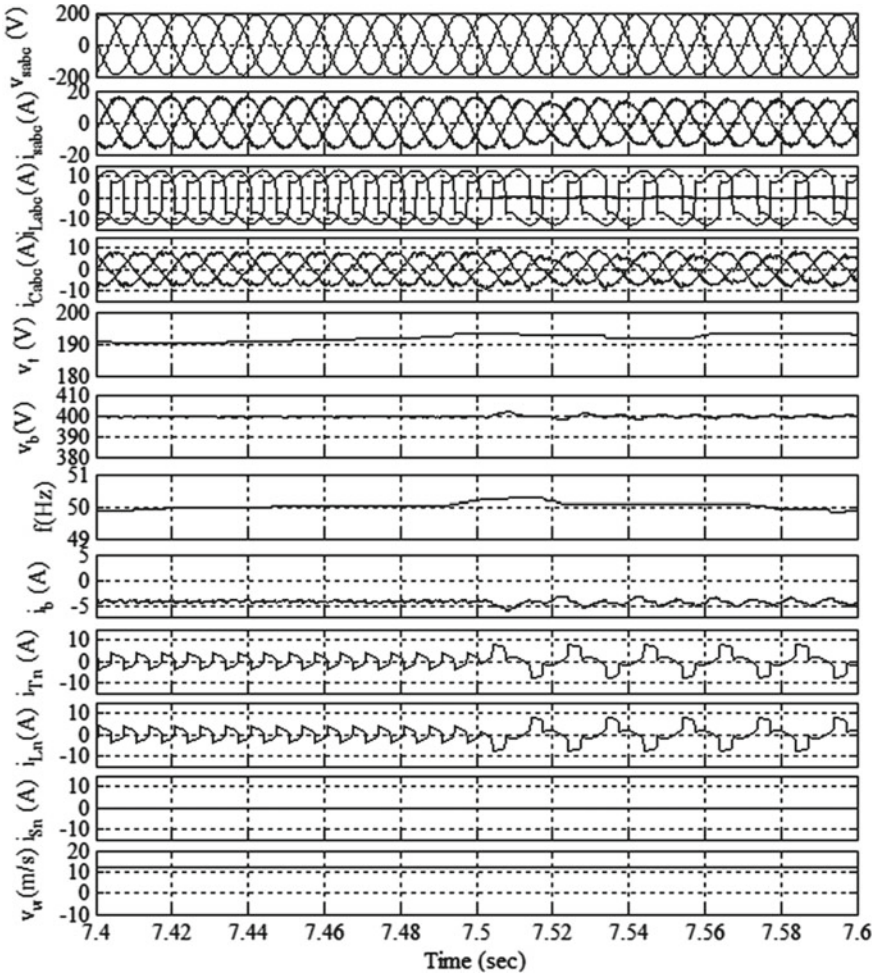

Fig. 14 Dynamics response of distributed power generation system under variable load with fixed wind speed

and total harmonics distortion is observed and plotted in Fig. 15b. The total harmonics distortion in the supply current is controlled, and observed value is 3.54% while load current THD is 32.25%. This shows the very effective compensation done by the VSC operated by NAVF control algorithm.

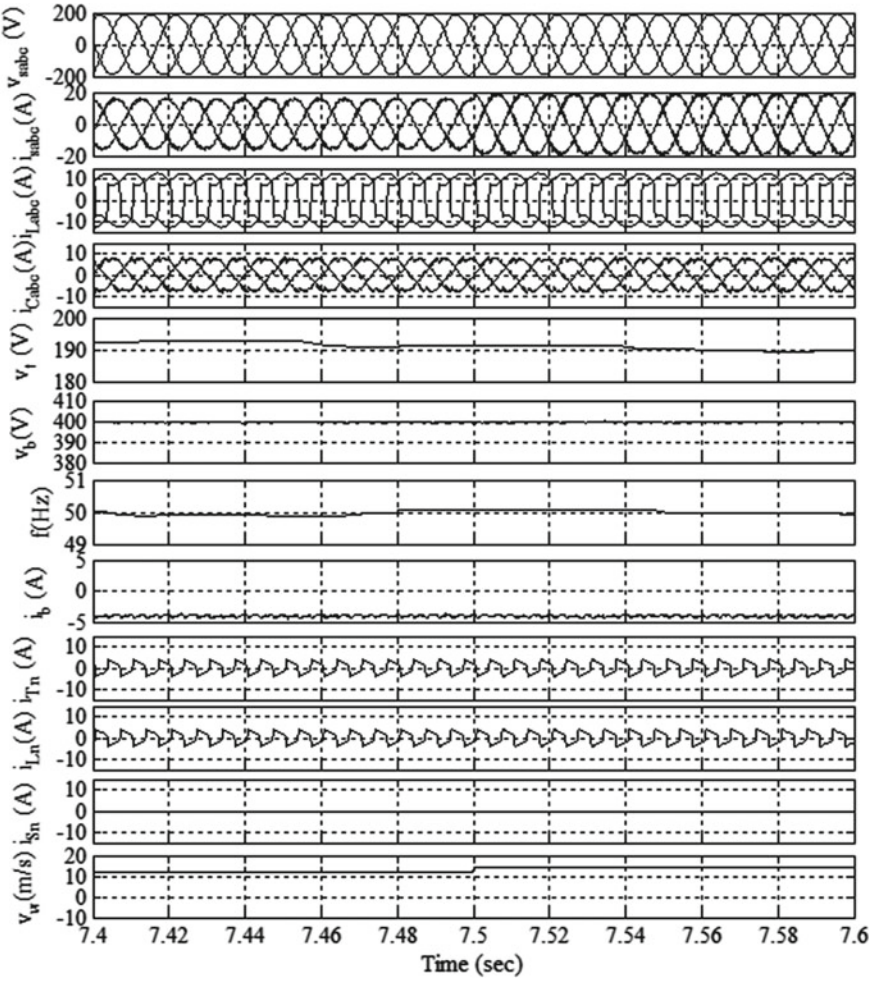

Fig. 15 **a** Dynamics response of distributed power generation system under variable wind speed and fixed load

5 Hardware Development and Discussion

The proposed distributed generation system is developed in its prototype form in laboratory. The major components are listed below:

- Variable frequency drive of ABB make
- Generator coupled with three-phase induction motor
- Three-phase linear/nonlinear load with multi-winding transformer
- Sensor circuits
- d-SPACE 1104

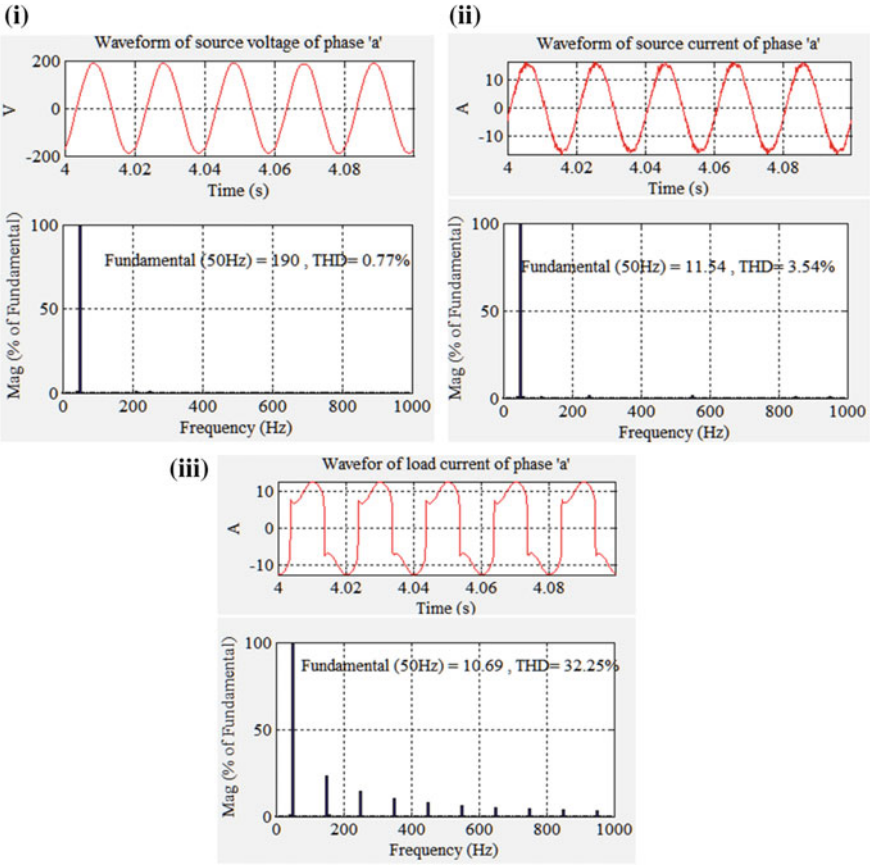

Fig. 15 **b** Steady-state results (i) THD in source voltage (ii) THD in source current (iii) THD in load current

- Dead band circuit
- Optocoupler isolation circuit
- Semicron four-leg inverter module
- Battery.

The brief discussion of the above components is provided here in subsections given below.

5.1 Variable Frequency Drive (VFD)

This is used to control the speed of prime mover (induction motor) by changing the voltage and frequency across the terminal of the motor. Actually, it consists

Fig. 16 Photograph of VFD

of back-to-back power electronics series convertor with dc link. At first stage of conversion, AC voltage is converted into fixed DC voltage and then in the second stage of conversion, the dc voltage is converted into variable ac voltage with variable frequency. This drive is shown in Fig. 16.

5.2 Generation System with Excitation Capacitor

The ABB makes 3.7 kW, 240 V (L-L); four-pole three-phase self-excited induction generator has been used as a standalone generation system. It is coupled with similar rating induction motor which is working as a prime mover. For excitation purpose, the three-wire star-connected capacitive bank is used across the terminals of the generator. The combined arrangement of generator and capacitor is shown in Fig. 17.

5.3 Three-Phase Linear/Nonlinear Load with Multi-winding Transformer

Three units of single-phase rectifier bridge connected with resistance and inductance are used as a nonlinear load. Dawn electrical make multi-winding transformer is used for compensating the neutral current of the load. The three-phase inductor of 100 mH is used for creating the distortion in the load current. The set-up is shown in Fig. 18.

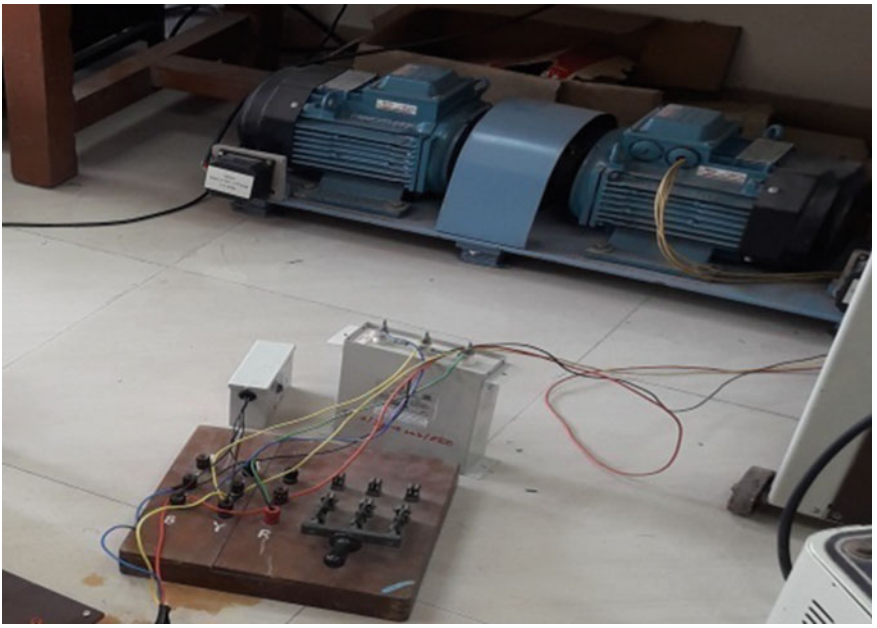

Fig. 17 Photograph of generation system

Fig. 18 Photograph of loads

5.4 Sensor Circuits

The voltage and current sensors are bridging the control circuit and power system. The following sensors are used and designed as discussed in the following subsections.

5.4.1 Design of Current Sensing Circuit

The source current of two phases and load currents of all the three phases are required to feedback into the control algorithms for reference current generation. Due to the balanced source current, third-phase source current can be calculated in the processor by just knowing the two-phase current. Therefore, only two current sensors are required at the source end. Due to natural load unbalanced in the case of three-phase four-wire system, all the three-phase load currents are required to sense. Hence, five LEM make current sensors (LA 55-P) having 50 A capacity of each are employed on the two different sensor cards as shown in Fig. 19. The sensed current signals are further given to operational amplifiers (LM324)-based signal conditioning circuits. The interfacing circuit of current sensor board is shown in Fig. 16. As per the datasheet of LA 55-P, the current transformation ratio of transducer is 1:1000 with primary winding current of 50 A. It means that if 50 A of current are flowing through the primary line, then according to conversion ratio of current sensors only 50 mA is flowing from the output terminals. Similarly, if line current is 10 A then corresponding output current is 10 mA. Therefore, in order to calibrate 10 A line current as an output voltage of 1 V, the minimum value of output resistance is somewhat greater than 100 Ω, and its power rating can be calculated as 0.01 W. However, the actual value will be selected based on the availability in the market. Generally, the available value in the market is 100-ohm 0.25 W, and hence, it is selected for this purpose.

5.4.2 Design of Voltage Sensing Circuit

The source voltages (L-N) of all the three phases are needed for running the control algorithms in the processor. Basically, any two line-to-line voltages are sensed and third (L-L) voltage is calculated. Further, these are converted into phase voltages for calculation of unit templates and PCC voltage magnitude. Therefore, two LEM make voltage sensors (LV 25-P) are needed, and it is shown in Fig. 19. Essentially, the aim of the voltage sensors is to reduce the power voltage level to the voltage level of ADC of d-SPACE 1104 that is ±10 V. Further, the equivalent gains are used to regain the originality of the signals before feeding to the control algorithm. The low voltage side of the hall effect voltage sensor is further connected to the signal conditioning circuits. The LM324 ICs are used as operational amplifiers as well as providing buffer stages.

The complete interfacing circuit of voltage sensor board is shown in Fig. 19. As per the datasheet of LV 25-P, each sensor or transducer is having rated current

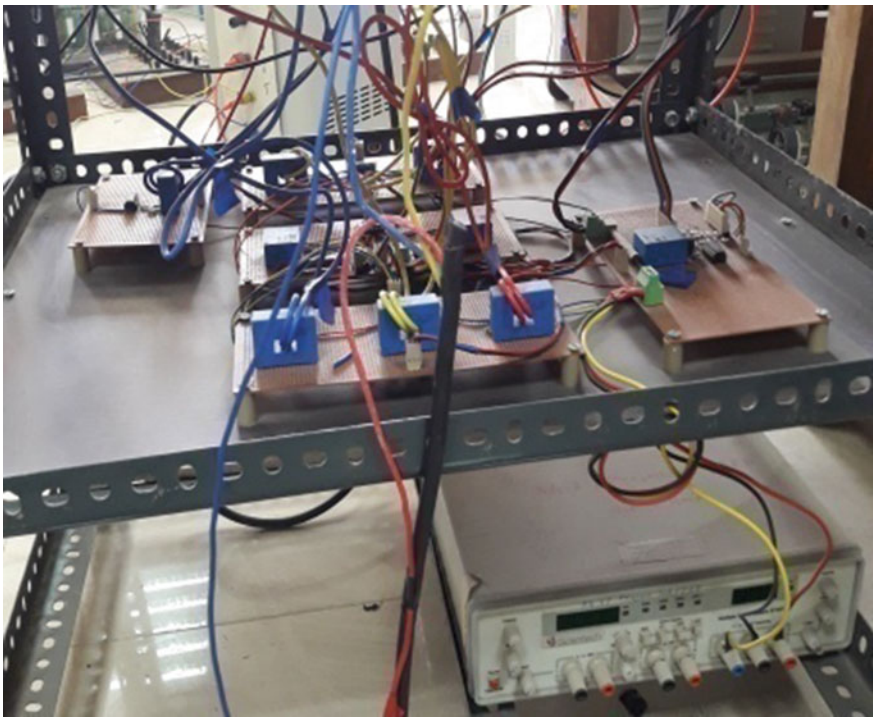

Fig. 19 Photograph of sensor circuit

transformation ratio of 10 mA/25 mA and 500 V input voltage rating. It means primary winding should not carry more than 10 mA current at any point of voltage. Therefore, an appropriate input resistance is inserted in series to limit the primary current. The value of input resistance can be calculated and found 50 KΩ. The power rating is found to be 5 watts. Therefore, the power resistor of 50 KΩ, 5 W value is selected as an input resistance (R_{in}). In order to obtain output voltage near 5 V with secondary current less than 25 mA, the minimum value of output resistance is 200 Ω. From the available range of resistor, the selected value of output resistance (*Ro*) is 270 Ω. From the available range of resistor, the selected value of output resistance (*Ro*) is 270 Ω. Therefore, an input voltage of 500 V is calibrated to an output voltage of 6.75. Therefore, an output resistance (*Ro*) is selected as 270Ω, 0.25 W value. From this conversion, the power-level voltage of ±240 V is scaled to signal-level voltage of ±3.15 V with isolation.

5.5 d-SPACE 1104

The software implementation is based on MATLAB Simulink model, having feature of easy interface with d-SPACE 1104 controller that uses programming code, built by MATLAB software. The proposed control algorithms are digitally implemented using d-SPACE controller (DS1104). The host PC made by IBM with 2 GB RAM is required to installed MATLAB 6.5 and Control Desk software. The d-SPACE 1104 processor includes master and slave DSP 210 subsystem based on the d-SPACE controller. Out of these pins, 6 digital I/O channels are utilized to implement the proposed classical control algorithms in real time. The eight ADC channels are available as four-multiplexed and four-parallel channels. The Control Desk software is worked as a compiler and uploads the programming code (C language) in DSP DS1104 controller board. The photograph of d-SPACE 1104 is shown in Fig. 20.

Fig. 20 Photograph of d-SPACE 1104

5.6 Dead Band Circuit

Dead band circuit is playing a very important role in satisfactory operation of voltage source converter. It provides necessary commutation time delay for the IGBT switches employed in the same leg of bridge converter module. For configuring this circuit, six number of 74F00PC ICs are employed for six PWM pulses. The main characteristics of this circuit are that it creates delay always at falling edge of each pulse, and therefore, generally the required time delay is created between two complementary PWM pulses. The dead band circuit is made on simple PCB and is presented in Fig. 21a. The circuit diagram of the same for initial two complimentary gate pulses is shown in Fig. 21b.

5.7 Opto-Coupler Isolation Circuit

The isolation is very important aspect between two circuits operating at different voltage level. The d-SPACE 1104 controller is supplying the PWM pulses to the

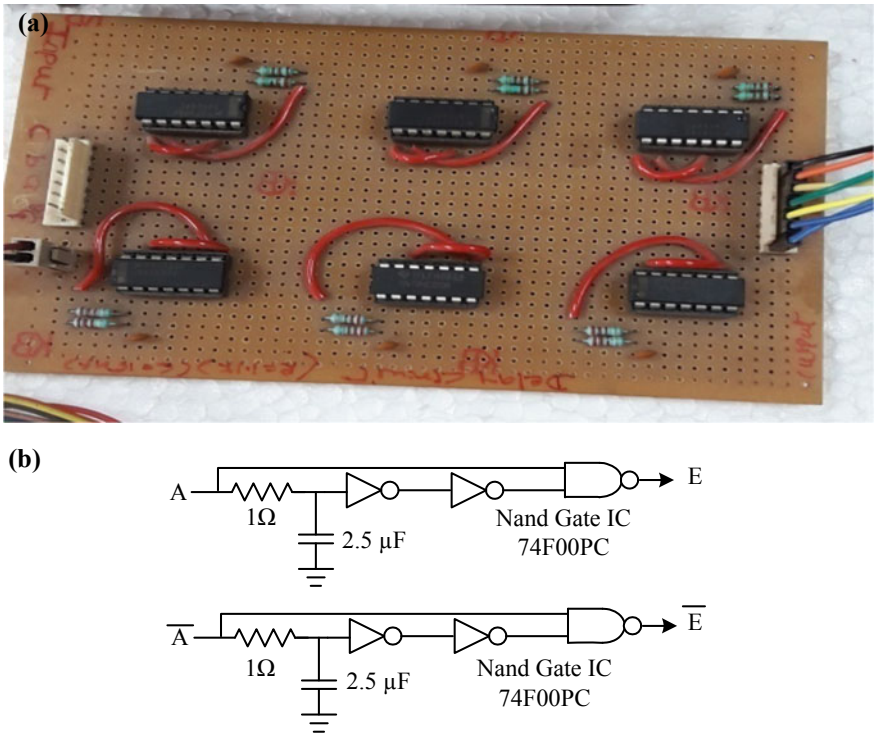

Fig. 21 **a** Photograph of dead band circuit **b** The circuit diagram of dead band circuit

dead band circuit. After creating the dead band of almost 2 microseconds between complementary pulses of in each phase, isolation circuit is needed for amplification of PWM pulses, providing isolation for gating of IGBTs of Semikron make VSC module. There are seven opto-coupler ICs 6N136, and a same number of transistor TL 2N2222 are used to configure this circuit. An opto-coupler ICs also require 0–5 V DC supply and transistor amplifier requires 0–15 V DC supply. The photograph and circuit diagram of isolation and amplification circuit are shown in Fig. 22a, b, respectively.

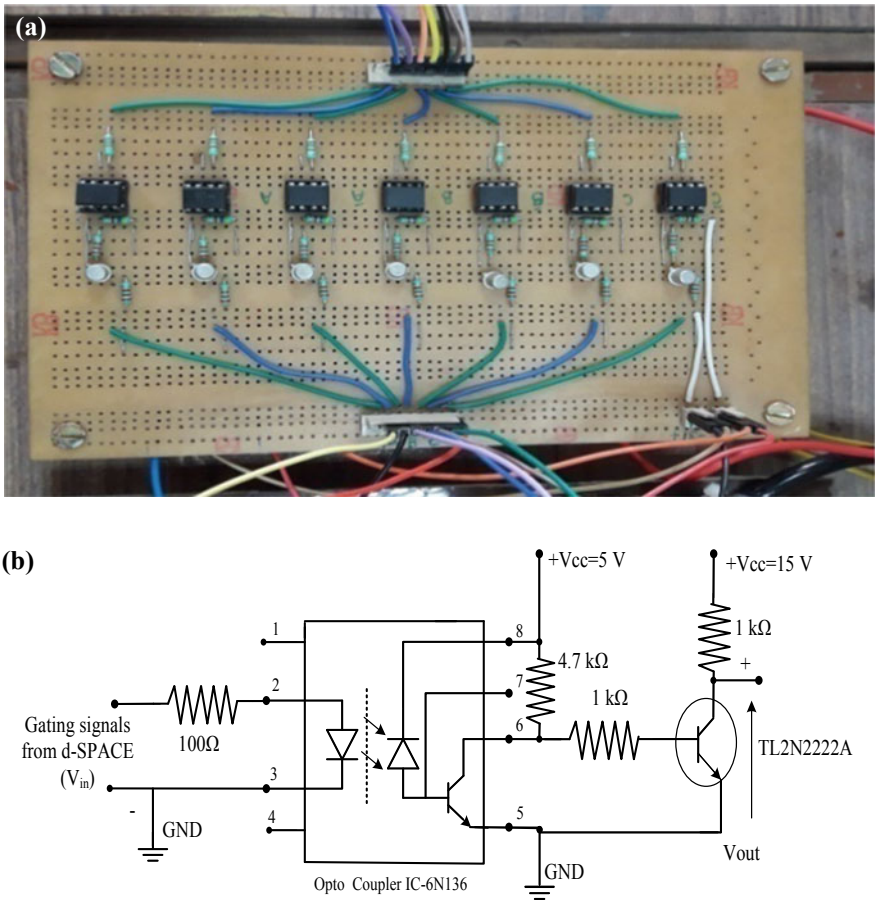

Fig. 22 **a** Photograph of the isolation circuit **b** the circuit diagram of the isolation circuit

5.8 Inverter Module

In distributed power generation system, the voltage source converter is major component. Therefore, 'Semikron' make intelligent power module (IPM) as shown in Fig. 23 is used as a voltage source converter. In this IPM, the driver circuit made by Skyper and DC bus capacitor is inbuilt with cooling fan. The converter is having bridge connection of IGBT modules (SKM GB 128DN). Each module of IGBTs contains two semiconductor switches connected in series and rated at 1200 V and 50 A. The voltage rating of driver circuit is 15 V with internal thermal overload protection and dead time features. The rating of DC bus capacitor used in the IPM is 1650 μF with its voltage capability of 750 V. The isolation and amplification circuit is also used for providing further protection.

5.9 BESS Unit

The battery unit is presented in Fig. 24 where 12-volt, 7.5 A, 36 cells are connected in series. Therefore, 434 V DC voltage is available at the input of the voltage source converter.

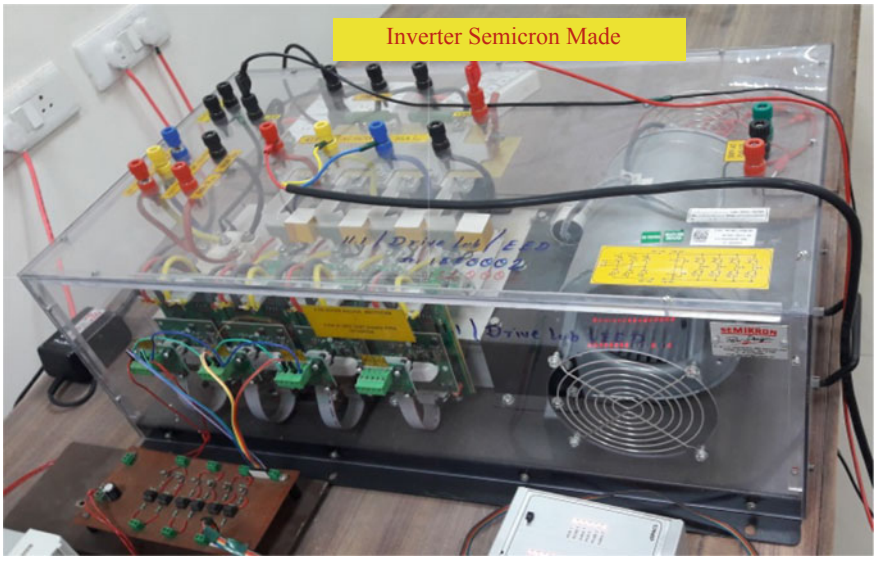

Fig. 23 Photograph of the four-leg IGBT module

Fig. 24 Photograph of the BESS

5.10 Experimental Set-up for Distributed Power Generation System

The individual components discussed above are arranged in the proper configuration to make the experimental set-up in the laboratory as shown in Fig. 25. The proposed control algorithms are built in d-SPACE 1104 platform and run in the control desk. The entire set-up is tested, and results are obtained satisfactory.

6 Test Results

Laboratory prototype of wind-based distributed generation system is developed, and Lorentzian norm-based adaptive Filter control (LAF), MLMS algorithm, VCO-less control AVF control and NAVF control algorithm are used to control the operation of VSC. The entire implementation is presented in four subsections. The complete set-up is tested experimentally on d-SPACE 1104 controller under nonlinear loading conditions. The results under dynamical conditions had been recorded. There are 8 channels of ADC and 8 channels of DAC. The first four ADC are multiplex in nature. The voltage-level capacity of ADC/DAC is 10 volts. The DG system had been studied under dynamical conditions as well as steady state. Moreover, input variations are also included, and test results are shown in Figs. 26, 27, 28 and 29. Dynamic of algorithms and SEIG is discussed as follows.

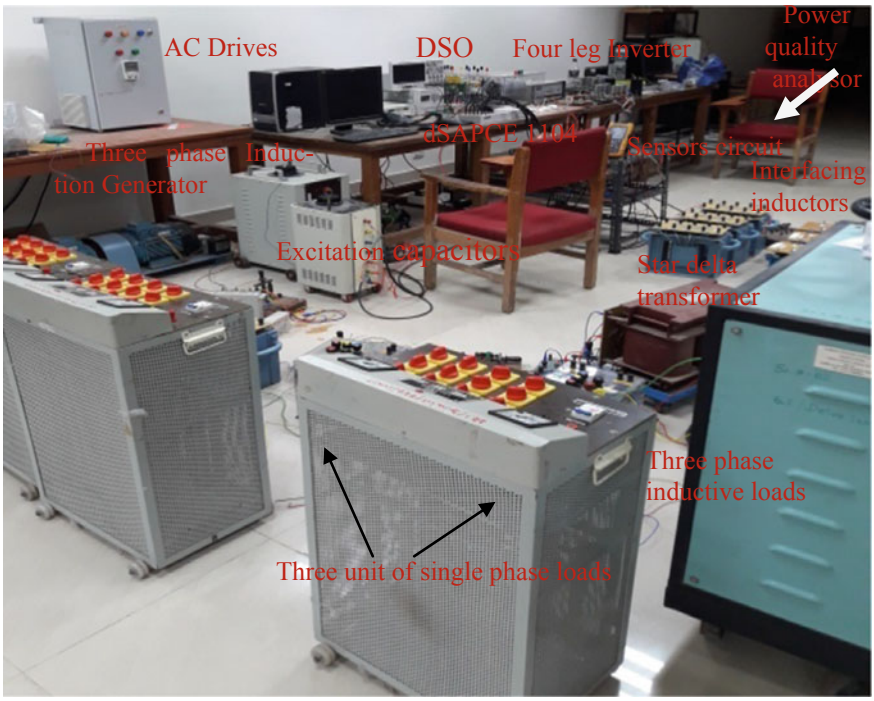

Fig. 25 Photograph of the experimental set-up

6.1 Performance of LAF-Based Control Algorithm

The experimental performance of Lorentzian adaptive filter (LAF) for power quality features in wind-based distributed generation system is carried out. The operating conditions include dynamic as well as steady-state operation of the system. The extraction process of fundamental component of load current for reference current estimation is also elaborated. The accuracy of dynamic performance of LAF for reference current estimation followed by gate pulse generation is also closely observed. The performance discussion is outlined below in the subsequent sections.

6.1.1 Control Signals Generation Using LAF Control Algorithms

The implementation of LAF control algorithm is carried out on d-SPACE 1104, and results are shown in Fig. 26a–d. The control signals generated in various stages of LAF control algorithm known as current error (e), unit template (u_{pa}) derived from the balanced phase voltages and load current (i_L) are shown in results. The Lorentzian objective function is minimized by means of square of error (e^2). These control signal parameters are illustrated in Fig. 26a. However, the active weight (w_{pa}) and reactive

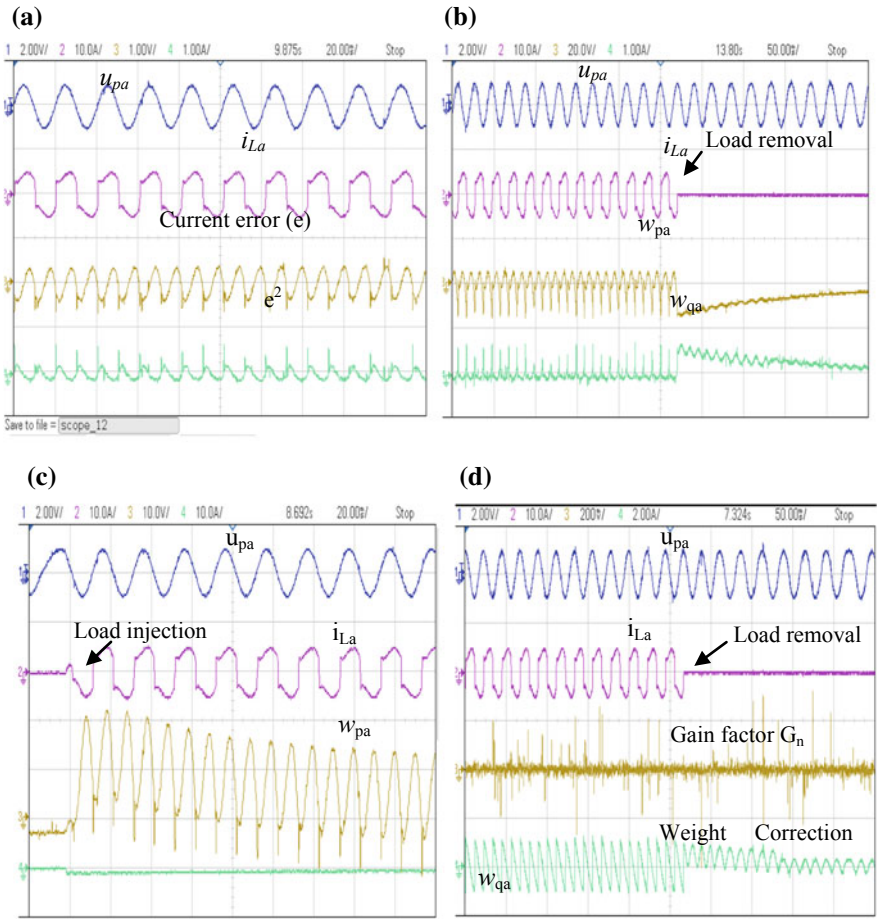

Fig. 26 **a** u_{pa}, i_{La}, e and e^2 **b** u_{pa}, i_{La}, w_{pa} and w_{qa} **c** u_{pa}, i_{La}, w_{pa} and w_{qa} **d** u_{pa}, i_{La}, gain factor (G_n), factor for error correction

weight (w_{qa}) of load current are estimated in the next stage. The estimated active as well as reactive weights of phase '*a*', load current (i_{La}), in-phase unit templates (u_{pa}) are displayed in Fig. 26b. For the load injection case, the same signals are displayed in Fig. 26c. The control signals at final stage of LAF control algorithm namely weight factors g_n (i) are estimated and are shown in Fig. 26d. Its normal range of variation lies between (0, 1), and it decreases as magnitude of the error increases.

6.1.2 Performance of DPG System Under Dynamic Condition

The performance of SEIG under nonlinear load variations is illustrated in Fig. 27a–h. The three-phase system voltage is measured with respect to neutral wire for power

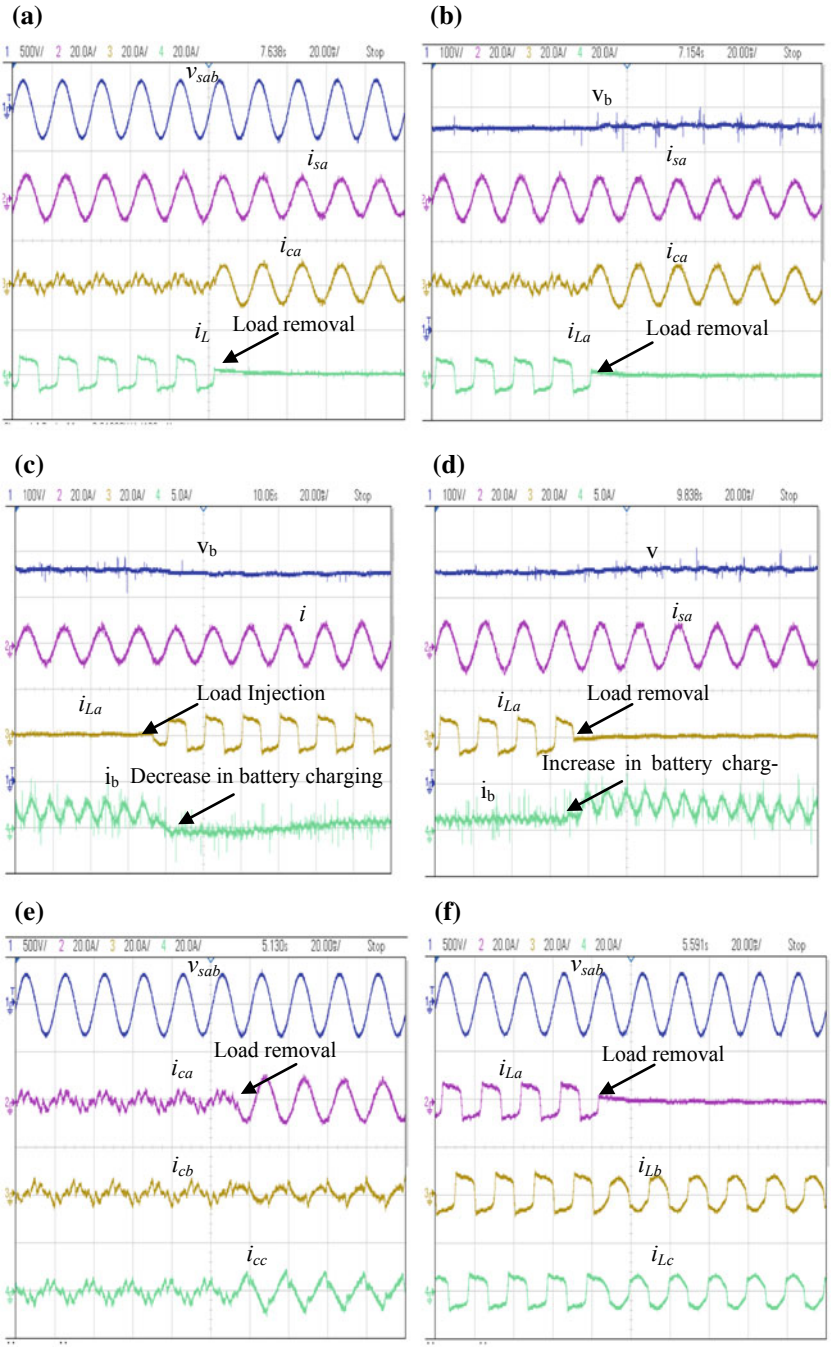

Fig. 27 Dynamic state results of DG system performance **a** waveforms of v_{sab}, i_{sa}, i_{ca}, i_{La} **b** waveforms of v_{sab}, i_{sa}, i_{ca}, i_{La} **c** waveforms of V_b, i_{sa}, i_{La}, i_b with load injection **d** waveforms of V_b, i_{sa}, i_{La}, i_b with load removal **e** waveforms of v_{sab}, i_{ca}, i_{cb}, i_{cc} **f** waveforms of v_{sab}, i_{La}, i_{Lb}, i_{Lc} **g** waveforms of v_{sab}, i_{sa}, i_{sb}, i_{sc} **h** waveforms of v_{sab}, i_{La}, i_{Ln}, i_{Tn} **i** waveforms of v_{sab}, P_g, P_L, i_b

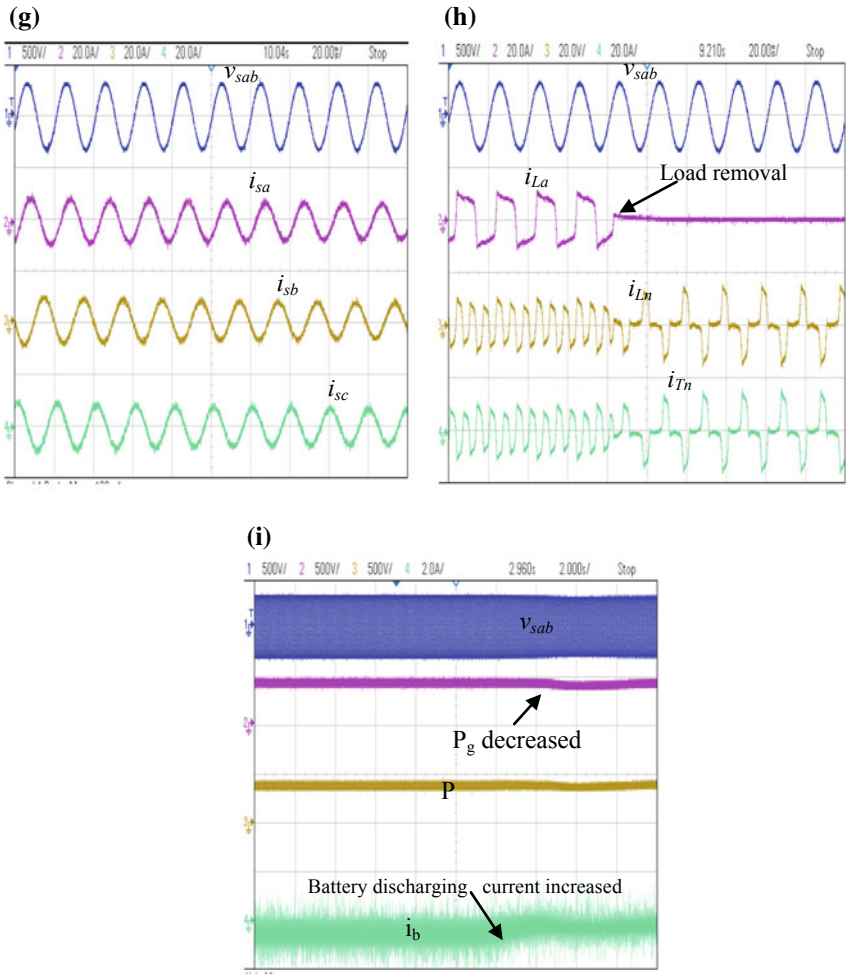

Fig. 27 (continued)

measurement only; otherwise for remaining results, it is line-to-line voltage of 235 V. The load dynamics with supply voltage (v_{sab}), source current (i_{sa}), load current (i_{La}) and compensator current (i_{ca}) of phase '*a*' are shown in Fig. 27a. The studies of battery terminal voltage (v_b), supply current with load variation (i_{La}) and compensator current (i_{ca}) have been shown in Fig. 27b. The dynamics of battery system is shown in Fig. 27c, d under the load current variation. From the results, it is evident that the battery either charge or discharge to balance the real power at PCC. The system dynamics related to PCC voltage (v_{sab}), compensator current (i_{ca}, i_{cb}, i_{cc}), load currents (i_{La}, i_{Lb}, i_{Lc}) and supply current (i_{sa}, i_{sb}, i_{sc}) have been presented in Fig. 27e–g under load unbalance. These are following kirchoff's current rule at the PCC. From these results, it is evident that all the supply currents are balance in magnitude and

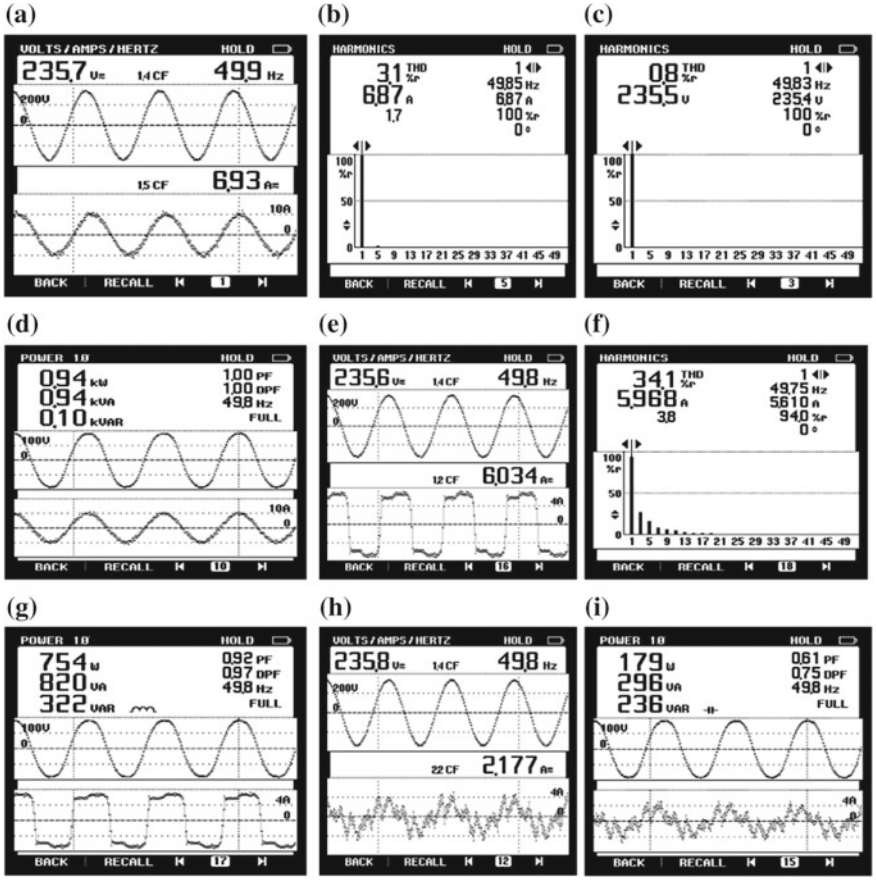

Fig. 28 Steady-state waveform and harmonic spectrum **a** V_{sa} and i_{sa} **b** THD of i_{sa} **c** THD of v_{sa} **d** Generator powers of phase '*a*' **e** V_{sa} and i_{La} **f** THD of i_{La} **g** Load powers of phase '*a*' **h** V_{sa} and i_{sa} **i** Compensator powers of phase '*a*'

phase despite the load disturbances. The waveforms of supply voltage (v_{sab}), transformer neutral current (i_{Tn}) and load neutral current (i_{Ln}) along with load currents are shown in Fig. 27h. In Fig. 27i, mechanical power is reduced at some moment and its effect on the phase–phase voltage (v_{sab}) is observed. It is evident from the results that line voltage remains constant due to proposed control's dynamic response.

6.1.3 Performance of DPG System Under Steady State

The performance of DG system under steady state is carried out, and results shown in Fig. 28a–i. In Fig. 28a, the supply current (i_{sa}) of phase '*a*' and supply voltage (v_{sab}) are shown. The THD in source current is recorded and is shown in Fig. 28b.

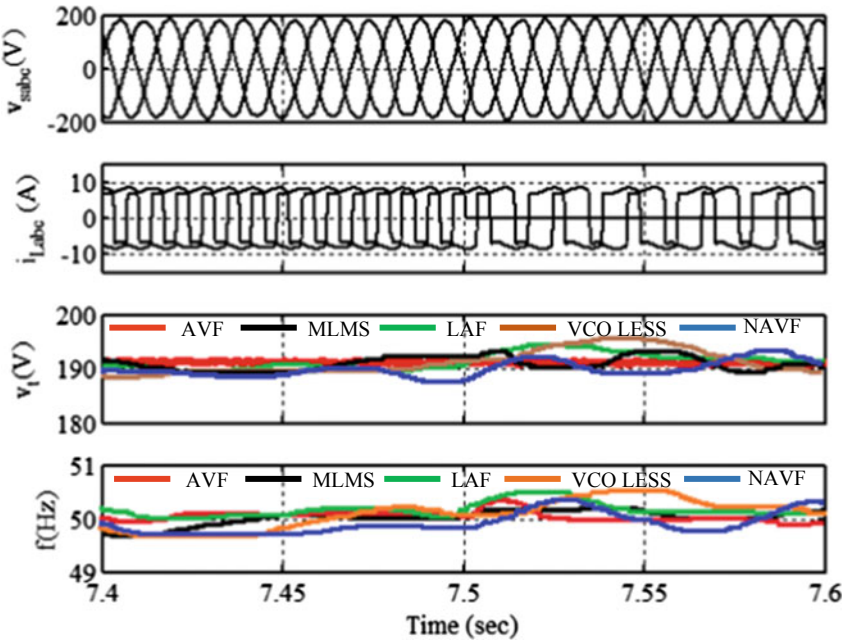

Fig. 29 Comparative analysis of LAF, MLMS, VCO-less PLL and AVF control algorithm implemented in three-phase SEIG

It is clear from the results that the THD in the source side current is 3.1% in steady state at rated load. This value is within the limit of IEEE Standards 519. In Fig. 28c, the THD of supply voltage is presented and this is 0.8% with 235.6 V RMS value phase to phase. The per phase steady-state power generated by generator is (0.94 kW, 0.94 KVA, 0.10 kVAR). It is revealed in Fig. 28d. The load current (i_{La}) waveform of phase 'a' along with PCC phase voltage of 'v_{sab}' is presented in Fig. 28e. Its THD is revealed in Fig. 28f.

Per phase of load power, compensator power and its waveform are presented in Fig. 28g–i. The steady-state execution of the generator under various operating conditions is found effective. Here, it can be said that the control response of LAF is also effective in nature.

7 Comparative Analysis of Control Algorithm in Three-Phase SEIG

The Lorentzian adaptive filter (LAF), momentum least mean square (M-LMS), VCO-less PLL, NAVF and adaptive vectorial filter (AVF) are implemented for power quality features in three-phase SEIG-based wind energy distributed power generation system, and results are compared on the basis of capability to track reference frequency and terminal voltage. The waveforms of load dynamics are shown here. The

transient in the load is introduced at the moment of 7.5 s, and the tracking response for frequency and terminal voltage is observed in each case. From the voltage and frequency response of the proposed controls, it is evident that adaptive vectorial filter (AVF) has performed relatively better in terms of settling time and peak overshoot. The other adopted control techniques have also shown the satisfactory response. From the experimental performance point of view, it was easy to implement due to less number of algebraic loop involved in the estimation of fundamental component of load current. The detailed comparison is provided below.

All the proposed controls have shown good performance within their operating constraints of stability on the basis of power quality indices. The results are shown in Fig. 29 and are tabulated in Table 4.

Table 4 Detailed comparative analysis of proposed controls

Proposed controls	Settling time (s)		Steady-state error		Sampling time required (μS)	Remarks
	v_t	f	v_t (%)	f (%)		
LAF	Less than 0.03	Less than 0.06	0.8	0.4	60	It has shown stable operation for wide range wind speed fluctuation as well as less noisy nonlinear loads
M-LMS	Less than 0.09	Less than 0.01	0.75	0.5	70	It has shown stable operation for narrow range wind speed fluctuation as well as noisy nonlinear loads
VCO-less PLL	Less than 0.08	Less than 0.10	0.5	1.05	60	It has shown more stable operation for narrow range wind speed fluctuation and less noisy loads

(continued)

Table 4 (continued)

Proposed controls	Settling time (s)		Steady-state error		Sampling time required (μS)	Remarks
	v_t	f	v_t (%)	f (%)		
AVF	Less than 0.02	Less than 0.02	0.25	0.4	45	It has shown stable operation for wide range wind speed fluctuation as well as noisy nonlinear loads
NAVF	Less than 0.06	Less than 0.08	0.45	0.8	120	It has shown stable operation for wide range wind speed fluctuation as well as noisy nonlinear loads. However, it requires high-speed processor

8 Conclusion

This review work is carried out based on control algorithm implementation in wind energy-driven standalone distributed power generation system. The power quality issues in three-phase system comprising self-excited induction generator had been the focal point of discussion. Some control algorithms stated above are implemented, and results obtained are as per IEEE-519-2014 standards. The total harmonic distortion in the current and voltage is less than 5% that is the standard requirement. The comparison of dynamic results of all control algorithms is also presented in the subsequent section, and results are shown. From the results, it is evident that AVF control algorithm is performing better than other adopted control algorithms in this work.

Appendix

A1. Three-Phase SEIG Rating and Parameters

Ratings: 4-pole, 50 Hz, 230 V and 3.7 kW;

Parameters: Rotor and stator resistance per phase $R_r = 0.4816\ \Omega$ and $R_s = 2.93\ \Omega$, rotor and mutual inductance $L_r = 0.002016$ H and $L_m = 0.0267544$ H, constant of friction = 0.0023, Inertia constant (H) = 0.0011 J (Kg m^2),

Capacitor for excitation (C_{eg}) = 4000 VAR;

A2. Compensator parameters: $L_s = 10$ mH; $C_{dc} = 2300\ \mu$F, Six IGBT having 1200 V, 50 A.

A3. BESS: Lithium-ion type, 400 V, 7.5 AH, SOC (10–90%), $r_s = 0.05\ \Omega$

A4. Nonlinear load in phases '*a*', '*b*' and phase '*c*': Diode bridge *ac*/*dc* converter with $R = 30\ \Omega$, $L = 100$ mH in each phase.

Wind turbine simulation parameters [3]: 5 kW, radius of blades $r = 1.4$ m, C_P (λ, β) = 0.87, $V_W = 12.5$ m/s and $\rho = 0.48$.

References

1. Simoes M, Farret F (2008) Alternate energy systems, design and analysis with induction generators, 2nd edn. CRC Press, Tailor and Fransis, London
2. Lai L, Chan T (2007) Distributed generation: induction and permanent magnet generators. Wiley, London
3. Fox B, Flynn D (2007) Wind power integration connection and system operational aspects. The Institution of Engineering and Technology, London, United Kingdom
4. Chapallaz J (1992) Manual on induction motors used as generators. Vieweg, Braunschweig
5. Stiebler M (2008) Wind energy systems for electric power generation. Green energy and technology. Springer, Berlin
6. IEEE (1993) 519–1992 IEEE recommended practices and requirements for harmonic control in electrical power systems. ISBN-978-0-7381-0915-2
7. Borbely A, Kreider J (2001) Distributed generation: the power paradigm for the new millennium. CRC Press, Boca Raton, Florida (USA)
8. Jha A (2011) Wind turbine technology. CRC Press, Taylor and Fransis Group, London
9. Boldea I (2016) Synchronous generators hand book. CRC Press, Tailor and Fransis Group
10. Akagi H, Kanazawa Y, Nabae A (1983) Generalized theory of the instantaneous reactive power in three-phase circuits. In: Proceeding IEEE/JIEE international power electronics conference (IPEC'83), pp 821–827
11. Singh B, Verma V (2008) Selective compensation of power-quality problems through active power filter by current decomposition. IEEE Trans Power Delivery 23:792–799. https://doi.org/10.1109/tpwrd.2007.911108
12. Valdez-Fernandez A, Martinez-Rodriguez P, Escobar G et al (2013) A model-based controller for the cascade H-bridge multilevel converter used as a shunt active filter. IEEE Trans Industr Electron 60:5019–5028. https://doi.org/10.1109/tie.2012.2218558
13. Al Chaer T, Gaubert J, Rambault L, Najjar M (2009) Linear feedback control of a parallel active harmonic conditioner in power systems. IEEE Trans Power Electron 24:641–653. https://doi.org/10.1109/tpel.2008.2008186

14. Rao U, Mishra M, Ghosh A (2008) Control strategies for load compensation using instantaneous symmetrical component theory under different supply voltages. IEEE Trans Power Delivery 23:2310–2317. https://doi.org/10.1109/tpwrd.2008.923053
15. Singh B, Arya S (2014) Back-propagation control algorithm for power quality improvement using DSTATCOM. IEEE Trans Industr Electron 61:1204–1212. https://doi.org/10.1109/tie.2013.2258303
16. Luo A, Xu X, Fang L et al (2010) Feedback-feedforward PI-type iterative learning control strategy for hybrid active power filter with injection circuit. IEEE Trans Industr Electron 57:3767–3779. https://doi.org/10.1109/tie.2010.2040567
17. Zou Z, Zhou K, Wang Z, Cheng M (2015) Frequency-adaptive fractional-order repetitive control of shunt active power filters. IEEE Trans Industr Electron 62:1659–1668. https://doi.org/10.1109/tie.2014.2363442
18. Sreeraj ES, Prejith EK, Chatterjee K, Bandyopadhyay S (2014) An active harmonic filter based on one-cycle control. IEEE Trans Ind Electron 61:3799–3809. https://doi.org/10.1109/tie.2013.2286558
19. Kanjiya P, Khadkikar V, Zeineldin H (2013) A noniterative optimized algorithm for shunt active power filter under distorted and unbalanced supply voltages. IEEE Trans Industr Electron 60:5376–5390. https://doi.org/10.1109/tie.2012.2235394
20. Singh B, Raj Arya S (2013) Composite observer-based control algorithm for distribution static compensator in four-wire supply system. IET Power Electron 6:251–260. https://doi.org/10.1049/iet-pel.2012.0412
21. Yazdani D, Bakhshai A, Joos G (2008) A real-time sequence components decomposition for transient analysis in grid-connected distributed generation systems. In: Proceedings IEEE symposium on industrial electronics, pp 1651–1656
22. Yazdani D, Mojiri M, Bakhshai A, Joos G (2009) A fast and accurate synchronization technique for extraction of symmetrical components. IEEE Trans Power Electron 24:674–684. https://doi.org/10.1109/tpel.2008.2010321
23. Cirrincione M, Pucci M, Vitale G, Miraoui A (2009) Current harmonic compensation by a single-phase shunt active power filter controlled by adaptive neural filtering. IEEE Trans Industr Electron 56:3128–3143. https://doi.org/10.1109/tie.2009.2022070
24. Tey L, So P, Chu Y (2005) Improvement of power quality using adaptive shunt active filter. IEEE Trans Power Delivery 20:1558–1568. https://doi.org/10.1109/tpwrd.2004.838641
25. Huang Shyh-Jier, Jinn-Chang Wu (1999) A control algorithm for three-phase three-wired active power filters under nonideal mains voltages. IEEE Trans Power Electron 14:753–760. https://doi.org/10.1109/63.774215
26. Tolbert LM, Hablter TG (2000) Comparison of time-based non-active power definitions for active filtering. In: Proceedings of CIEP, Acapulco, Mexico, pp 73–79
27. Cardenas V, Moran L, Bahamondes A, Dixon J (2003) Comparative study of real time reference generation techniques forfour-wire shunt active power filters. In: Proceedings of IEEE (PESC), Acapulco, Mexico, pp 791–796
28. Chilipi R, Singh B, Murthy S (2014) Performance of a self-excited induction generator with DSTATCOM-DTC drive-based voltage and frequency controller. IEEE Trans Energy Convers 29:545–557. https://doi.org/10.1109/tec.2014.2321184
29. Kasal G, Singh B (2011) Voltage and frequency controllers for an asynchronous generator-based isolated wind energy conversion system. IEEE Trans Energy Convers 26:402–416. https://doi.org/10.1109/tec.2010.2102029
30. Ouazenne L, McPherson G (1983) Analysis of the Isolated Induction generator. IEEE Power Eng Rev PER 3:59–59. https://doi.org/10.1109/mper.1983.5518898
31. Alolah A, Alkanhal M (2000) Optimization-based steady state analysis of three phase self-excited induction generator. IEEE Trans Energy Convers 15:61–65. https://doi.org/10.1109/60.849117
32. Al Jabri A, Alolah A (1990) Capacitance requirement for isolated self-exicted induction generator. IEE Proc B Electr Power Appl 137:154. https://doi.org/10.1049/ip-b.1990.0016

33. Murthy S, Singh B, Sandeep V (2012) A novel and comprehensive performance analysis of a single-phase two-winding self-excited induction generator. IEEE Trans Energy Convers 27:117–127. https://doi.org/10.1109/tec.2011.2170072
34. Singh B, Kasal G, Chandra A, Haddad KA (2007) Battery based voltage and frequency controller for parallel operated isolated asynchronous generators. In: Proceedings of IEEE international symposium on industrial electronics (ISIE-2007), Vigo, Spain
35. Rajagopal V, Singh B, Kasal G (2011) Electronic load controller with power quality improvement of isolated induction generator for small hydro power generation. IET Renew Power Gener 5:202. https://doi.org/10.1049/iet-rpg.2010.0081
36. Kalla U, Singh B, Murthy S (2014) Normalised adaptive linear element-based control of single-phase self excited induction generator feeding fluctuating loads. IET Power Electron 7:2151–2160. https://doi.org/10.1049/iet-pel.2013.0652
37. Singh B, Murthy S, Gupta S (2006) A voltage and frequency controller for self-excited induction generators. Electr Power Compon Syst 34:141–157. https://doi.org/10.1080/15325000500244567
38. Singh B, Murthy SS, Gupta S (2005) An electronic voltage and frequency controller for single-phase self-excited induction generators for pico hydro applications. Proc IEEE Power Electron Drives Syst Conf 1:240–245
39. Yazdani D, Bakhshai A, Jain P (2010) A three-phase adaptive notch filter-based approach to harmonic/reactive current extraction and harmonic decomposition. IEEE Trans Power Electron 25:914–923. https://doi.org/10.1109/tpel.2009.2036621
40. Mojiri M, Bakhshai A (2007) Stability analysis of periodic orbit of an adaptive notch filter for frequency estimation of a periodic signal. Automatica 43:450–455. https://doi.org/10.1016/j.automatica.2006.08.018
41. Yin G, Guo L, Li X (2013) An amplitude adaptive notch filter for grid signal processing. IEEE Trans Power Electron 28:2638–2641. https://doi.org/10.1109/tpel.2012.2226752
42. Blaabjerg F, Teodorescu R, Liserre M, Timbus A (2006) Overview of control and grid synchronization for distributed power generation systems. IEEE Trans Industr Electron 53:1398–1409. https://doi.org/10.1109/tie.2006.881997
43. Rao U, Mishra M, Ghosh A (2008) Control strategies for load compensation using instantaneous symmetrical component theory under different supply voltages. IEEE Trans Power Deliv 23:2310–2317. https://doi.org/10.1109/tpwrd.2008.923053
44. Karimi-Ghartemani M, Karimi H, Bakhshai A (2009) A filtering technique for three-phase power systems. IEEE Trans Instrum Meas 58:389–396. https://doi.org/10.1109/tim.2008.2003331
45. Arya S, Singh B (2013) Performance of DSTATCOM using leaky LMS control algorithm. IEEE J Emerg Sel Top Power Electron 1:104–113. https://doi.org/10.1109/jestpe.2013.2266372
46. Shinnaka S (2008) A robust single-phase PLL system with stable and fast tracking. IEEE Trans Ind Appl 44:624–633. https://doi.org/10.1109/tia.2008.916750
47. Guo X, Wu W, Chen Z (2011) Multiple-complex coefficient-filter-based phase-locked loop and synchronization technique for three-phase grid-interfaced converters in distributed utility networks. IEEE Trans Industr Electron 58:1194–1204. https://doi.org/10.1109/tie.2010.2041738
48. Arablouei R, Werner S, Dogancay K (2014) Analysis of the gradient-descent total least-squares adaptive filtering algorithm. IEEE Trans Signal Process 62:1256–1264. https://doi.org/10.1109/tsp.2014.2301135
49. Shuai Z, Luo A, Tu C, Liu D (2011) New control method of injection-type hybrid active power filter. IET Power Electron 4:1051. https://doi.org/10.1049/iet-pel.2010.0353
50. Bhattacharya A, Chakraborty C, Bhattacharya S (2009) Shunt compensation. IEEE Ind Electron Mag 3:38–49. https://doi.org/10.1109/mie.2009.933881
51. Suresh Y, Panda A, Suresh M (2012) Real-time implementation of adaptive fuzzy hysteresis-band current control technique for shunt active power filter. IET Power Electron 5:1188–1195. https://doi.org/10.1049/iet-pel.2011.0371

52. Wu J, Jou H, Feng Y et al (2007) Novel circuit topology for three-phase active power filter. IEEE Trans Power Delivery 22:444–449. https://doi.org/10.1109/tpwrd.2006.881416
53. Bristow D, Tharayil M, Alleynea A (2006) Learning-based method for high-performance tracking control. IEEE Control Syst Mag 96–114
54. Vazquez S, Sanchez J, Reyes M et al (2014) Adaptive vectorial filter for grid synchronization of power converters under unbalanced and/or distorted grid conditions. IEEE Trans Industr Electron 61:1355–1367. https://doi.org/10.1109/tie.2013.2258302
55. Wang X, Sun L, Wen F, Salam MA, Ang SP (2015) Control strategies of battery energy storage systems for smoothing wind power fluctuations. In: 10th International conference on advances in power system control, operation and management (APSCOM 2015), Hongkong, China
56. Godavarti M, Hero A (2005) Partial update LMS algorithms. IEEE Trans Signal Process 53:2382–2399. https://doi.org/10.1109/tsp.2005.849167
57. Kohli A, Mehra D (2006) Tracking of time-varying channels using two-step LMS-type adaptive algorithm. IEEE Trans Signal Process 54:2606–2615. https://doi.org/10.1109/tsp.2006.874779
58. Choi Y, Shin H, Song W (2006) Robust regularization for normalized LMS algorithms. IEEE Trans Circuits Syst II Express Briefs 53:627–631. https://doi.org/10.1109/tcsii.2006.877280
59. Das D, Mohapatra S, Routray A, Basu T (2006) Filtered-s LMS algorithm for multichannel active control of nonlinear noise processes. IEEE Trans Audio Speech Lang Process 14:1875–1880. https://doi.org/10.1109/tsa.2005.858543
60. Das D, Kuo S, Panda G (2007) New block filtered-X LMS algorithms for active noise control systems. IET Signal Proc 1:73–81. https://doi.org/10.1049/iet-spr:20060220
61. Vega L, Rey H, Benesty J, Tressens S (2009) A fast robust recursive least-squares algorithm. IEEE Trans Signal Process 57:1209–1216. https://doi.org/10.1109/tsp.2008.2010643
62. Bhotto M, Antoniou A (2011) Robust recursive least-squares adaptive-filtering algorithm for impulsive-noise environments. IEEE Signal Process Lett 18:185–188. https://doi.org/10.1109/lsp.2011.2106119
63. Singh B, Arya S (2013) Adaptive theory-based improved linear sinusoidal tracer control algorithm for DSTATCOM. IEEE Trans Power Electron 28:3768–3778. https://doi.org/10.1109/tpel.2012.2228884
64. Foley J, Boland F (1987) Comparison between steepest descent and LMS algorithms in adaptive filters. IEE Proc F Commun Radar Signal Process 134:283. https://doi.org/10.1049/ip-f-1.1987.0056
65. Gorriz J, Ramirez J, Cruces-Alvarez S et al (2009) A novel LMS algorithm applied to adaptive noise cancellation. IEEE Signal Process Lett 16:34–37. https://doi.org/10.1109/lsp.2008.2008584
66. Srar J, Chung KS, Mansour A (2010) Adaptive array beam forming using a combined LMS-LMS algorithm. IEEE Trans Antennas Propag 58:3545–3557. https://doi.org/10.1109/tap.2010.2071361
67. Zanella A, Chiani M, Win M (2011) Statistical analysis of steepest descend and LMS detection algorithms for MIMO systems. IEEE Trans Veh Technol 60:4667–4672. https://doi.org/10.1109/tvt.2011.2170185
68. Andrade J Jr, de Campos M, Apolinário J Jr (2019) L1-constrained normalized LMS algorithms for adaptive beam forming. IEEE Trans Signal Process 63:6524–6539
69. Das B, Chakraborty M (2014) Sparse adaptive filtering by an adaptive convex combination of the LMS and the ZA-LMS algorithms. IEEE Trans Circuits Syst I Regul Pap 61:1499–1507. https://doi.org/10.1109/tcsi.2013.2289407
70. Chien Y, Tseng W (2013) Switching-based variable step-size approach for partial update LMS algorithms. Electron Lett 49:1081–1083. https://doi.org/10.1049/el.2013.1762
71. Eweda E, Bershad N (2017) Stochastic analysis of the signed LMS algorithms for cyclostationary white gaussian inputs. IEEE Trans Signal Process 65:1673–1684. https://doi.org/10.1109/tsp.2016.2646666

72. Kelly J, Siewiorek D, Smailagic A, Wang W (2016) An adaptive filter for the removal of drifting sinusoidal noise without a reference. IEEE J Biomed Health Inform 20:213–221. https://doi.org/10.1109/jbhi.2014.2375318
73. Das R, Narwaria M (2017) Lorentzian based adaptive filters for impulsive noise environments. IEEE Trans Circuits Syst I Regul Pap 64:1529–1539. https://doi.org/10.1109/tcsi.2017.2667705
74. Narasimhan S, Veena S, Lokesha H (2009) Variable step-size Griffiths' algorithm for improved performance of feedforward/feedback active noise control. SIViP 4:309–317. https://doi.org/10.1007/s11760-009-0120-9
75. Chan T, Lai L, Yan Lie-Tong (2003) Finite element analysis of a single-phase grid-connected induction generator with the Steinmetz connection. IEEE Trans Energy Convers 18:321–329. https://doi.org/10.1109/tec.2003.811737
76. Sayed A (2003) Fundamentals of adaptive filtering. IEEE Press [u.a.], [Piscataway, NJ]
77. Koike S (1997) Adaptive threshold nonlinear algorithm for adaptive filters with robustness against impulse noise. IEEE Trans Signal Process 45:2391–2395. https://doi.org/10.1109/78.622963
78. Carrillo R, Barner K, Aysal T (2010) Robust sampling and reconstruction methods for sparse signals in the presence of impulsive noise. IEEE J Sel Top Signal Process 4:392–408. https://doi.org/10.1109/jstsp.2009.2039177
79. Das RL, Chakraborty M (2012) Sparse adaptive filters—an overview and some new results. In: Proceedings of ISCAS, Seoul, South Korea, pp 2745–2748
80. Shao Tiange, Zheng Y, Benesty J (2010) An affine projection sign algorithm robust against impulsive interferences. IEEE Signal Process Lett 17:327–330. https://doi.org/10.1109/lsp.2010.2040203
81. Singh B, Rajagopal V (2011) Neural-network-based integrated electronic load controller for isolated asynchronous generators in small hydro generation. IEEE Trans Industr Electron 58:4264–4274. https://doi.org/10.1109/tie.2010.2102313
82. Bhotto Z, Antoniou A (2013) A family of shrinkage adaptive-filtering algorithms. IEEE Trans Signal Process 61:1689–1697. https://doi.org/10.1109/tsp.2012.2236831
83. Rey Vega L, Rey H, Benesty J, Tressens S (2008) A new robust variable step-size NLMS algorithm. IEEE Trans Signal Process 56:1878–1893. https://doi.org/10.1109/tsp.2007.913142
84. Gansler T, Gay S, Sondhi G, Benesty J (2000) Double-talk robust fast converging algorithms for network echo cancellation. IEEE Trans Speech Audio Process 8:656–663. https://doi.org/10.1109/89.876299
85. Kuruoğlu E, Rayner P, Fitzgerald W (1998) Least Lp-norm impulsive noise cancellation with polynomial filters. Sig Process 69:1–14. https://doi.org/10.1016/s0165-1684(98)00083-8
86. Sayin M, Vanli N, Kozat S (2014) A novel family of adaptive filtering algorithms based on the logarithmic cost. IEEE Trans Signal Process 62:4411–4424. https://doi.org/10.1109/tsp.2014.2333559
87. Chen WL, Lin YH, Gau HS, Yu CH (2008) STATCOM Controls for a self-excited induction generator feeding random loads. IEEE Trans Power Delivery 23:2207–2215. https://doi.org/10.1109/tpwrd.2008.923160
88. Chilipi R, Murthy S, Madishetti S et al (2014) Design and implementation of dynamic electronic load controller for three-phase self-excited induction generator in remote small-hydro power generation. IET Renew Power Gener 8:269–280. https://doi.org/10.1049/iet-rpg.2013.0087
89. Sharma S, Singh B (2014) Asynchronous generator with battery storage for standalone wind energy conversion system. IEEE Trans Ind Appl 50:2760–2767. https://doi.org/10.1109/tia.2013.2295475
90. Chauhan P, Chatterjee J, Bhere H et al (2015) Synchronized operation of DSP-based generalized impedance controller with variable-speed isolated SEIG for novel voltage and frequency control. IEEE Trans Ind Appl 51:1845–1854. https://doi.org/10.1109/tia.2014.2356642

91. Das R, Chakraborty M (2015) On convergence of proportionate-type normalized least mean square algorithms. IEEE Trans Circuits Syst II Express Briefs 62:491–495. https://doi.org/10.1109/tcsii.2014.2386261
92. Kim S, Jeong J, Koo G, Kim S (2016) Robust convex combination of affine projection-type algorithms using an impulsive noise indicator. Sig Process 129:33–37. https://doi.org/10.1016/j.sigpro.2016.05.034
93. Huang F, Zhang J, Zhang S (2016) Combined-step-size affine projection sign algorithm for robust adaptive filtering in impulsive interference environments. IEEE Trans Circuits Syst II Express Briefs 63:493–497. https://doi.org/10.1109/tcsii.2015.2505067
94. Singh B, Sharma S (2012) Stand-alone single-phase power generation employing a three-phase isolated asynchronous generator. IEEE Trans Ind Appl 48:2414–2423. https://doi.org/10.1109/tia.2012.2227136
95. Widrow B, Walach E (1984) On the statistical efficiency of the LMS algorithm with nonstationary inputs. IEEE Trans Inf Theory 30:211–221. https://doi.org/10.1109/tit.1984.1056892
96. Patel S, Arya S, Maurya R (2017) Nonlinear adaptive Volterra filter for control of distribution static compensator. IEEE J Emerg Sel Top Power Electron 5:559–567. https://doi.org/10.1109/jestpe.2016.2633481
97. Sharma P, Bhatti T (2013) Performance investigation of isolated wind-diesel hybrid power systems with WECS having PMIG. IEEE Trans Industr Electron 60:1630–1637. https://doi.org/10.1109/tie.2011.2175672
98. Pathak G, Singh B, Panigrahi B (2016) Control of wind-diesel microgrid using affine projection-like algorithm. IEEE Trans Industr Inf 12:524–531. https://doi.org/10.1109/tii.2016.2518643
99. Chittora P, Singh A, Singh M (2017) Gauss–Newton-based fast and simple recursive algorithm for compensation using shunt active power filter. IET Gener Transm Distrib 11:1521–1530. https://doi.org/10.1049/iet-gtd.2016.1222
100. Roy S, Shynk J (1990) Analysis of the momentum LMS algorithm. IEEE Trans Acoust Speech Signal Process 38:2088–2098. https://doi.org/10.1109/29.61535
101. Sharma R, Sethares W, Bucklew J (1998) Analysis of momentum adaptive filtering algorithms. IEEE Trans Signal Process 46:1430–1434. https://doi.org/10.1109/78.668805
102. Niwas R, Jain C, Goel S, Singh B (2015) Unity power factor operation and neutral current compensation of diesel generator set feeding three-phase four-wire loads. IET Gener Transm Distrib 9:1738–1746. https://doi.org/10.1049/iet-gtd.2014.0745
103. Tong Li, XudongZou ShuShuaiFeng et al (2014) An SRF-PLL-based sensorless vector control using the predictive deadbeat algorithm for the direct-driven permanent magnet synchronous generator. IEEE Trans Power Electron 29:2837–2849. https://doi.org/10.1109/tpel.2013.2272465
104. Geng H, Xu D, Wu B (2011) A novel hardware-based all-digital phase-locked loop applied to grid-connected power converters. IEEE Trans Industr Electron 58:1737–1745. https://doi.org/10.1109/tie.2010.2053338
105. Chen L (2004) PLL-based battery charge circuit topology. IEEE Trans Industr Electron 51:1344–1346. https://doi.org/10.1109/tie.2004.837891
106. Barbosa Rolim L, Rodrigues da Costa D, Aredes M (2006) Analysis and software implementation of a robust synchronizing PLL circuit based on the pq theory. IEEE Trans Industr Electron 53:1919–1926. https://doi.org/10.1109/tie.2006.885483
107. Luna A, Rocabert J, Candela J et al (2015) Grid voltage synchronization for distributed generation systems under grid fault conditions. IEEE Trans Ind Appl 51:3414–3425. https://doi.org/10.1109/tia.2015.2391436
108. Ama N, Martinz F, Matakas L, Kassab F (2013) Phase-locked loop based on selective harmonics elimination for utility applications. IEEE Trans Power Electron 28:144–153. https://doi.org/10.1109/tpel.2012.2195506
109. Freijedo F, Yepes A, Lopez Ó et al (2011) An optimized implementation of phase locked loops for grid applications. IEEE Trans Instrum Meas 60:3110–3119. https://doi.org/10.1109/tim.2011.2122550

110. Chung SK (2000) A phase tracking system for three phase utility interface inverters. IEEE Trans Power Electron 15:431–438. https://doi.org/10.1109/63.844502
111. Chung S (2000) Phase-locked loop for grid-connected three-phase power conversion systems. IEE Proc Electr Power Appl 147:213. https://doi.org/10.1049/ip-epa:20000328
112. Freijedo F, Doval-Gandoy J, Lopez O, Acha E (2009) Tuning of phase-locked loops for power converters under distorted utility conditions. IEEE Trans Ind Appl 45:2039–2047. https://doi.org/10.1109/tia.2009.2031790
113. Gonzalez-Espin F, Figueres E, Garcera G (2012) An adaptive synchronous-reference-frame phase-locked loop for power quality improvement in a polluted utility grid. IEEE Trans Industr Electron 59:2718–2731. https://doi.org/10.1109/tie.2011.2166236
114. Hadjidemetriou L, Kyriakides E, Blaabjerg F (2015) A robust synchronization to enhance the power quality of renewable energy systems. IEEE Trans Industr Electron 62:4858–4868. https://doi.org/10.1109/tie.2015.2397871
115. Aiello M, Cataliotti A, Cosentino V, Nuccio S (2007) Synchronization techniques for power quality instruments. IEEE Trans Instrum Meas 56:1511–1519. https://doi.org/10.1109/tim.2007.903585
116. Li W, Ruan X, Bao C et al (2014) Grid synchronization systems of three-phase grid-connected power converters: a complex-vector-filter perspective. IEEE Trans Industr Electron 61:1855–1870. https://doi.org/10.1109/tie.2013.2262762
117. Park Y, Sul S, Kim W, Lee H (2014) Phase-locked loop based on an observer for grid synchronization. IEEE Trans Ind Appl 50:1256–1265. https://doi.org/10.1109/tia.2013.2279194
118. Golestan S, Guerrero J, Vasquez J (2017) Three-phase PLLs: a review of recent advances. IEEE Trans Power Electron 32:1894–1907. https://doi.org/10.1109/tpel.2016.2565642
119. Zheng L, Geng H, Yang G (2016) Fast and robust phase estimation algorithm for heavily distorted grid conditions. IEEE Trans Industr Electron 63:6845–6855. https://doi.org/10.1109/tie.2016.2585078
120. BarghiLatran M, Yoldaş Y, Teke A (2015) Mitigation of power quality problems using distribution static synchronous compensator: a comprehensive review. IET Power Electronics 8:1312–1328. https://doi.org/10.1049/iet-pel.2014.0531
121. Sebastián R (2016) Application of a battery energy storage for frequency regulation and peak shaving in a wind diesel power system. IET Gener Transm Distrib 10:764–770. https://doi.org/10.1049/iet-gtd.2015.0435
122. Jou H, Wu J, Wu K et al (2005) Analysis of zig-zag transformer applying in the three-phase four-wire distribution power system. IEEE Trans Power Delivery 20:1168–1173. https://doi.org/10.1109/tpwrd.2005.844281
123. Singh B, Sharma S (2012) Design and implementation of four-leg voltage-source-converter-based VFC for autonomous wind energy conversion system. IEEE Trans Industr Electron 59:4694–4703. https://doi.org/10.1109/tie.2011.2179271
124. Perales M, Mora J, Carrasco J, Franquelo L (2001) A novel control method for active filters, based on filtered current. In: 2001 IEEE 32nd annual power electronics specialists conference (IEEE Cat No01CH37230). https://doi.org/10.1109/pesc.2001.954317
125. Rodriguez P, Luna A, Candela I et al (2011) Multiresonant frequency-locked loop for grid synchronization of power converters under distorted grid conditions. IEEE Trans Industr Electron 58:127–138. https://doi.org/10.1109/tie.2010.2042420
126. Mojiri M, Karimi-Ghartemani M, Bakhshai A (2007) Time-domain signal analysis using adaptive notch filter. IEEE Trans Signal Process 55:85–93. https://doi.org/10.1109/tsp.2006.885686
127. Yazdani D, Bakhshai A, Joos G, Mojiri M (2009) A real-time extraction of harmonic and reactive current in a nonlinear load for grid-connected converters. IEEE Trans Industr Electron 56:2185–2189. https://doi.org/10.1109/tie.2009.2017100
128. Wang F, Benhabib M, Duarte J, Hendrix M (2009) High performance stationary frame filters for symmetrical sequences or harmonics separation under a variety of grid conditions. In: 2009 24th annual IEEE applied power electronics conference and exposition. https://doi.org/10.1109/apec.2009.4802877

129. Guo X (2010) Frequency-adaptive voltage sequence estimation for grid synchronisation. Electron Lett 46:980. https://doi.org/10.1049/el.2010.0843
130. Asiminoael L, Blaabjerg F, Hansen S (2007) Detection is key—Harmonic detection methods for active power filter applications. IEEE Ind Appl Mag 13:22–33. https://doi.org/10.1109/mia.2007.4283506
131. Chang G, Chen CI, Teng YF (2010) Radial-basis-function-based neural network for harmonic detection. IEEE Trans Industr Electron 57:2171–2179. https://doi.org/10.1109/tie.2009.2034681
132. Lin H (2007) Intelligent neural network-based fast power system harmonic detection. IEEE Trans Industr Electron 54:43–52. https://doi.org/10.1109/tie.2006.888685
133. Dong Gan, Ojo O (2007) Current regulation in four-leg voltage-source converters. IEEE Trans Industr Electron 54:2095–2105. https://doi.org/10.1109/tie.2007.895140
134. Rahmani S, Mendalek N, Al-Haddad K (2010) Experimental design of a nonlinear control technique for three-phase shunt active power filter. IEEE Trans Industr Electron 57:3364–3375. https://doi.org/10.1109/tie.2009.2038945
135. Griffith D, Arce G (1997) Partially decoupled Volterra filters: formulation and LMS adaptation. IEEE Trans Signal Process 45:1485–1494. https://doi.org/10.1109/78.599973
136. Sayadi M, Fnaiech F, Najim M (1999) An LMS adaptive second-order Volterra filter with a zeroth-order term: steady-state performance analysis in a time-varying environment. IEEE Trans Signal Process 47:872–876. https://doi.org/10.1109/78.747794
137. Tan Li, Jiang J (2001) Adaptive Volterra filters for active control of nonlinear noise processes. IEEE Trans Signal Process 49:1667–1676. https://doi.org/10.1109/78.934136
138. Krall C, Witrisal K, Leus G, Koeppl H (2008) Minimum mean-square error equalization for second-order Volterra systems. IEEE Trans Signal Process 56:4729–4737. https://doi.org/10.1109/tsp.2008.928167

Modern Control Methods for Adaptive Droop Coefficients' Design

Y. V. Pavan Kumar and Ravikumar Bhimasingu

Abstract The microgrid controller comprises of cascaded "droop–voltage–current" control modules. The voltage and current controllers are basically proportional plus integral (PI)-type control logics. So, the efficacy of these controllers depends on the accuracy of the PI gain parameter tuning. Besides, the droop control logic supplies the reference voltage required for voltage control and the voltage control logic supplies the reference current required for the current control. Therefore, the total control operation depends on the effective design of droop control logic, which depends on the design of droop coefficients and their adaptivity to respond with respect to a disturbance. There are many conventional methods available as mentioned in the literature; however, to meet the modern power system requirements, these conventional methods have to be updated with features such as adaptivity, disturbance rejection, capability to address inertia related issues. With this intent, this chapter provides modern control methods for adaptive droop coefficients' design. In brief, this chapter presents a novel droop controller design method that involves fuzzy logic-based adaptive $p - \omega$ droop coefficient design and model reference-based adaptive $q - v$ droop coefficient design. This method facilitates the controller to adaptively respond according to the disturbances and thereby provides effective closed-loop control actions to improve the transient response of the system. The comparisons with the conventional methods are presented with the help of simulation and experimental results to persuade the importance of the proposed adaptive droop control method.

Keywords Adaptive inertia · Droop coefficients · Droop controller · Fuzzy logic control · Microgrids · Model-based control · Transient response · Virtual inertia

Y. V. Pavan Kumar
School of Electronics Engineering, Vellore Institute of Technology-Andhra Pradesh (VIT-AP) University, Inavolu (V), Amaravati, Andhra Pradesh 522237, India
e-mail: pavankumar.yv@vitap.ac.in

R. Bhimasingu (✉)
Department of Electrical Engineering, Indian Institute of Technology Hyderabad (IITH), Kandi (V), Sangareddy, Telangana 502285, India
e-mail: ravikumar@iith.ac.in

P. Ray and M. Biswal (eds.), *Microgrid: Operation, Control, Monitoring and Protection*, Lecture Notes in Electrical Engineering 625,
https://doi.org/10.1007/978-981-15-1781-5_4

Nomenclature

C_f^{abc}, G_f^{abc}	Filter shunt branch capacitance (μF), conductance (℧)
C_f, G_f	Single-phase representation of C_f^{abc}, G_f^{abc}
FODDC	First-order delayed droop control
FLADC	Fuzzy logic control-based adaptive droop coefficients
I_i^{abc}	Total current drawn from the inverter (A)
I_c^{abc}	Current flowing through filter's shunt branch (A)
I_i, I_c, I_o	Single-phase representation of I_i^{abc}, I_c^{abc}, I_o^{abc}
$I_o^{dq} = I_{do}, I_{qo}$	$D-q$ components of I_o^{abc} (A)
K_{PV}, K_{IV}	Proportional, integral gains of voltage controller
K_{PA}, K_{IA}	Proportional, integral gains of current controller
MRADC	Model reference-based adaptive droop coefficients
PEVSI	Power electronic-based static voltage source inverter
PI	Proportional plus integral
PWM	Pulse width modulation
R_f, L_f	Single-phase representation of R_f^{abc}, L_f^{abc}
R_g, L_g	Single-phase representation of R_g^{abc}, L_g^{abc}
R_f^{abc}, L_f^{abc}	Filter series branch resistance (Ω), inductance (mH)
R_g^{abc}, L_g^{abc}	Grid line resistance (Ω), inductance (mH) parameters
V/I Controller	Voltage and current controller
V_{do}^{ref}, V_{qo}^{ref}	Reference voltage inputs of voltage controller (V)
$V_o^{dq} = V_{do}, V_{qo}$	$D-q$ components of V_o^{abc} (V)
V_o^{abc}, I_o^{abc}	Voltage (V), current (A) measured at load bus
$V_{\text{pwm}}^{\text{ref}}$	Reference signal input to PWM generator (V)
V_s^{abc}	Output voltage produced by the inverter (V)
V_i^{abc}	Voltage across series branch of the filter (V)
V_g^{abc}	Utility grid voltage (V)
V_s, V_i, V_o	Single-phase representation of V_s^{abc}, V_i^{abc}, V_o^{abc}
ω	Angular frequency (rad/s)

1 Introduction

The microgrids are low-to-medium voltage distribution plants, which constitutes an interconnection of renewable or alternative energy sources (e.g., solar photovoltaics, wind power, fuel cells, diesel generators, etc.), energy storage units (batteries, supercapacitors, electric vehicles, etc.), suitable power conversion devices, flexible loads, and control units. The fashion in which all these constituents are interconnected is called as an "architecture" for the microgrid. The microgrid can operate as a single entity in an island mode of operation or in parallel with electric utility grid in

grid-connected mode of operation. Grid-connected mode of operation is typically preferred to endorse reliable and continuous supply to the local loads. Such introduction of microgrids enables larger distributed generation by interconnecting many micro-sources, which generally uses a single interface (usually power electronic-based static voltage source inverter (PEVSI)) to the utility grid. Therefore, for the effective utilization of all the sources, some key power system concepts such as active power vs. frequency controls, reactive power vs. voltage controls, hierarchical control systems to be adopted for microgrids to improve their stability, active and reactive power support, ride through capability, etc. Besides, the microgrid should exhibit stable responses to operate in grid-connected mode; unless, it can disturb the other generators connected in parallel to it. The fruitful operation of the microgrid depends on four key aspects such as (i) intermittent nature of the energy sources due to their environmental dependency, (ii) suitable architecture selection to interconnect all the constituents, (iii) design of suitable power conversion devices, and (iv) design of effective controllers.

In the literature, the renewable energy intermittency was addressed by considering hybrid energy source (the combination of different sources instead of the single type of source) and usage of energy storage units, so that the stored energy can be used in contingencies. Similarly, three physical architectures such as central DC bus architecture, central AC bus architecture, and hybrid (AC–DC) coupled architecture, whose selection impacts the number of power converters required, power conversion efficiency, and quality were developed based on the type of major power flow (AC or DC) in the system. In "power conversion" point of view, due to the concerns with energy conversion efficiency of conventional electromechanical (rotary)-type inverters, and fortunately owing to quick progress in improvement of power switching devices and substantial evolution in the power converter topologies from early 2-level to multi-levels in output voltage to approximate it to sinusoidal shape, certainly encourage the use of more and more power electronic devices.

So, PEVSIs are widely used for renewable energy-based microgrid applications. However, unlike the bulk power system that depends upon the operation of synchronous generators, which ensures a relatively large kinetic energy and inertia that helps to address the power swings, microgrids possess negligible inertia characteristics due to the involvement of PEVSIs. This lack of inertial capability for converters can degrade system voltage and frequency response during disturbances, which can promote into transient stability issue, if not controlled suitably. This issue becomes severe in weak-grid operation that can destroy the neighboring generators/loads connected to the utility grid. So, to effectively address this critical issue of voltage and frequency deviations that are occurred during disturbances, the converter should have a robust controller association, which can effectively control the system against those disturbances.

The microgrid controller comprises of cascaded "droop–voltage–current" control modules. The voltage and current controllers are basically proportional plus integral (PI)-type control logics. So, the efficacy of these controllers depends on the accuracy of the PI gain parameter tuning. Besides, the droop control logic supplies the reference voltage required for voltage control and the voltage control logic supplies

the reference current required for the current control. Therefore, the total control operation depends on the effective design of droop control logic, which depends on the design of droop coefficients and their adaptivity to respond with respect to a disturbance. The detailed information about the available key literature works is given as follows. Furthermore, three control schemes to incite inertial responses have been developed for the microgrids as follows: (1) swing equation method, (2) low-pass filter, and (3) an adjustable rate limiter. The required inertia that is adjusted virtually through the variation in filter cutoff frequency facilitates the power sharing between different microgrids. But, this inertia may not be adequate for addressing the transients. This requires the inertia to be adaptive with respect to the severity of the disturbance to improve the transient response. Therefore, the droop methods implemented for microgrids to transfer the power should be effective enough to address the issues with transients [1]. However, there is not much literature about addressing the voltage droop concepts.

The conventional $q - v$ and $p - \omega$ droop control methods can only assist the power transitions in steady state, but not able to address the transient instabilities [2, 3]. So, modern developments have brought new design for droop controllers, which can virtually inject the required moment of inertia for the operation of PEVSI. These contemporary methods can be grouped as fixed inertia injection methods and adaptive (or) variable inertia injection methods as described below.

A droop control method based on virtual impedance theory was given in [4]. Instead of active power, this method leads to the consumption of the reactive power through the injected virtual impedance. So, this method improves $q - v$ droop control action. However, this method won't have any impact on efficacy of $p - \omega$ droop control action. So, to address transient response issues in both voltage and frequency, droop control law with a first-order time delay was given in [5]. The usefulness of this approach over inertia injection through virtual synchronous machines was estimated in [6]. From the analysis, it was observed that the droop control with time-delay approach improves both frequency and voltage responses for given load disturbances. However, emulating fixed inertia characteristic is not sufficient in case of huge disturbances such as tripping of power factor improvement devices or circuit breakers, switching of nonlinear loads, line faults. So, later, adaptive virtual inertia injection approaches were discussed in [7–12].

In view of adaptive virtual inertia injection, an improvement was suggested to vary the droop gain based on variation in frequency in [7] and based on variation in the rate of change of frequency in [8]. However, these methods did not study the deviations (under/over) of frequency, which may influence the controller action in severe disturbances. Another variable inertia injection technique was given in [9] to addresses the limitation given in [8]. There are two limitations that exist for this approach: one is the non-consideration of frequency derivative and the other is consideration of only two values for variable inertia, which may not address all varieties of disturbances. Similarly, the methods presented in [10–12] produces adaptive inertia, where it was achieved by translating droop curves in [10], by combining fixed inertia and variable inertia (derived by change in frequency) in [11], and by self-adaptive inertia mechanism through change of frequency rate in [12]. But, all these methods given

in [10–12] for injecting adaptive virtual inertia have improved transient frequency response, but not the voltage response.

Besides, to address both the frequency and voltage response issues, a droop control method, where $p - \omega$ droop equation was adjusted based on the rate of active power change and $q - v$ droop equation was adjusted based on the rate of reactive power change was given in [13]. This approach is restricted for smaller power variations (such as a lower sensitive load variation or disturbance in the system), where the deviations in voltage and frequency are high, which may not have sensed by the lower rate of change of reactive and active powers. Further, a new mechanism of adaptive inertia injection through virtual synchronous generator theory with the help of state of charge value-based use of energy storage element was given in [14]. This approach has successfully emulated desired inertia, but the complexity presented in the storage control logic limits its usage for real-time applications. All other major droop control methods discussed in the literature are segregated into different relative groups, and their cumulative merits and demerits are compared as shown in Table 1.

Therefore, from the literature it is understood that the droop methods used for transferring power across microgrids must be effective to address the transients. Besides, the offline droop coefficient tuning methods need to be converted to online methods to adaptively vary them with respect to the output conditions to achieve better $p - \omega$ and $q - v$ correlations and control. This helps the controller to respond according to various critical disturbances that occur in the system such as unpredictable linear and nonlinear load dynamics, momentary line faults, trippings of power factor improvement devices or circuit breakers, flicker sensations.

Hence, with the motivation of calculating the adaptive droop coefficients to inject moment of inertia virtually into the microgrid's operation to address the issues in frequency and voltage deviations and to overcome the limitations of the state-of-the-art design methods, this chapter proposes "fuzzy logic and model reference-based control methods" for the adaptive $p - \omega$ and $q - v$ droop coefficients' estimation. The philosophy in the proposed methods is changing the $p - \omega$ and $q - v$ droop coefficients based on the deviations in frequency and voltage responses that are obtained during disturbances. These proposed methods inject adaptive virtual inertia in the place of using a fixed inertia, with respect to the voltage and frequency deviations under disturbances. This facilitates the controller to produce control actions according to a disturbance in a closed loop, which improves the performance of the microgrid.

2 Analysis on the Importance of Adaptive Droop Control

Many control methods have been used for enhancing the microgrid performance against different events. The most common way is the use of droop characteristics for $p - \omega$ and $q - v$ correlation management as per the relations given in (1) and (2), respectively. Besides, in the microgrid's cascaded droop–voltage–current controller, the droop controller provides the reference values ($V = V_{\mathrm{do}}^{\mathrm{ref}}$ *or* $V_{\mathrm{qo}}^{\mathrm{ref}}$) to the V/I

Table 1 Brief details about various droop control methods available

Method	Merits	Demerits	References
Traditional droop control method	• This method is easy and simple in implementation	• The effectiveness of the method is affected by the other system parameters • This is only applicable to highly inductive transmission lines • These approaches cannot handle nonlinear loads • Another major limitation is the voltage regulation which is not sure • Adjusting the controller speed for the active and reactive power controllers can affect the frequency and voltage controls	[15]
Voltage-active Power Droop (VPD) and Frequency-Reactive Power Boost (FQB) droop method	• Adjusting the controller speed for the active and reactive power controllers is possible without compromising the frequency and voltage controls • This method is easy and simple in implementation	• This is only applicable to highly resistive transmission lines • The effectiveness of this method is affected by the accurate tracking of other parameters of the system • Another major limitation is that this method cannot handle nonlinear or highly reactive loads	[16]
Adjustable load sharing method	• Adjusting the controller speed for the active and reactive power controllers is possible without compromising the frequency and voltage controls • Robust to the system parameter variations • Improved voltage regulation can be achieved	• The major limitation of this method is that it cannot handle nonlinear loads or disturbances	[17, 18]

(continued)

Table 1 (continued)

Method	Merits	Demerits	References
Adaptive voltage droop method	• The effectiveness of this method won't be affected by the system parameters • This method leads to improved voltage regulation against disturbances in the system	• This cannot handle nonlinear loads. • Adjusting the controller speed for the active and reactive power controllers can affect the frequency and voltage controls • Prior information about system parameters is needed for the design	[19]
Virtual output impedance method	• This method is simple in implementation • The effectiveness of this method won't be affected by system parameters • Applicable to both linear and nonlinear loads • This method can mitigate the harmonic distortion of the output voltage • Also, this can control the output voltage unbalances	• Adjusting the controller speed for the active and reactive power controllers can affect the frequency and voltage controls • Another major limitation is the voltage regulation which is not guaranteed	[20–22]
Virtual frame transformation method	• This is an easier method • This method can provide decoupled active and reactive power controls. So, thereby there is a possibility of achieving better controls for both active and reactive powers	• This method is ineffective for handling nonlinear loads • Adjusting the controller speed for the active and reactive power controllers can affect the frequency and voltage controls • The line impedances should be known a priori • Voltage regulation is not sure	[23–25]

(continued)

Table 1 (continued)

Method	Merits	Demerits	References
Signal injection method	• The major advantage of this method is that it can be applied to both linear and nonlinear loads • Also, the effectiveness of this method is not affected by the system parameters	• This is very complicated to implement compared to other methods • Adjusting the controller speed for the active and reactive power controllers can affect the frequency and voltage controls • Voltage regulation is not guaranteed	[16, 26, 27]
Nonlinear load sharing techniques	• Properly shares the current harmonics between the available distributed generation units. Therefore, it can cancel out the voltage harmonics • Thus, the improved harmonic profile can be obtained when compared to other methods	• The effectiveness of this method is affected by the accurate tracking of other parameters of the system • This method exhibits poor voltage regulation in the case of precise reactive power sharing • Adjusting the controller speed for the active and reactive power controllers can affect the frequency and voltage controls	[28, 29]

controller and thereby affects the operation of the V/I controller to produce PWM control signals to the PEVSI. Further, a key advancement that has been referred in the recent researches is the droop controller design with the ability of virtual inertia emulation to make the frequency response stable during transients [4–14]. However, in all these usages, the effectiveness of the droop controller depends on the design of its coefficients and their adaptivity to respond with respect to a disturbance as discussed in the above section. In line with this, a quantitative analysis is presented as follows to understand the importance of adaptive droop coefficients' design in addressing the stability issues during disturbances.

$$\omega = \omega_{\text{ref}} + D_{p\omega}(P_{\text{ref}} - P) \tag{1}$$

$$V = V_{\text{do}}^{\text{ref}} \text{ or } V_{\text{qo}}^{\text{ref}} = V_{\text{ref}} + D_{qv}(Q_{\text{ref}} - Q) \tag{2}$$

$$D_{p\omega} = \frac{\omega\text{max} - \omega\text{min}}{P_{\text{ref}}} \tag{3}$$

$$D_{qv} = \frac{V\text{max} - V\text{min}}{Q_{\text{ref}}} \tag{4}$$

where V, ω are the output voltage (V) and frequency (rad/s) of the droop controller. P (in kW) and Q (in kVAR) are the output instantaneous active and reactive powers. V_{ref}, ω_{ref}, Q_{ref}, P_{ref} are the reference values of V, ω, Q, P, respectively. $D_{p\omega}$ and D_{qv} are the coefficients of $p - \omega$ and $q - v$ droop laws as given in (3) and (4). ω_{min} and ω_{max} are the minimum and maximum values of ω. V_{min} and V_{max} are the respective minimum and maximum values of V.

Among various conventional droop control methods, a first-order delayed droop control (FODDC) method given in Fig. 1 shows the superior performance among the other conventional methods in both the transient responses of voltage and frequency under load disturbances [5]. This method uses first-order delay coefficient in addition to the droop coefficient to inject virtual inertia into the traditional droop laws. This method is used as the prime conventional method to evaluate the relative effectiveness of the proposed methods in this chapter.

In order to understand the importance of the adaptive droop control, various test conditions given in Table 2 are implemented on the microgrid system that is being controlled by conventional FODDC method. For the analysis, the droop coefficients ($D_{p\omega}$, D_{qv}) that are designed based on (3) and (4) are considered as the 100% values, and these are varied by ±80% to study their impact on the system stability. An RL

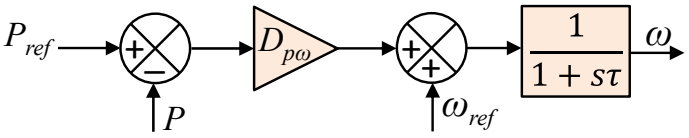

(a) *p-ω* Droop controller model based on FODDC method

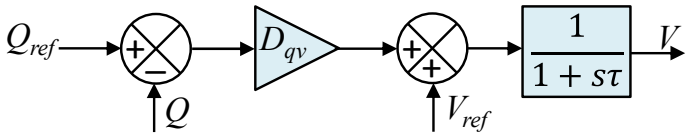

(b) *q-v* Droop controller model based on FODDC method

Fig. 1 Model of the delayed droop control method

Table 2 Test conditions to check FODDC method

Test case	Load	$p - \omega$ Droop coefficient ($D_{p\omega}$)	$q - v$ Droop coefficient (D_{qv})
T_1	Constant	Varying	Constant
T_2	Varying	Varying	Constant
T_3	Constant	Constant	Varying
T_4	Varying	Constant	Varying

load of 0.7 power factor lagging is connected to the system for a certain amount of time to simulate varying load condition. Based on these parameters, various test conditions are developed as shown in Table 2 and the respective stability response plots are shown in Figs. 2, 3, 4, and 5.

- From Fig. 2, by computing the stability margins (gain and phase margins), it is observed that the microgrid system is stable with respect to 100% of $D_{p\omega}$. This indicates the accuracy of considered conventional FODDC method for the design

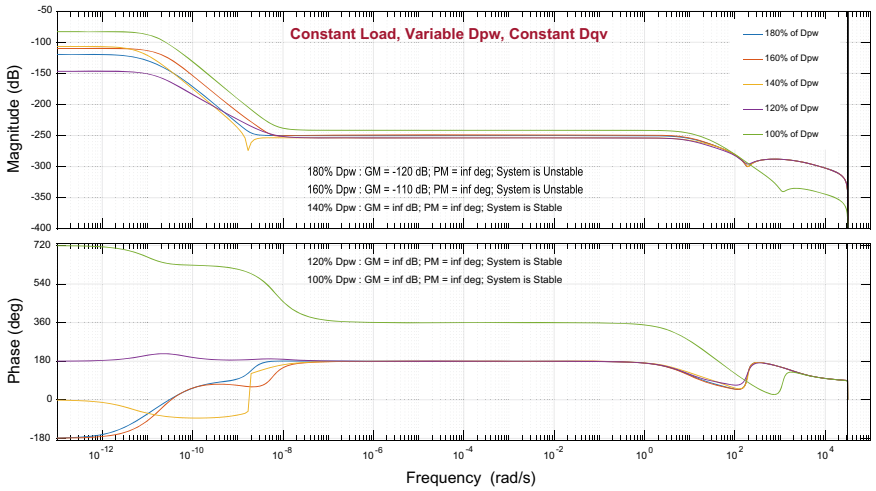

(a) Variation of stability characteristic with respect to $D_{p\omega}$ variation of (0-80) % upwards

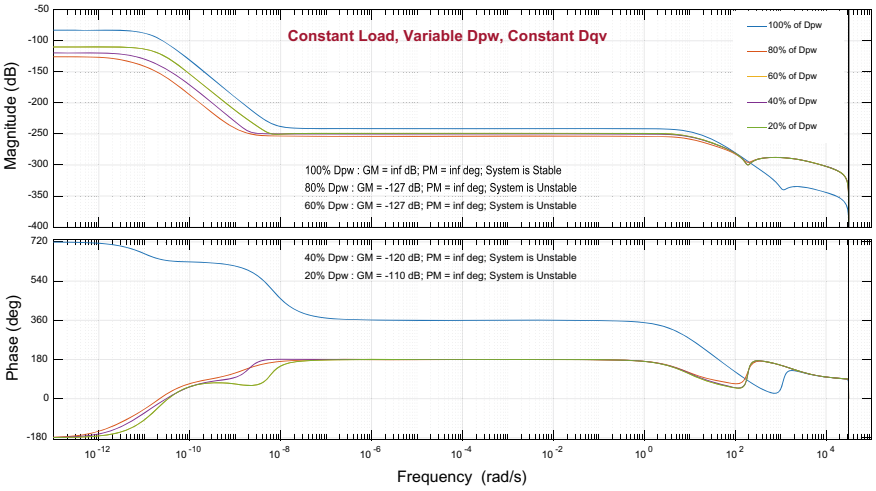

(b) Variation of stability characteristic with respect to $D_{p\omega}$ variation of (0-80) % downwards

Fig. 2 Stability analysis plots with respect to test case-T_1

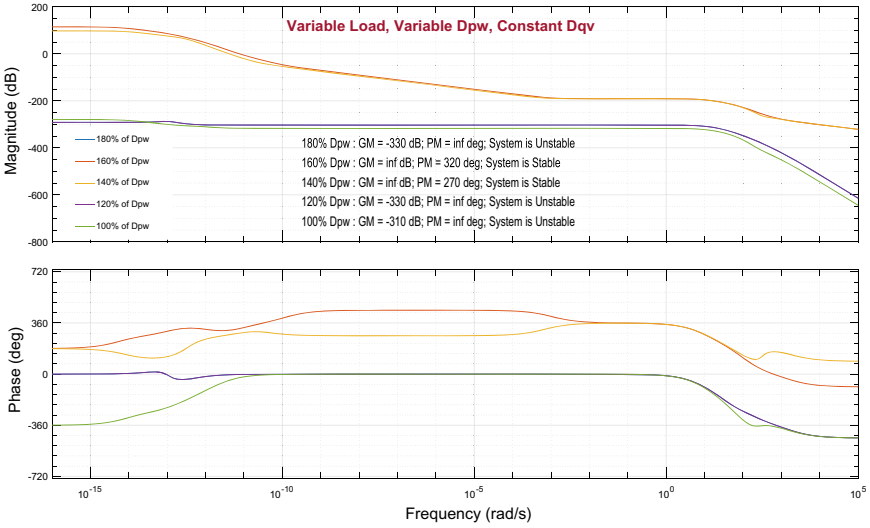

(a) Variation of stability characteristic with respect to $D_{p\omega}$ variation of (0-80) % upwards

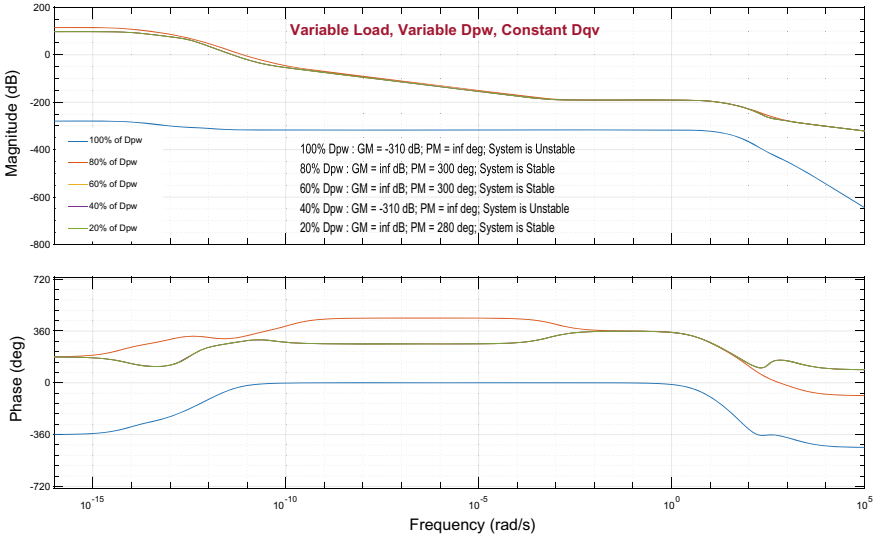

(b) Variation of stability characteristic with respect to $D_{p\omega}$ variation of (0-80) % downwards

Fig. 3 Stability analysis plot with respect to test case-T_2

of $p - \omega$ droop coefficient under the condition that the microgrid is supplying to a constant load.

- However, from Fig. 3, it is observed that the system becomes unstable for the value of 100% of $D_{p\omega}$ during a reactive load change. Instead of 100% of $D_{p\omega}$, now, the system possesses stability characteristics for 140% of $D_{p\omega}$, 160% of $D_{p\omega}$, 80% of

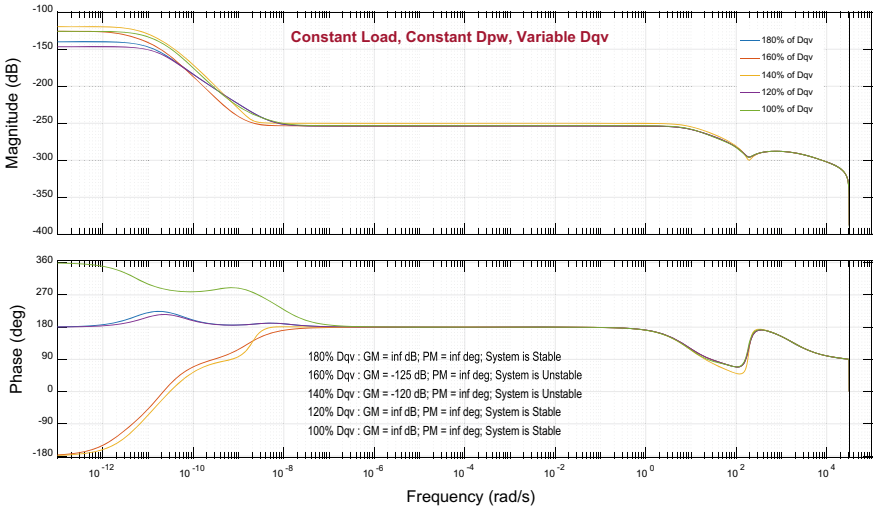

(a) Variation of stability characteristic with respect to D_{qv} variation of (0-80) % upwards

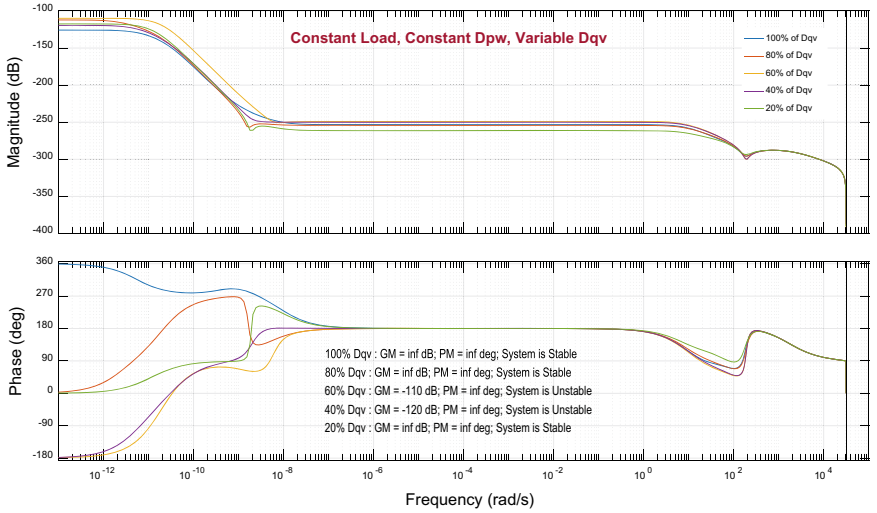

(b) Variation of stability characteristic with respect to Dqv variation of (0-80) % downwards

Fig. 4 Stability analysis plot with respect to test case-T_3

$D_{p\omega}$, 60% of $D_{p\omega}$, and 20% of $D_{p\omega}$. Hence, bearing a constant value of $p-\omega$ droop coefficient leads to system instability, which suggests an adjustment of $D_{p\omega}$ with respect to a disturbance triggered in the plant to retain the system stability during transients.

A similar analysis for $q-v$ droop coefficient (D_{qv}) is also conducted, and the respective observations are given follows.

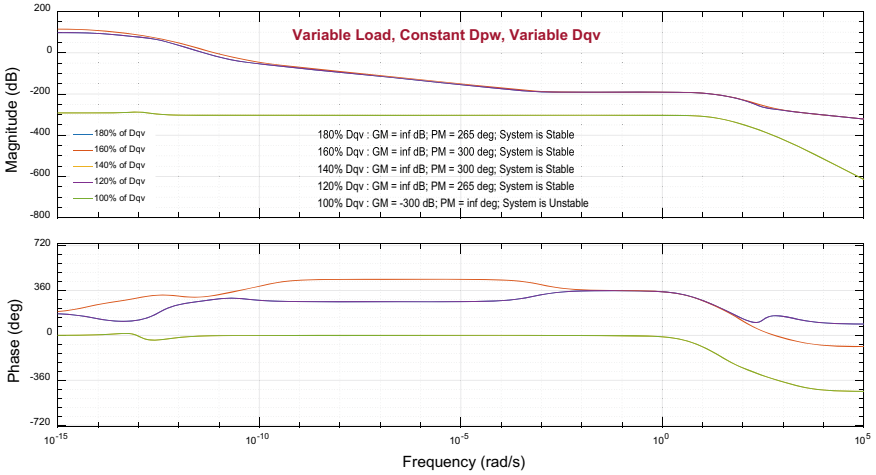

(a) Variation of stability characteristic with respect to D_{qv} variation of (0-80) % upwards

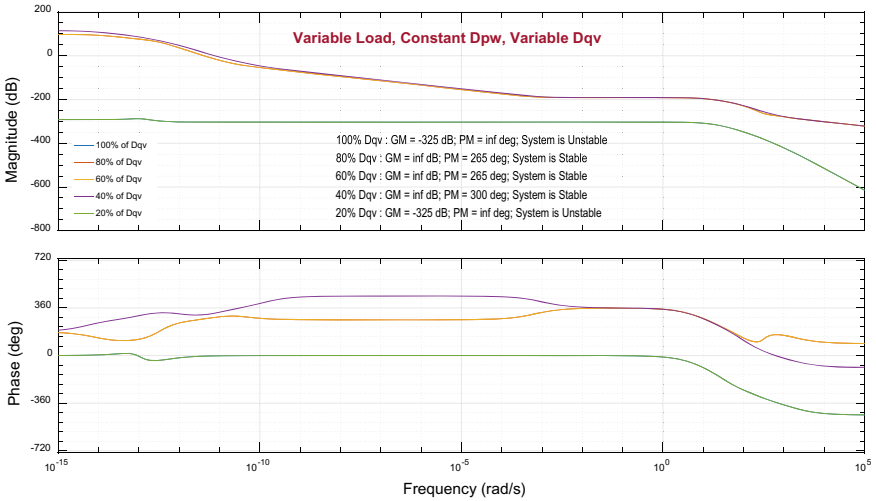

(b) Variation of stability characteristic with respect to D_{qv} variation of (0-80) % downwards

Fig. 5 Stability analysis plot with respect to test case-T_4

- From Fig. 4, by computing the stability margins (gain and phase margins), it is observed that the microgrid system is stable with respect to 100% of D_{qv}. This indicates the accuracy of the conventional FODDC method for the design of $q - v$ droop coefficient under the condition that the microgrid is supplying to a constant load.
- However, from Fig. 5, it is observed that the system becomes unstable for the value of 100% of D_{qv} during a reactive load change. Instead of 100% of D_{qv}, now, the system possesses stability characteristics around the neighborhood of 100%

of D_{qv}, i.e., the system possesses stability for 120% of D_{qv}, 140% of D_{qv}, 160% of D_{qv}, 180% of D_{qv}, 80% of D_{qv}, 60% of D_{qv}, and 40% of D_{qv}.

Therefore, bearing a constant value of $q - v$ droop coefficient leads to system instability, which suggests an adjustment of D_{qv} with respect to the disturbance occurred in the plant to retain the system stability during transients.

Hence, from the above-mentioned analysis on the effect of varying droop control coefficients on the system stability, it is understood that the adaptivity is a major feature that the droop controller should possess to provide better control actions in according to the disturbances occurred in the system and thereby produces stable output responses from the microgrids.

***Keeping the aforesaid issue in view, this chapter proposes two methods,* viz.**

- ***Fuzzy logic control-based adaptive droop coefficients' ($p - \omega$ and $q - v$) design, named as FLADC method with a major benefit of injecting virtual inertia into the controller operation, that helps in retaining frequency stability.***
- ***Model reference-based adaptive $q - v$ droop coefficient design, named as MRADC method to further improve the voltage response compared to FLADC method.***

3 Virtual Inertia Injection Through Adaptive Droop Control

The proposed FLADC method uses fuzzy logic control concepts to vary the droop controller coefficients. The corresponding variability in the $p - \omega$ droop coefficient introduces an adaptive virtual moment of inertia into the plant's operation as explained below and thereby enhances its frequency stability under disturbances.

The process of virtual inertia injection can be understood by comparing the microgrid's $p - \omega$ droop controller equation with the swing equation of the conventional electromechanical generator-based power plant as given in Eq. (5) [30]. From this equation, the relation between the angular frequency (ω) and the system moment of inertia (J) can be derived as Eq. (6). Also, from Fig. 1, the droop controller operation can be derived as Eqs. (7) and (8). Owing to high inertia, capability of synchronous generator-based power plants can effectively control the frequency variations as per Eq. (6). But this is a major concern in PEVSI-based microgrids, which possess negligible inertia. However, the necessary inertia can be injected virtually into the PEVSI's operation by an adaptively varying $p - \omega$ droop controller coefficient ($D_{p\omega}$) as explained follows.

$$P_{\text{ref}} - P = J\omega_{\text{ref}}\frac{\mathrm{d}\omega}{\mathrm{d}t} - D(\omega_{\text{ref}} - \omega) \tag{5}$$

$$\Rightarrow \frac{\mathrm{d}\omega}{\mathrm{d}t} \propto \frac{1}{J} \tag{6}$$

$$\omega = \frac{\omega_{\text{ref}} - D_{p\omega}(P - P_{\text{ref}})}{1 + s\,\tau} \tag{7}$$

$$V = \frac{V_{\text{ref}} - D_{qv}(Q - Q_{\text{ref}})}{1 + s\,\tau} \tag{8}$$

Readjusting the terms of (5) will produce (9),

$$\begin{cases} \Rightarrow P_{\text{ref}} - P = J \cdot \omega_{\text{ref}} \cdot \omega \cdot s - D\,\omega_{\text{ref}} + D\,\omega \\ \Rightarrow P_{\text{ref}} - P + D\,\omega_{\text{ref}} = \omega(D + J\omega_{\text{ref}}s) \\ \Rightarrow \omega = \frac{P_{\text{ref}} - P + D\omega_{\text{ref}}}{D + J\,\omega_{\text{ref}}s} \\ \therefore \omega = \frac{\omega_{\text{ref}} + \left(\frac{P_{\text{ref}} - P}{D}\right)}{1 + \left(\frac{J\omega_{\text{ref}}}{D}\right)s} \end{cases} \tag{9}$$

Therefore, by equating Eqs. (7) and (9), the equation for virtual inertia (J) is obtained as Eq. 10.

$$\begin{cases} \Rightarrow \tau = \frac{J\omega_{\text{ref}}}{D} \text{and } D = \frac{1}{D_{p\omega}} \\ \Rightarrow J = \frac{D\tau}{\omega_{\text{ref}}} = \frac{\tau}{D_{p\omega}\omega_{\text{ref}}} \\ \therefore J \propto \frac{1}{D_{p\omega}}, \quad \text{since, } \tau \text{ and } \omega_{\text{ref}} \text{ are constants} \end{cases} \tag{10}$$

where J is moment of inertia in Kg m^2; is time constant of the low-pass filter; D is damping factor.

Hence, from Eq. (10), it is observed that by regulating the value of $p - \omega$ droop coefficient ($D_{p\omega}$), the moment of inertia (J) can be regulated. This controls the transient frequency response disturbances. Similarly, the transient voltage response is controlled by regulating $q - v$ droop coefficient (D_{qv}). Figure 6 gives the corresponding droop philosophies.

4 Description of the Proposed FLADC Method

To address the limitations of state-of-the-art methods presented in the literature, which injects fixed or variable inertia to handle frequency and voltage transient response issues, this section explains the proposed FLADC method. Fuzzy logic-based control philosophy is beneficial compared to traditional control laws or methods in terms of the points mentioned below [31, 32].

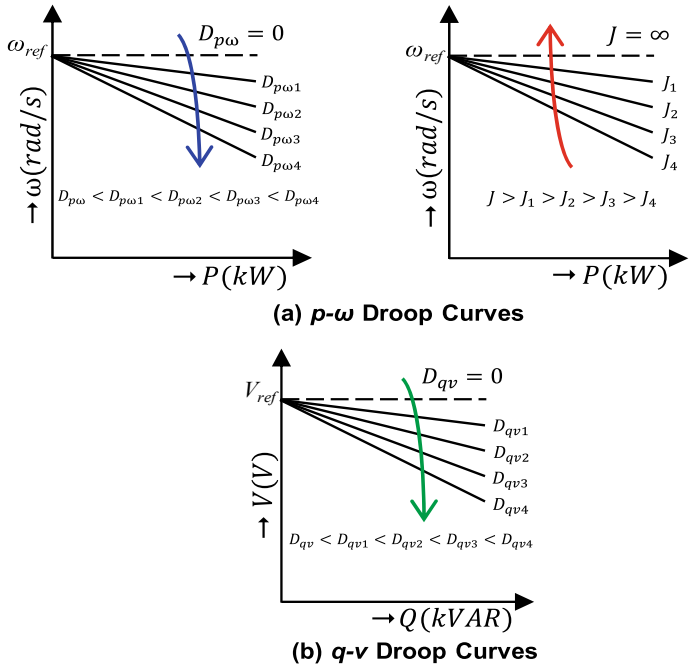

Fig. 6 $p - \omega$ and $q - v$ droop responses

- It offers nonlinear and flexible input and output mapping with multi-variety membership functions and a wide range of inference systems. Therefore, these logics can effectively handle different uncertainties with better sensitivity.
- These logics can be implemented (defining the linguistic variables and rules) just by knowing system's behavior instead of actually knowing the system's mathematical model, which is the key requirement of traditional approaches.

4.1 Proposed Design of Droop Controller Coefficients

The concept involved in the proposed FLADC method is tuning the droop controller coefficients ($p - \omega$ and $q - v$) based on the variations in frequency and voltage responses that are caused due to system disturbances. As per Eq. (10), the deviation in the $p - \omega$ droop coefficient ($D_{p\omega}$) virtually introduces and regulates the moment of inertia (J) that reflects through PEVSI's operation. This helps for the improvement of transient frequency response. In the same way, adaptive variation in $q - v$ droop coefficient (D_{qv}) helps for the improvement of transient voltage response.

- The droop coefficients ($D_{p\omega}$ and D_{qv}) that are designed by the proposed method are given by Eqs. (11) and (12), respectively. These coefficients have two parts: a fixed quantity ($D^0_{p\omega}/D^0_{qv}$) and a variable quantity ($D^f_{p\omega}/D^f_{qv}$).
- The fixed droop quantities given in Eqs. (13) and (14) are defined as half of the fixed values provided by Eqs. (3) and (4), respectively.
- Another half value of Eqs. (11) and (12), i.e., the variable quantity, is provided by the proposed fuzzy logic control model. Referring to a disturbance, these variable droop quantities are constantly provided by the fuzzy logic controller.

The above-mentioned proposed mixture of fixed and variable quantitates leads to wide-range variation (0–100% of the actual fixed values set in Eqs. (3) and (4)) in the droop coefficients with the advantage of injecting an adaptive virtual inertia. Figure 7 shows the corresponding proposed droop controller model.

$$D_{p\omega} = D^0_{p\omega} + D^f_{p\omega} \tag{11}$$

$$D_{qv} = D^0_{qv} + D^f_{qv} \tag{12}$$

$$D^0_{p\omega} = \frac{D_{p\omega}}{2} = \frac{\omega\text{max} - \omega\text{min}}{2P_{\text{ref}}} \tag{13}$$

$$D^0_{qv} = \frac{D_{qv}}{2} = \frac{V\text{max} - V\text{min}}{2Q_{\text{ref}}} \tag{14}$$

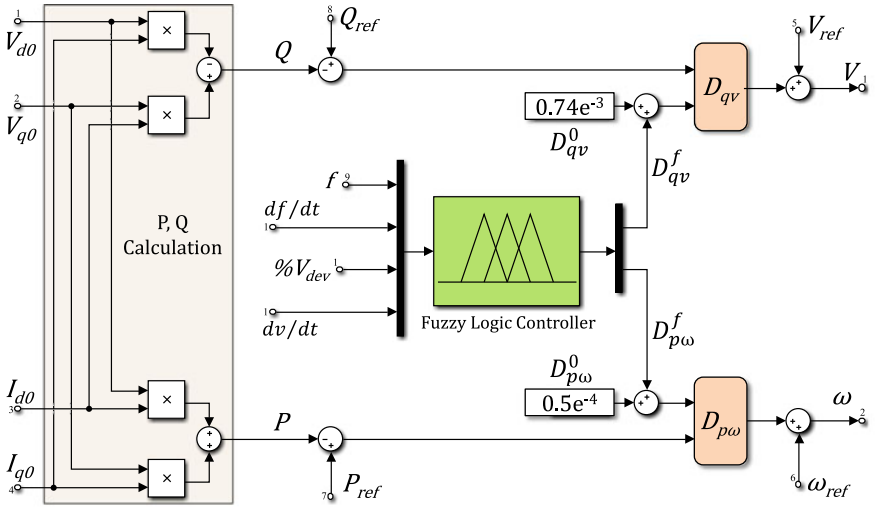

Fig. 7 Model of the proposed fuzzy logic droop controller

where $D^0_{p\omega}$, D^0_{qv} are the constant parts of $D_{p\omega}$ and D_{qv} coefficients, respectively. $D^f_{p\omega}$, D^f_{qv} are the variable parts of $D_{p\omega}$ *and* D_{qv} coefficients, respectively, that are obtained by the proposed FLADC method.

4.2 Implementation of the Fuzzy Logic Controller

The proposed fuzzy logic-based controller to estimate the variable parts of the droop coefficients is implemented with 4-input and 2-output membership functions as shown in Fig. 8. These functions are designed as triangular functions with training reference data given in Table 3. The fuzzy inference system shown in Fig. 8a connects the input and output (I/O) membership functions, and these I/Os are mapped using various fuzzy rules as given in Fig. 8b, which are developed based on Fig. 9.

Selection of fuzzy rules influences the effectiveness of the fuzzy logic controller. Thus, for the proposed approach, the fuzzy rules are methodically developed by the observation of voltage and frequency responses that are obtained when subjected to particular disturbances. These responses normally follow an under-damped behavior

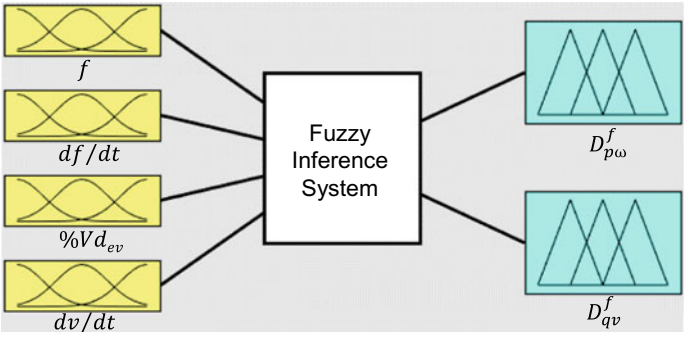

(a) I/O membership functions connected to fuzzy inference system.

1. If (f is P) and (df/dt is P) then (Dpw is N) (1)
2. If (f is P) and (df/dt is N) then (Dpw is Z) (1)
3. If (f is N) and (df/dt is N) then (Dpw is N) (1)
4. If (f is N) and (df/dt is P) then (Dpw is Z) (1)
5. If (f is Z) and (df/dt is Z) then (Dpw is Z) (1)
6. If (Vdev is P) and (dv/dt is P) then (Dqv is N) (1)
7. If (Vdev is P) and (dv/dt is N) then (Dqv is Z) (1)
8. If (Vdev is N) and (dv/dt is N) then (Dqv is N) (1)
9. If (Vdev is N) and (dv/dt is P) then (Dqv is Z) (1)
10. If (Vdev is Z) and (dv/dt is Z) then (Dqv is Z) (1)

(b) I/O mapping fuzzy rules

Fig. 8 Implementation of the fuzzy inference system

Table 3 Reference values for developing the proposed fuzzy rules

Type of Function		Data range	
Input variables	Frequency (f) in Hz	N:	(49.4)–(49.7)–(50)
		Z:	(49.7)–(50)–(50.3)
		P:	(50)–(50.3)–(50.6)
	Rate of change of frequency (df/dt) in Hz/s	N:	(−1)–(−0.5)–(0)
		Z:	(−0.5)–(0)–(0.5)
		P:	(0)–(0.5)–(1)
	Percentage of voltage deviation ($\%V_{\text{dev}}$)	N:	(−10)–(−5)–(0)
		Z:	(−5)–(0)–(5)
		P:	(0)–(5)–(10)
	Rate of change of voltage (dv/dt) in V/s	N:	(−2)–(−1)–(0)
		Z:	(−1)–(0)–(1)
		P:	(0)–(1)–(2)
Output variables	Variable part of droop coefficient $D_{p\omega}$, i.e., ($D^f_{p\omega}$)	N:	($-0.5e^{-4}$)–($-0.25e^{-4}$)–(0)
		Z:	($-0.25e^{-4}$)–(0)–($0.25e^{-4}$)
		P:	(0)–($0.25e^{-4}$)–($5e^{-4}$)
	Variable part of droop coefficient D_{qv}, i.e., (D^f_{qv})	N:	($-0.74e^{-3}$)–($-0.37e^{-3}$)–(0)
		Z:	($-0.37e^{-3}$)–(0)–($0.37e^{-3}$)
		P:	(0)–($0.37e^{-3}$)–($0.74e^{-3}$)

df/dt / f	P	Z	N
P	N		Z
Z		Z	
N	Z		N

(a) Rules to obtain D^f_p

dv/dt / $\%V_{dev}$	P	Z	N
P	N		Z
Z		Z	
N	Z		N

(b) Rules to obtain D^f_{qv}

Fig. 9 Proposed fuzzy rules to develop fuzzy inference system

as shown in Fig. 10. Critically deviated regions of these responses are separated as four different segments and are designated with a value in each segment such as P (a positive value, indicating upper deviation), Z (a zero, indicating normal value), N (a negative value, indicating lower deviation), whose ranges for various parameters are given in Table 3. Similarly, for the frequency response correction, the rules are realized such that a huge inertia is injected for the segments 1 and 3 (where the characteristic is moving away from the normal value) and to recover the frequency, a much lower inertia value is injected for the segments 2 and 4 (where the characteristic

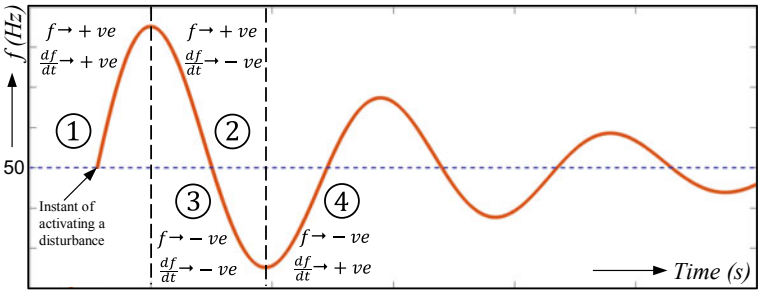

(a) Frequency response subjected to a disturbance

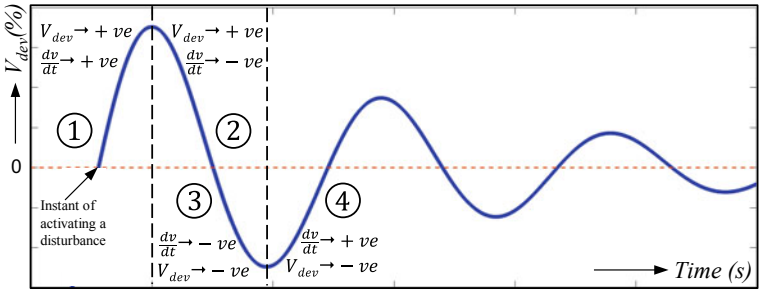

(b) Voltage response subjected to a disturbance

Fig. 10 Response deviations observed to develop the proposed fuzzy rules

is moving toward the normal value). Thus, this proposed procedure facilitates slow deviation and fast restoration of the frequency and thereby provides adaptive virtual inertia. Similarly, in the same way, the voltage response transient deviations are also controlled.

4.3 Summary of the Proposed FLADC Method

Due to the provision of adaptively varying droop coefficients, the proposed FLADC method can improve the system responses when compared to conventional methods, which is analyzed based on the simulation results presented in Sect. 6. However, the effectiveness of the proposed FLADC method majorly depends upon the training of the fuzzy inference system, which further involves the selection of membership functions and their operating ranges, and the input/output mapping rules. So, the FLADC method works very effectively even with limited training data for the controlled variables (or membership functions) whose operating neighborhood/range is small. On the other hand, more effective rules have to be developed if the function range is big.

In the case of considered application, there are two controlled variables exists, one is frequency, which has to be controlled over a range of $\pm 1\%$ of the nominal

value and another one is voltage, which has to be controlled over a range of ±10% of the nominal value. These ranges are set by the standard tolerances defined by IEEE 1547 [33] and EN 50160 [34]. Hence, the control neighborhood for voltage response is very high compared to that of frequency, which needs more effective training to produce better results.

Hence, to reduce the dependency on training based logics, an alternative way, named MRADC method, is proposed in the subsequent section to design the $q - v$ droop controller coefficient, such that the combined operation of FLADC method (for improving frequency response) and MRADC method (for improving voltage response) results in improved system performance during disturbances as justified from the simulation results presented in Sect. 6.

5 Description of the Proposed MRADC Method

The proposed MRADC method uses the small signal model of the microgrid as a reference model that produces a correction coefficient to design the $q - v$ droop coefficient (D_{qv}). The correction coefficient is produced by comparing plant's ideal response that is produced by the small signal model and the plant's actual response produced during the real-time operation. This correction coefficient helps to tune the response of the plant to gradually align with the ideal response in a closed loop and thereby produces a better response as desired. Figures 11 and 12 represent the microgrid's equivalent circuit and its small signal modeling block diagram that is used to implement the proposed MRADC method. The modified droop coefficient (D_{qv}) obtained by MRADC method is represented as (Eq. 15). This involves two parts, viz. fixed part (D^0_{qv}) and variable part or correction coefficient, (D^{ssm}_{qv}) as given by (Eqs. 16 and 17), respectively. The closed-loop transfer function of the small signal model shown in Fig. 12 is obtained as (Eq. 18). By substituting the parameters given in Table 4, the small signal model (Eq. 18) is simplified as (Eq. 19), which is

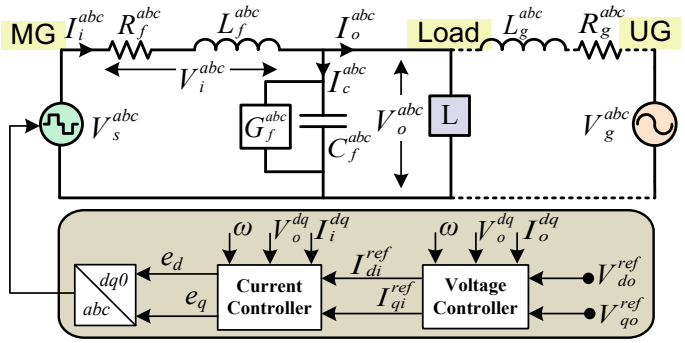

Fig. 11 Equivalent circuit of the microgrid system

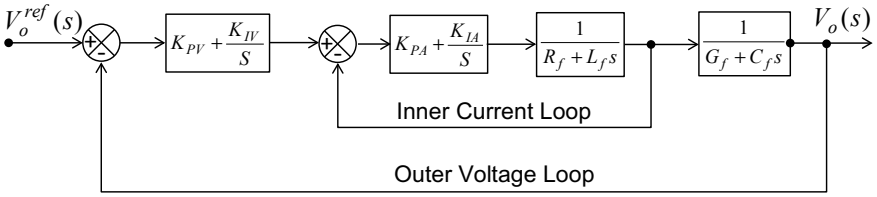

Fig. 12 Small signal modeling block diagram of the microgrid system

Table 4 Parameters considered for microgrid'smodel

Parameter	Description	Value
C_f	Filter capacitance	50 μF
L_f	Filter inductance	1.35 mH
R_f	Filter resistance	0.1 Ω
G_f	Filter conductance	0 ℧
K_{PA}	Proportional gain of current controller	0.09
K_{IA}	Integral gain of current controller	6.67
K_{PV}	Proportional gain of voltage controller	5.6×10^{-4}
K_{IV}	Integral gain of voltage controller	0
D_p	$p - \omega$ droop coefficient obtained by conventional FODDC method	1×10^{-4}
D_{qv}	$q - v$ droop coefficient obtained by conventional FODDC method	1.47×10^{-3}
D_p^0	Fixed part of $p - \omega$ droop coefficient obtained by proposed FLADC method	0.52×10^{-4}
D_{qv}^0	Fixed part of $q - v$ droop coefficient obtained by proposed FLADC method	0.74×10^{-3}
	Fixed part of $q - v$ droop coefficient obtained by proposed MRADC method	1.48×10^{-3}

used as the reference model in the development of the proposed MRADC method. The proposed FLADC plus MRADC method-based droop controller model is shown in Fig. 13.

$$D_{qv} = D_{qv}^0 + D_{qv}^{ssm} \tag{15}$$

$$D_{qv}^0 = \frac{V\max - V\min}{Q_{\text{ref}}}$$

This is equal to the value given in (Eq. 4) (16)

$$D_{qv}^{ssm} = \frac{V_i - V_a}{Q_{\text{ref}}} \tag{17}$$

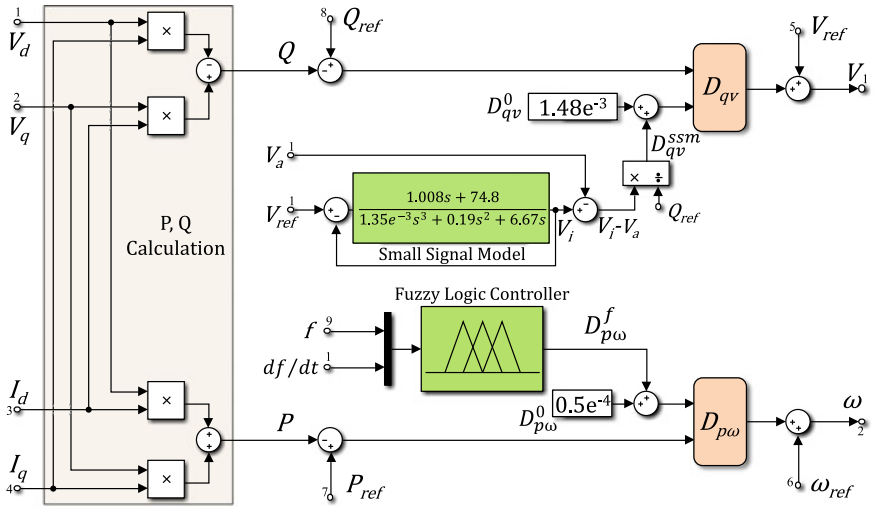

Fig. 13 Proposed FLADC plus MRADC-based droop controller model

$$\frac{V_i}{V_{\text{ref}}} = \frac{K_{PV}K_{PA}s^2 + (K_{PV}K_{IA} + K_{IV}K_{PA})s + K_{IV}K_{IA}}{\begin{bmatrix} C_fL_fs^4 + (G_fL_f + C_fK_{PA} + C_fR_f)s^3 \\ +(G_fK_{PA} + G_fR_f + C_fK_{IA} + K_{PV}K_{PA})s^2 \\ +(G_fK_{IA} + K_{PV}K_{IA} + K_{IV}K_{PA})s + K_{IV}K_{IA} \end{bmatrix}} \tag{18}$$

$$\left.\frac{V_i}{V_{\text{ref}}}\right|_{\text{closed\_loop}} = \frac{1.008s + 74.8}{1.35e^{-3}s^3 + 0.19s^2 + 7.678s + 74.8} \tag{19}$$

where V_i is the ideal output produced by the small signal model of the microgrid for a reference input of V_{ref}. V_a is the actual output generated by the system under any real-time condition.

6 Results and Discussions

To persuade the importance of the proposed FLADC and MRADC methods against the conventional methods, the analysis is carried out on different performance index such as voltage characteristics, frequency characteristics, active power, and reactive power characteristics as described below. Various test cases mentioned in Table 5 are considered for the performance analysis. These test cases are implemented with respect to various load patterns and disturbance patterns that are given in Tables 6 and 7, respectively, which comprehensively covers the possible key real-time disturbances in microgrid scenarios. The results obtained from these tests are shown in Figs. 14, 15, 16, 17, 18, 19, 20, 21, 22, 23, 24, 25, 26, 27, 28, and 29. The obtained

Table 5 Test cases used for the performance analysis

S. no	Performance index		Test case no.	Disturbance
1	Voltage response	3-Phase waveform shape (V)	TC_1	D_1
			TC_2	D_2
			TC_3	D_3
		rate of change of voltage (V/s)	TC_4	D_1
		Voltage deviation (%)	TC_5	D_1
			TC_6	D_2
			TC_7	D_4
		Positive sequence voltage (pu)	TC_8	D_1
			TC_9	D_2
		Negative sequence voltage (pu)	TC_{10}	D_1
			TC_{11}	D_2
		Voltage imbalance (%)	TC_{12}	D_1
			TC_{13}	D_2
2	Frequency response	Frequency (Hz)	TC_{14}	D_1
			TC_{15}	D_3
		Rate of change of frequency (Hz/s)	TC_{16}	D_1
3	Power response	Active power (kW)	TC_{17}	D_1
		Reactive power (kVAR)	TC_{18}	D_1

Table 6 System load patterns considered for the analysis

S. no	Type of load		Specifications	Duration (50 Hz signal)	
L_1	Base load	RL type	25.0 kW + j6.25 kVAR, 0.97 Lag	0–160 s	8000 cycles
L_2	Test load-1	RL type	6.25 kW + j6.25 kVAR, 0.7 Lag	80–90 s	500 cycles
L_3	Test load-2	RC type	6.25 kW − j6.25 kVAR, 0.7 Lead	125–135 s	500 cycles
L_4	Test load-3	RL type	6.25 kW + j6.25 kVAR, 0.7 Lag	80–100 s	1000 cycles
L_5	Test load-4	Electric Arc Furnace (EAF)	3-Phase AC, 25A, 0.72 Lag	80–90s	500 cycles
L_6	Test load-5	Instantaneous Flicker Sensation (IFS)	3-Phase AC, 20A, UPF	80–120 s	2000 cycles

Note
All the above-mentioned loading effects are considered with respect to the droop controller reference power = 25 kW + j25 kVAR

Table 7 Disturbance patterns considered for the analysis

S. no	Disturbance type		Procedure for injecting the disturbance
D_1	Balanced load variations		Apply $L_1 + L_2 + L_3$ on three phases (A, B, C) {i.e., for the balanced/base load (L_1) system, Test Load-1 (L_2) is connected during (80–90)s and Test Load-2 (L_3) during (125–135)s}
D_2	Unbalanced load variations		Apply L_1 on three phases $+ L_4$ on phase-A and phase-B only {i.e., for the balanced/base load (L_1) system, Test Load-3 (L_4) is connected during (80–100)s on Phase-A and Phase-B}
D_3	Nonlinear load variations	Arc furnace loading	Apply L_1 on three phases $+ L_5$ on three phases {i.e., for the balanced/base load (L_1) system, Test Load-4 (L_5) is connected during (80–90)s}
D_4		Flicker sensation injections	Apply L_1 on three phases $+L_6$ on three phases {i.e., for the balanced/base load (L_1) system, Test Load-5 (L_6) is connected during (80–120)s}

results for both the conventional and proposed methods are compared to understand their effectiveness during different disturbances.

6.1 Observations on Voltage Response Variations

To observe the variations in voltage performance index such as waveform shape, rate of change of voltage, over and under magnitude deviations, imbalances, various test cases as per Table 5 are implemented through the injection of various disturbances such as balanced load variations, unbalanced load variations, and nonlinear load variations, into the system as per the specifications are given in Table 6. Here, the reactive load variations (balanced or unbalanced) are considered as the normal disturbances and nonlinear variations (e.g., arc furnace, flickers, etc.) are considered as the high impact events. The corresponding results are given in Figs. 14, 15, 16,

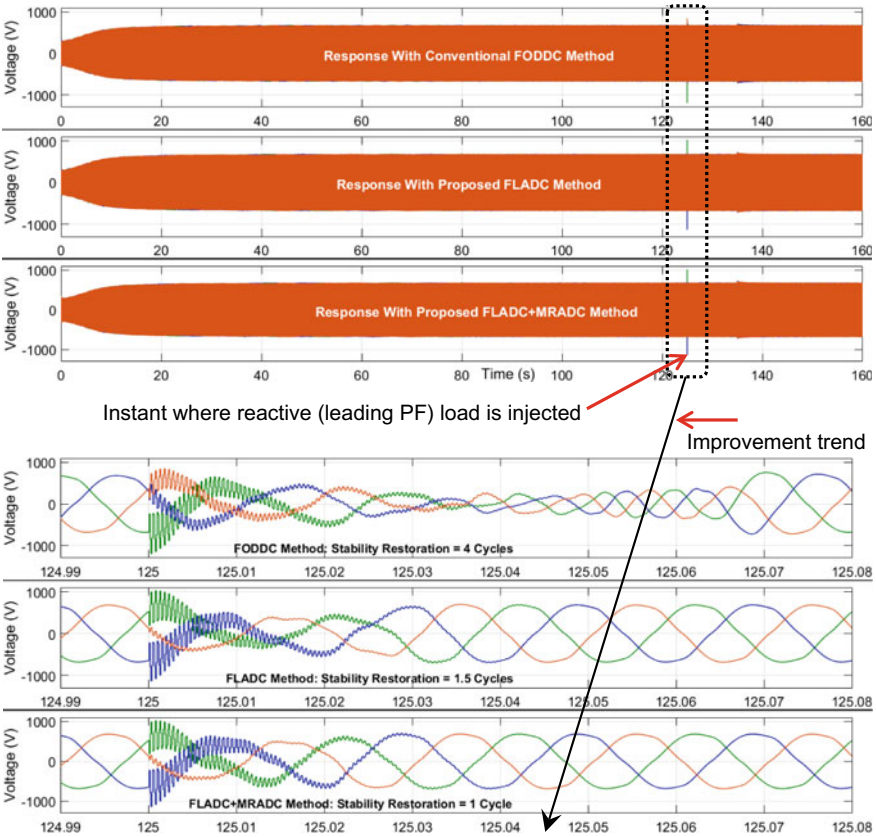

Fig. 14 Voltage response for balanced load variations as per test case-TC_1 of Table 5

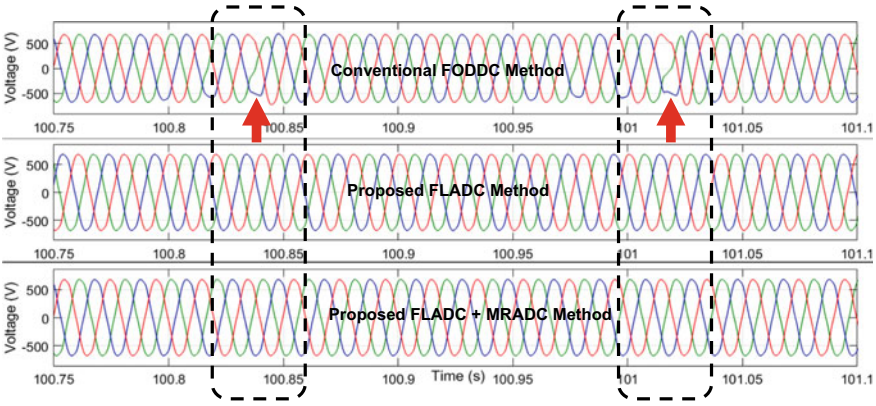

Fig. 15 Voltage response for unbalanced load variations as per test case-TC_2 of Table 5

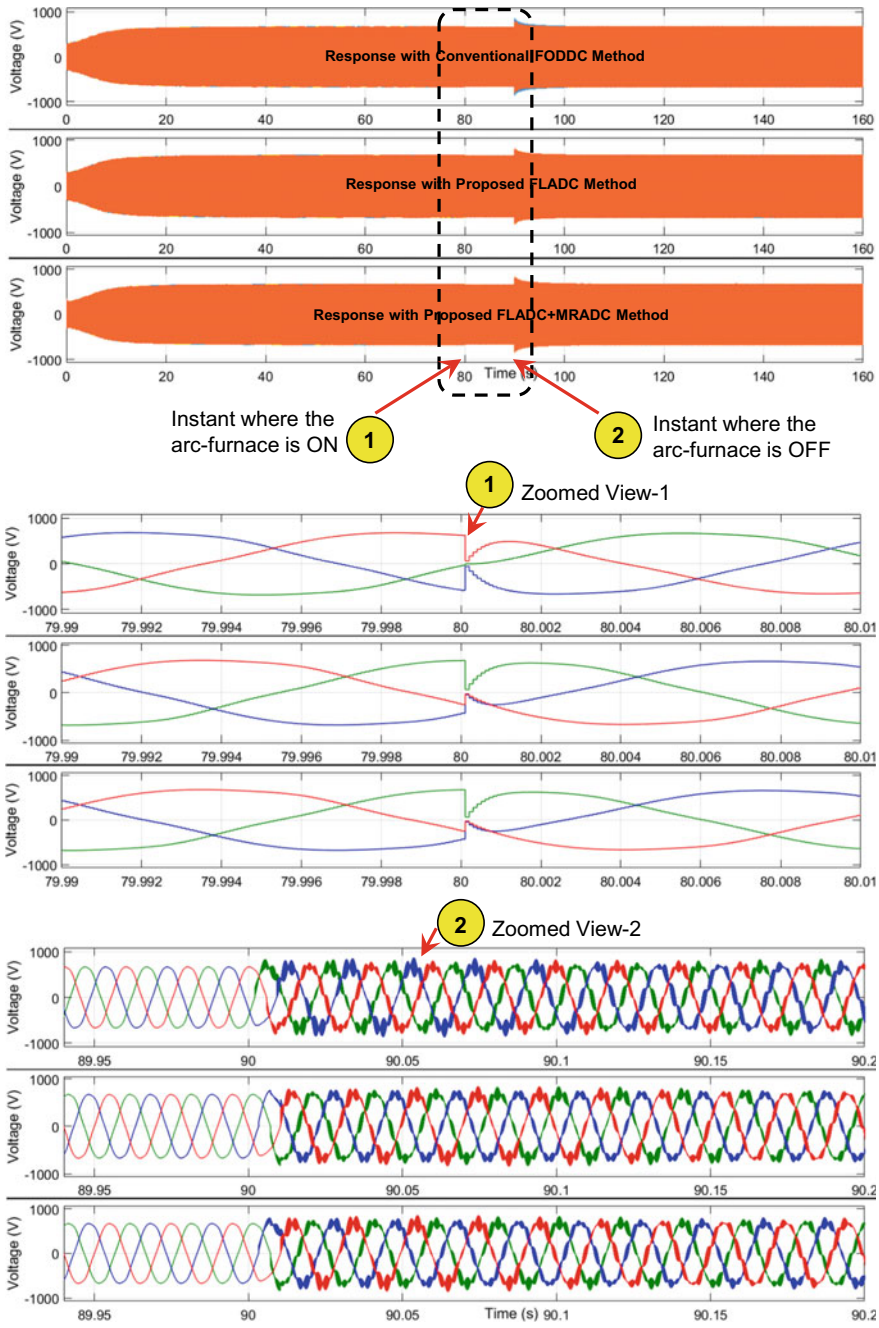

Fig. 16 Voltage response for arc furnace loading as per test case-TC_3 of Table 5

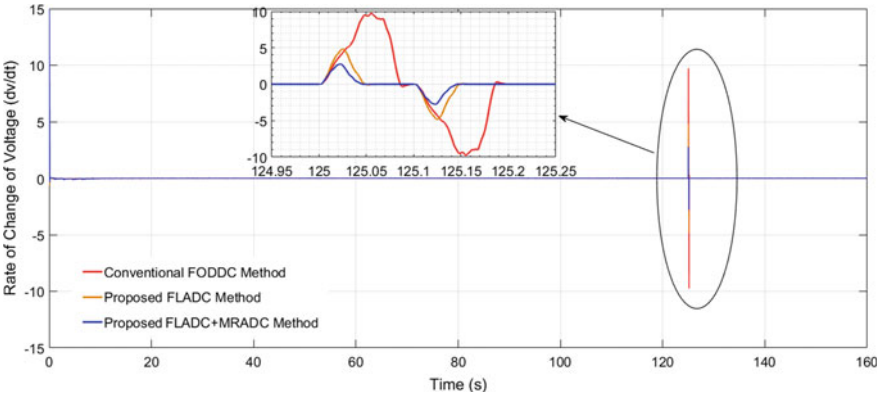

Fig. 17 Rate of change of voltage for load variations as per test case-TC_4 of Table 5

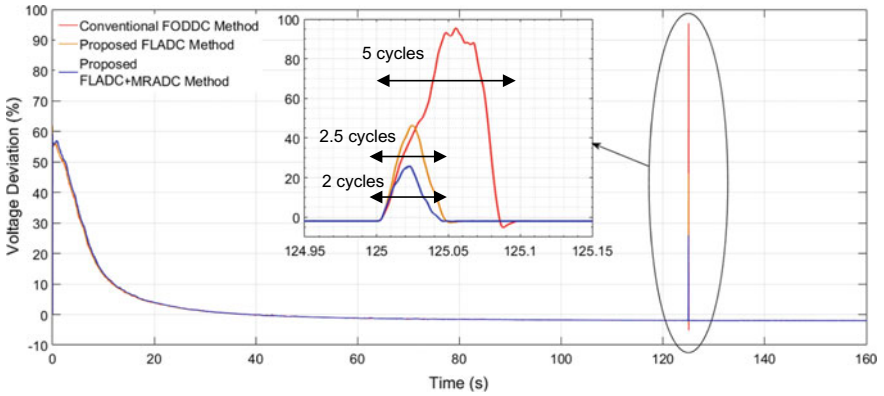

Fig. 18 Voltage deviation for balanced load variations as per test case-TC_5 of Table 5

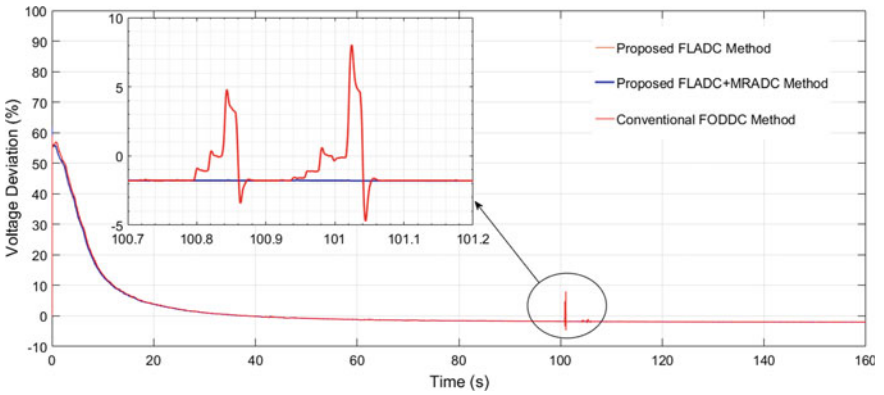

Fig. 19 Voltage deviation for unbalanced load variations as per test case-TC_6 of Table 5

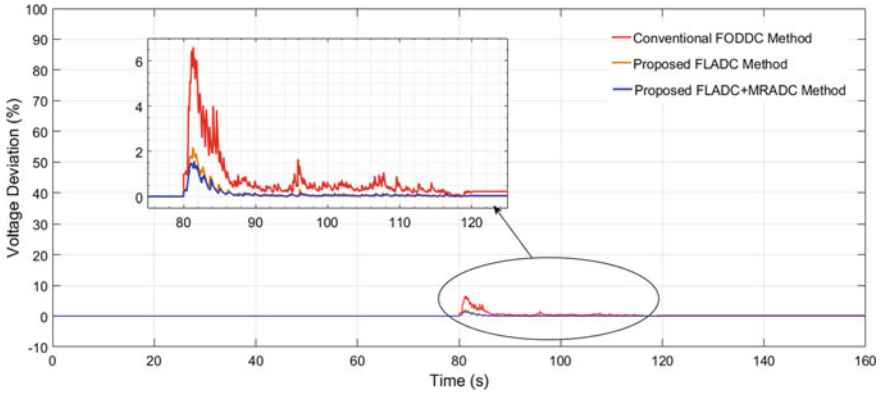

Fig. 20 Voltage deviation for flicker sensations as per test case-TC_7 of Table 5

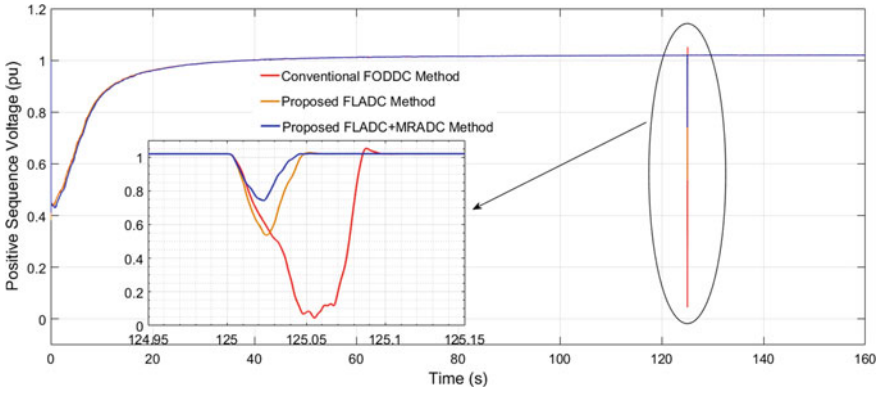

Fig. 21 Positive sequence voltage for balanced load variation as per test case-TC_8 of Table 5

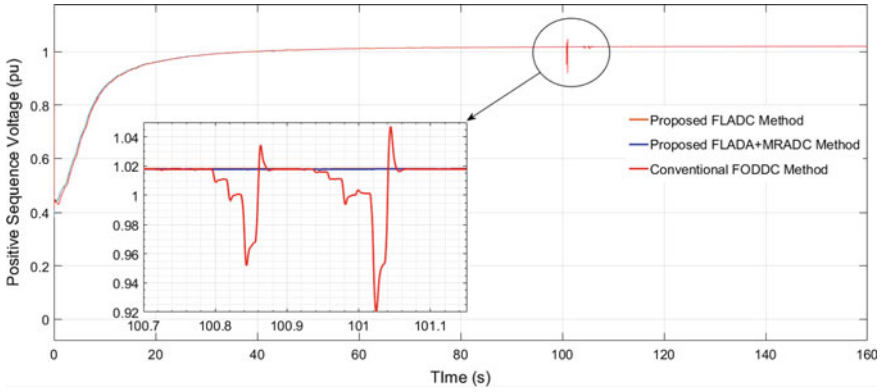

Fig. 22 Positive sequence voltage for unbalanced load variations as per test case-TC_9

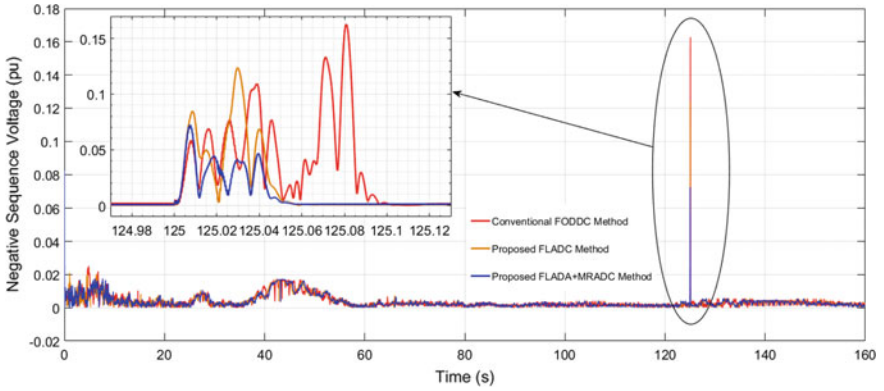

Fig. 23 Negative sequence voltage for balanced load variations as per test case-TC_{10}

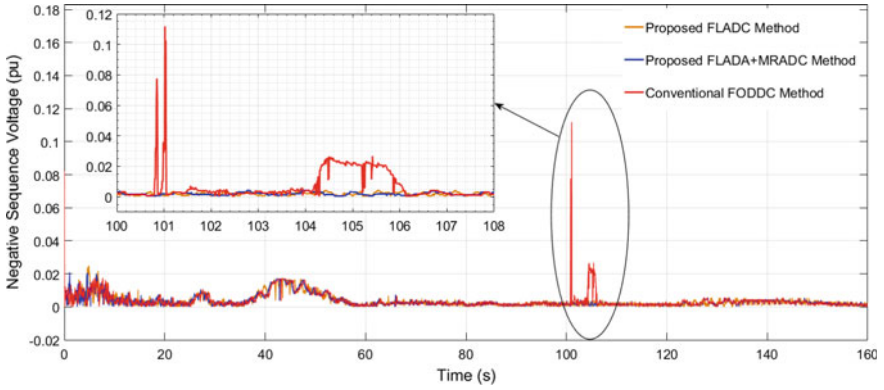

Fig. 24 Negative sequence voltage for unbalanced load variations as per test case-TC_{11}

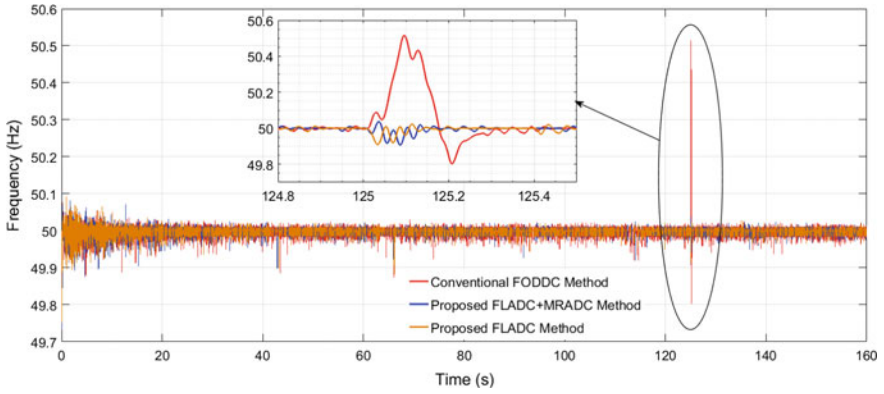

Fig. 25 Frequency response under balanced load variations as per test case-TC_{14}

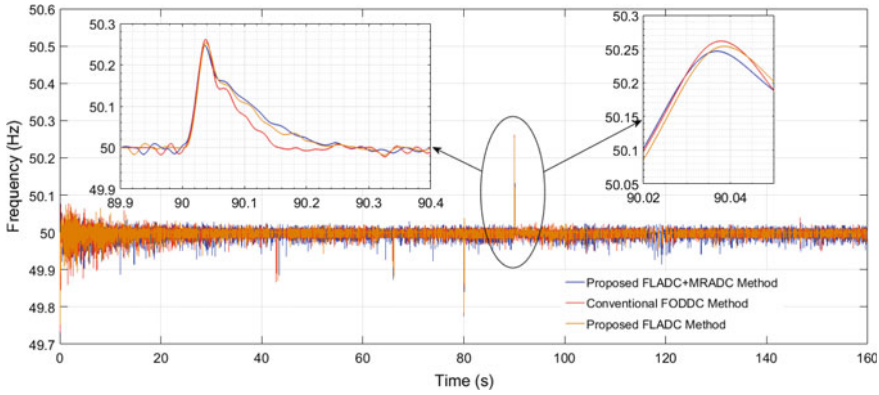

Fig. 26 Frequency response under arc furnace loading as per test case-TC_{15} of Table 5

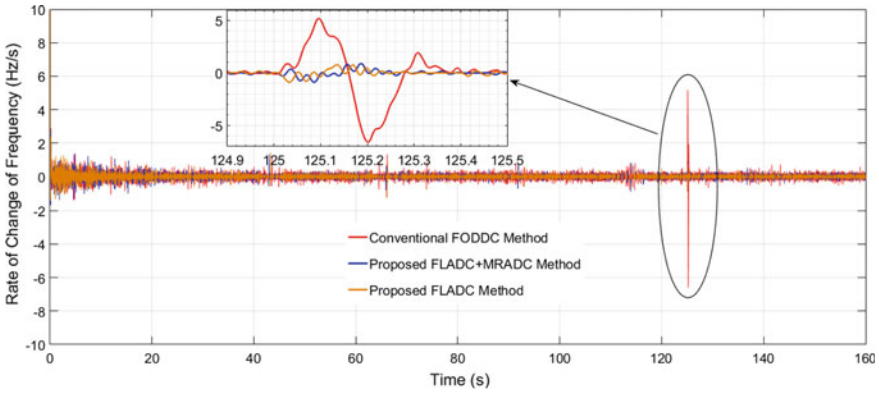

Fig. 27 Rate of frequency change under balanced load variations as per test case-TC_{16}

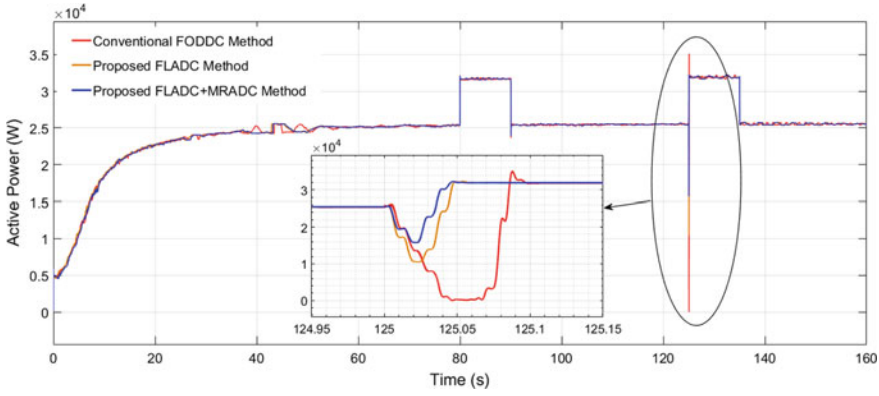

Fig. 28 Active power profile for load variations as per test case-TC_{17} of Table 5

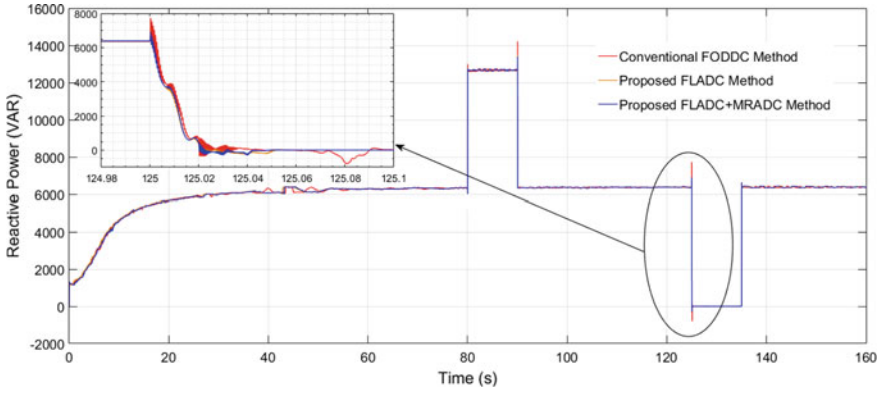

Fig. 29 Reactive power profile for load variations as per test case-TC_{18} of Table 5

17, 18, 19, 20, 21, 22, 23, and 24. Finally, a cumulative comparison of all the results is summarized in Table 8.

To analyze the impact of balanced reactive load variations on the voltage response, test case-TC_1 of Table 5 is implemented, where inductive and capacitive-type loads are injected during (80–90)s and (125–135)s, respectively, as per the specifications given in Tables 6 and 7. From the corresponding simulation result shown in Fig. 14, it is observed that the injected reactive load variations affected the voltage profile critically when using the conventional FODDC method, which takes a restoration time of 4 cycles subjected to a balanced capacitive load variation on the three phases. This effect is sequentially reduced when using the proposed methods, which reduces the restoration time to 1.5 cycles and 1 cycle with the FLADC and FLADC + MRADC methods, respectively.

Similarly, test case-TC_2 of Table 5 is implemented to understand the impact of unbalanced loading on the three phases. From the respective result shown in Fig. 15, it is observed that the conventional FODDC method causes little distortions in the voltage profile during the restoration process after the disturbance is removed, which are nullified when using the proposed FLADC and FLADC + MRADC methods. Besides, to analyze the effects of high impact disturbances, an arc furnace load is injected into the system during (80–90)s as per the test case-TC_3 of Table 5. From the corresponding simulation result shown in Fig. 16, it is observed that the variation of highly nonlinear load, critically disturbed the system voltage profile that is obtained with conventional as well as proposed control methods. Similarly, the other key performance index of voltage characteristics such as rate of change of voltage, voltage deviations, voltage imbalances is also computed as given in Figs. 17, 18, 19, 20, 21, 22, 23, and 24 with respect to different test cases given in Table 5.

As per the test case-TC_4 of Table 5, the rate of change of voltage is measured subjected to balanced reactive load variations in the system, where inductive and capacitive-type loads are injected during (80–90)s and (125–135)s, respectively, as per the specifications given in Tables 6 and 7. The corresponding result is shown in

Table 8 Summary of key performance index obtained with conventional and proposed methods

Performance index		Test case no.	Conventional FODDC method	Proposed FLADC method	Proposed FLADC + MRADC method
Waveform shape distortions	Stability restoration time	TC_1	4 cycles	1.5 cycles	1 cycle
	Deviations	TC_2	Major deviation	Minor deviation	Minor deviation
		TC_3	Major deviation	Major deviation	Major deviation
Rate of change of voltage (V/s)		TC_4	9.95	4.7	2.75
Voltage deviation (%)		TC_5	95	46	25
		TC_6	8	0	0
		TC_7	6.5	2	1.5
Positive sequence voltage		TC_8	0.04	0.54	0.75
		TC_9	0.92	1.02	1.02
Negative sequence voltage		TC_{10}	0.165	0.122	0.07
		TC_{11}	0.11	0.005	0.003
Voltage imbalance (%)		TC_{12}	412.5	22.59	9.33
		TC_{13}	11.96	0.49	0.29
Over frequency deviations (Hz)		TC_{14}	50.52	50.02	50.01
		TC_{15}	50.253	50.251	50.245
Under frequency deviations (Hz)		TC_{14}	49.8	49.9	49.9
		TC_{15}	49.78	49.8	49.86
Rate of change of frequency (Hz/s)		TC_{16}	+5, −6.5	+0.9, −1	+0.9, −1
Active power deviation ΔP (%)		TC_{17}	100	61.54	38.46
Reactive power deviation ΔQ (%)		TC_{18}	21.09	6.25	6.25

Fig. 17, from which, it is observed that the system can tolerate the inductive load variations, but, exhibits disturbed response during the capacitive load variations. This leads to a rate of change of voltage of 9.95% when using the conventional FODDC method, which violated the standard tolerance of 3% [33, 34]. This undesired deviation is considerably reduced especially to 2.75% with the use of the proposed FLADC + MRADC method. The deviation in the average value of three-phase voltage is measured as per the test cases-TC_5 to TC_7 of Table 5 subjected to balanced/unbalanced reactive load variations and nonlinear load variations based on the specifications

given in Tables 6 and 7. The corresponding simulation results are shown in Figs. 18, 19 and 20.

- As shown in Fig. 18, use of conventional FODDC method leads to huge voltage deviation of 95% that lasts for almost 5 cycles for balanced capacitive load injection. This undesired deviation is considerably reduced to 46% for 2.5 cycles and 25% for 2 cycles duration, respectively, with the proposed FLADC and FLADC + MRADC methods.
- As shown in Fig. 19, use of conventional FODDC method leads to voltage deviation of 8% subjected to unbalanced load variations as given in test case-TC_6. This deviation is fully nullified to 0% when using proposed methods.
- As shown in Fig. 20, use of conventional FODDC method leads to voltage deviation of 6.5% subjected to flicker sensations. This undesired deviation is effectively reduced to 2% and 1.5%, respectively, with the proposed FLADC and FLADC + MRADC methods.

Any deviation in voltage and current waveform from perfect sinusoidal in terms of magnitude or phase shift is termed as an imbalance. The voltage imbalance is one of the key power quality performance indexes, which generally occurs because of the following reasons.

- Switching of three-phase heavy loads, which results in current and voltage surges, causes an imbalance in the system.
- Any large single-phase load or a number of small loads connected to only one phase causes more current to flow from that particular phase. This leads to voltage drop in that phase and can cause three-phase voltage imbalance.

To analyze the voltage imbalance characteristics, various test cases-TC_8 to TC_{13} are implemented, and the corresponding results are given in Figs. 21, 22, 23 and 24. The imbalance is calculated in terms of maximum deviation of voltage in a phase from the mean of three phases. Alternatively, voltage imbalances can be calculated as a ratio of negative sequence value to positive sequence value.

- In Figs. 21 and 23, the positive and negative sequence voltages are resulted, respectively, from activating a balanced three-phase capacitive-type load during (125–135)s. Similarly, in Figs. 22 and 24, the positive and negative sequence voltages are resulted, respectively, from activating unbalanced loads as defined by D_2 of Table 7.
- During all these above-mentioned disturbances, the deviations in the sequence voltages reduce with the use of proposed methods as shown in Figs. 21, 22, 23 and 24. This helps in reducing corresponding voltage imbalances in the system.

6.2 Observations on Frequency Response Variations

Frequency is another important power quality indices that is to be maintained satisfactorily within the tolerance limits to develop seamless microgrid and utility grid

integration as recommended by IEEE 1547 standard [33], as well as to ensure the safe operation for the connected devices to the microgrid. The deviations in the frequency response are normally occurring due to switching of large reactive loads, nonlinear loads, supply discontinuities, etc.

To understand the impacts of various disturbances on the frequency characteristics, two indices are considered, viz. frequency deviations (over and under frequency) and rate of change of frequency. Various test conditions as described in Table 5 are implemented, and the corresponding frequency responses are plotted as shown in Figs. 25, 26 and 27. The collective quantitative comparisons of all these results are given in Table 8. From these results, the following comparative remarks could be made.

- To analyze the impact of balanced reactive load variations on the frequency response, test case-TC_{14} of Table 5 is implemented, where inductive and capacitive-type loads are injected during (80–90)s and (125–135)s, respectively, as per the specifications given in Tables 6 and 7. From the corresponding simulation result shown in Fig. 25, it is observed that the injected reactive load variations critically affected the frequency profile when using the conventional FODDC method. This deviation in frequency response is considerably reduced when using the proposed FLADC and FLADC + MRADC methods.
- Similarly, test case-TC_{15} of Table 5 is implemented to understand the effects of high impact disturbances. For this, an arc furnace load is injected into the system during (80–90)s. From the corresponding simulation result shown in Fig. 26, it is observed that there is a little improvement in this characteristic when using the proposed methods compared to conventional method.
- The rate of change of frequency under balanced reactive load variations is measured as shown in Fig. 27 with respect to test case-TC_{16} of Table 5. From this, it is observed that, the injected disturbance leads to a rate of change of frequency value of +5 Hz/s (above) and −6.5 Hz/s (below) when using the conventional method. So, these values are violated the standard tolerance limits of ±1 Hz/s [33, 34]. But, the usage of the proposed methods reduces this effect, which leads to values of +0.9 Hz/s (above) and −1 Hz/s (below).

6.3 Observations on Active and Reactive Power Profiles

The characteristics of active and reactive power flows in the system are supposed to be smooth with respect to the loading conditions. To understand these characteristics, inductive and capacitive load change as per the test cases-TC_{17} and TC_{18} is injected into the system during (80–90) s and (125–135) s, respectively, as described in Table 5.

The corresponding simulation results are given in Figs. 28 and 29 for active and reactive power profiles, respectively. From these results, it is observed that the proposed methods shown the improved transient responses of active and reactive

powers under the considered test conditions. This indicates smooth power transitions in the system, which is one of the requisites for the microgrid and utility grid seamless integrations [33]. The collective quantitative comparisons of all these results are given in Table 8.

7 Conclusion

To overcome the limitations of conventional droop controllers in view of inertia emulation characteristics, this chapter proposes adaptive virtual inertia-based droop controller coefficients' design with the use of fuzzy logic and model reference-based control concepts. The proposed FLADC has fuzzy logic-based trained loop continuously adjusts $p - \omega$ droop coefficient according to the deviation in system frequency. Similarly, the proposed MRADC uses small signal model of the microgrid as a reference model that produces a correction coefficient to design the $q - v$ droop coefficient. The combination of both these proposed approaches helps to tune the response of the plant to gradually align with the ideal response in a closed loop and thereby produces a better response as desired. It is proved through extensive simulation cases. From results, it is observed that the proposed method improves the transient response during key disturbances and shows superior performance when compared to the conventional method.

The salient merits of the proposed method for microgrid application are given as follows.

- It corrects both the frequency and voltage responses according to the disturbances occurred in the system.
- Instead of emulating fixed inertia as stated in state-of-the-art approaches, the proposed method injects adaptive virtual inertia according to the voltage and frequency deviations during disturbances.
- Emulation of adaptive inertia virtually through the variation of $p - \omega$ droop coefficient according to the frequency deviation subjected to a disturbance helps the controller to commendably respond to the disturbances and thereby delivers better control actions to improve the system performance. Similarly, by adaptively regulating $q - v$ droop coefficient according to the voltage deviation during disturbances, the voltage can be improved as desired.
- From the quantitative results shown in Table 8, it is observed that all the performance indices of voltage, frequency, and power characteristics have been improved with the proposed FLADC plus MRADC method. This improvement in system transient response during key disturbances helps in ensuring stability requirements for seamless integration of microgrids and utility grid power export or import as suggested by IEEE-1547 standard [33].

Hence, as per the aforesaid salient features, it is concluded that the proposed FLADC + MRADC method is a preferable method to design microgrid's droop

controller parameters that help to considerably improve the microgrid performance during various disturbances.

References

1. Alaboudy AK, Zeineldin H, Kirtley J (2012) Microgrid stability characterization subsequent to fault-triggered islanding incidents. IEEE Trans Power Deliv 27:658–669. https://doi.org/10.1109/tpwrd.2012.2183150
2. Katiraei F, Iravani M (2006) Power management strategies for a microgrid with multiple distributed generation units. IEEE Trans Power Syst 21:1821–1831. https://doi.org/10.1109/tpwrs.2006.879260
3. Piagi P, Lasseter R (2006) Autonomous control of microgrids. In: 2006 IEEE power engineering society general meeting. https://doi.org/10.1109/pes.2006.1708993
4. Liu H, Chen Y, Li S, Hou Y (2013) Improved droop control of isolated microgrid with virtual impedance. In: 2013 IEEE power and energy society general meeting. https://doi.org/10.1109/pesmg.2013.6672849
5. Liu J, Miura Y, Ise T (2016) Comparison of dynamic characteristics between virtual synchronous generator and droop control in inverter-based distributed generators. IEEE Trans Power Electron 31:3600–3611. https://doi.org/10.1109/tpel.2015.2465852
6. Zhong Q (2016) Virtual synchronous machines: a unified interface for grid integration. IEEE Power Electron Mag 3:18–27. https://doi.org/10.1109/mpel.2016.2614906
7. Dheer D, Soni N, Doolla S (2016) Improvement of small signal stability margin and transient response in inverter-dominated microgrids. Sustain Energy Grids Netw 5:135–147. https://doi.org/10.1016/j.segan.2015.12.005
8. Soni N, Doolla S, Chandorkar M (2013) Improvement of transient response in microgrids using virtual inertia. IEEE Trans Power Deliv 28:1830–1838. https://doi.org/10.1109/tpwrd.2013.2264738
9. Alipoor J, Miura Y, Ise T (2015) Power system stabilization using virtual synchronous generator with alternating moment of inertia. IEEE J Emerg Sel Top Power Electron 3:451–458. https://doi.org/10.1109/jestpe.2014.2362530
10. Xiaobo Z, Kangda W, Baohui Z (2016) An improved droop controller for eliminating control error in microgrid. In: 2016 IEEE PES Asia-Pacific power and energy engineering conference (APPEEC). https://doi.org/10.1109/appeec.2016.7779661
11. Hou X, Han H, Zhong C et al (2016) Improvement of transient stability in inverter-based AC microgrid via adaptive virtual inertia. In: 2016 IEEE energy conversion congress and exposition (ECCE). https://doi.org/10.1109/ecce.2016.7855195
12. Li D, Zhu Q, Lin S, Bian X (2017) A self-adaptive inertia and damping combination control of VSG to support frequency stability. IEEE Trans Energy Convers 32:397–398. https://doi.org/10.1109/tec.2016.2623982
13. Yajuan G, Weiyang W, Xiaoqiang G, Herong G (2010) An improved droop controller for grid-connected voltage source inverter in microgrid. In: 2nd international symposium on power electronics for distributed generation systems. https://doi.org/10.1109/pedg.2010.5545801
14. Meng J, Wang Y, Fu C, Wang H (2016) Adaptive virtual inertia control of distributed generator for dynamic frequency support in microgrid. In: 2016 IEEE energy conversion congress and exposition (ECCE). https://doi.org/10.1109/ecce.2016.7854825
15. Bidram A, Davoudi A (2012) Hierarchical structure of microgrids control system. IEEE Trans Smart Grid 3:1963–1976. https://doi.org/10.1109/tsg.2012.2197425
16. Guerrero J, Matas J, Garcia de Vicuna L et al (2007) Decentralized control for parallel operation of distributed generation inverters using resistive output impedance. IEEE Trans Ind Electron 54:994–1004. https://doi.org/10.1109/tie.2007.892621

17. Sao C, Lehn P (2005) Autonomous load sharing of voltage source converters. IEEE Trans Power Deliv 20:1009–1016. https://doi.org/10.1109/tpwrd.2004.838638
18. Sao C, Lehn P (2008) Control and power management of converter fed microgrids. IEEE Trans Power Syst 23:1088–1098. https://doi.org/10.1109/tpwrs.2008.922232
19. Rokrok E, Golshan M (2010) Adaptive voltage droop scheme for voltage source converters in an islanded multibus microgrid. IET Gener Transm Distrib 4:562. https://doi.org/10.1049/iet-gtd.2009.0146
20. Guerrero J, Matas J, De Vicuna LGDV et al (2006) Wireless-control strategy for parallel operation of distributed-generation inverters. IEEE Trans Ind Electron 53:1461–1470. https://doi.org/10.1109/tie.2006.882015
21. Mehrizi-Sani A, Iravani R (2010) Potential-function based control of a microgrid in islanded and grid-connected modes. IEEE Trans Power Syst 25:1883–1891. https://doi.org/10.1109/tpwrs.2010.2045773
22. Yao W, Chen M, Matas J et al (2011) Design and analysis of the droop control method for parallel inverters considering the impact of the complex impedance on the power sharing. IEEE Trans Ind Electron 58:576–588. https://doi.org/10.1109/tie.2010.2046001
23. Li Y, Li YW (2009) Virtual frequency-voltage frame control of inverter based low voltage microgrid. In: 2009 IEEE electrical power and energy conference (EPEC). https://doi.org/10.1109/epec.2009.5420973
24. Li Y, Li YW (2011) Power management of inverter interfaced autonomous microgrid based on virtual frequency-voltage frame. IEEE Trans Smart Grid 2:30–40. https://doi.org/10.1109/tsg.2010.2095046
25. Li Y, Vilathgamuwa D, Loh P (2004) Design, analysis, and real-time testing of a controller for multibus microgrid system. IEEE Trans Power Electron 19:1195–1204. https://doi.org/10.1109/tpel.2004.833456
26. Kwasinski A (2011) Quantitative evaluation of DC microgrids availability: effects of system architecture and converter topology design choices. IEEE Trans Power Electron 26:835–851. https://doi.org/10.1109/tpel.2010.2102774
27. Tuladhar A, Jin H, Unger T, Mauch K (2000) Control of parallel inverters in distributed AC power systems with consideration of line impedance effect. IEEE Trans Ind Appl 36:131–138. https://doi.org/10.1109/28.821807
28. Borup U, Blaabjerg F, Enjeti P (2001) Sharing of nonlinear load in parallel-connected three-phase converters. IEEE Trans Ind Appl 37:1817–1823. https://doi.org/10.1109/28.968196
29. Zhong Q (2013) Harmonic droop controller to reduce the voltage harmonics of inverters. IEEE Trans Ind Electron 60:936–945. https://doi.org/10.1109/tie.2012.2189542
30. Pavan Kumar YV, Ravikumar B (2017) Fuzzy logic based adaptive virtual inertia in droop control operation of the microgrid for improved transient response. In: 2017 IEEE PES Asia-Pacific power and energy engineering conference (APPEEC). https://doi.org/10.1109/appeec.2017.8309006
31. Yen J, Langari R (1999) Fuzzy logic. Prentice Hall, Upper Saddle River, N.J
32. Murthy BV, Kumar YP, Kumari UR (2012) Fuzzy logic intelligent controlling concepts in industrial furnace temperature process control. In: 2012 IEEE international conference on advanced communication control and computing technologies (ICACCCT). https://doi.org/10.1109/icaccct.2012.6320801
33. Tagare MD (2011) Interconnecting distributed resources with electric power systems. In: Tagare MD (ed) Electric power generation. The changing dimensions, Wiley, pp 301–313. https://doi.org/10.1002/9780470872659.ch15
34. Voltage Characteristics of Electricity Supplied by Public Electricity Networks, Voltage Disturbances Standard EN 50160 2013

Design of Linear and Nonlinear Controllers for a Grid-Connected PV System for Constant Voltage Applications

Nibedita Swain and Nivedita Pati

Abstract As the assimilation of photovoltaic (PV) systems with grid is having an exponential growth, design of an appropriate controller gains a higher priority. The PV system output changes with solar irradiation and cell temperature, and also the power converters are variable structure devices which further assist in making the entire system as a highly nonlinear system. The control system in a two-stage PV system is achieved through two different control approaches. One is to make the PV work so as to extract maximum power from it, and the other control strategy aims at regulating the output of the converter. In order to satisfy both the control objectives simultaneously, controllers are segregated based on its work. In order to make the system continuously adapt and extract maximum power from PV, an algorithm exists known as Maximum Power Point Tracking (MPPT). The MPPT provided voltage as a reference is used which is further compared to converter output through a closed loop. The closed-loop voltage regulation of converter output is further dealt with a controller which varies the duty cycle of the power converter through the pulse width modulation (PWM) process.

Keywords Solar PV module · Nonisolated boost converter · Maximum Power Point Tracking · PI controller · H-infinity controller · Sliding mode controller · Full-bridge boost inverter

Nomenclature

ARE Algebraic Ricatti equation
CCM Continuous conduction mode

N. Swain · N. Pati (✉)
Department of Electrical Engineering, Silicon Institute of Technology, Bhubaneswar, Odisha, India
e-mail: niveditapati1981@gmail.com

N. Swain
e-mail: nibeditaswain@gmail.com

P. Ray and M. Biswal (eds.), *Microgrid: Operation, Control, Monitoring and Protection*, Lecture Notes in Electrical Engineering 625,
https://doi.org/10.1007/978-981-15-1781-5_5

DCM	Discontinuous conduction mode
FLC	Fuzzy logic controller
GM	Gain margin
IC	Incremental conductance
MPPT	Maximum Power Point Tracking
MRAS	Model reference adaptive system
MRAC	Model reference adaptive control
MPP	Maximum power point
LQG	Linear quadratic Gaussian
LQR	Linear quadratic regulator
LQE	Linear quadratic estimator
P&O	Perturb and observe
PI	Proportional integral
PID	Proportional integral derivative
PM	Phase margin
PV	Photovoltaic
PWM	Pulse width modulation
SM	Sliding mode
SMC	Sliding mode control
SC	Solar cell
SSA	State-space averaging technique
SVC	Static VAR compensator
ZN	Ziegler–Nichols method

1 Introduction

The increase in demand for a clean and green energy requirement has facilitated the use of renewable energy sources, more significantly the photovoltaic (PV) system. The large-scale power generation requires a grid-connected PV system with several interfacing units. A power conditioning device along with controllers helps in regulating the voltage fed to the inverter.

1.1 General Overview

This chapter discusses and compares the performance of various controllers for a grid-connected (photovoltaic) PV system more specifically the conversion stage. The conversion stage mainly comprises a power (DC-DC) converter fed from a variable PV output. The PV system can be classified as, whether they are connected to grid or not, well known as grid-connected and isolated PV systems. The isolated PV system is utilized for low energy consuming application, specially required in

rural areas, where there is a scarcity of electricity. These systems perform efficiently using simple controllers, but the control system required should be robust enough when PV penetrates into grid. In grid-coupled solar PV systems, improvement of efficiency and reliability of the overall system is always desired as energy usage efficiency plays a vital role which can be done by controlling the PV as well as the conversion part. Apart from this reason, staging of power conversion should be done in order to maintain a healthy quality of output power.

The PV side control is achieved through Maximum Power Point Tracking (MPPT) technology which works by optimizing the power flow from solar panel to load or battery. MPPT controllers convert module operating voltage to battery voltage and enhance output current in that process. The word "tracking" used in this chapter is electrical tracking done through shifting the operating point of solar PV system as discussed in [1]. By implementing the MPPT methods, the solar installations will benefit significantly. The gain will be increased by increasing the module operating voltage (V_{MPP}). For standalone systems, the MPPT is connected in series with PV arrays to draw high voltage which can reach up to 600 V. There are various MPPT algorithms validated for several factors associated with the PV system like change in irradiance and temperature to give an optimum performance. Design of the algorithm should be such that it could adapt to full utilization of power from the PV array under certain loading conditions such as partial load shading and disturbances. Popularly used algorithms are perturb and observe (P&O) and incremental conductance (INC) which function by varying the panel voltage to extract maximum power as discussed in [2]. The output of such algorithms could be duty cycle or a reference voltage.

The step-up transformation from low PV output to a higher one is done through the converters. There are two major distinct DC-DC converters based on the isolation separating the output and input. They are classified as nonisolated and isolated switching regulator, and nonisolated configurations are used mostly due to its simple structure. Buck, boost, buck–boost, and Cuk configurations are under nonisolated switching regulator, and push–pull and fly back to name a few are under isolated switching regulator as described in [3]. As compared to buck DC-DC converter, boost converters' input current is continuous in nature.

The universal power converters are illustrated according to their circuit configuration concisely as in [4]. The comparison in [5] shows that buck converter requires a high value of capacitance to smooth the PV current, and also the RMS value of ripple current is more; therefore, the boost converter is used to test optimality of a controller. The converter is mounted with a MPPT used to capture power from solar PV module. In DC-DC conversion, MPPT is used, and the voltage is reduced by increasing the current. Depending on whether the voltage is increased or decreased, the current will vary accordingly. Finally, the power remains constant. The second phase then involves regulation of converter output so as to provide a regulated input to inverter. Converter control is done through duty cycle using pulse width modulation (PWM) process. Converter control can be achieved by linear and nonlinear control laws. The various controllers used are the conventional PI controller, H-infinity, sliding mode (SM), hysteresis and fuzzy controllers. Compensator design is also possible

by proper estimation of the parameters. The purpose of all the controllers is same, but the design procedure and performance vary within certain trade-off.

1.2 Literature Review

Substantial literature is available on controlling the output voltage of the DC-DC converter. Several studies and topologies describing the performance and analysis of switching mode regulators have been completed using various techniques. The DC-DC power converter employed in solar systems is to identify and monitor the MPP generated by a PV module, under different climatic conditions and load variations.

The nonisolated power converter is fed with a variable DC voltage and produced a fixed DC output voltage. By using a proper voltage regulator, the output voltage remains constant in spite of load current (I_0) and input voltage (V_{in}) variation. Various types of voltage controllers are employed to improve the output voltage of power converters. Due to recent improvement in science and latest electronic components, an accurate and reliable regulation is required. The aim of this chapter is to discuss the control strategies employed to assist the realization of DC-DC converters. Different control techniques are described in this chapter.

1.2.1 Regulation of Converter Output Voltage Using Conventional PID Controller

PID controller is the oldest and classical controller used for DC-DC power converters. It uses different combinations like proportional, proportional plus integral, proportional plus derivative, and proportional plus integral plus derivative controllers. These different combinations are used to control the voltage output in these power converters. Due to many advantages of PID controller, it is mostly used in industry where power electronic converters are employed. The tuning method is based upon Ziegler–Nichols (ZN) method of controller tuning to produce the desired closed-loop performance. PID controllers are frequently used as controller for PV-based converter systems [6]. PID controllers are easy to apply and understand. It is reliable for linear single-input single-output (SISO) systems. Some disadvantages of PID controllers are that they are not dependable and acceptable for nonlinear systems and more rise time results in decreasing the overshoot of output voltage which affects the dynamic response of the converter.

1.2.2 Regulation of Converter Output Voltage Using Lead Compensator

An open-loop DC-DC power converter cannot regulate its output voltage due to fluctuation in input voltage and changing output load. A compensator is used to

overcome this problem, so that the power converter will produce stable output voltage. They are designed to provide a specific gain and phase shift at one frequency. The term compensation is linked to the bode design, but a classical controller design is much linked with root locus technique. A controller is a much more general term which refers to the block that is inserted to produce the desired closed-loop response in either t-domain or in s-domain. The controller assists the output towards its nominal set point and tries to nullify the error. PID controller is the best choice in this regard. On the other hand, a compensator is needed to alternate the entire system characteristics; it is operated besides the control functions. A compensator is an additional element embedded into a system to compensate for a deficient performance of the overall system as stated in [7]. The lead compensator is commonly used as PD controller to reshape the root locus to improve the transient response. A larger phase margin indicates a more stable control system but more sluggish response. The choice of phase margin between 40° and 60° can achieve a good trade-off between system stability and responsiveness. A lead compensator will make the phase margin become larger. Similarly, PD controller will make the system more stable.

1.2.3 Regulation of Converter Output Voltage Using Optimal Control

Linear quadratic Gaussian (LQG) controller problem is the optimal control problems and is applicable to the systems those are disturbed by additive white Gaussian noise and having incomplete state information. The control technique is also used for minimizing the cost function in [8] and also needs a feedback control law which has to be implemented. The LQG regulator is a combination of Kalman filter or called as linear quadratic estimator (LQE) and a linear quadratic regulator (LQR) as stated in [9]. These two can be designed independently by using the separation principle. LQG controller is applicable to linear system which is variable and also nonvariable with respect to time. The controller is designed properly for a reduced-order model where the dimension of system state is quite small. The application of LQG controller to a large system is very difficult because the number of states is no longer separable.

1.2.4 Regulation of Converter Output Voltage Using Model Reference Adaptive Control

Model reference adaptive control is coming under nonlinear control and is one of the major approaches to adaptive control. The desired performance is expressed in terms of a reference model that gives the expected response to a command signal. The system also has a standard feedback loop composed of the plant and the controller. The error is the difference between the system output and reference model. The regulator has parameters that are changed based on the error. Out of the pair loops, one is the feedback loop that provides the standard control feedback, and the other loop adjusts the parameters in the feedback loop. The inner loop is assumed to be faster than the outer loop. The gradient approach to MRAC is developed in this paper

[10]. The difficulty of this controller is the adjustment of the regulator parameters such that difference between the plant output and the reference model is driven towards zero.

1.2.5 Regulation of Output Voltage Using H-Infinity Controller

H-infinity control is a mathematical optimization process which deals with the minimization of the H_∞ norm of a transfer matrix from an external disturbance to a pertinent controlled output of a given plant. H_∞ norm of any transfer matrix is maximum or supremum value over all frequencies. The controller implementation includes two outputs, one is the error signal which is to be minimized and the other is the measured variables that are used to control the system as in [11]. Due to robust nature of this controller, it is used in this chapter.

1.2.6 Regulation of Converter Output Voltage Using SMC

Sliding mode control (SMC) is a nonlinear control technique that develops the dynamic model of the nonlinear system. SMC systems drive the system states onto a particular called sliding surface. Once the sliding surface is reached, SMC keeps the states on the close region of the sliding surface. Hence, the sliding mode control is a two-section controller design. The first section involves the sliding surface design to satisfy the sliding motion design specifications. The second section selects a relevant control law for the switching surface [12].

1.3 Conclusion from Literature Review

The present work focuses in the area of designing several control techniques for various power electronic converter systems used for grid-connected PV system. The improvement of dynamic stability of power converter ensures secure and stable operation of the grid-connected PV system. The controllers are structured in both PID and fuzzy, and a comparison study has been done between the performances of both the structures [13]. For improving the stability and for achieving the desired response, a lead compensator is designed for the system. The converter closed-loop design is carried with LQG regulator to minimize the cost function, hence improving the overall performance [14].

2 Modeling and Design of Overall System

The realization of solar PV system depends upon changing environmental conditions and also depends upon the uses of MPPT. PV system generates maximum power by utilizing MPPT. The primary purpose of a controller is to adjust the operating point while climatic conditions vary. The power converter along with PV module adjusts the operating point through MPPT controller.

The output power of PV module varies due to fluctuation in solar radiation, temperature conditions, and under consumer load variations. The output voltage of the converter can be controlled by controlling duty cycle of the switch S. Duty ratio measures the ratio of ON time to OFF time over one switching period. Here different controllers are discussed for PV-fed boost converter. The proposed model is depicted in Fig. 1.

In Fig. 1, V_{ODC} represents the converter output voltage which has to be controlled by using different controllers and fed to the input of the inverter. V_{OAC} represents inverter output voltage which is sinusoidal in nature and fed to the AC load. V_{PV} and I_{PV} represent PV voltage and PV current, respectively. V_{MAX} represents the maximum voltage from the output of the MPPT.

2.1 Design of PV System

The photovoltaic (PV) systems had gained a higher priority among other renewable energy sources. The grid-connected PV systems consist of a conversion stage, where the PV generator output is fed to electronic converters to process electricity. The PV system is also highly nonlinear in nature as it depends upon sun's irradiation which is

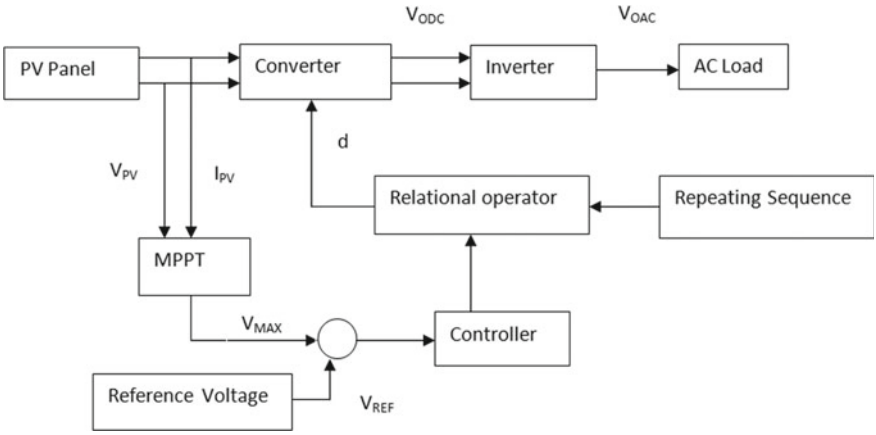

Fig. 1 Proposed model of grid-connected PV system

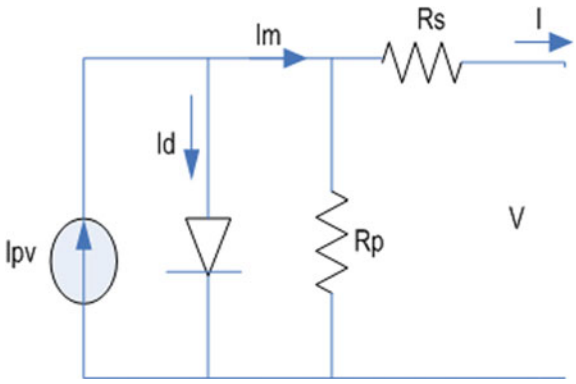

Fig. 2 Equivalent circuit of single-diode PV cell

continuously varying throughout the day. The mathematical model of the PV device is thus useful in the dynamic study and analysis of the device as a source. The purpose of mathematical model is to simulate the true PV system which converts the irradiance into a variable DC voltage and current. Several literatures reveal various configurations of a PV model varying in accuracy and complexity. The single-diode model is considered as it is simple and easily accessible physical model used to represent the electric characteristics of a single PV cell. The model consists of: (1) a current source, I_{pv}, illustrating the light-induced current generated in the cell, (2) p-n junction diode for PV cell, (3) parallel resistance, R_{sh}, and (4) a series resistance, R_s shown in Fig. 2.

I-V characteristic of the array can be achieved on application of the Shockley diode equation and Kirchhoff's current law as in Eq. 1.

$$I = I_{pv} - I_0\left[\exp\left(\frac{V + R_s I}{V_t a}\right) - 1\right] - \frac{V + R_s I}{R_p} \tag{1}$$

where I_{pv}, I_0 are the PV current and saturation current of the array, and V_t is the thermal voltage, respectively. I-V characteristic also depends on several other parameters like irradiance level and cell temperature. The equations required to include all the parameter dependence and improvement of the model are described as in Eqs. 2–4. The array is modeled through various subsystems of I_{pv}, I_0, I_m, a dependent current source and the resistors.

$$I_{pv} = \left(I_{pv,n} + K_i \Delta_T\right)\frac{G}{G_n} \tag{2}$$

$$I_{0,n} = \frac{I_{sc,n}}{\exp\left(\frac{V_{oc,n}}{aV_{t,n}}\right) - 1} \tag{3}$$

$$I_0 = \frac{I_{sc,n} + K_i \Delta_T}{\exp\left(\frac{V_{oc,n} + K_v \Delta_T}{aV_t}\right) - 1} \tag{4}$$

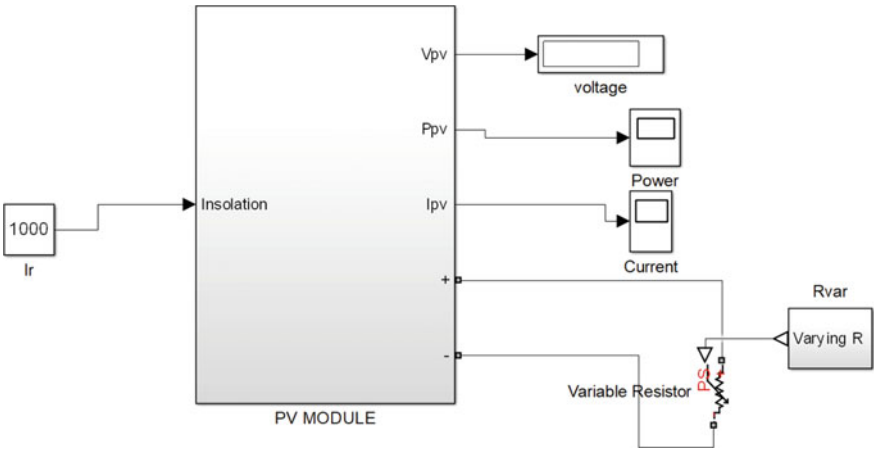

Fig. 3 Simulink model of PV source

In this chapter, the entire PV module consists of 26 solar cells, each is having open-circuit voltage of 0.6 V and short-circuit current of 4.75 A in series along with the Simulink-PS converter and PS-Simulink converter to generate a voltage of 15 V which is fed to the nonisolated boost converter. Figure 3 represents the PV module in a Simulink environment. It has two main characteristics, P-V and I-V characteristics [15], from where the operating point is calculated.

2.2 Maximum Power Extraction Through MPPT

MPPT is an algorithm that maximizes the power extraction from a PV system under all climatic situations. The photovoltaic system's performance can be enhanced by using a high-efficiency power control device to control the voltage to assure that the system operates under maximum power. MPPT can be designed in various ways, but all functions are moving around the P-V curves depending upon light intensity and temperature conditions. It is not fixed over a particular operating point. The mostly used MPPT algorithms are (i) perturb and observe and (ii) incremental conductance

(i) *Perturb and Observe Method*

This algorithm works on by deliberately creating disturbances with the help of increasing or decreasing the duty cycle to monitor its effect on power output. In this method, the variation in power is determined by changing the operating voltage and the operating point oscillates around the MPP along the PV curve. If $\Delta P > 0$, the operating point shifts closer to the MPP, and if $\Delta P < 0$, the operating point is far away from MPP, resulting sign of the perturbed voltage to be reversed and again to move the operating point to the MPP. The maximum power obtained at ΔP is zero.

(ii) *Incremental Conductance Method*

The algorithm is derived by taking the derivative of the power equation of PV module with respect to voltage and makes it to zero. The set of governing equations are given in Eqs. 5 and 6.

$$P = V * I \tag{5}$$

$$\frac{\mathrm{d}P}{\mathrm{d}V} = I + V * \frac{\mathrm{d}I}{\mathrm{d}V} \tag{6}$$

The conditions that need to be satisfied to shift the operating point to MPP are followed by Eqs. 7, 8, and 9.

$$\frac{\mathrm{d}P}{\mathrm{d}V} = -\frac{I}{V}, \frac{\mathrm{d}P}{\mathrm{d}V} = 0 \tag{7}$$

$$\frac{\mathrm{d}P}{\mathrm{d}V} > \frac{I}{V}, \frac{\mathrm{d}P}{\mathrm{d}V} > 0 \tag{8}$$

$$\frac{\mathrm{d}P}{\mathrm{d}V} < \frac{I}{V}, \frac{\mathrm{d}P}{\mathrm{d}V} < 0 \tag{9}$$

The disturbances are continuously repeated until the first condition is satisfied. When the irradiation increases or decreases, the MPP shifts to the right or left of the operating voltage. The function of MPPT is to increase or decrease the operating voltage, respectively, under these varying conditions. The PV and IV characteristics for different irradiance levels are depicted in Figs. 4 and 5, respectively.

From the above characteristics, it is observed that the maximum power varies by increasing the irradiance level, and also the operating point is shifted. For 900 W/m^2, the maximum power is 48 W, whereas for 1100 W/m^2 the maximum power is 58 W. V_{MPP} remains constant, but I_{MPP} is varying.

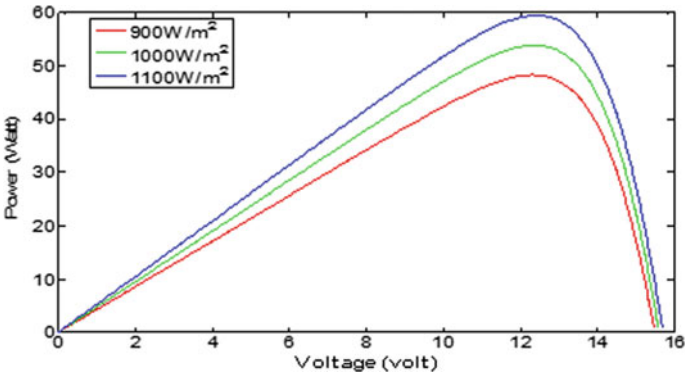

Fig. 4 PV characteristic

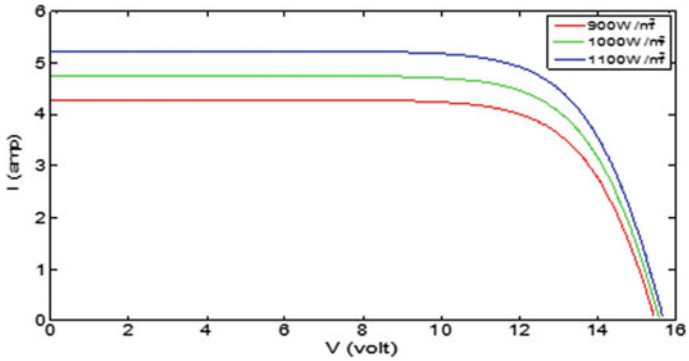

Fig. 5 I-V characteristic

From I-V characteristics, it is noticed that the current value increases with increasing insolation keeping voltage constant. The maximum power is 54 W at 1000 W/m^2 irradiance, and the corresponding V_{MPP} and I_{MPP} are 12.5 V and 4.9 A, respectively.

2.3 Mathematical Linearization of DC-DC Converters

The DC-DC power converters are frequently used devices in applications like power management and voltage regulation. The basic converter configuration consists of an inductor, a capacitor, a diode, and a controlled switch. Its operation and performance are governed by the switch which operates in two binary states, on and off. Thus, the inherent switching operation results in a configuration which is periodically changing. This leads to a variable set of equations which makes the system complicated for analysis and controlling view point. Various techniques are formulated to linearize such systems so as to avoid the modeling uncertainties and make the system work optimally for some specific condition. State-space averaging (SSA) method [16] is one such process of modeling through which an equivalent circuit of any DC-DC converters can be derived. The equivalent circuit helps in developing a transfer function model of the nonlinear power converter. The transfer function can be developed with respect to input as well as duty ratio as duty ratio control is mostly implemented to achieve a desired performance. The outline of the linearization process is presented through a flowchart in Fig. 6.

The following notations and conventions are common to describe the equations in continuous conduction mode.

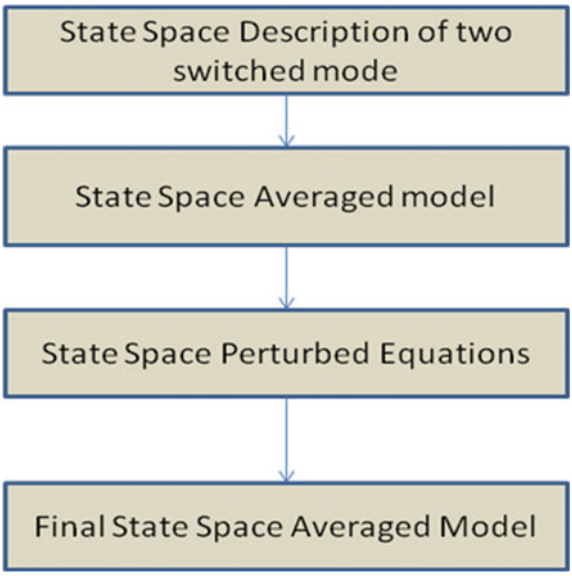

Fig. 6 Outline of the linearization process

d = duty ratio
$d' = 1 - d$
X = State Vector
V_0 = Output Voltage
V_{in} = Input Voltage

During each switching period, the converter is described by a set of state-space equations given in Eqs. 10–13.

$$\dot{X} = A_1 X + B_1 V_{\text{in}} \tag{10}$$

$$V_0 = C_1 X \tag{11}$$

$$\dot{X} = A_2 X + B_2 V_{\text{in}} \tag{12}$$

$$V_0 = C_2 X \tag{13}$$

Equations 10 and 11 are during on state ($d \bullet T_s$), and Eqs. 12 and 13 are during off state $[(1 - d)\, T_s]$. The above equations are combined to get a single state-space matrix to describe the averaged model as given in Eqs. 14 and 15, respectively.

$$\dot{X} = \left[A_1 d + A_2 d'\right] X + \left[B_1 d + B_2 d'\right] V_{\text{in}}$$

$$\dot{X} = AX + BV_{\text{in}} \tag{14}$$

$$\begin{aligned} V_0 &= \left[C_1 d + C_2 d'\right] X \\ V_0 &= CX \end{aligned} \tag{15}$$

Introducing certain perturbations in the variables and applying the superposition principle, transfer function model can be derived and is given in Eq. 16.

$$\dot{\tilde{x}} = AX + BV_{\text{in}} + A\tilde{x} + [(A_1 - A_2)X + (B_1 - B_2)V_{\text{in}}]\tilde{d} + \text{negligible terms} \tag{16}$$

Equations 15 and 16 can thus be reduced to Eqs. 17 and 18, respectively.

$$\dot{\tilde{x}} = A\tilde{x} + [(A_1 - A_2)X + (B_1 - B_2)V_{in}]\tilde{d} \tag{17}$$

$$\tilde{v}_0 = C\tilde{x} + [(C_1 - C_2)X]\tilde{d} \tag{18}$$

Taking Laplace transformation and solving, the transfer functions are as given in Eqs. 19 and 20, respectively. Transfer function analysis for duty cycle is carried out by taking input voltage perturbations zero, and for input voltage, duty ratio perturbation is considered as zero.

$$\frac{V_0(s)}{d(s)} = C[sI - A]^{-1} \cdot [(A_1 - A_2)X + (B_1 - B_2)V_{\text{in}}] + (C_1 - C_2)X \tag{19}$$

$$\frac{V_0(s)}{V_{\text{in}}(s)} = C[sI - A]^{-1} \cdot B \tag{20}$$

The above equations are helpful for linearization of any type of converter configuration. In this chapter, the dynamic model of DC-DC boost converter is analyzed, circuit parameter specification is given in Table 1, and the circuit is given in Fig. 7.

The dynamic equations of boost converter for ON and OFF state are provided in Eqs. 21 and 22, respectively.

Table 1 Circuit parameter specification

Circuit parameters	Values
Input voltage (V_{in})	15 V
Set point voltage $(V_{\text{s}})_{\text{desired}}$	30 V
Inductance (L)	500 μH
Capacitance (C)	300 μF
Load resistance (R)	20 Ω
Switching frequency (f_{s})	5 kHz

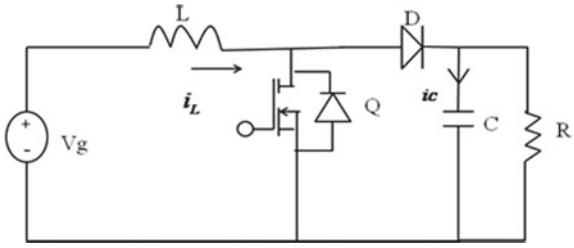

Fig. 7 Circuit model of boost converter

$$V_{\text{in}} - \frac{\mathrm{d}i_L}{\mathrm{d}t} = 0$$
$$\frac{V_{\text{c}}}{R} - \frac{C\mathrm{d}V_{\text{c}}}{\mathrm{d}t} = 0 \tag{21}$$

$$V_{\text{in}} - V_{\text{c}} - L\frac{\mathrm{d}i_L}{\mathrm{d}t} = 0$$
$$i_{\text{L}} - \frac{V_{\text{c}}}{R} + C\frac{\mathrm{d}V_{\text{c}}}{\mathrm{d}t} = 0 \tag{22}$$

The transfer function is derived from its switching state equations using SSA [16, 17] and is given in Eq. 23.

$$\frac{V_{\text{o}}(s)}{d(s)} = \frac{-10{,}000s + 1 \times 10^8}{s^2 + 166.7s + 1.667 \times 10^6} \tag{23}$$

The magnitude and phase angle plot of boost converter are illustrated in Fig. 8.

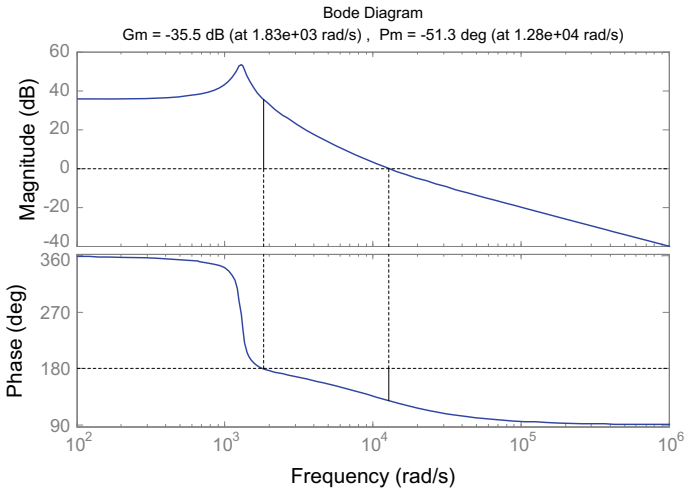

Fig. 8 Bode plot of the open-loop boost converter

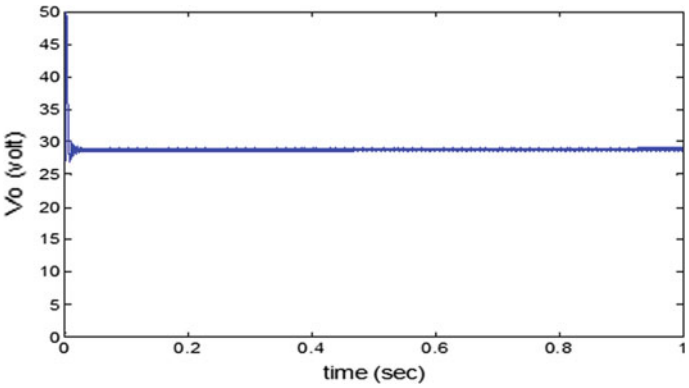

Fig. 9 Voltage output of boost converter

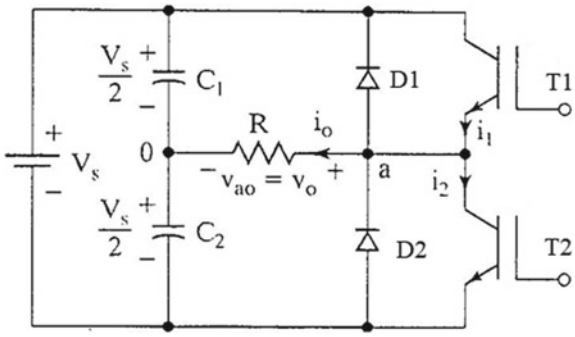

Fig. 10 1-φ half-bridge inverter

From Fig. 8, it can be observed that gain margin and phase margin both are negative making the system highly unstable. To make it stable, different control mechanisms are described later in this chapter. The output voltage of boost converter is illustrated in Fig. 9.

From above plot, it is observed that the overshoot is very large at the beginning and simultaneously it is reduced. The output is approximated to 30 V and is pulsating in nature. For generation of AC, this output voltage of boost converter is fed to the inverter circuit. Various inverter structures are explained in the next section. As the output voltage magnitude is less to produce 230 V AC, a boost transformer is used to improve the voltage at the output side.

2.4 Design of Different Inverter Configurations

Figure 10 shows that the 1-φ half-bridge inverter consists of two switches T_1, T_2 and two diodes D_1 and D_2 with a load. During the positive half cycle, T_1 is ON and V_o

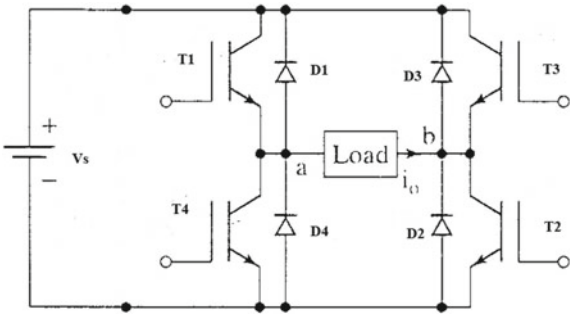

Fig. 11 1-φ full-bridge inverter

$= V_s/2$. During the negative half cycle, T_2 is ON and $V_o = -V_s/2$. Figure 11 shows the full-bridge inverter circuit consisting of T_1, T_2, T_3, T_4 and four diodes. T_1 and T_2 are operating for positive half cycle, and $V_o = V_s$ and $V_o = -V_s$ for negative half cycle when T_3 and T_4 are conducting. The peak value of the load voltage and load current for resistive load is calculated by using Eqs. 24 and 25, respectively.

$$V_{o(peak)} = \frac{4V_s}{\Pi} \tag{24}$$

$$i_{o(peak)} = \frac{4V_s}{\Pi R} \tag{25}$$

To increase the AC voltage to a high value, boost transformer is connected at the load side. The inverter structure is different from the full-bridge inverter configuration. The Simulink model of the full-bridge inverter with step-up transformer is illustrated in Fig. 12.

The inverter output is shown in Fig. 13 which is sinusoidal in nature and produces a voltage of 230 AC.

It is observed that peak inverter voltage is approximately 230 V which can be connected to any AC load.

3 Issues and Challenges in Grid Integrated PV System

The power quality issues addressed are mostly reactive power compensation and suppression of load harmonic currents. Generally, a phase-locked loop (PLL) is implemented in the synchronous frame to deal with the power quality-related problems.

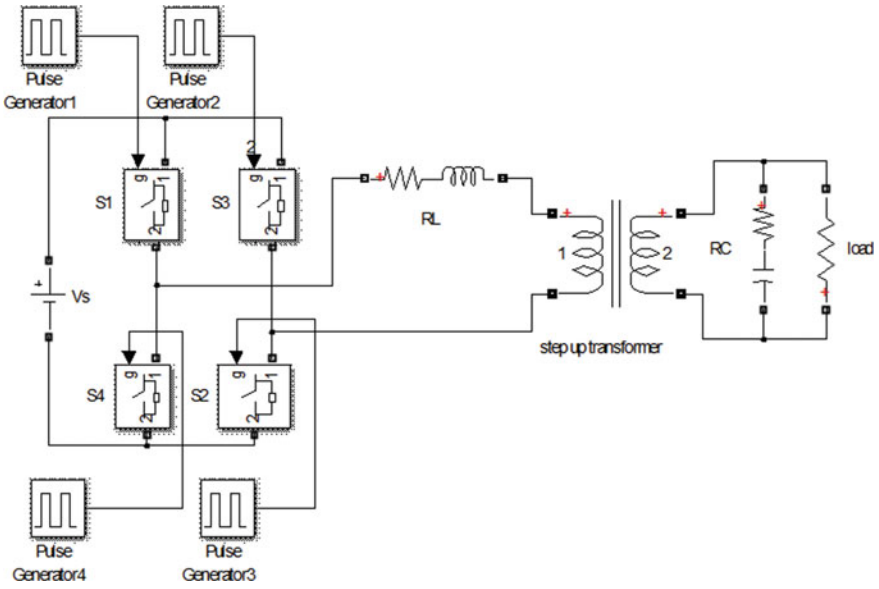

Fig. 12 1-φ full-bridge inverter plus step-up transformer

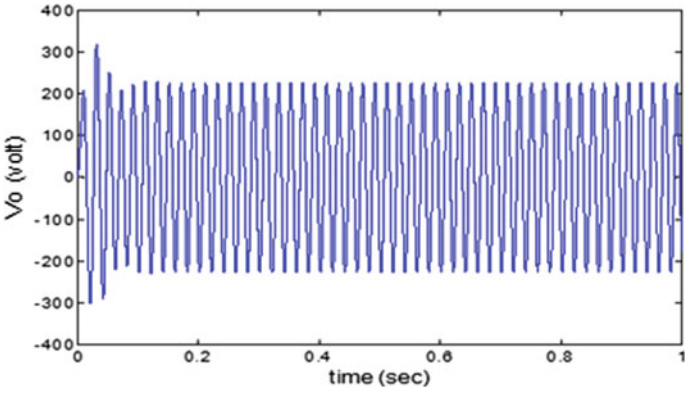

Fig. 13 Inverter output

3.1 Power Quality Issues

The need for a pollution-free, green, and clean energy system has facilitated the abundant use of sustainable energy systems and its assimilation with grid. The interdependence of various devices in the overall system gives rise to several Power quality issues. Power quality means maintaining the parameters of power like voltage, power factor, and harmonics within a prescribed and bounded range. The power

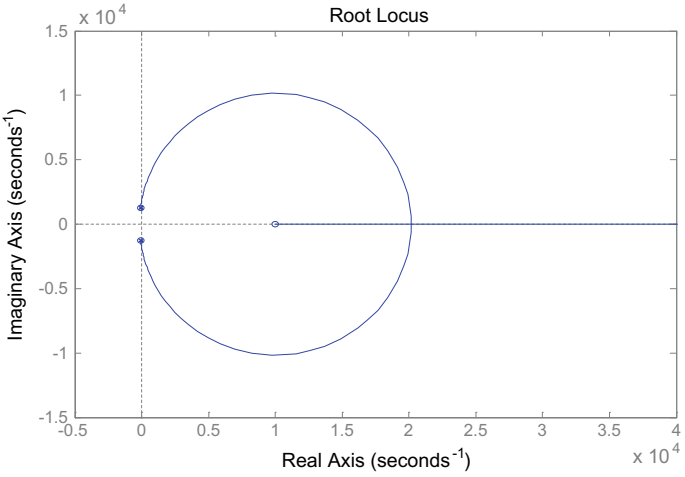

Fig. 14 Root locus plot

quality issues are gaining a lot of attention due to the penetration of enormous non-linear loads in entire power system. The priority is given to problems like harmonics, frequency, and voltage fluctuations.

Current harmonics or voltages harmonics are the frequencies that are integral multiples of the fundamental power frequency. Most of the electrical appliances used frequently everywhere like computers, rectifiers, furnaces, power electronics devices, etc., produces large number of harmonics that give rise to possibility of an unreliable power system. Harmonic distortion occurs due to the use of power inverters; hence, properly designed inverter configuration is beneficial. The produced harmonics can cause resonances, overheating in capacitor banks, transformers, and also lead to faulty operation of protection devices. There are various ways in which voltage and frequency fluctuations get injected to the system. It may occur due to sudden change in grid voltage if it moves beyond the set parameters; therefore, inverters operating in voltage regulating mode act as a protection against unnecessary islanding conditions. It should be properly configured so as to provide reactive power compensation during voltage sag and draw excess of it during voltage rise.

Another important factor responsible for voltage fluctuation is poor power factor which causes losses and therefore poor voltage regulation. A VAR compensator along with inverter is used in places of large load transients. Frequency fluctuations are result of imbalance between the produced power and the consumed power. Frequency fluctuation is negligible in small-size PV systems compared with other renewable energy resources.

4 Design of Converter Controller

For grid-coupled PV system to implement optimal utilization of energy and stable running of a system, the switched mode power converter has to switch frequently between MPPT control and constant voltage control. Under MPPT control mode, it tracks the MPPT rapidly, and in constant voltage mode, output rapidly reaches the reference voltage and keeps small voltage oscillation.

4.1 Existing Solution

Existing solutions are based on conventional control design like the proportional and integral controller as its parameter tuning is simple and is based on linear control theory of root locus or bode plot. The only requirement is the transfer function of the plant. It can be well applied to nonminimum phase systems also (Fig. 14).

4.1.1 Classical PI Controller

The magnitude of open-loop converter output is found to be 28 V from Fig. 15 which is approximately equal to 30 V, but it is having a very large overshoot of 42.8% at the beginning. To reduce the overshoot at the beginning and to control the converter output voltage, PI controller is required. The classical PI controller design is based on Ziegler–Nichols method shown in Table 2 as described in [18].

The transfer function of PI controller is obtained by Eq. 24.

$$G_c(s) = \frac{0.00835s + 4.91}{s} \tag{26}$$

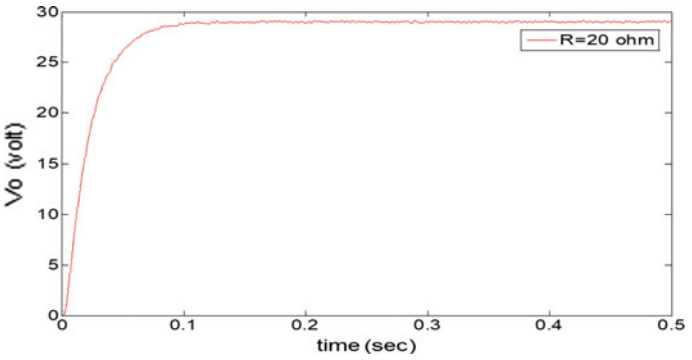

Fig. 15 Converter output voltage with PI controller

Table 2 Classical PI controller design

Controller	Proportional gain (K_p)	Integral time (T_i)	Derivative time (T_d)
PID	0.6 K_{cr}	$T_{cr}/2$	$T_{cr}/8$

From Fig. 15, it is found that the peak overshoot drastically reduces to zero value and the output voltage is constant DC voltage with a magnitude of approximately 30 V.

4.2 Proposed Methods

The proposed methods are based on nonlinear and robust control theory which can work properly and efficiently in varying environmental conditions. The controller inherent design considers nonlinearities and worst-case disturbances which make them robust to different types of variations.

4.2.1 Robust Controller

H_∞ control is an optimization process that deals with both performance and stability of the control system [19]. Robust H_∞ controllers are developed to provide a highly robust control environment to linear systems. H_∞ norm shows its peak value over the entire frequency range and is given in Eq. 25.

$$\|G\| = \sup \sigma(G(j\omega)) \tag{27}$$

Here, σ is the largest singular value of a transfer function. The objective of the synthesis is to design a controller such that the H_∞ norm of the plant transfer function is bound within the limits. The robust property of the controller requires minimization of error in the presence of disturbances. As sensitivity (S) and the complementary sensitivity (T) functions are measures of disturbance effect, thus has to be reduced. In this chapter, both sensitivity and complementary sensitivity functions are used to design weight functions, and the equations are given in Eqs. 28 and 29, respectively.

$$S = (I + GK)^{-1} \tag{28}$$

$$T = GK(I + GK)^{-1} \tag{29}$$

For this problem, two weight functions are assigned. One is performance weight function (W_s) to reduce the value of the sensitivity function, and another is the robustness weight function (W_t) to minimize the value of the complementary sensitivity function. The selections of weighting functions are based upon hit-and-trial method.

The weight functions are selected by an empirical formula given by Eqs. 30 and 31, respectively.

$$W_s = \frac{\frac{s}{M} + \omega_b}{s + \omega_b A} \tag{30}$$

$$W_t = \frac{Ls + 1}{Ls + 2} \tag{31}$$

where ω_b is the cut off frequency, M is the high frequency disturbance gain, A is the gain of the control signal having low frequency, and L is the any constant.

The magnitudes of A, M, and L are chosen in such a way that the cost function γ is less, and also it satisfies the condition $\|T\|_\infty < \gamma.\gamma$ is greater than zero. The weight functions for this system are given in Eqs. 32 and 33.

$$W_s(s) = \frac{s + 1360}{s + 136} \tag{32}$$

$$W_t(s) = \frac{0.01s + 1}{0.01s + 2} \tag{33}$$

where $\omega_b = 1.36 \times 10^3$ rad/s.

Using MATLAB code, H-infinity controller transfer function, γ, and $\|T\|_\infty$ are obtained as in Eq. 34.

$$K(s) = \frac{0.0077s + 1.5420}{0.0003s^2 + 0.1144s + 9.2473}$$
$$\gamma = 1.1475, \qquad \|T\|_\infty = 1 \tag{34}$$

The closed-loop model using controller is depicted in Fig. 16.

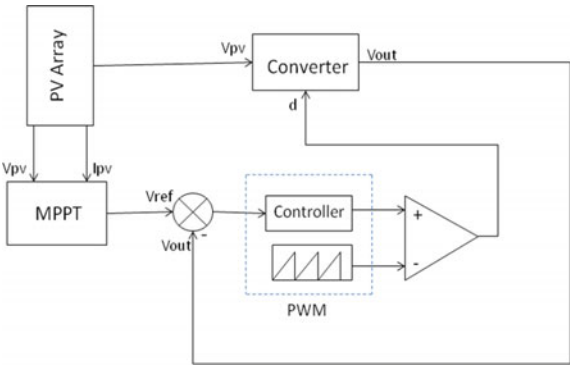

Fig. 16 Closed-loop model with H-infinity controller

4.2.2 Nonlinear Controller

Sliding mode is a nonlinear control method [20] that develops the dynamics of nonlinear system by application of discontinuous control signal which forces the system to slide along a cross section of systems normal behavior [21]. SMC design involves two steps: One is selection of the sliding surface; another is the switching function. The technique consists of two modes: reaching mode and sliding mode. In reaching mode state trajectory moves toward the sliding surface from any initial point, and system output is sensitive to parameter variations. In sliding mode, the state trajectory moves to origin along the switching surface, and the states never leave the switching surface [22].

In SMC, the control input consists of two components: a discontinuous component u_n and a continuous component u_{eq} as given in Eq. 35.

$$u = u_n + u_{eq} \tag{35}$$

The continuous component ensures the motion of the system on the sliding surface, while the system is on the surface. The equivalent control maintains the sliding mode by satisfying the condition given in Eq. 36.

$$\dot{S} = 0 \tag{36}$$

The solution is called equivalent control u_{eq}. The sliding surface for boost converter is illustrated in Eq. 37.

$$s = Ke + \dot{e} \tag{37}$$

"e" is the error between reference voltage and output voltage. The general state equations for boost converter combining two states with control parameter u are shown in Eq. 38.

$$\begin{aligned} \frac{\mathrm{d}i_L}{\mathrm{d}t} &= \frac{V_i}{L} + \frac{v_C}{L}(u-1) \\ \frac{\mathrm{d}v_C}{\mathrm{d}t} &= -\frac{v_C}{RC} + \frac{i_L}{C}(1-u) \end{aligned} \tag{38}$$

The sliding surface can be considered by the following equations as stated in Eqs. 39 and 40, respectively.

$$\begin{aligned} s &= K(V_{ref} - V_o) + \frac{\mathrm{d}}{\mathrm{d}t}(V_{ref} - V_o) = KV_{ref} - Kv_C - \frac{\mathrm{d}v_C}{\mathrm{d}t} \\ &= KV_{ref} - v_C\left[K - \frac{1}{RC}\right] - (1-u)\frac{i_L}{C} \end{aligned} \tag{39}$$

$$\dot{s} = v_C\left[\frac{KRC-1}{RC}\times\frac{1}{RC}+\frac{(1-u)^2}{LC}\right]+i_L\left[\frac{(1-KRC)}{RC}\times\frac{(1-u)}{C}\right] - \frac{(1-u)}{LC}V_{in} \tag{40}$$

Putting $\dot{s}=0$ as in Eq. 41

$$\dot{s}=0 \tag{41}$$

We get Eq. 42

$$0 = v_C\left[\frac{KRC-1}{RC}\times\frac{1}{RC}+\frac{(1-u)^2}{LC}\right]+i_L\left[\frac{(1-KRC)}{RC}\times\frac{(1-u)}{C}\right] \tag{42}$$

Here u is the control input, and in this work, the control input is the duty cycle given by Eq. 43.

$$u_{eq}^2\left(\frac{v_c}{LC}\right)+u_{eq}\left(\frac{-2v_c}{LC}+\frac{V_{in}}{LC}-\frac{(1-KRC)}{RC^2}i_L\right) + \left(-\frac{V_{in}}{LC}+v_c\left(\frac{-1}{LC}-\frac{(1-KRC)}{R^2C^2}\right)\right) + \frac{(1-KRC)}{RC^2}i_L = 0 \tag{43}$$

Solving Eq. 43, a, b, c values are obtained as in (44)

$$a=\frac{V_o}{LC}, b=-\frac{2V_o}{LC}+\frac{V_{in}}{LC}-\frac{1-KRC}{RC^2}i_L, \quad c=\frac{-V_{in}}{LC}+V_o\left(\frac{-1}{LC}-\frac{(1-KRC)}{R^2C^2}\right)+\frac{(1-KRC)}{RC^2}i_L \tag{44}$$

where a, b, c are the coefficients of s^2, s^1, s^0 respectively. By putting the above data as specified in Table 1 for second boost converter, the values of a, b and c are obtained as in Eq. 45.

$$\begin{aligned} a &= 0.066\times10^8 V_o \\ b &= -0.132\times10^8 V_o + 0.99\times10^8 - \left(18.18\times10^{-7} - K\times0.33\times10^4\right)i_L \\ c &= -0.99\times10^8 - 0.066\times10^8 V_o - 0.0275\times10^6 V_o + 222.22 V_o K \\ &\quad + 0.055\times10^7 - 0.33\times10^4 K \end{aligned} \tag{45}$$

By putting the values of a, b, and c, equivalent component of u can be calculated.

For designing a control law, the Lyapunov function V can be specified in Eq. 46.

$$V = 0.5S^2 \tag{46}$$

$\dot{V} < 0$ ensures a stable system, and it makes the sliding surface S attractive. Such condition marks to the following inequality as given in Eq. 47.

$$S\dot{S} < 0 \tag{47}$$

To satisfy above condition, the nonlinear control component can be stated in Eq. 48.

$$u_n = \text{sign}(S) \tag{48}$$

5 Performance Evaluation and Comparison Through Simulations

The proposed model is simulated by varying irradiance level keeping the temperature constant. Average annual solar radiation arriving at the top of the atmosphere of the earth is roughly 1366 W (peak)/m^2. So here the irradiance value is varied between the range of 900 and 1100 W (peak)/m^2, approximately above and below of the standard irradiance level. Table 3 shows the maximum power, V_{MPP} and I_{MPP} at different insolation levels.

From Table 3, it is observed that the operating point will change at each time by varying the irradiance level keeping constant V_{MPP}. The efficiency will be increased by decreasing the irradiance level. I-V and P-V plots for various insolation levels are already shown in Figs. 4 and 5, respectively. The efficiency can be measured by applying the formula given in Eq. 49. The formula represents maximum usable energy from the solar PV module.

$$\eta = \frac{P\text{max}}{V_{\text{MPP}} I_{\text{MPP}}} \times 100 \tag{49}$$

From P-V and I-V plots, it can be inferred that the system tracks the MPP successfully despite of variation in irradiance. The entire PV system can track MPP very fast by changing the environmental conditions. The output power is shown in Fig. 17 at 1000 Wp/m^2 irradiance level.

Table 3 Maximum power, V_{MPP} and I_{MPP} at different insolation levels

Irradiance (Wp/m^2)	V_{out} (V)	P_{out} (W)	V_{MPP} (V)	I_{MPP} (A)	P_{max} (W)	Efficiency (%)
900	28.5	40.7	12.5	4.2	48	91.9
1000	29	40	12.5	4.9	54	88.1
1100	28	39.8	12.5	5.5	58	84.36

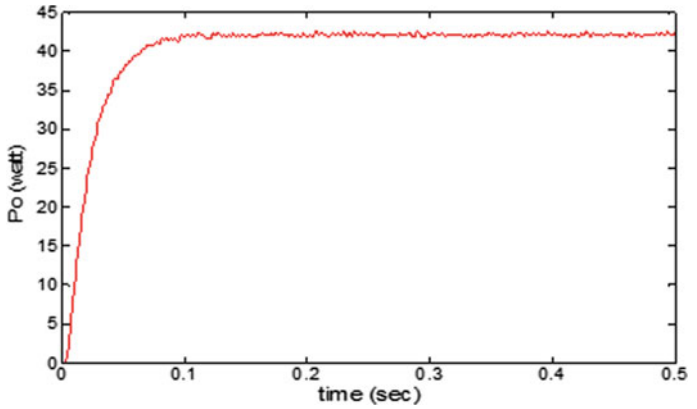

Fig. 17 Power output of the converter using MPPT

The power output is nearly about 42.5 W. It also remains constant irrespective of the changing irradiance level.

Figure 18 shows converter output voltage using MPPT and H-infinity controller for different loading conditions. Here, the load resistance is varied between the ranges 15 and 25 Ω. It is understood that voltage output remains constant by varying load resistance, and the overshoot is zero and also it tracks the voltage.

Figure 19 shows voltage output of the converter for different input irradiance. The irradiance level changes from 900 to 1100 Wp/m^2, and the output voltage remains constant at all levels. Hence, it is concluded that the system is robust irrespective of the input and load variations. The effect of PI controller under different loading conditions on the converter output is shown in Fig. 20.

From Fig. 20, it is observed that the output voltage remains fixed irrespective of the loading condition. The overshoot is also reduced to zero, but output voltage is not

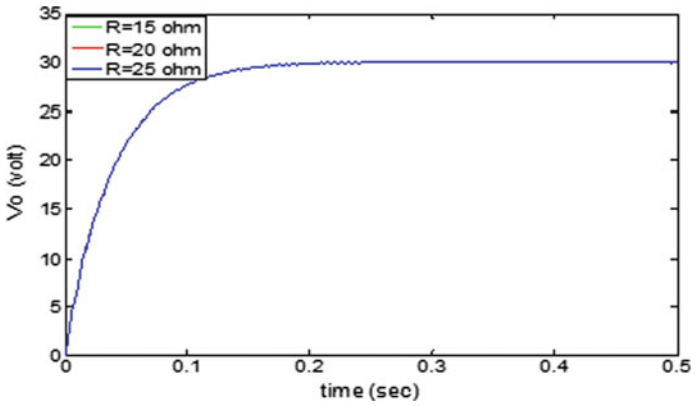

Fig. 18 Converter output with H-∞ controller for different load

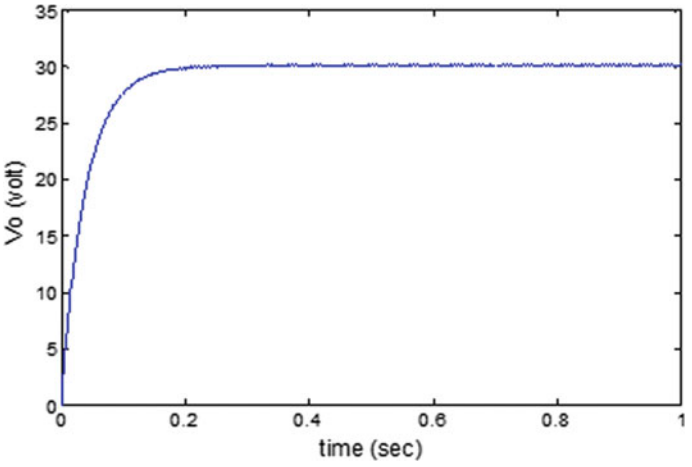

Fig. 19 Converter output with H-∞ controller for different input

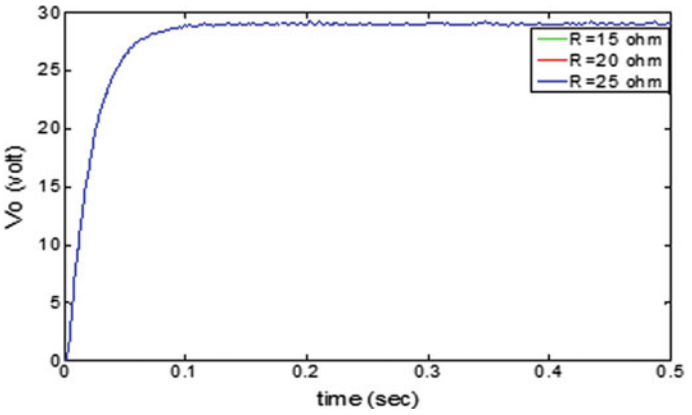

Fig. 20 Converter output with PI controller for different load

exactly 30 V. So tracking is poor in comparison to H-infinity controller. Figure 21 shows the converter output voltage using PI controller for different input condition. Figures 22 and 23 show the sensitivity and complementary sensitivity plot for open-loop converter and closed-loop converter using H-infinity controller.

The output voltage under different input conditions of the converter is nearly 30 V. Figure 22 presents the sensitivity plot for open-loop and closed-loop converter with H-infinity controller.

The sensitivity for the open-loop plant is 1.3 dB at 1.33×10^4 rad/s, and it is reduced to 0 dB at a frequency of 1×10^{20} rad/s. Sensitivity of a system is closely associated with the robustness of the system. It relates to the disturbance rejecting

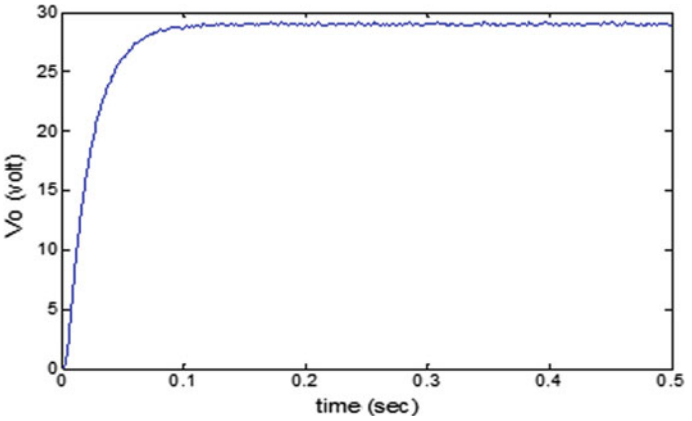

Fig. 21 Converter output with PI controller for different input

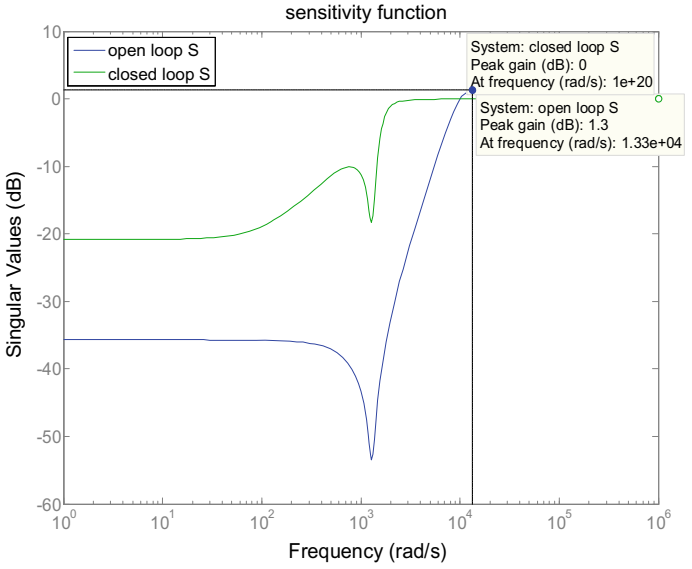

Fig. 22 Sensitivity plot

property. Figure 23 shows the complementary sensitivity plot for open-loop and closed-loop converter using H-infinity controller.

From Fig. 23, the complementary sensitivity for open-loop plant is found to be 3.42 dB at a frequency of 8.56×10^3 rad/s, and in closed-loop system, it is reduced to 1.06 dB at a frequency of 1.3×10^3 rad/s. From above results, it is observed that the plant is completely robust to input variation and load variation using H-infinity controller.

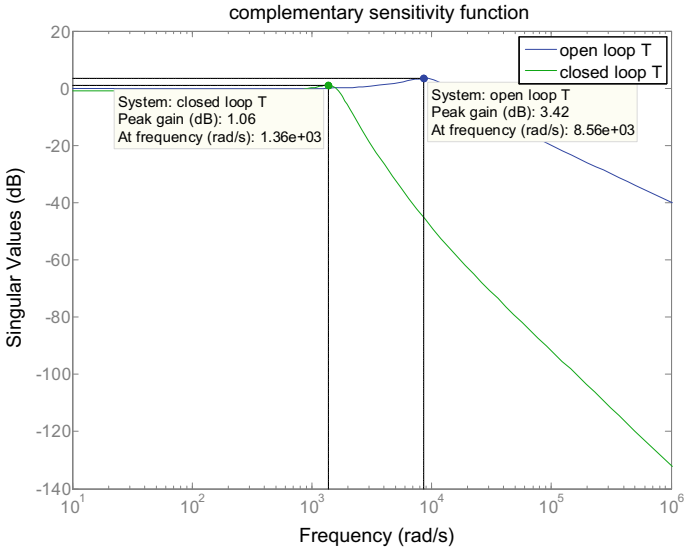

Fig. 23 Complementary sensitivity plot

The effect of SMC on the converter output under various input conditions is shown in Fig. 24. Here input is the solar irradiance. It is varying from 900 to 1100 Wp/m^2. Figure 9 shows the output voltage for different load at standard irradiance condition. Here the resistive load is varied in between the range 15 and 25 Ω. Figure 25 shows the output voltage for different values of controller gain k. Here k is varied from 1 to 1000 range keeping the input and output fixed.

From Fig. 24, it is observed that the output voltage is controlled by varying the input and it is tracking the output voltage of 30 V.

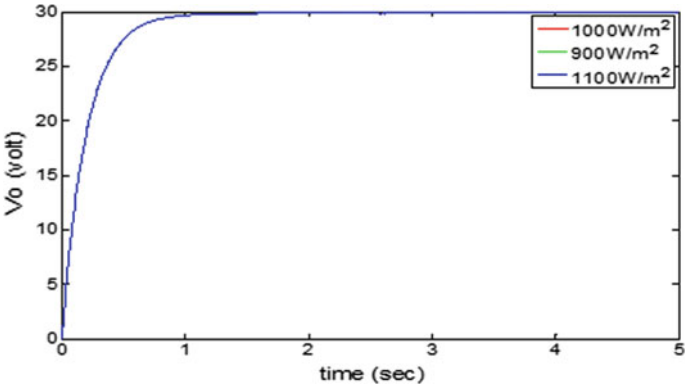

Fig. 24 Converter output voltage using SMC for different input

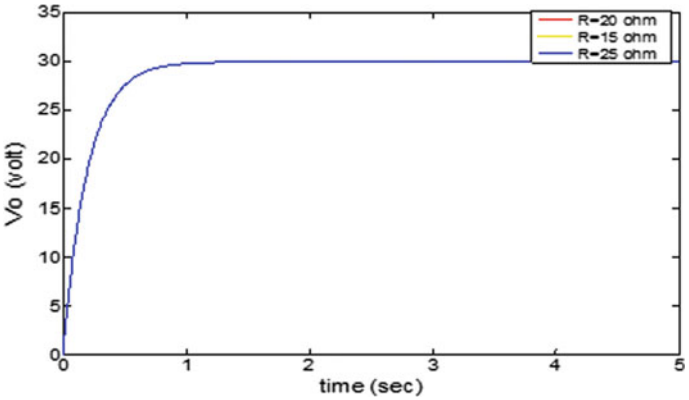

Fig. 25 Converter output voltage with SMC for different load

Figure 25 gives 30-V output for various values of load resistance. Hence, it is concluded that the output voltage is also regulated by varying the load.

In Fig. 26, the output voltage is drawn for different values of the SMC parameter k, and it is observed that the output voltage is nearly about 32 V when the range of k is in between 1 and 1000. When k value is further increased the output, voltage is regulated to 30 V which is desired for the converter. In this chapter, k value is chosen by hit-and-trial basis. Table 4 discusses the performance variation without controller and by using different types of controllers for a constant input of 15 V at standard irradiance and a constant resistance of 20 Ω.

From the above Table 4, it is noticed that the output response settles very fast without controller having an overshoot of 42.8% and a steady-state error of 6.66%. By the use of PI controller, the overshoot is reduced to zero. The use of H-infinity controller gives less steady-state error, less overshoot than PI controller. Settling time

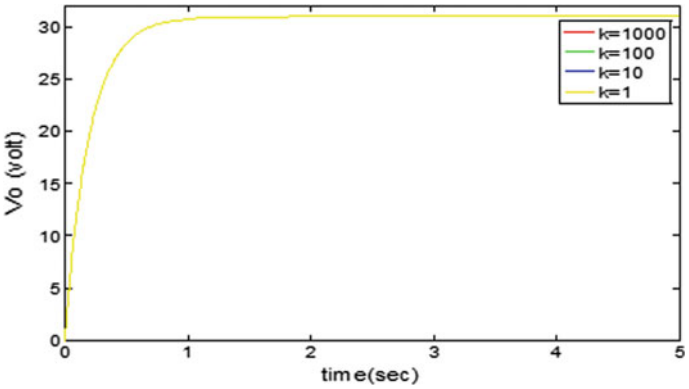

Fig. 26 Converter output voltage with SMC for different values of k

Table 4 Performance variation without controller and by using different types of controllers

	Input voltage—15 V at 1000 Wp/m^2			
	t_s (s)	M_p (%)	Steady-state error (%)	Stability
Without controller	0.025	42.8%	6.66	Unstable
With PI controller	0.15	0	3.33	Stable
With H-∞ controller	0.20	0	0.99	Stable
With SMC	1.4	0	0.56	Stable

is little bit higher than PI controller. By using SMC, the settling time is improved with a less steady-state error and zero overshoot.

6 Conclusion

In this chapter, PV-fed boost regulator is constructed by using PI, SMC, and H-∞ controller, and the outcomes are analyzed using the MATLAB/Simulink platform with different irradiance levels and also for different load condition. From the steady-state analysis, it can be inferred that the system reaches an MPP successfully despite of variation in irradiance. The efficiency goes on decreasing by increasing insolation levels from 900 to 1100 W (peak)/m^2. All the controllers are satisfying the required objective with improved time response specifications but with certain trade-offs. The tracking and robustness of the controllers are verified by varying the input and load within a certain range.

References

1. Lal V, Singh S (2017) Control and performance analysis of a single-stage utility-scale grid-connected PV system. IEEE Syst J 11:1601–1611. https://doi.org/10.1109/jsyst.2015.2408055
2. Zainudin H, Mekhilef S (2010) Comparison study of maximum power point tracker techniques for PV systems. In: 14th international middle east power systems conference (MEPCON-10), Cairo University, Egypt
3. Rashid M (2007) Power electronics handbook. Academic, Amsterdam
4. Forsyth A, Mollov S (1998) Modelling and control of DC-DC converters. Power Eng J 12:229–236. https://doi.org/10.1049/pe:19980507
5. Xiao W, Ozog N, Dunford W (2007) Topology study of photovoltaic interface for maximum power point tracking. IEEE Trans Industr Electron 54:1696–1704. https://doi.org/10.1109/tie.2007.894732
6. Ang Kiam Heong, Chong G, Li Yun (2005) PID control system analysis, design, and technology. IEEE Trans Control Syst Technol 13:559–576. https://doi.org/10.1109/tcst.2005.847331
7. Thau F (1979) A feedback compensator design procedure for switching regulators. IEEE Trans Ind Electron Control Instrum IECI 26:104–110. https://doi.org/10.1109/tieci.1979.351582

8. Bagheri AM, Zaeri N, Yaghoobi M (2011) Comparison performance between PID and LQR controllers for 4-leg voltage-source inverters. In: International conference on circuits, system and simulation IPCSIT, vol 7. IACSIT Press, Singapore
9. Anderson BDO, Moore JB (1990) Optimal control: linear quadratic methods. Prentice Hall Inc, Englewood Cliffs, NJ
10. Mao P et al (2015) MIT MRAC based boost converter with modified 2nd-order reference model. In: 3rd international conference on material, mechanical and manufacturing engineering
11. Doyle J, Glover K, Khargonekar P, Francis B (1989) State-space solutions to standard H/sub 2/ and H/sub infinity/control problems. IEEE Trans Autom Control 34:831–847. https://doi.org/10.1109/9.29425
12. Mahdavi J, Emadi A, Toliyat HA (1997) Application of state space averaging method to sliding mode control of PWM DC/DC converters. Proc IEEE IAS Ann Meet 2:820–827
13. Raviraj V, Sen P (1997) Comparative study of proportional-integral, sliding mode, and fuzzy logic controllers for power converters. IEEE Trans Ind Appl 33:518–524. https://doi.org/10.1109/28.568018
14. Nasir ANK, Ahmad MA, Rahmat MF (2008) Performance comparison between LQR and PID Controller for an inverted pendulum system. In: Proceedings of international conference on power control and optimization, Chiang May, Thailand, pp 18–20
15. Durán E, Ferrera MB, Andújar JM, Mesa MS (2010) I-V and P-V curves measuring system for PV modules based on DC-DC converters and portable graphical environment. In: Proceedings of 2010 IEEE international symposium on industrial electronics, Bari, Italy, pp 3323–3328
16. Su H-H, Chen J-J, Wu D-S (2002) Learning feedback controller design of switching converters via MATLAB/SIMULINK. IEEE Trans Educ 45:307–315. https://doi.org/10.1109/te.2002.803403
17. Pati N, Swain N (2015) Application of H-infinity controller to boost converter using model order reduction. In: Proceedings of 2015 annual IEEE India conference (INDICON), New Delhi, India, pp 1–6
18. O'Dwyer A (2009) Handbook of PI and PID controller tuning rules. Imperial College Press, London
19. Guldemir H (2005) Sliding mode control of Dc-Dc boost converter. J Appl Sci 5:588–592. https://doi.org/10.3923/jas.2005.588.592
20. He Y, Luo F (2006) Sliding-mode control for dc–dc converters with constant switching frequency. IEE Proc Control Theory Appl 153:37–45. https://doi.org/10.1049/ip-cta:20050030
21. Bibel J, Malyevac D (1992) Guidelines for the selection of weighting functions for H-infinity control. Defense Technical Information Center, Ft. Belvoir
22. Utkin V (1993) Sliding mode control design principles and applications to electric drives. IEEE Trans Industr Electron 40:23–36. https://doi.org/10.1109/41.184818

Protection Challenges with Microgrid

Pinku Das and Monalisa Biswal

Abstract In the modern power system, more penetration of renewable sources is encouraging to reduce the consumption of fossil fuel, to get clean energy, to reduce transmission losses, better utilization of natural sources, avoid, etc. Although the penetration of distributed energy resources (DER) is advantageous but with such modifications in the existing system, the protection system-related issues will be more pronounced, which required further modifications. Existing protection schemes are suitable for the conventional system but are unsuitable for the new renewable integrated microgrid system. To mitigate the new challenges, different techniques have been developed. Generally, microgrid system can be of AC or DC type. Again, the different protection issues associated with AC/DC type microgrid are islanding detection, fault detection/classification, and relay coordination. In this chapter, a detailed description of all the available techniques with the existing merits and demerits is provided.

Keywords AC microgrid · DC microgrid · Active method · Passive method · Hybrid method · Fault detection · Overcurrent relay coordination

Nomenclature

cf	Chopping fraction
df/dt	Rate of change of frequency
dP/dt	Rate of change of DG power output
DG	Distributed generation
DNN	Deep neural network
EBSA	Enhanced back search algorithm

P. Das (✉) · M. Biswal
Department of Electrical Engineering, National Institute of Technology Raipur, Chhattisgarh 492010, India
e-mail: pinku.das776@gmail.com

M. Biswal
e-mail: monalisabiswal22@gmail.com

P. Ray and M. Biswal (eds.), *Microgrid: Operation, Control, Monitoring and Protection*,
Lecture Notes in Electrical Engineering 625,
https://doi.org/10.1007/978-981-15-1781-5_6

H	Generator inertia constant
IDM	Islanding detection method
NDZ	Non-detection zone
P_{load}, Q_{load}	Active and reactive power of the load
PLL	Phase-locked loop
Q	Quality factor
PTS	Plug tap setting
PCC	Point of common coupling
t_{d}	Zero time
TDS	Time dial setting
WSE	Wavelet singular entropy
ΔP, ΔQ	Change in active and reactive power

1 General Introduction

The ever-increasing and unpredictable load demand of future power sector can only be handled wisely by enhancing power generation through renewable sources. Best utilization of natural resources, such as encouraging pollution-free power generation and reducing the transmission cost and losses, should be the main aim in the power sector so that a safe, reliable, and developed nation can be built. A small initiation from distributed level is a best example of such developments where micro-sources or distributed generators (DG), mainly in the level of 500 kW such as micro-hydro and wind turbines, solar plants are connected to low voltage side to meet the local power demands. Such a distribution grid with available renewable power generation is known as "Microgrid."

For better energy management, microgrids are designed with storage units [1]. Through the storage unit, uninterrupted power can be supplied to the distribution side. The second most important point is to achieve stable, reliable, and quality power supply from microgrid. Basically, the renewable source connected to microgrid system provides either AC or DC supply, which is further converted to the required supply with the help of converters. So, depending on the classification, microgrid can be of AC type, DC type, or hybrid type [2–4]. For different configuration, the structure of microgrid will change with new interconnection points. The conventional distribution system, which is passive in nature, is further diverted to active distribution system, which is only to achieve reliable and quality power supply. Due to the modification of the system, the existing conventional protection systems, which are equipped continuously to monitor the healthiness of power supply, will face challenges due to unexpected signal variations. In this chapter, a detailed discussion about the existing protection challenges associated with AC, DC, and hybrid microgrid systems is presented.

2 Protection Challenges with Microgrid

The protection algorithms that are applied to analyze and detect the abnormal events and discriminate from main grid side events in a microgrid are islanding detection, fault detection/classification, and overcurrent relay coordination [3]. According the type of microgrid the protection challenges are also different and more challenging. In Fig. 1, the typical structures of an AC and DC microgrid are shown. In this chapter, the details of all the protection algorithms available in the literature are discussed briefly.

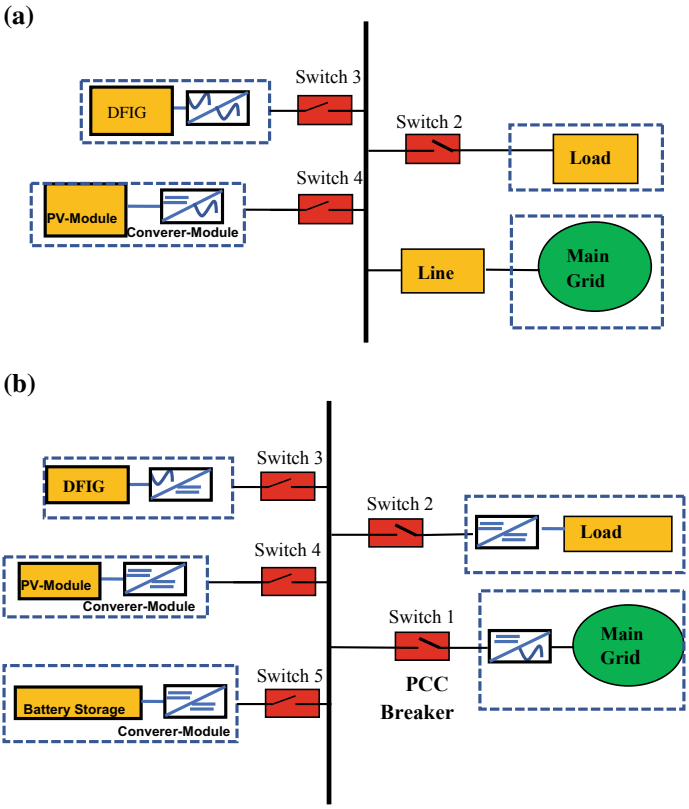

Fig. 1 **a** Structure of AC microgrid. **b** Structure of DC microgrid

2.1 Islanding Detection Techniques

Islanding is an observed circumstance when a DG and its connected local load become electrically isolated from the main power grid and the local load is still connected and energized by the DG. Islanding is broadly classified into two groups: one is intentional islanding and another one unintentional islanding [5]. Intention islanding is normally done for maintenance purposes and load shedding conditions. Unintentional islanding arises due to equipment failure and fault conditions. Detection of islanding in the power system is very essential as it drifts the system frequency, and voltage outside safety limits during load switching. Also, it can lead to out of phase reclosure of DG unit during instantaneous reclosing.

In the next subsection, the details about different types of islanding detection techniques for AC and DC microgrid are discussed.

2.1.1 Islanding Detection for AC Microgrid

In AC microgrid, islanding can be detected using active, passive, remote methods. Active method injects the disturbance in the network, and then, it monitors the system parameters deflection to detect islanding. Passive method monitors the magnitude and amount of deviation in parameters such as voltage, frequency, power, phase, harmonics, and oscillation to detect islanding. Remote methods are the communication-based methods in which the main grid side information is transmitted to the DG end to detect islanding. Individual active and passive methods have their own non-detection zones (NDZs). Remote methods have no NDZs, but they require high investments to install.

(a) **Active Methods**

In the literature, different active islanding detection techniques are available which are explained in details below.

(i) **Active Frequency Drift (AFD) Method** [5, 6]

AFD method is generally applied on a system consisting of only resistive loads, and it is based on injecting intentional distorted current waveform into the distribution network through the inverter. As shown in Fig. 2, due to intentional injected current disturbance in the positive half cycle of the DG system, output frequency of the DG side current signal is slightly higher than main grid side frequency of the voltage/current signal. When the DG output current reaches zero, it remains at zero for a short time duration t_d (zero time) before the initiation of the negative half cycle. During first half of the negative cycle, DG output current has negative value and when DG current reaches zero, it remains at zero until the main grid side voltage will rise and reach the zero crossing. The duration of zero time in negative half cycle is not fixed and it may not be equal to t_d.

Due to distortion in current waveform, PCC voltage maintains its frequency when main grid is connected. But when main grid is disconnected, the zero crossing point

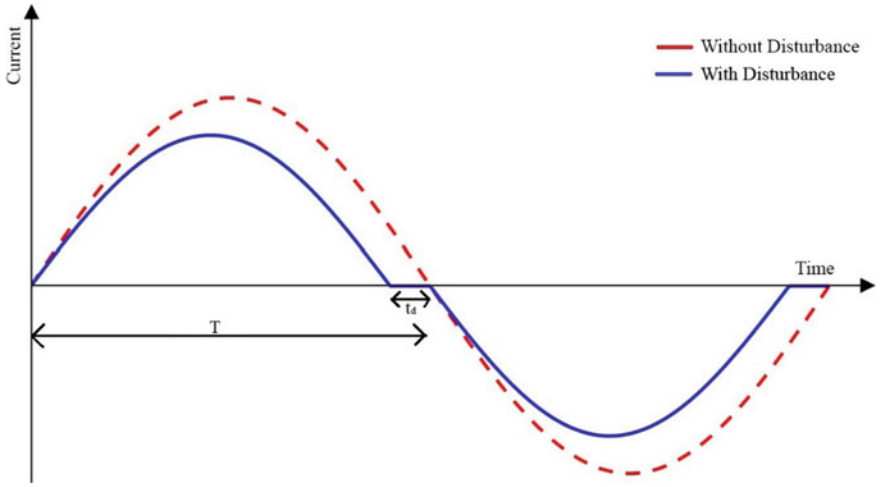

Fig. 2 Current waveform with or without injecting disturbance

of PCC voltage appears before the expected time due to the distortion in the current waveform. In case of resistive load, PCC voltage waveform responds to the distorted current waveform which results in advanced zero crossing time. Now PCC voltage and inverter current still contain phase error after first cycle, and the frequency of PCC voltage again increases. This process continues till the rise of in the frequency of PCC voltage. This increase in frequency can be detected by Over Frequency Relay (OFR) to detect the islanding condition.

The parameter which is used to describe the distortion of the inverter injected current is called chopping fraction (cf)

$$\text{cf} = \frac{2t_\text{d}}{T} \tag{1}$$

where t_d is the zero time and T is the time period of the half cycle.

AFD method is easy to implement. It has small NDZ and works well with resistive loads. But when the loads are not resistive, the detection time and the NDZ will rise with increasing value of quality factor (Q). AFD method also suffers when the DG system contains multiple inverters, as each inverter in the multi-inverter system gives different deviation of frequency bias and under such a condition it is difficult to detect islanding. Another disadvantage of AFD method is that it degrades the power quality of inverter output.

(ii) **Improved AFD/AFDPF (Active Frequency Drift Positive Feedback)** [7]

The main disadvantage of AFD method is that it requires many cycles for PCC voltage frequency to drift for OVR relay to detect the islanding condition, and it can be overcome by AFDPF method in which positive feedback is used to increase the chopping fraction, as it results in increase in the frequency deviation to detect

islanding. The chopping fraction can be estimated as

$$\mathrm{cf}_n = \mathrm{cf}_{n-1} + F(\Delta\omega_n) \tag{2}$$

where

cf_n	chopping fraction of nth cycle
cf_{n-1}	chopping fractionof $n-1$th cycle
error in frequency in nth cycle	$\Delta\omega_n = \omega_{n-1} - \omega_n$ and
F	is linear function of $\Delta\omega_n$.

AFDPF has following advantages over AFD

i. AFDPF has much better performance, and it has reduced NDZ as compared to AFD.
ii. In AFDPF, the value of the chopping fraction can be positive or negative according to the frequency error and for that condition F should be properly chosen. It means during negative frequency error, the AFDPF could reinforce the downward frequency drift instead of counteracting it.
iii. AFDPF is much more effective in multi-inverter DG system as comparison to AFD due to the fact that the positive feedback enables us to reinforce any frequency deviation produced by the DG system.

(iii) **Sandia Frequency Shift (SFS)** [8, 9]

SFS method has also have a similar working principle like AFDPF technique in which positive feedback is given to the inverter voltage frequency.

The formula for chopping fraction in this method is

$$\mathrm{cf} = \mathrm{cf}_0 + k\left(f_{\mathrm{pcc}} - f_{\mathrm{g}}\right) \tag{3}$$

where

cf_0	chopping fraction with no deviation in f,
k	acceleration gain,
f_{pcc}	frequency of voltage at PCC
f_{grid}	frequency of grid.

When the DG network is connected to main grid, there is no change in frequency of voltage at PCC due to large inertia of the main grid. But when the DG network is isolated, the chopping factor rises due to increase in frequency of f_{pcc}. This process of shifting the frequency continues until the islanding is detected. SFS has a reduced NDZ as compared to other methods.

(iv) **Sandia Voltage Shift (SVS)** [8, 9]

SVS has a similar working principle as SFS, and it also utilizes a positive feedback which is applied to the magnitude of PCC voltage [9]. When there will be any distortion in voltage signal, the inverter output current also changes with the output

power. Thus, the distortion f_{PCC} voltage due to positive feedback is negligible. During islanding, the variation in output power will speed up the drift voltage and thus can be used for islanding detection. Under voltage or over voltage protection will detect the deviation in voltage and compare it with the threshold. When threshold is reached, inverter is disconnected from the network.

The detection time of islanding through SVS is almost equal to SFS, and SVS method is easy to implement. The inverter controller reference current can be calculated as [7]

$$I_{\text{ref}} = \frac{k_v \cdot \Delta V + P_{\text{DG}}}{V} \tag{4}$$

where I_{ref} is the inverter controller reference current, ΔV is the change in voltage, V is the PCC voltage, P_{DG} is the DG output power. k_v is factor which helps the output current of the inverter to vary in proportional to the PCC voltage.

The SVS method is although better than SFS but this method degrades the power quality of the network and in PV system tracking of MPPT is difficult with the implementation of SVS algorithm.

(v) **Slide Mode Frequency Shift (SMS)** [10]

Sliding mode frequency method employs positive feedback to the PCC side voltage phase angle, and frequency drift is monitored to detect the islanding situation.

The output current of the inverter can be represented as

$$i = I_{\text{m}} \sin(2\pi f t + \theta_{\text{sms}}) \tag{5}$$

where f is the frequency of the PCC voltage signal and θ_{sms} is the phase angle in degree can be calculated as

$$\theta_{\text{sms}} = \frac{2\pi}{360} \times \theta_{\text{m}} \times \sin\left(\frac{\pi}{2} \times \frac{f - f_{\text{grid}}}{f_m - f_{\text{grid}}}\right) \tag{6}$$

where f_{grid} is the grid frequency, θ_{m} is the maximum phase angle in degrees, and f_m is the frequency at which θ_{m} occurs.

When the main grid is connected to the DG, the magnitude of the frequency at PCC and the grid frequency are identical ($f = f_{\text{grid}}$), thus the phase angle during the grid connected mode is almost equal to zero. Islanding of DG system from the main grid leads to change in phase angle of the load. For this situation, the SMS curve will vary due to change in frequency ($f \neq f_{\text{grid}}$) and thus detects islanding when frequency deviation exceeds the threshold.

Unlike other active methods, SMS method is efficient for multi-inverter system. It is also easy to implement and also have small NDZ. However, it affects the system transient stability, and it degrades the power quality of the network.

(vi) **Negative Sequence Current Injection** [11–13]

In this method, a negative sequence current is injected as a disturbance signal through the voltage source converter (VSC). From the presence of negative sequence voltage at the PCC, islanding can be detected. VSC controls the active power and reactive power flow, and the quantities are controlled using *d-q* reference frame. The magnitude of negative sequence voltage is continuously monitored at the PCC end, and islanding can be detected once the voltage index exceeds the threshold.

The local load is tuned at resonant frequency (50 Hz), and when the operating frequency matches with the resonant frequency, the local load becomes a purely resistive circuit which withdraws power from the DG at rated PCC voltage. As shown in Fig. 3a, when the DG is connected to main grid, the system frequency is at the resonant frequency and local load contains only the fundamental component of current. For grid connected mode, if any disturbance occurs, the negative sequence injected current flows toward the main grid as it provides the low impedance path. But during islanded mode (Fig. 3b), the injected negative sequence current will move toward the local load due to the absence of low impedance path. Through proper monitoring and measurement, the magnitude of negative sequence voltage measured at PCC can be utilized for islanding detection when the voltage index exceeds the threshold. Under islanding condition, the PCC voltage in an unbalance voltage and the percentage of voltage unbalance can be defined as

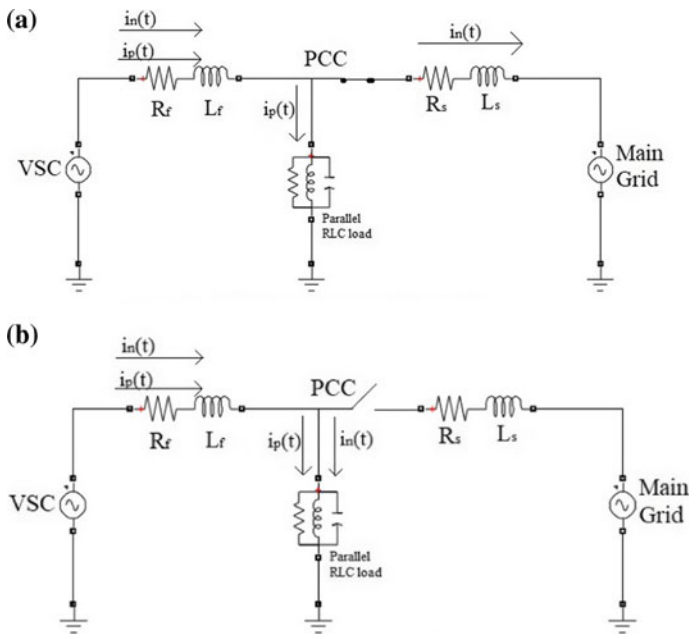

Fig. 3 **a** Main grid connected mode. **b** Main grid disconnected mode

$$= \frac{V_n}{V_p} \times 100\% \tag{7}$$

where V_p and V_n are the instantaneous positive sequence and negative sequence voltage magnitudes in abc-reference frame. It is also true that during islanding the V_p and V_n are proportional to the magnitudes of the related current components, and the voltage unbalance in terms of current components can be expressed as

$$= \frac{I_n}{I_p} \times 100\% \tag{8}$$

where I_p is proportional to V_p and I_n is proportional to V_n.

Negative sequence current injection method has a very fast detection time and the response time improved with more injected current. Also, it is immune to noise, less sensitive toward low resistance load change and variation of inductance and capacitance. It has no NDZ.

(vii) **Impedance Measurement** [14]

Impedance measurement method is based on frequency-dependent impedances at PCC which measures the notable existing harmonics injected by the main grid and DG system. When intentional harmonics are not injected, this is considered as passive method, and considering the injection of external harmonics, this is considered as active method.

Disconnection of DG from main grid leads to change in the topology of the network, which results in the variation of voltage due to perturbation of current. To distinguish between islanding and non-islanding conditions, intentional harmonic frequencies are injected through the inverter. Islanding condition can be confirmed when impedance values for different harmonic frequency can be traced. In normal condition, the impedance measured through the injected harmonic frequency at PCC is very less due to low impedance path of main grid. But in the islanded condition, the estimated impedance for different injected harmonic frequency will be significant and thus declares the islanding condition.

The impedance measurement method has very fast detection time and has small NDZ for single inverter system. But it suffers in case of multi-inverter system and obtaining a proper threshold value is difficult as it requires exact grid impedance.

(b) **Passive Methods**

(i) **Rate of Change of Frequency (ROCOF)** [8, 15]

During islanding, the topology of the network changes which results in power imbalance between the load and the generation. Due to islanding, there will be change in frequency of the DG network. This results in frequency change at PCC. The rate of change of frequency ($\mathrm{d}f/\mathrm{d}t$) over once cycle can be estimated to detect the islanding condition. With islanding, the operation of DG can be interrupted. Flowchart of ROCOF method is shown in Fig. 4.

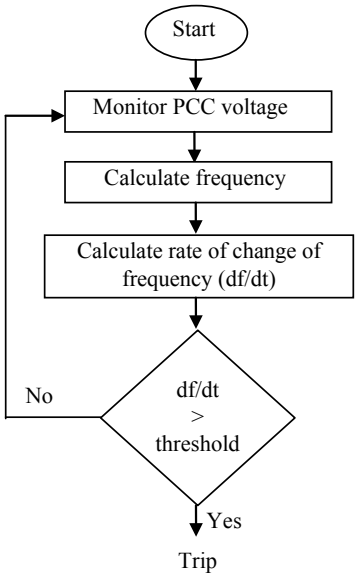

Fig. 4 Flowchart of ROCOF method

ROCOF provides a better result when the active power imbalance between DG and load is large. When the magnitude of ROCOF is higher, rate of islanding detection is also more possible, reliable, and faster. But the ROCOF method fails mainly during active power mismatch situation when it is less than 15% [8]. The rate of frequency change will be small as it does not reach threshold to detect islanding condition. Also, ROCOF is sensitive to load switching and load fluctuation as under such condition threshold setting is difficult. This method is best suited for loads with less fluctuation.

(ii) **Rate of Change of Power (ROCOP)** [8]

ROCOP measures rate of change in DG power output (dp/dt). During islanding, there will be heavy power unbalance situation develop. Due to this, dp/dt will be high as during islanding as compared to non-islanding situation. As a result, when the dp/dt exceeds the predefined threshold, the ROCOP method detects the islanding condition and the DG will stop supplying power to the load.

ROCOP has faster detection time when the power mismatch between DG and load is high, and it takes around 24–26 ms to detect islanding in this condition [8]. Also, this method has the ability to detect unsynchronized reconnection of the grid supply to the DG unit. Such a method suffers under there will be low power mismatch situation, and under such a condition, the method suffers from high non-detection zone. But this method works perfectly when the power mismatch between DG and load is high.

(iii) **Rate of Change of Frequency Over Power (ROCOFOP)** [4, 8]

Principle of this method is to monitor the changes in df/dP_{L} for identifying whether the DG is in islanding condition or not, where P_{L} indicates the load power.

ROCOFOP works better than ROCOF under low power mismatch condition. ROCOFOP has higher reliability, low error detection ratio, and smaller non-detection zone. The detection time for ROCOFOP detection is about 100 ms [8]. But threshold selection is difficult for ROCOFOP method as it requires two predefined thresholds setting namely frequency and power for the successful implementation of the method. However, such a method can work perfectly under lower power imbalance condition.

(iv) **Over/Under Voltage (UV/OV) and Over/Under Frequency (OF/UF)** [8, 16]

This method monitors the variation of voltage and frequency during normal and islanding conditions at the DG location. In this method, the maximum and minimum voltage and frequency ranges are set and when either of the measured value will cross, the threshold is detected as an islanding condition. Due to islanding, the topology will change. This results in changing the active and reactive power demands of the network. This change in active power demand leads to change in voltage magnitude, and the change in reactive power demand leads to change in voltage frequency at PCC and can be estimated as

$$\Delta P = P_{\text{Load}} - P_{\text{DG}} \tag{9}$$

$$\Delta Q = Q_{\text{load}} - Q_{\text{DG}} \tag{10}$$

Usually when the main grid is connected, the variation of active power and reactive power is injected from the main grid. But when islanding occurs, the load variation produces significant variation in voltage and frequency and thus islanding can be detected. The detection time of the (UV/OV) and (OF/UF) methods depend on the power mismatch between the DG and load. When the power mismatch is considerably less, this method will fail to detect islanding. So, for this method it is difficult to set threshold values. Also, these methods have large non-detection zone under low power mismatch condition. The OUV/OUF methods have other related advantages such no impact on power quality and works perfectly when the power imbalance between load and DG is high.

(v) **Phase Jump Detection (PJD)** [17, 18]

The PJD method monitors the phase difference between the inverter terminal voltage and current. To detect the zero crossing point of the PCC voltage, phase-locked loop (PLL) is required. During normal condition, the phase difference between the inverter current and the PCC voltage will be synchronized. When islanding occurs, the PCC voltage loses synchronism from main grid voltage, but the inverter output current remains unchanged. During islanding, the PCC voltage will jump to a new phase to exhibit the same load phase angle. So, the PCC voltage jumps to a new value. If the phase difference between the PCC voltage and inverter output current exceeds the threshold setting, islanding can be detected and inverter stop operating.

The PJD scheme is easy to implement, and it has no such effect on the system transient response. The detection speed is also fast, and unlike active methods, it does

not deteriorate power quality. But PJD method suffers during load switching which causes error in detecting islanding. Under such a condition, threshold selection is also challenging. The PJD method is suitable for less frequent switching loads and load with sufficient phase angle difference.

(vi) **Voltage Unbalance and Total Harmonics Distortion (VU and THD)** [19]

After the loss of the utility, the DG will still be connected to the remaining local loads. Due to sudden loss of the utility during islanding, the system topology will change and this introduces harmonics in the voltage and current signal. Generally, the load which is connected to the distribution network is single-phase loads, and due to islanding, it is difficult to balance load from power generation from DG end. Since the topology of the network changes, it results in different harmonic content in the signal.

The UV and THD method monitor the voltage unbalance and total harmonic distortion of current for detecting the islanding condition, along with the above two parameter voltage magnitude of the system is also monitored. So, in this method three parameters are monitored to detect the islanding condition.

During islanding, due to large load variation there will be sudden change in voltage magnitude, frequency and phase displacement. In this case by monitoring the variation of voltage, we can detect islanding for large load variations.

For small load variation after islanding, the variation in voltage magnitude, frequency, and phase displacement may not reach the predetermined threshold, and thus, islanding detection will be difficult. For such a situation, percentage variation in the voltage unbalance (VU) and total harmonic distortion (THD) present in current signal can be monitored to detect the islanding.

The flow diagram of the VU and THD methods is shown in Fig. 5 [19]. Individually, a single parameter is suitable to detect islanding for all conditions but combinedly they can provide better result. This method is very reliable and has very small non-detection zone.

(vii) **Oscillation Frequency Estimation** [20]

The method is based on monitoring the frequency oscillation to differentiate between the islanding conditions from other situation that occurs in distribution system.

In synchronous machine when sudden any disturbance occurs, the angle between rotor angle and resulting magnetic field oscillates dynamically according to the swing condition as given in Eq. 11,

$$\frac{2H}{\omega_0}\frac{\mathrm{d}^2\delta}{\mathrm{d}t^2} + \frac{D\mathrm{d}\delta}{\mathrm{d}t} = P_\mathrm{m} - P_\mathrm{e} \tag{11}$$

where H is the generator inertia constant, ω_0 is the synchronous speed, δ is the rotor angle, D is the damping coefficient, P_m is the mechanical input of DG, and P_e is the electrical power output of DG.

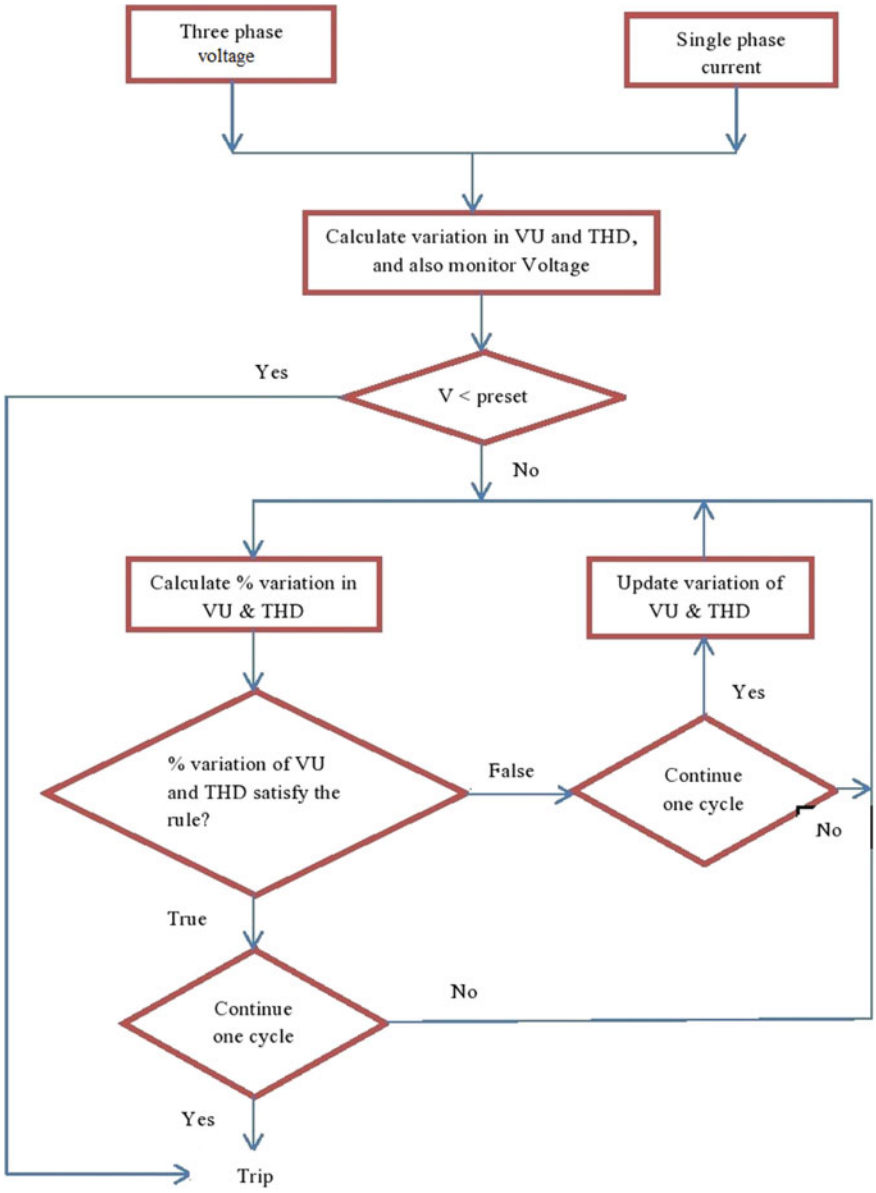

Fig. 5 Flowchart of VU and THD method

During non-islanding condition, a small perturbation of $\Delta\delta$ is introduced. Solving the swing equation for this condition for the frequency deviation of the synchronous speed is given by

$$\Delta\omega = -\frac{\omega_n \Delta\delta(0)}{\sqrt{1-\xi^2}} e^{-\xi\omega_n t} \sin\omega_d t \tag{12}$$

where

ξ damping ratio,
ω_n natural frequency of oscillation,
ω_d damped frequency of oscillation, and the above equation frequency response is a damped sinusoidal waveform.

During islanded condition, the frequency deviation of the synchronous speed is given by

$$\Delta\omega = -\frac{\Delta P}{D}\left(1 - e^{-(\omega_0 D/2H)t}\right) \tag{13}$$

During islanding, the frequency at the first instant gives exponential response and the frequency deviation is compared with first threshold (Th1). If the threshold frequency exceeded, then the oscillation frequency is measured. Oscillation frequency is measured using this formula

$$f_{\text{osc}}(\text{k}) = \frac{f_S}{2\pi N} \text{acos}\left(\frac{f(k) + f(k-2N) - 2f_0}{2f(k-N) - 2f_0}\right) \tag{14}$$

where

f_s is the sampling frequency,
N is the number of samples,
f_0 is the nominal frequency.

The oscillated frequency is calculated and compared with the threshold (Th2). If the oscillation frequency is greater than the threshold (Th2), it is due to heavy load switching, and if the oscillation frequency is less than threshold (Th2), then the counter is started. When the counter reaches its preset delay, a signal will be given to disconnect the DG. The flow diagram of the oscillation frequency method is shown in Fig. 6 [20].

(c) **Remote Techniques**

(i) **Power Line Carrier Communication (PLCC)-Based Method** [21]

In this method at the grid side of the network, transmitters are set and the transmitter sends continuous signals through the power lines to the receiver. Receivers are generally equipped at the DG side.

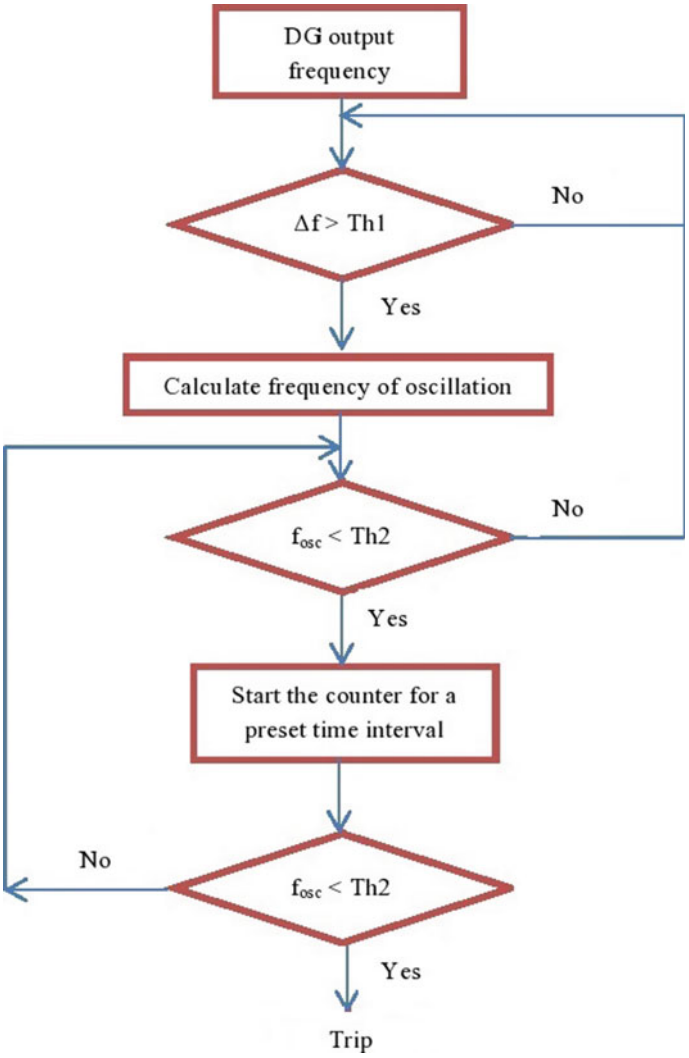

Fig. 6 Flowchart of oscillation frequency estimation technique

To detect the islanding condition from normal condition, the transmitter sends continuous signal to the receiver about its current status. When the PLCC receiver does not receive any signal from the transmitter end, it detects the islanding condition. Normally, islanding condition is considered if the receiver does not receive any signal from transmitter continuously for three to four cycles. PLCC signal propagation determines the reliability of this method. PLCC signals are free from high frequency component as the distribution transformer series inductance attenuates the

high frequency signals. So, sub-harmonic frequency signals is used for PLCC signal propagation.

This method has no NDZ, effective in multi-DG system, fast detection time and does not degrade the power quality like active methods. The only limitation of this method is the cost that is required to set up the transmitter and receiver for the transmission of the PLCC signals. That is why, such a method is not feasible in low-density DG system.

(ii) **Supervisory Control and Data Acquisition (SCADA)** [4, 8]

SCADA method monitors the status of the auxiliary contacts of the main grid circuit breakers. SCADA method detects the islanding condition when the main grid circuit breakers are opened due to any fault condition at the main grid side. Then, the corresponding circuit breakers that are tripped of the DG side are opened during the islanding operation.

Advantage of SCADA method is that it has no NDZ even in multi-DG system and it also does not degrade the power quality. Like PLCC-based technique, the only disadvantage with such a technique is the installation cost.

2.1.2 Islanding Detection for DC Microgrid

The islanding detection techniques used in AC microgrid are generally classified into passive methods, active methods, and remote techniques. In the above-listed techniques, frequency change, power mismatch, harmonic content, and phase angle difference factors are considered and monitored continuously to detect islanding. But in the literature, only few techniques are reported for islanding detection in DC microgrid as the voltage signal will only vary under such a situation. So, in the present scenario this is an emerging topic for research.

The available islanding detection techniques for DC microgrid are given described below:

(i) **Rate of Change of Voltage (ROCOV) and Rate of Change of Current (ROCOC)** [22]

When the DG is connected to the main grid, DC voltage is kept constant by controlling the power exchange between the DG and the main grid. But during islanded mode, the power exchange between DG and main grid is null and storage device is the only source which controls the DC voltage by controlling the switching of buck boost converter.

At each instant, DC voltage and current magnitudes are monitored and the equation of ROCOV and ROCOC can be written as

$$\text{ROCOV} = \frac{V(n) - V(n - \Delta n)}{\Delta n} \tag{15}$$

$$\text{ROCOC} = \frac{I(n) - I(n - \Delta n)}{\Delta n} \tag{16}$$

where $V(n)$ and $I(n)$ are the magnitude of voltage and current at nth sample and Δn is the step size of the algorithm.

ROCOV and ROCOC monitor the real power mismatch between the load and generation from the DG units. Real power mismatch during islanding mode creates a large deviation, and the magnitude of ROCOV and ROCOC has a significant value. When the magnitude of ROCOV and ROCOC exceeds threshold, islanding is detected.

As there is continuous power mismatch at PCC and load, there is dynamic change in voltage and current, thus the dynamic behavior of ROCOV and ROCOC can be expressed as

$$\text{ROCOV} = \frac{V}{2 * P_{\text{load}}} * \frac{\Delta P}{\Delta n} \tag{17}$$

$$\text{ROCOC} = \frac{I}{2 * P_{\text{load}}} * \frac{\Delta P}{\Delta n} \tag{18}$$

where

ΔP active power mismatch
V terminal voltage
I terminal current
P_{load} active power of the DC load.

From above equation, it can be shown that during islanded mode, ROCOV and ROCOC are directly proportional to ΔP. Also, the higher active power mismatch leads to small NDZ and smaller detection time. However, this method suffers when active power mismatch is less which results in the increase of NDZ. The method is unable to discriminate between the high resistive fault and islanding condition.

(ii) **Islanding Detection Based on Deviation of Voltage and Frequency at PCC** [23]

This method is based on changing the DC voltage of the DC-link based on the fluctuation of the voltage and frequency at the PCC on the AC side.

When the main grid is connected, power mismatch will not cause any significant change in the voltage and frequency, so the deviation is almost zero. But when the main grid is disconnected from DG, the deviations in voltage and frequency are significant with higher power mismatch. In this method, the DC bus voltage is continuously changing according to the deviation of the voltage and frequency of the AC side. In the islanded mode, the deviation of voltage and frequency is significant, and when the threshold value of the DC voltage is reached, DC relay is triggered to disconnect the DG system.

Reference DC bus voltage (V_{dcref}) is given as:

$$V_{\text{dcref}} = V_{\text{dcref,steady}} + \alpha * \Delta V_{\text{PCC}} + \beta * \Delta f_{\text{PCC}} \tag{19}$$

where

α and β	constant coefficients
$V_{\text{dcref,steady}}$	reference DC bus voltage at steady state
ΔV_{PCC}	deviation in PCCvoltages
Δf_{PCC}	deviation in PCC frequency PCC frequency.

α and β are chosen in such a way that it pushes the DC-link voltage of DG toward threshold to detect the islanding condition. Normally in islanding condition, the voltage and frequency deviations occur at the same instant. Under such a condition, the DC-link voltage deviates much faster and it results in fast islanding detection.

(iii) **DC-link Voltage Control** [24]

This method is based on changing the magnitude of DC-link voltage (V_{dc}) when the PCC voltage (V_{PCC}) changes at the instant of islanding condition. DG side is to be designed as a controllable voltage source. For islanding detection, over/under voltage protection can be used to detect the islanding condition. As the magnitude of voltage exceeds threshold, islanding can be detected.

In this method, the lower and upper voltage limits are considered properly to avoid unnecessary tripping. If V_{dc} is within the upper and lower limits even after islanding occurs, islanding cannot be detected as this range represents the NDZ zone.

The relationship between V_{dc} and V_{PCC} can be represented as

$$V_{\text{dc}} = X_1^* V_{\text{PCC}} + X_2 \tag{20}$$

In Eq. 20, by changing the values of X_1 and X_2, area of the NDZ can be varied.

This method can be used as both an active or passive method. When intentional disturbance is injected to drift the voltage of PCC, the method is considered as active method. It can change the DC-link voltage by continuously feeding the PCC voltage, and thus, islanding can be detected if it crosses the threshold.

(iv) **Electrolyte Capacitor Less PV Interface in DC Distribution System** [25]

In this technique, PV system is used only in the microgrid system and the algorithm injected current perturbation for detecting the islanding condition.

During normal condition when main grid is connected to DG, current injection does not affect the DC-link voltage. However, when main grid is disconnected, and current perturbation is given to the system. So, the voltage will be affected due to that perturbation. Injecting a current disturbance at a scheduled frequency can drift the voltage magnitude toward under voltage protection scheme to detect islanding.

In this method, the performance of the algorithm depends upon the perturbation factor (k), perturbation frequency (f_{P}), and perturbation time (t_{P}). The PV converter is modeled as a current source and provides current I_{D} with an output capacitor C_0 and load resistance R_0 connected in parallel. After islanding, the DC-link voltage can be expressed as

$$\frac{\mathrm{d}V_{\mathrm{dc}}(t)}{\mathrm{d}t} = \frac{1}{C_0}\left(kI_{\mathrm{D}} - \frac{1}{R_0}V_{\mathrm{dc}}(t)\right) \tag{21}$$

Solving this above equation, we get

$$V_{\mathrm{dc}}(\mathrm{t}) = \mathrm{k}I_{\mathrm{d}}R_0 + \left[(V_{\mathrm{dc}} - \mathrm{k}I_{\mathrm{d}}\mathrm{R}_0)\mathrm{e}^{-1/(R_0C_0)t}\right] \tag{22}$$

where

$V_{\mathrm{dc}}(t)$ DC-link voltage
C_0 PV converter capacitance
I_{d} current from PV converter to output capacitor
R_0 equivalent load resistance.

It can be easily observed that $V_{\mathrm{dc}}(t)$ and k are related to each other as a function of time. Detection time decreases when the value of k decreases. Initial value of k is taken, and it is decreased continuously in a stepwise manner. When islanding occurs due to change in the value of k, the DC-link voltage decreases continuously, and it detects islanding when under-voltage threshold is reached. During normal condition, even after the change in the value of k, the DC-link voltage is tightly regulated due to the presence of main grid. This indicates normal operation, and then, the value of k is preset to the initial value of k.

2.2 Overcurrent Relay Coordination

Introduction of DG in the main grid changes the property of the network. It also changes the network control and protection strategy due to the inclusion of DG. When fault occurs in the grid connected mode, high fault current flows from main grid to reach the pickup values of the overcurrent relays. But in islanded mode, the DG inverter does not provide enough current to reach the pickup values.

Therefore, there is a need of revision of the existing scheme for setting the pickup value of overcurrent relay and to set proper coordination time intervals between the operating time of primary relay and backup relay. For the AC/DC microgrid, the available conventional approach required for DG side isolation during fault scenario is not reliable and require complete revision. Therefore, there is a need for redefined protection and control schemes of overcurrent relays during fault conditions when applied for AC/DC microgrid.

2.2.1 Method 1 [26]

In this method, the energy storage devices such as flywheel unit are used so to reach the pickup value of the overcurrent relay during fault in islanded condition. During a grid-connected mode, the main grid provides the high fault current to reach the

pickup value of the overcurrent relay and trip the circuit breaker to isolate the fault. However, in islanded mode the DG inverter has a limited current due to which the pickup value of the overcurrent relay cannot be reached, and relay does not operate for the provided settings. The inclusion of energy storage devices contributed the fault current during islanded fault.

Energy storage system such as flywheel unit sets the voltage and frequency during islanded operation, and it maintains both the parameters within the threshold of operating limits by injecting or absorbing real power or reactive power. When the presence of main grid is detected, feedback from main grid voltage and frequency is considered and applied to the control loops to synchronize the microgrid with the main grid voltage and frequency.

In islanded mode, the fault current from DG is very less for the overcurrent relay to detect fault condition and the flywheel unit is the only source for providing fault current. The flywheel unit provides significant fault current results in overall current to reach the pickup value of the overcurrent relay during fault conditions. Thus, without using additional equipment, fault can be detected in islanded mode by classical overcurrent relay with preset setting by coordinating primary relay and backup relay.

2.2.2 Method 2 [27]

This method uses the fault current limiter (FCL) for maintaining the coordination between the directional overcurrent relays. Fault current limiter is a series connected device which has resistive or inductive characteristics and it also limits the current during faulted condition. During normal operation, it remains in in-active mode in the network.

For maintaining the coordination between directional overcurrent relay with DG system, the available FCL can provide a better option. During faulted condition, it limits the current draw from DG side and restores the original relay coordination setting without altering the relay setting or disconnecting the DG.

For implementing this method, we need to identify the individual DG capacity (IDG), number of DG (NDG), DG location (DGL), and fault location (FL). In the presence of the DG, we need to modify the power distribution scheme including the DG system. During normal operation, the pre-fault bus voltage and load flow into the distribution system are required to monitor. Considering a close-in fault condition, the primary relay and backup relay currents are required to monitor to set the pickup value and to check whether the coordination time interval is proper between the primary relay and backup relay or not.

With the inclusion of fault current limiter at the DG end, the current during fault condition can be limited. During fault, the power distribution scheme can be modified according to the type of the fault current limiter used and number of DG present in the system. For close-in fault to source end, the primary relay and backup relay currents are required to monitor to set the pickup value and then to check the coordination between primary relay and backup relay. If the coordination time interval is not

achieved between the primary relay and backup relay, the impedance of the fault current limiter will be increased, and it is required to run the whole process to modify the power distribution scheme during fault condition. This is required to obtain new coordination time intervals between primary relays and backup relays.

When the proper value of the impedance of FCL can be selected, the network can achieve proper coordination time intervals between primary relays and backup relays.

2.2.3 Method 3 [28]

Optimized techniques are generally used to obtain global/local maxima or minima of the given objective function. Conventional optimization techniques are sometimes inefficient for finding out the global points, as they get normally stuck toward the nearby local optimized points. Evolutionary methods use its search space more efficiently to obtain the global values by considering all the constraints.

There are numerous evolutionary techniques available for the coordination of overcurrent relay such as genetic algorithm (GA) and particle swarm optimization (PSO). In [28], enhanced back search algorithm (EBSA) is used for its ability to solve complex nonlinear optimization problem. It has single control parameter without being affected with the initial setting of the parameter. EBSA contains two crossovers and mutation operation for obtaining the optimal solution, and EBSA also has a memory to obtain advantages of previous population during creating new population which helps it to find the global optimized solution.

In this technique, EBSA method is used for obtaining the optimal values of time dial settings (TDS), pickup current/plug tap setting (PTS), and optimal parameters for inverse relay characteristics. Objective function of the relay coordination time is to minimize the operating time of the primary relay and to keep the coordination between the backup relays. Coordination of relay is done by the following steps

i. TDS is taken on first stage to obtain the optimal values.
ii. Both TDS and PTS are taken together to obtain the optimized values.
iii. At final stages, simulation is done to obtain the optimal values of TDS, PTS, and parameters for the inverse relay characteristics.

By using digital relay, different inverse relay characteristics can be programmed by using Eq. 23 as given.

$$t = \frac{\beta}{\left[\left(\frac{I}{\mathrm{CT}\times I_{\mathrm{p}}}\right)^{\theta} - 1\right]} * \mathrm{TDS} \tag{23}$$

where t is the operating time of the relay, I is the fault current on primary side of CT, I_{p} is the pickup current, and β, θ is the relay characteristic parameters.

The characteristic of the inverse relay can be varied by varying β and θ, and this will be considered as an optimized variable for the coordination problem. The

objective function (OF) used is to minimize the operating time of the primary relay at all fault location and to keep the coordination of main relay and backup relay. The EBSA method is used for obtaining the above objective.

2.3 Fault Classification

To restore the healthy supply system, quick detection and classification of fault type is essential in microgrid. The conventional fault-type selection techniques may not be suitable for microgrid system [29]. The penetration of renewable sources introduces new challenges such as distortions in signals which will further lead to phasor estimation issue [29]. Under the new developed constraints, obtaining adequate information is not possible. This will create fault phase selection issue. Some of the available techniques for the fault classification are given below.

2.3.1 Voltage Angle and Magnitude-Based Classifier [29]

In this method, the three-phase voltage phasor are estimated at local end relay. Next, the sequence components are estimated from the voltage phasors. The angle difference between the negative sequence and zero sequence voltage is estimated and represented by δ^0. The rule diagram for fault classification based on δ^0 is shown in Fig. 7.

With the monitoring of change in phase voltage magnitude with the above-mentioned logic can provide better information about fault type. In this technique, if at any situation none of the conditions will satisfy then relay output will be void. With the proper design of logic circuit, all faults can be detected and classified properly.

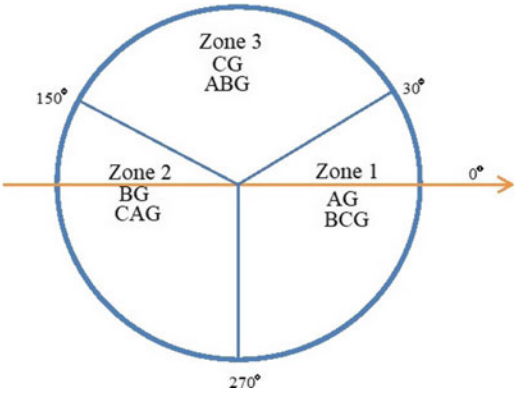

Fig. 7 Delta-zero zones for different fault types considering phase-a as reference

2.3.2 Combination of Wavelet Singular Entropy (WSE) and Fuzzy Logic (FL) [30]

In this method, a combination of wavelet singular entropy (WSE) and fuzzy logic (FL) is used for detecting and classifying the grid side fault with or without the presence of the DG.

In this technique, wavelet singular entropy (WSE) combines the benefits of wavelet transform theory (WTT), singular value decomposition (SVD) and spectrum theory (ST) calculations to generate index, and next, it is applied to the fuzzy logic system. Initially from the relay end, three-phase current signals are taken and then the positive sequence components of the phase current are calculated and analyzed by the wavelet transform theory to obtain detail coefficients of the three-phase signals. Now using SVD technique, we can compute the singular value from the detailed coefficient matrix. The singular value obtained from SVD is then used to calculate the entropy for evaluating the structures and patterns of the analyzed data. Again, from that data probability data array is created. First, the wavelet singular entropy for each phase current signal is computed, and the maximum and minimum values are estimated to classify the fault type.

WSE and fuzzy logic (FL) techniques are combined to detect and classify different types of fault in the microgrid system. Membership function and rules are implemented to the fuzzy decision system to classify the fault. Fault classification index is defined for each phase, and WSE of positive sequence component of current signals is defined for fault detection.

Such a method is highly effective and has faster detection and classification capability in the presence of DG systems.

2.3.3 Wavelet-Based Deep Neural Network (WBDNN) [31]

In this fault detection method, the discrete wavelet transform (DWT) is used along with deep neural network (DNN). DWT extracts all the information from the signal in time frequency domain, and DNN contains multiple hidden layers of neurons between input layer and output layer which is helpful to solve nonlinear phenomenon-related issues. DNN can be trained offline for fault detection task.

In this method, initially the three-phase current signals can be obtained from the measuring instrument, and then, it is processed through DWT to extract the time frequency domain information of the signal. Next, the DWT signal is feed to the DNN. Here by this method, the fault detection task can be further executed and extended by performing the following steps:

i. Type of fault occurred
ii. Phase at which fault has occurred
iii. Location at which fault has occurred.

So, to solve the above task, three different DNN are required, i.e., one for each problem.

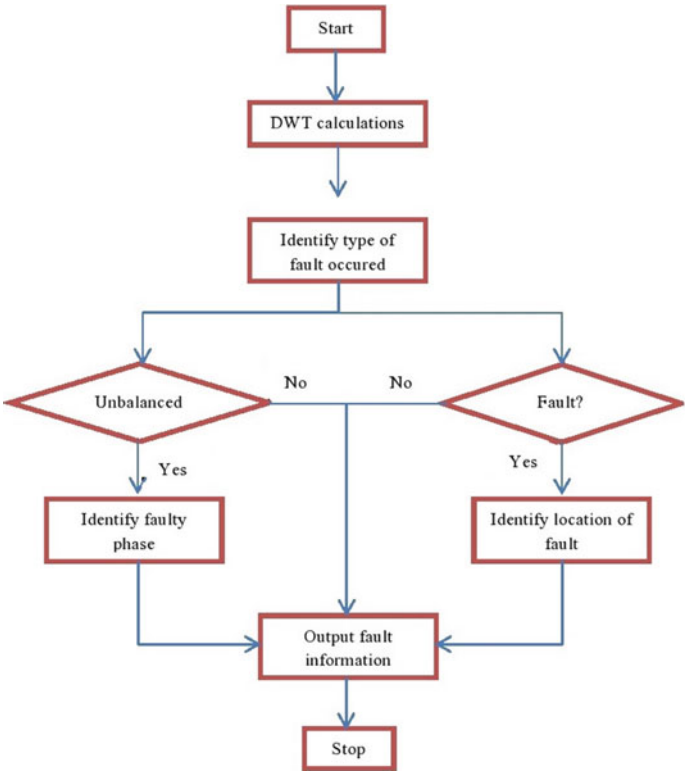

Fig. 8 Flow diagram of wavelet-based deep neural network technique

During fault condition, first DNN is employed to identify the type of fault, whether the fault is a balanced fault or unbalanced fault which can be observed from Fig. 8. Also, at the same time second DNN is employed to find out the fault location. If the first DNN identifies the fault as an unbalanced fault, then the third DNN is employed to identify the faulty phase. If the first identifies it as a balanced fault, then the first DNN continues to classify the type of fault, whether it is a triple line fault or triple line to ground fault. The WBDNN method is fast, and it can give accurate result. It also identifies the fault type, faulty phase, and fault location (Fig. 8).

3 Conclusion

The use of nonconventional resources for power generation is a better choice for future power section, and the reasons are not very limited. Microgrid is an active distribution network where renewable energy sources are integrated. From this reformed distribution network, uninterrupted and green power can be obtained. Local operation

and control are the other merits that can be possible in such a system. But due to the inclusion of different control systems and conversion mediums, the generated signals are more distorted. This is the main issue in a microgrid to deal with that distorted signal. Protection challenges arise due to the reformation of existing distribution network. Islanding detection, fault detection/classification, and relay coordination are one of them. Several algorithms have been developed to mitigate these issues and the existing problems with those techniques have been discussed briefly in this chapter.

References

1. Chandrakar R, Nale R, Biswal M (2019) Uninterrupted power supply to microgrid during Islanding. In: Handbook of research on smart power system operation and control, IGI Global, pp 96–128
2. Nale R, Biswal M, Kishor N (2019) A transient component based approach for islanding detection in distributed generation. IEEE Trans Sustain Energy 10(3):1129–1138
3. Nale R, Biswal M, Abdelaziz AY (2019) Protection schemes for sustainable microgrids. In: Sustainable interdependent networks: from theory to application. Springer, Berlin, pp 267–296
4. Nale R, Biswal M (2017) Comparative assessment of passive islanding detection techniques for microgrids. In: Proceedings IEEE conference on innovations in information, embedded and communication system (ICIIECS-2017), 17–18 Mar, 2017, Coimbatore
5. Lopes L, Sun H (2006) Performance assessment of active frequency drifting islanding detection methods. IEEE Trans Energy Convers 21:171–180. https://doi.org/10.1109/tec.2005.859981
6. Ropp M, Begovic M, Rohatgi A (1999) Analysis and performance assessment of the active frequency drift method of islanding prevention. IEEE Trans Energy Convers 14:810–816. https://doi.org/10.1109/60.790956
7. Yafaoui A, Wu B, Kouro S (2012) Improved active frequency drift anti-islanding detection method for grid connected photovoltaic systems. IEEE Trans Power Electron 27:2367–2375. https://doi.org/10.1109/tpel.2011.2171997
8. Li C, Cao C, Cao Y et al (2014) A review of islanding detection methods for microgrid. Renew Sustain Energy Rev 35:211–220. https://doi.org/10.1016/j.rser.2014.04.026
9. El-Moubarak M, Hassan M, Faza A (2015) Performance of three islanding detection methods for grid-tied multi-inverters. In: 2015 IEEE 15th international conference on environment and electrical engineering (EEEIC). https://doi.org/10.1109/eeeic.2015.7165481
10. Liu F, Kang Y, Zhang Y et al (2010) Improved SMS islanding detection method for grid-connected converters. IET Renew Power Gener 4:36. https://doi.org/10.1049/iet-rpg.2009.0019
11. Hernandez-Gonzalez G, Iravani R (2006) Current injection for active islanding detection of electronically-interfaced distributed resources. IEEE Trans Power Deliv 21:1698–1705. https://doi.org/10.1109/tpwrd.2006.876980
12. Karimi H, Yazdani A, Iravani R (2008) Negative-sequence current injection for fast islanding detection of a distributed resource unit. IEEE Trans Power Electron 23:298–307. https://doi.org/10.1109/tpel.2007.911774
13. Tuyen ND, Fujita G (2011) Negative-sequence current injection of dispersed generation for islanding detection and unbalanced fault ride-through. In: International conference universities power engineering, pp 1–6
14. O'Kane P (1997) Loss of mains detection for embedded generation by system impedance monitoring. In: 6th international conference on developments in power systems protection. https://doi.org/10.1049/cp:19970037
15. Freitas W, Xu W, Affonso C, Huang Z (2005) Comparative analysis between ROCOF and Vector surge relays for distributed generation applications. IEEE Trans Power Deliv 20:1315–1324. https://doi.org/10.1109/tpwrd.2004.834869

16. Zeineldin H, El-Saadany E, Salama M (2006) Impact of DG interface control on islanding detection and nondetection zones. IEEE Trans Power Deliv 21:1515–1523. https://doi.org/10.1109/tpwrd.2005.858773
17. Samui A, Samantaray S (2011) Assessment of ROCPAD relay for islanding detection in distributed generation. IEEE Trans Smart Grid 2:391–398. https://doi.org/10.1109/tsg.2011.2125804
18. Singam B, Hui L (2006) Assessing SMS and PJD schemes of anti-islanding with varying quality factor. In: 2006 IEEE international power and energy conference. https://doi.org/10.1109/pecon.2006.346645
19. Jang S, Kim K (2004) An islanding detection method for distributed generations using voltage unbalance and total harmonic distortion of current. IEEE Trans Power Deliv 19:745–752. https://doi.org/10.1109/tpwrd.2003.822964
20. Marchesan G, Muraro M, Cardoso G et al (2016) Passive method for distributed-generation island detection based on oscillation frequency. IEEE Trans Power Deliv 31:138–146. https://doi.org/10.1109/tpwrd.2015.2438251
21. Ropp M, Aaker K, Haigh J, Sabbah N (2000) Using power line carrier communications to prevent islanding [of PV power systems]. In: Conference record of the twenty-eighth IEEE photovoltaic specialists conference—2000 (Cat No00CH37036). https://doi.org/10.1109/pvsc.2000.916224
22. Makkieh A, Florida-James A, Tzelepis D et al (2019) Assessment of passive islanding detection methods for DC microgrids. In: 15th IET international conference on AC and DC power transmission (ACDC 2019). https://doi.org/10.1049/cp.2019.0016
23. Papadimitriou C, Kleftakis V, Hatziargyriou N (2017) A novel method for islanding detection in DC networks. IEEE Trans Sustain Energy 8:441–448. https://doi.org/10.1109/tste.2016.2604419
24. Vahedi H, Noroozian R, Jalilvand A, Gharehpetian G (2011) A new method for islanding detection of inverter-based distributed generation using DC-Link voltage control. IEEE Trans Power Deliv 26:1176–1186. https://doi.org/10.1109/tpwrd.2010.2093543
25. Seo G, Lee K, Cho B (2013) A new DC anti-islanding technique of electrolytic capacitor-less photovoltaic interface in DC distribution systems. IEEE Trans Power Electron 28:1632–1641. https://doi.org/10.1109/tpel.2012.2208226
26. Yang M, Chang L (2013) Optimal protection coordination for microgrid under different operating modes. Math Probl Eng 2013:1–15. https://doi.org/10.1155/2013/404086
27. El-Khattam W, Sidhu T (2008) Restoration of directional overcurrent relay coordination in distributed generation systems utilizing fault current limiter. IEEE Trans Power Deliv 23:576–585. https://doi.org/10.1109/tpwrd.2008.915778
28. Othman A, Abdelaziz A (2015) Enhanced backtracking search algorithm for optimal coordination of directional over-current relays including distributed generation. Electric Power Compon Syst 44:278–290. https://doi.org/10.1080/15325008.2015.1111468
29. Hooshyar A, El-Saadany E, Sanaye-Pasand M (2016) Fault type classification in microgrids including photovoltaic DGs. IEEE Trans Smart Grid 7:2218–2229. https://doi.org/10.1109/tsg.2015.2451675
30. Dehghani M, Khooban M, Niknam T (2016) Fast fault detection and classification based on a combination of wavelet singular entropy theory and fuzzy logic in distribution lines in the presence of distributed generations. Int J Electr Power Energy Syst 78:455–462. https://doi.org/10.1016/j.ijepes.2015.11.048
31. Yu J, Hou Y, Lam A, Li V (2019) Intelligent fault detection scheme for microgrids with wavelet-based deep neural networks. IEEE Trans Smart Grid 10:1694–1703. https://doi.org/10.1109/tsg.2017.2776310

Hybrid Event Classification Scheme for Converter-Based DG with Improved Power Quality

Om Hari Gupta, Manoj Tripathy and Vijay K. Sood

Abstract With the integration of renewable energy-based distributed generations (DGs), there are a few challenges in the protection of microgrid (i.e., a distribution system employed with DGs—mostly the renewable energy-based) which are required to be addressed. Detection of an islanding event has been one of such challenges in microgrid protection. There are several techniques for the detection of islanding event such as passive, active, hybrid, and communication-based techniques. However, most of them are either affected by fault event or inject disturbances and thereby, degrade the power quality. Moreover, communication-based techniques are expensive in terms of installing a signal generator, transmitter, and receiver. This chapter presents a method to detect and differentiate between islanding and fault events in microgrids with embedded converter-based DG. Unlike other schemes, the proposed scheme injects negligibly small disturbance into the microgrid when some change in the extracted features is detected. The proposed scheme is based on an alert signal (generated using several features) and a parameter called superimposed impedance (SI) that has never been used for such application. The SI is calculated only when the alert signal is high. The SI is characterized by a low value during grid-connected mode and a high value during the islanded mode. Furthermore, for a fault at the point of common coupling (PCC), the SI is very small and PCC voltage is virtually close to zero. Therefore, an islanding event can be detected if SI is high, while a fault event is detected if SI is very low and the PCC voltage is also very low.

O. H. Gupta (✉)
Department of Electrical Engineering, National Institute of Technology Jamshedpur, Jamshedpur, Jharkhand, India
e-mail: omhari.ee@nitjsr.ac.in

M. Tripathy
Department of Electrical Engineering, Indian Institute of Technology Roorkee, Roorkee, Uttarakhand, India
e-mail: manojfee@iitr.ac.in

V. K. Sood
Department of Electrical, Computer and Software Engineering, Ontario Tech University, 2000 Simcoe St N, Oshawa, ON L1G 0C5, Canada
e-mail: vijay.sood@uoit.ca

P. Ray and M. Biswal (eds.), *Microgrid: Operation, Control, Monitoring and Protection*,
Lecture Notes in Electrical Engineering 625,
https://doi.org/10.1007/978-981-15-1781-5_7

The robustness of the proposed scheme is tested against different islanding conditions and a fault at the PCC first by using off-line MATLAB-based simulator and secondly by using real-time digital simulator (RTDS). Additionally, a comparison with recently published schemes shows the superiority of the proposed scheme. The results obtained from the off-line and real-time simulations show that the scheme is accurate for different islanding, fault, and other events and successfully classifies different events.

Keywords Islanding · Microgrid · Distributed generation · Superimposed impedance · RTDS

Nomenclature

DG	Distributed generation
ΔP	Active power supplied by grid
P_{dg}	DG output power
PCC	Point of common coupling
V_{PCC}	PCC voltage
f_{PCC}	PCC frequency
R	Load resistance
ΔQ	Reactive power supplied by grid
Q_{dg}	DG output power
L	Load inductance
C	Load capacitance
ω	PCC frequency
$\left\lvert\frac{\mathrm{d}V_{\mathrm{PCC}(-)}}{\mathrm{d}t}\right\rvert$ or ROCONSV	Rate-of-change-of-negative-sequence-voltage
V_{dthN}	Threshold for ROCONSV
$\left\lvert\frac{\mathrm{d}f_{\mathrm{PCC}}}{\mathrm{d}t}\right\rvert$ or ROCOF	Rate-of-change-of-frequency
f_{dth}	Threshold for ROCOF
PDM	PCC disturbances per minute
THD	Total harmonic distortion
ΔZ or SI	Superimposed impedance
$\lvert\Delta Z_{\mathrm{thr}}\rvert$	Threshold for ΔZ
AS	Alert signal
P_{ref}	Reference active power
I_{d}	Direct axis reference current
i_{ref}	Reference current
i_{DG}	DG current
VSC	Voltage Source Converter
LoG	Loss-of-grid
RPS	Rate of power shift
NDZ	Non-detectable zone

Z_{IB}	Grid impedance
$\left\lvert \frac{\mathrm{d}V_{\text{PCC}}}{\mathrm{d}t} \right\rvert$	Rate-of-change-of-voltage or ROCOV
V_{dth}	Threshold for ROCOV
Z_L	Load impedance
PPAM	Perturbation amount per minute
I_{q}	Quadrature axis reference current
I_0	Zero sequence reference current

1 Introduction

1.1 General Overview

Microgrids are small-scale replicas of the main (distribution) grid but now with distributed generation (DG) incorporated. Microgrids, therefore, have the flexibility to operate in either grid-connected or islanded modes. The microgrid is capable of injecting locally generated power into the main grid to fill the gap between demand and supply in grid-connected mode. In islanded mode, the microgrid with its DG is capable of feeding its local load (all or part of it) when the main grid is unavailable for whatever reason. Solar-based DGs are the fastest-growing segment of DGs and are widely used [1]. Solar-based DG produces DC power from sunlight which is converted to AC power by means of electronic converters. Therefore, in this chapter, only converter-based DG system is considered. The presence of DG within the microgrid introduces new challenges for the distribution system protection due to bi-directional current/power flow. Within the microgrid, there are mainly two protection concerns: first, protection against (internal) faults and second, protection against Loss-of-grid (LoG). For any fault within the distribution system, the point of common coupling (PCC) voltage will be small (or nearly zero) and the superimposed impedance (SI) will also be very small (or nearly zero). The objective here is mainly to identify the islanding event and fault event at the PCC.

LoG (or microgrid islanding) is the condition in which microgrid is energized by the DGs, while the utility grid is removed. As per IEEE STD 1547-2003 [2], it is the duty of the DG to detect the islanding and disconnect itself within two seconds. However, for best utilization of DGs, they should be capable to operate itself either grid-connected mode or islanded mode [3, 4] with the use of load shedding if required [5, 6]. More importantly, DGs should be able to switch from power control mode (or current control mode) to voltage control mode in the event of islanding in order to maintain the PCC voltage and frequency at their rated values [7, 8]. Therefore, islanding detection is mandatory in both cases either to disconnect the DG unit or to switch the mode of operation of the voltage source converter (VSC).

Overall, there may be two desired conditions after an islanding event:

- DG must be disconnected.
- DG has to change its mode of operation (from power/current control to voltage/frequency control).

For the first case, islanding can be detected within two seconds and DG should be disconnected. This condition is desirable when the DG is incapable of supplying the local load alone or load shedding cannot be applied.

For the second case, after the detection of an islanding event, DG should change its mode of operation from power/current control to voltage/frequency control. This condition is desirable when the DG alone is capable of supplying the local load or load shedding can be used. Therefore, the second case may sometimes require the islanding detection to be a little faster. In this proposed work, the islanding events (under different system conditions) are detected nearly in 0.7 s, i.e., in less than half of the time specified in IEEE STD 1547-2003.

In the literature, mainly, four types of islanding detection methods are identified, namely passive methods [9–13], active methods [14–25], communication-based methods [26] and hybrid methods [27, 28] (i.e., use both active and passive techniques). These are discussed next.

1.2 Passive Methods

After an islanding event, the PCC voltage goes beyond its desired limits (0.8–1.1 PU) due to sufficient active power mismatch. Similarly, the PCC frequency may cross its minimum (49.5 Hz) or maximum (50.5 Hz) limits (in the case of a 50 Hz system) if sufficient mismatch of reactive power exists. Therefore, the passive methods find limitation when the small mismatch of powers exists. Figure 1a depicts the non-detectable zone (NDZ) for passive methods. The islanding event is not detected if ΔQ and ΔP (the reactive and active mismatch powers, respectively, supplied by the main/utility grid) lie within the dashed area. The NDZ is described next.

Consider Fig. 1b which depicts a DG connected to the main grid with local load at point of common coupling. Load-active power can be defined as follows:

$$P_{\mathrm{L}} = P_{\mathrm{dg}} + \Delta P = \frac{V_{\mathrm{PCC}}^2}{R}$$

where ΔP = the active power supplied by the utility grid, P_{dg} = DG output power, V_{PCC} = PCC voltage, R = load resistance.

Above equation can be re-written as:

$$V_{\mathrm{PCC}} = \sqrt{\left(P_{\mathrm{dg}} + \Delta P\right) R} \tag{1}$$

Similarly, the load reactive power consumption can be described as:

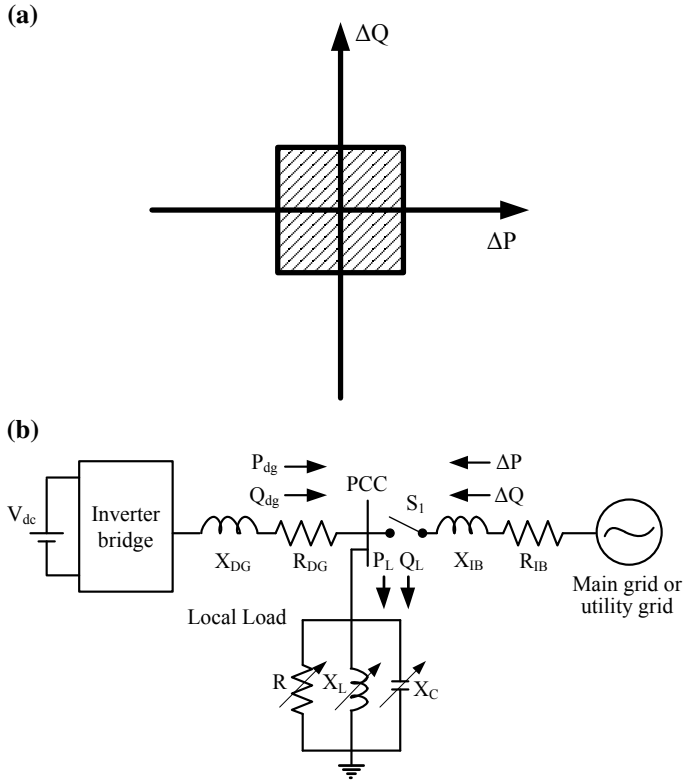

Fig. 1 **a** Representation of non-detectable zone and **b** an equivalent representation of microgrid

$$Q_{\mathrm{L}} = Q_{\mathrm{dg}} + \Delta Q = \frac{V_{\mathrm{PCC}}^2}{\omega L} - \frac{V_{\mathrm{PCC}}^2}{1/\omega C}$$
$$Q_{\mathrm{dg}} + \Delta Q = V_{\mathrm{PCC}}^2\left(\frac{1}{\omega L} - \omega C\right)$$

where $\Delta Q =$ the reactive power supplied by the utility grid, $Q_{\mathrm{dg}} =$ DG output power, $L =$ load inductance, $C =$ load capacitance, $\omega =$ PCC frequency (rad/s)

Above equation can also be re-written as:

$$\left(\frac{1}{\omega L} - \omega C\right) = \frac{Q_{\mathrm{dg}} + \Delta Q}{V_{\mathrm{PCC}}^2} \tag{2}$$

As per Eq. 1, if ΔP is zero and islanding occurs, there will not be any change in V_{PCC} and islanding will not be detected by under voltage/over voltage (UV/OV) relay. If ΔP is sufficiently high and islanding occurs, ΔP will become zero and V_{PCC} will deviate from its nominal value and UV/OV relay can detect the islanding event. Therefore, it is clear from (1) that after an islanding event, the PCC voltage will go beyond its desired limits (0.8–1.1 PU) if there is sufficient active power mismatch. Similarly, according to (2), the PCC frequency may cross its minimum (49.5 Hz) or

maximum (50.5 Hz) limits if ΔQ is sufficient. Therefore, the passive method finds limitation when the small mismatch of powers is there. Figure 1a depicts the NDZ for passive methods. The islanding event is not detected if ΔQ and ΔP are within the dashed area.

Several other passive islanding detection schemes are rate-of-change-of-frequency (ROCOF) [29], ROCOF over power [12], voltage unbalance [30], total harmonic distortion technique [31], etc. There are schemes which can reduce the area of this NDZ. However, these schemes fail to detect when closely matched DG and load powers exist. Several schemes use signal processing techniques such as wavelet transform [32] and S-transform [33] to extract new features of the measured signal. Moreover, several other intelligent methods, viz. artificial neural networks (ANNs) [34] and fuzzy logic [10], are also used for islanding detection.

Another simple passive islanding detection technique based on rate-of-change-of-voltage-phase-angle (ROCOVPA) [26] has been proposed that has very small NDZ but, if the converter mode is switched to independent mode, this scheme finds limit. Further, a fault event will also be mis-detected as an islanding event by ROCOVPA scheme.

1.3 Active Methods

To eliminate the problem of NDZ, active methods use intentional disturbance injection which deviates either PCC voltage or frequency from their desirable limits. These methods work even if there is a perfect match for DG and load powers. As per IEEE STD 1547-2003, islanding should be detected within 2 s. Therefore, these disturbances are injected at 2-s intervals. Although these schemes have the capability of detecting an island during perfectly matching conditions, they seriously degrade the power quality. Several schemes are available that comparatively reduce the amount of disturbance injection but not the rate of injection. Therefore, regular injections still largely degrade power quality. Several active islanding detection methods have been listed below:

- Slip-mode frequency shift [14]
- Negative sequence current injection [15]
- Phase-locked loop (PLL) perturbation [24]
- Voltage phase angle feedback-based active method [25]
- Negative sequence voltage injection [16]
- Active frequency drift [17]
- Current injection [18]
- Virtual capacitor [19]
- Virtual inductor [20]
- Sandia frequency shift [21]
- High-frequency signal injection [22]
- Sandia voltage shift [23].

All the above-mentioned methods inject regular disturbances into the PCC and, therefore, degrade the power quality at PCC.

1.4 Communication-Based Schemes

Such schemes detect an islanding event based on communication between utility and DG. These schemes are more reliable; nonetheless, these are quite expensive because of installation of peripheral signal equipment. Therefore, such schemes are not preferred [26].

1.5 Hybrid Methods

Hybrid methods make use of both passive and active techniques. The disturbance is injected only when islanding is suspected using the features extracted from PCC measurements. By doing this, the power quality of the system is not degraded on a large scale. However, the available schemes depend on the features which may not vary sufficiently during closely matched power conditions. There are several hybrid islanding detection techniques which use both the passive and active methods to detect an islanding event. In [27], the frequency set point is shifted to observe the deviation in PCC frequency. If the PCC frequency reaches a certain value, an islanding event is detected. The frequency set point is, however, shifted only after observing some voltage unbalance. The scheme finds its limitation if there is not sufficient voltage unbalance. Further, it may take around 1.5 s to detect an islanding event. Similarly, there must be some voltage variation at the PCC to apply the rate of power shift (RPS)-based scheme proposed in [28].

In this chapter, instead of injecting disturbances at regular intervals, a new alert signal is first generated before the injection of a very small disturbance. The alert signal is generated using several features extracted from the PCC voltage. These extracted features are PCC frequency (f_{PCC}), ROCOF, PCC voltage magnitude ($|V_{\mathrm{PCC}}|$), rate-of-change-of-voltage (ROCOV), and rate-of-change-of-negative-sequence-voltage (ROCONSV).

2 DG Description and Converter Control

The control process of the microgrid is shown in Fig. 2. The DG is normally operated at unity power factor to supply active power only [35]. The PCC voltage and DG current output are used to obtain active (P) and reactive (Q) power output of DG. The active power is compared with a reference active power ($\mathrm{P_{ref}}$) and an error signal (E_{P}) is generated. This error signal is given to an active power controller (an

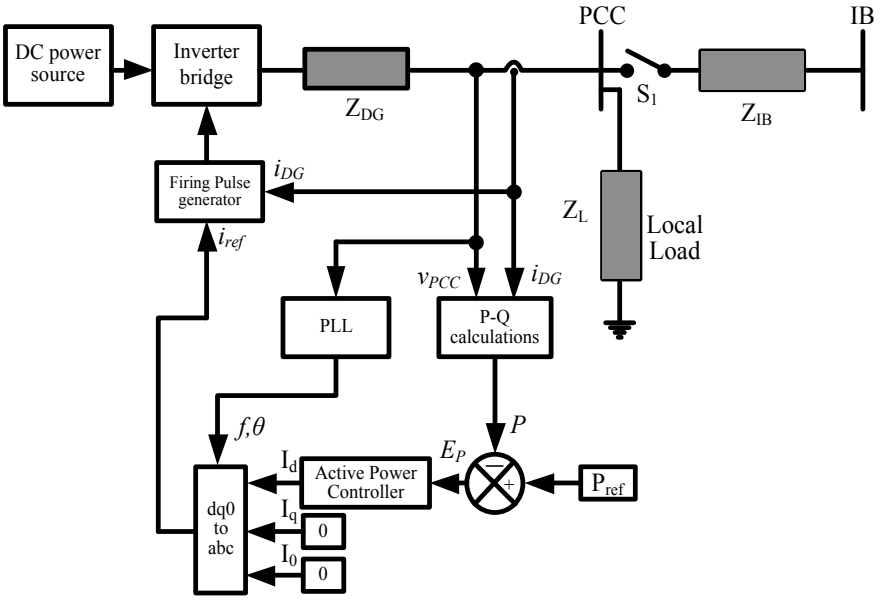

Fig. 2 Control scheme of grid-connected inverter-based DG

integrator) which gives the direct axis reference current (I_d). The quadrature axis reference current (I_q) and zero sequence reference current (I_0) are kept zero as only active power is to be delivered by the inverter. Then, using dq0-abc transformation, reference current (i_{ref}) is obtained. Firing pulses are generated using i_{ref} and i_{DG}. These firing pulses are generated with a hysteresis current controller and are fed to the inverter switches.

3 Islanding Event Detection Scheme

The presented hybrid islanding event detection scheme first generates an alert signal using several features extracted at the PCC (local end) and then injects a very small perturbation to the system to calculate the superimposed impedance (SI) at the PCC. If the magnitude of measured SI (or $|\Delta Z|$) is higher than a threshold value $|\Delta Z_{thr}|$, then the microgrid is considered as islanded, and if $|\Delta Z|$ is lower than the threshold $|\Delta Z_{thr}|$, then the microgrid is considered as grid connected, i.e.:

IF $|\Delta Z| > |\Delta Z_{thr}|$, **THEN** microgrid is islanded
IF $|\Delta Z| < |\Delta Z_{thr}|$, **THEN** microgrid is grid connected.

The procedure of obtaining $|\Delta Z_{thr}|$ (which is equal to 3 PU) to identify an islanding event has been given later in Sect. 3.2.

The $|\Delta Z|$ will be nearly zero in case of a solid or bolted fault at the PCC since it represents the short circuit impedance. Therefore, if the SI and PCC voltage both are nearly zero, a fault event is detected. The proposed event detection and classification scheme has been tested and works fine for all the cases including nearly perfect power match (both P and Q) of load and DG. The generation of an alert signal (i.e., AS) and SI (i.e., ΔZ) calculation are separately explained next.

3.1 Generation of an Alert Signal

The alert signal, AS, will be a logical 1 if any of the following conditions is true:

$$\left|\frac{\mathrm{d}V_{\mathrm{PCC}}(-)}{\mathrm{d}t}\right| > V_{\mathrm{dthN}} \tag{3}$$

$$|V_{\mathrm{PCC}}| < 0.88 \text{ or } |V_{\mathrm{PCC}}| > 1.1 \text{ or } \left|\frac{\mathrm{d}V_{\mathrm{PCC}}}{\mathrm{d}t}\right| > V_{\mathrm{dth}} \tag{4}$$

$$f_{\mathrm{PCC}} < 49.5 \text{ or } f_{\mathrm{PCC}} > 50.5 \text{ or } \left|\frac{\mathrm{d}f_{\mathrm{PCC}}}{\mathrm{d}t}\right| > f_{\mathrm{dth}} \tag{5}$$

where $\left|\frac{\mathrm{d}V_{\mathrm{PCC}}(-)}{\mathrm{d}t}\right|$ is ROCONSV, V_{dthN} is the threshold for ROCONSV, $\left|\frac{\mathrm{d}V_{\mathrm{PCC}}}{\mathrm{d}t}\right|$ is the ROCOV, V_{dth} is the threshold for ROCOV, $\left|\frac{df_{PCC}}{dt}\right|$ is the ROCOF, and f_{dth} is the threshold for ROCOF.

Sufficient deviation from their steady-state values is not possible during an islanding event for a negligible or close-to-zero mismatch between load and DG powers (both real and reactive) [12, 29–31]. However, it is found that there is always some deviation in the magnitude of the negative sequence voltage following an islanding event irrespective of the mismatch [36] between load and DG powers (both P and Q). It happens because of the error caused by sample-to-sample calculation of negative sequence voltage. Therefore, the ROCONSV is sufficient to generate an alert signal (AS) even if nearly perfect power match between load and DG powers (both real and reactive) exists.

For a case of nearly perfect power match in a microgrid of Fig. 1b, consider Fig. 3 which shows the change in ROCONSV after an islanding event. It is observed that there is sufficient change in the ROCONSV and it can cross the threshold to generate an alert signal.

3.2 Superimposed Impedance (SI) Calculation

Consider the microgrid shown in Fig. 1b and its superimposed component circuit, as shown in Fig. 4. If the AS is logical 1, a small intentional perturbation is injected in

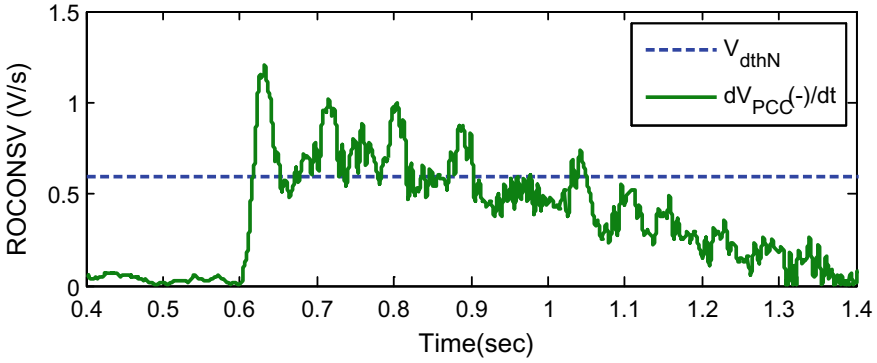

Fig. 3 ROCONSV for nearly perfect power match

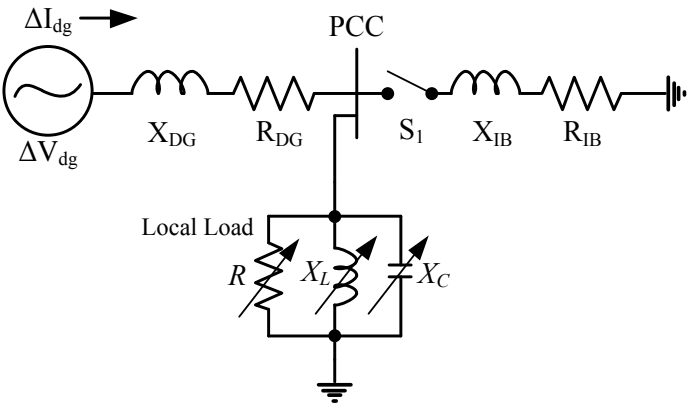

Fig. 4 Superimposed equivalent of the circuit of Fig. 1b

the DG supply and the SI (ΔZ) is calculated as per (6) below:

$$\Delta Z = \frac{\Delta V_{\mathrm{PCC}}}{\Delta I_{\mathrm{dg}}} \mathrm{AS} \tag{6}$$

Under the occurrence of different events, the calculated SI (ΔZ) will be different as given below in Eq. 7:

$$\Delta Z = \begin{cases} Z_{\mathrm{L}} \| Z_{\mathrm{IB}} & \ldots \text{ connected mode} \\ Z_{\mathrm{L}} & \ldots \text{ islanded mode} \\ 0 & \ldots \text{ fault mode} \end{cases} \tag{7}$$

where $Z_{\mathrm{L}} = R \| (jX_{\mathrm{L}} \| -jX_{\mathrm{C}})$

As depicted in Eq. 7, in connected mode (switch S_1 is closed), ΔZ is equal to the parallel combination of Z_L and Z_{IB}. The grid impedance, $|Z_{IB}|$, is very small compared to $|Z_L|$ and $|(Z_L \| Z_{IB})| < |Z_{IB}|$. Therefore, $|\Delta Z|$ is also very small and is less than $|Z_{IB}|$. During islanded mode (switch S_1 is open), $|\Delta Z|$ is equal to $|Z_L|$ which is very high compared to $|Z_{IB}|$, and during the fault at PCC, ΔZ represents the short circuit impedance which is nearly zero.

Overall, the scenario is that $|\Delta Z|$ is high and equal to $|Z_L|$ when the microgrid is islanded. For the other two cases (i.e., connected mode and fault mode), $|\Delta Z|$ is very small and less than $|Z_{IB}|$.

The threshold for SI ($|\Delta Z_{thr}|$) can be selected between $|Z_{IB}|$ and $|Z_L|$. The magnitude of load impedance, $|Z_L|$, is usually many times higher than grid impedance $|Z_{IB}|$. In this study, it is 12.5 times higher and the threshold ($|\Delta Z_{thr}|$) is set three times $|Z_{IB}|$ (considering 200% margin of safety). Considering the base value equal to $|Z_{IB}|$, the threshold value ($|\Delta Z_{thr}|$) in per unit will be 3 PU.

3.3 *Application of the Proposed Scheme with Improved Power Quality*

The proposed scheme utilizes the 1% perturbation ratio (i.e., 1% reduction in rated power takes place) to detect the islanding event and that too only when a disturbance is detected at the PCC. There are schemes which use periodical injections [37–40]. These disturbance injections are usually much higher than that of this proposed scheme. For instance, the scheme of [40] uses 10% perturbation ratio. Figure 5 shows a comparative analysis between the proposed scheme and a scheme which uses a regular perturbation, i.e., scheme of [40]. It presents the Percentage perturbation amount per minute (PPAM) with PCC disturbances per minute (*PDM*) for the existing [40] and the proposed scheme. The PCC disturbances include load disturbances,

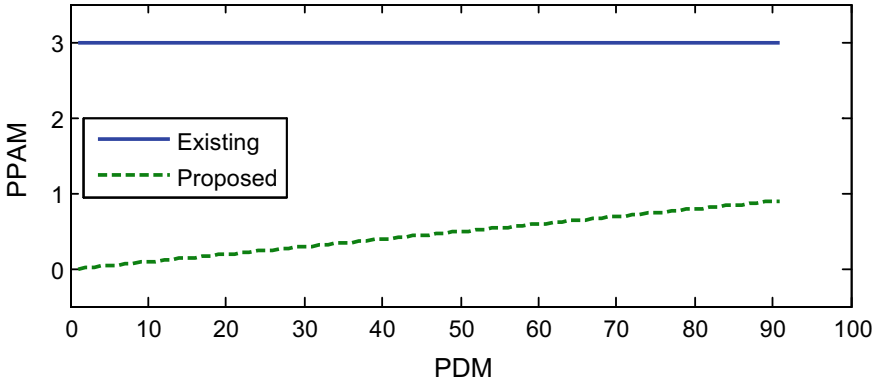

Fig. 5 A plot of PPAM versus PDM for the proposed scheme and scheme of [40]

capacitor switching, islanding event, fault event, etc. Further, the *PPAM* is calculated as:

$$\text{PPAM} = \%\ \text{perturbation} \times \text{frequency of perturbation (per minute)} \tag{8}$$

The schemes which use periodical perturbation injections have a constant frequency of perturbation, and usually, its minimum value can be 30 as per IEEE STD 1547-2003 [2]. Therefore, for the scheme of [40], the minimum value of *PPAM* using Eq. 8 will be constant and equal to 3 (i.e., 0.1 * 30). Overall, the PPAM is independent of the PDM.

On the other hand, in the proposed scheme, the frequency of perturbation (and thus PPAM) depends on the PCC disturbances (or PDM). Since only 1% perturbation is allowed in the proposed scheme, the *PPAM* for the proposed scheme can be written as:

$$\text{PPAM} = 0.01 \times \text{PDM} \tag{9}$$

It is clear from Eq. 9 that *PPAM* is directly proportional to the PDM. From Fig. 5, it can be observed that for a very large value of PDM, PPAM of the proposed scheme is still very small compared to that of an existing scheme [40].

Figure 6 depicts the flow diagram of SI-based islanding detection method. The 3-phase voltages and DG output currents are first measured at PCC; then using Eqs. 3–5, the disturbance at the PCC is detected. If a disturbance is not detected using Eqs . 3–5, the algorithm returns to the measurement block else the *AS* is generated and perturbation is injected by reducing the DG output by only 1% after 0.4 s (to let the transients die out). Now, the SI (ΔZ) is calculated at PCC using Eq. 6 and if the $|\Delta Z|$ is found to be more than the threshold ($|\Delta Z_{\text{thr}}|$) for the duration of 0.3 s (i.e., 15 cycles to avoid any false islanding event detection due to other switching events), islanding event is detected. Else if $|\Delta Z|$ is less than $|\Delta Z_{\text{thr}}|$, algorithm rechecks the PCC voltage and if PCC voltage is less than 0.88 PU, there is a fault event at the PCC. Else if the PCC voltage is found equal to or more than 0.88 PU, there is another type of switching event and algorithm returns to the measurement block.

4 Results

The proposed scheme is first evaluated using MATLAB simulations and then verified in a real-time environment using RTDS. The microgrid data is given in the Appendix.

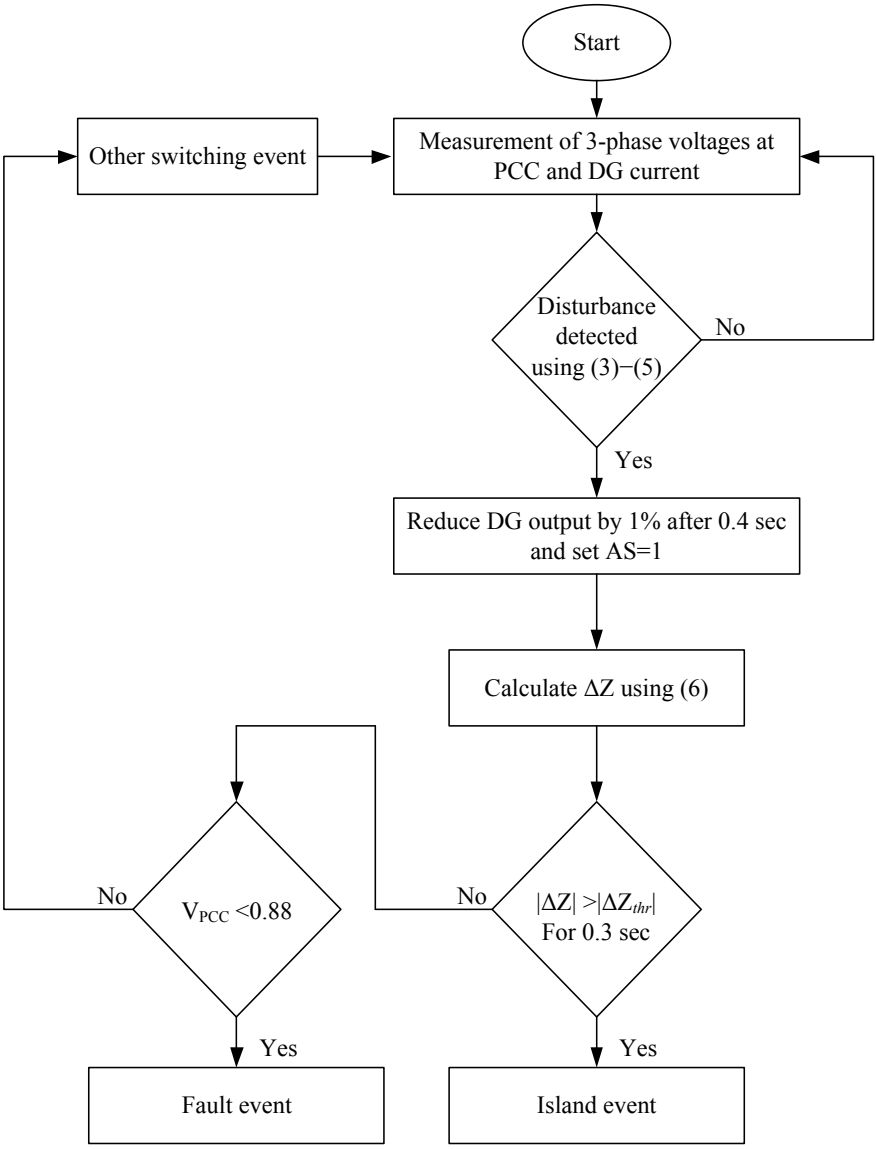

Fig. 6 Flow diagram of the presented scheme

4.1 MATLAB Simulation

The test model, as shown in Fig. 1b, is simulated using MATLAB with 100 kHz sampling frequency. The DG inverters are usually operated to supply constant active power, i.e., at unity power factor. The reactive power demand of load is supplied by

the grid. Therefore, in this work, the converter-based DG is providing only constant active power. Different conditions of microgrid have been used to investigate the effectiveness of the proposed scheme such as islanding during nearly perfect power match, active power mismatch, and reactive power mismatch, load switching, fault at PCC and DG output variation.

4.1.1 Islanding During Nearly Perfect Power Matching Condition

Figure 7 presents the results obtained for an islanding event occurring at 0.6 s during nearly perfect power match (i.e., ΔP and ΔQ are nearly zero). After the islanding event, ROCONSV and ROCOF cross their respective thresholds of 0.6 V/s (V_{dthN}) and 0.6 Hz/s (f_{dth}), which can be seen in Fig. 7a, b, respectively. The thresholds are chosen by observing the pre-islanding values and by keeping sufficient safety margin. The thresholds for ROCONSV and ROCOF are kept four times of their maximum pre-islanding values such as 0.15 V/s and 0.15 Hz/s, respectively. It is clear from Fig. 7c that as per the algorithm, the change in AS from zero to one is delayed by 0.4 s after detection of a disturbance at the PCC occurring at 0.6 s. The generation of AS decreases the DG output power by 1% of its rated value, as shown in Fig. 7d. Now, the SI (ΔZ) is calculated. The $|\Delta Z|$ settles at nearly 12.5 PU. Since the $|\Delta Z|$ is higher than the threshold value ($|\Delta Z_{\text{thr}}|$) for more than 0.3 s as depicted in Fig. 7e, the islanding event is detected and the islanding detection indicator (ID) moves from 0 to 1, see Fig. 7f. Further, it is also clear from Fig. 7g–j that post-islanding voltage, frequency, active power, and reactive power hardly change from their steady-state value after the occurrence of islanding. Therefore, passive techniques (e.g., UV/OV) find limitations.

To observe the power quality degradation due to perturbation injection, two cycles (one pre-islanding and one post-islanding) are considered and comparison of various parameters with that of [40] are presented in Table 1. It is found that the proposed scheme is better in all the aspects such as PCC voltage THD, DG current THD, and fundamental magnitudes of voltage and current. Moreover, the proposed scheme injects the perturbation only when any disturbance is detected but the scheme of [40] injects the perturbations at regular intervals which causes more degradation of power quality than the proposed scheme.

4.1.2 Islanding During Reactive Power Mismatch

When there is mismatching of reactive powers between load and DG (say 22%), the plots of AS, SI, and ID have been included in Fig. 8. The load requires 0.22 PU reactive power, while the DG supplies no reactive power as it is working at unity power factor. Therefore, during the pre-islanding condition, reactive power is supplied by the grid. After an islanding event, the ROCONSV, ROCOF, and frequency are high and generate an alert signal as shown in Fig. 8a. This causes the injection of 1% perturbation in DG power and ΔZ is calculated. The $|\Delta Z|$ crosses the

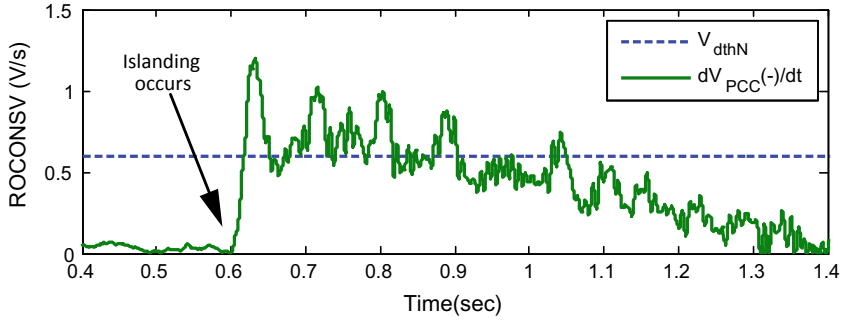

(a) ROCONSV

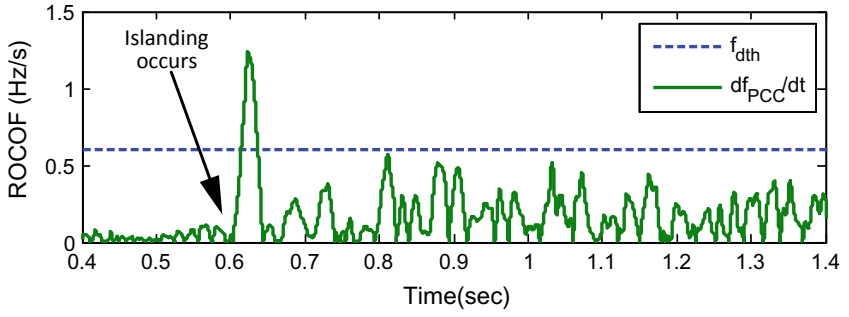

(b) ROCOF

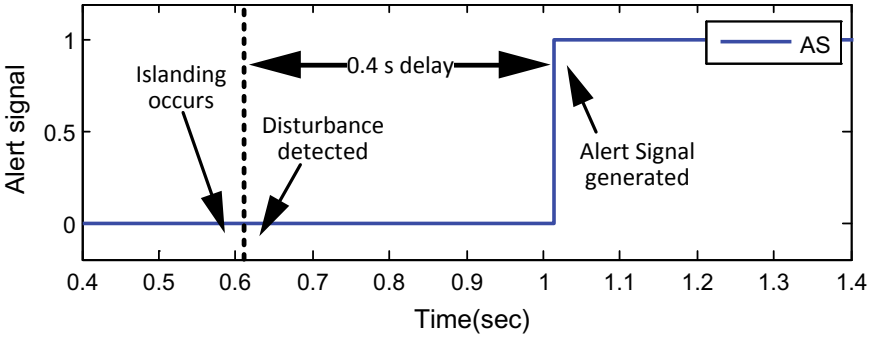

(c) Alert signal (AS)

Fig. 7 Different waveforms for islanding event with nearly perfect power match

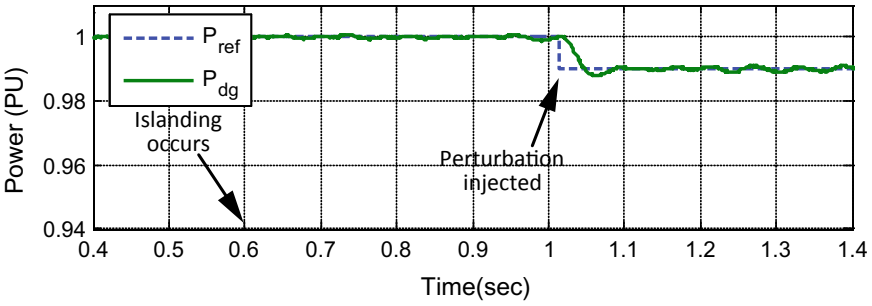

(d) DG output power

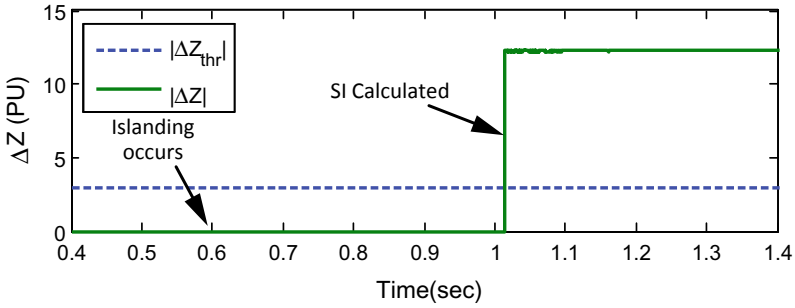

(e) Superimposed impedance (SI)

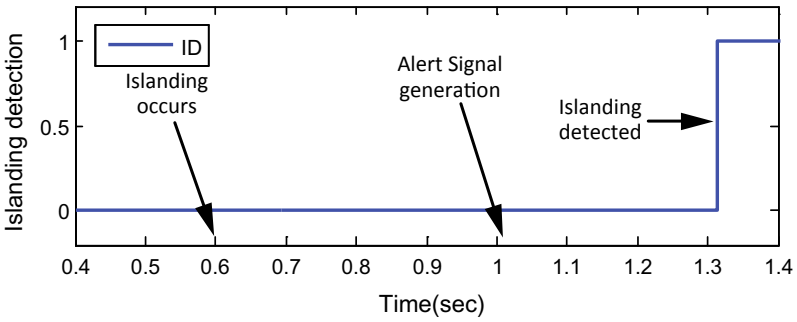

(f) Islanding detection indicator (ID)

Fig. 7 (continued)

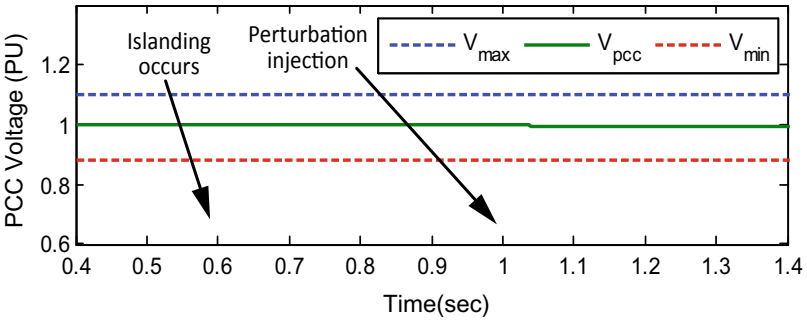

(g) PCC Voltage

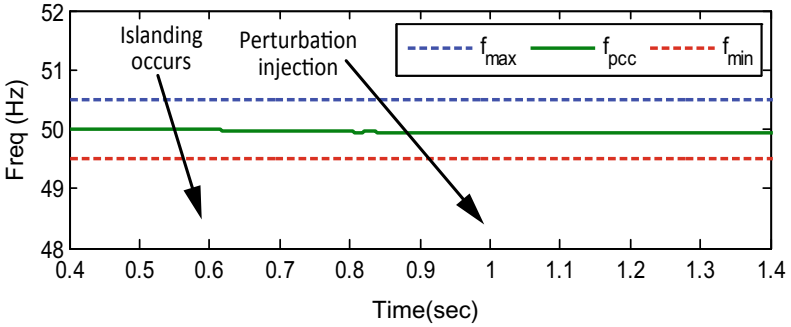

(h) PCC frequency

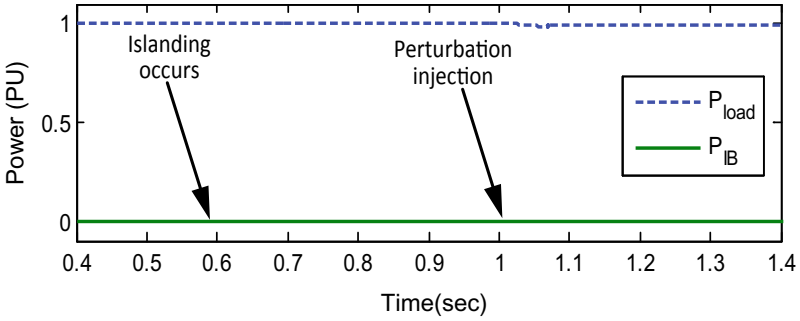

(i) Load and grid-supplied (i.e. IB-supplied) active powers

Fig. 7 (continued)

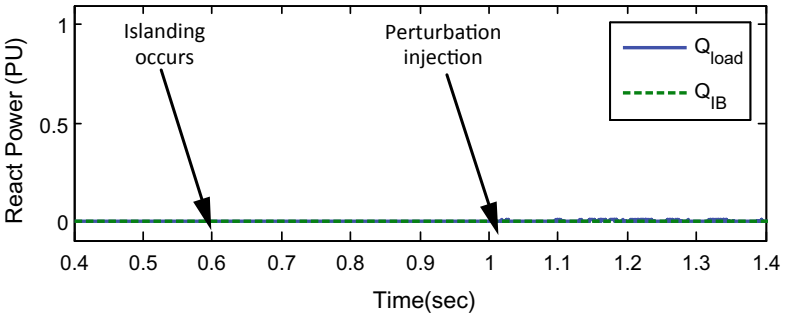

(j) Load and grid-supplied (i.e. IB-supplied) reactive powers

Fig. 7 (continued)

Table 1 Power quality comparison of proposed scheme with that of [40]

S. no.	Parameter	Proposed scheme	Scheme of [40]
1	PCC voltage THD (%)	0.24	0.49
2	Fundamental voltage (V)	439.88	437.34
3	DG current THD (%)	1.00	1.09
4	Fundamental current (A)	65.55	64.81

threshold and remains high for more than 0.3 s as depicted in Fig. 8b. Therefore, the proposed scheme successfully detects the islanding event at 1.3 s (approximately) which is clear from Fig. 8c.

4.1.3 Islanding During Active Power Mismatch

When islanding occurs at a time 0.6 s with the mismatch of active power (say 25%), the *AS* is generated since features of Eqs. 3–5 have crossed the corresponding thresholds and $|\Delta Z|$ is obtained by using Eq. 6 which remains higher than the $|\Delta Z_{thr}|$ for 0.3 s. Therefore, islanding is detected as shown in Fig. 9.

4.1.4 Effect of Load Switching

To study the effect of the sudden load jump, 50% of the rated load is suddenly increased at 0.6 s. The changes are found in the features of Eqs. 3–5, and therefore, an alert signal is generated as illustrated in Fig. 10a. The $|\Delta Z|$ momentarily crosses

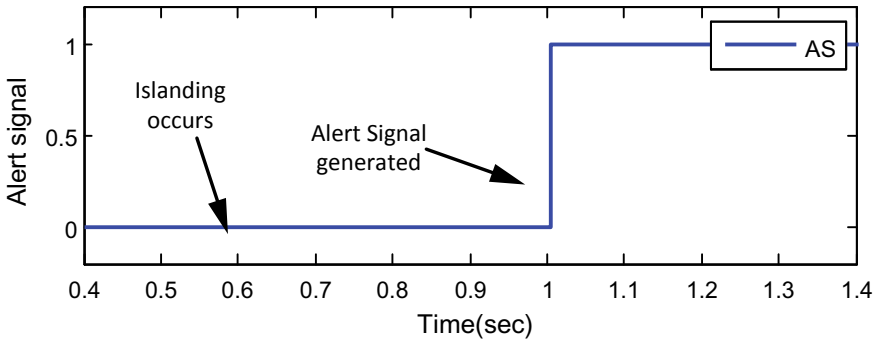

(a) Alert signal (AS)

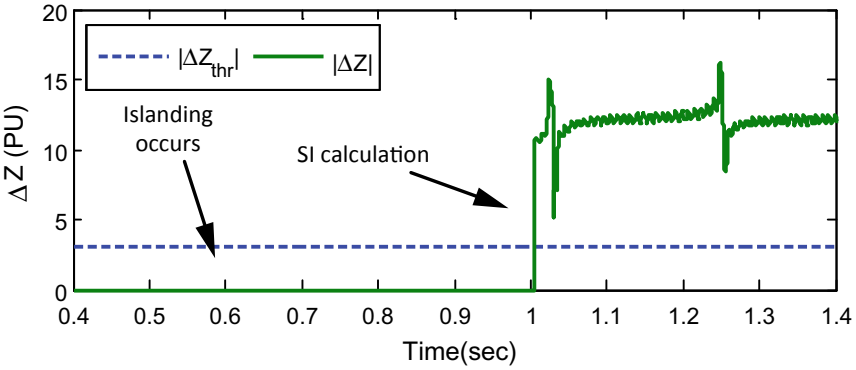

(b) Superimposed Impedance (SI)

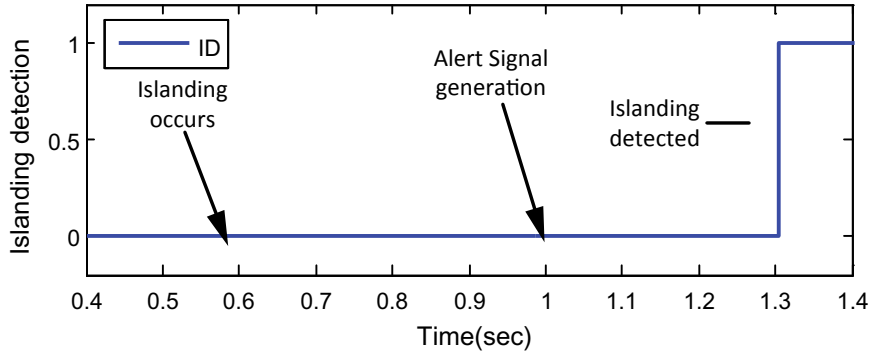

(c) Islanding detection indicator signal (ID)

Fig. 8 Different waveforms for islanding event during reactive power mismatch

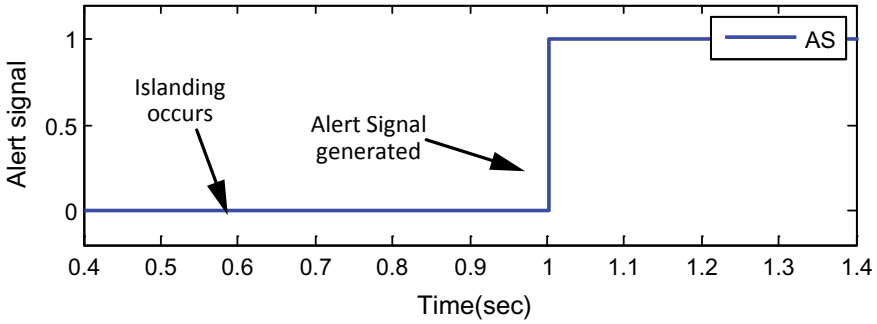

(a) Alert signal (AS)

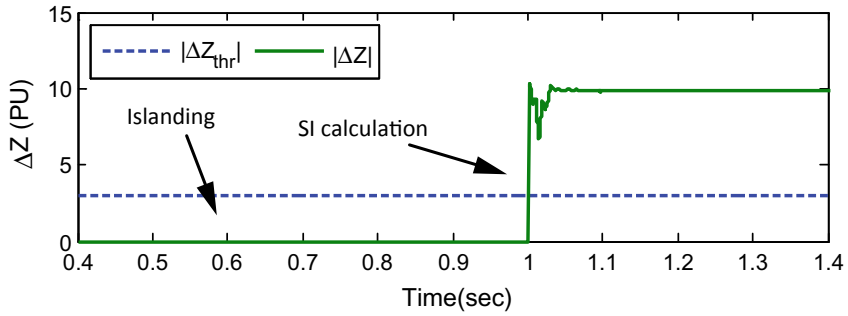

(b) Superimposed Impedance (SI)

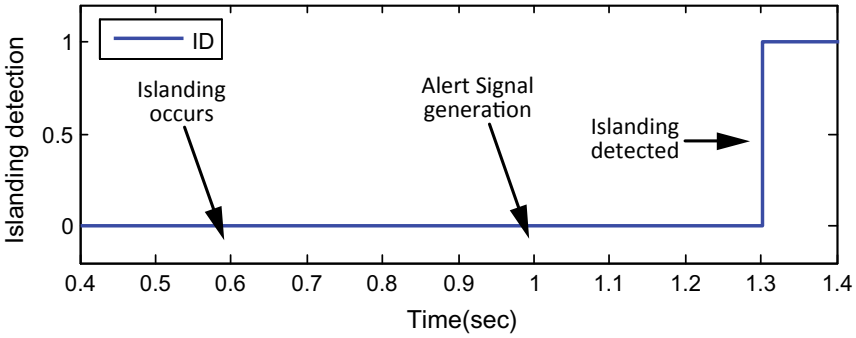

(c) Islanding detection indicator (ID)

Fig. 9 Different waveforms for islanding event during active power mismatch

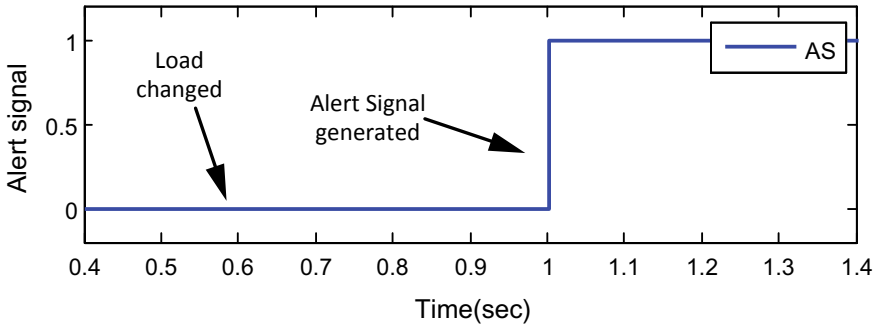

(a) Alert signal (AS)

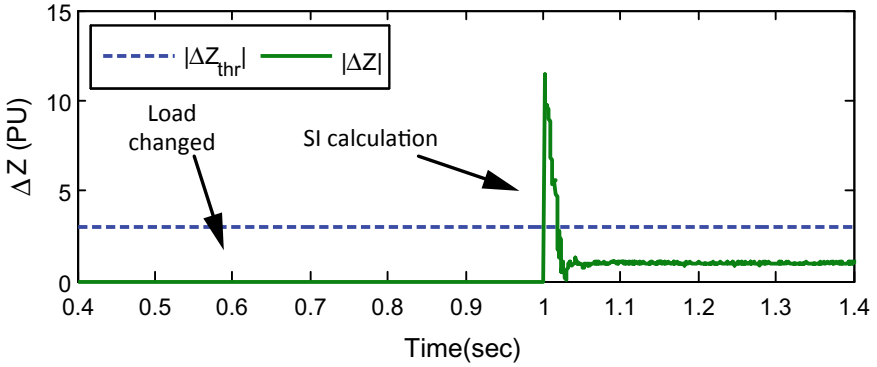

(b) Superimposed impedance (SI)

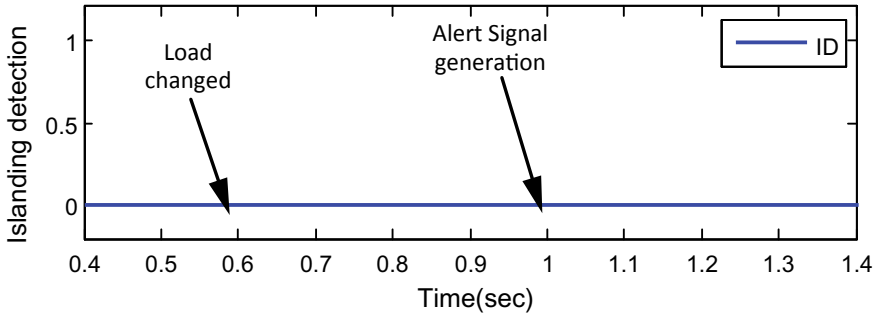

(c) Islanding detection indicator (ID)

Fig. 10 Load switching effect on the proposed scheme

the threshold but returns back to 1 PU within 0.05 s as shown in Fig. 10b. Thus, islanding event is not detected, and hence, ID remains zero as shown in Fig. 10c. Further, the PCC voltage is found more than 0.88 PU which indicates that there is no fault at PCC and algorithm returns to the measurement block (see Fig. 6) considering this as another switching event.

4.1.5 Fault at PCC

The ROCONSV, ROCOV, and ROCOF cross their respective threshold values when a 3-phase fault is created at PCC at $t = 0.6$ s, and then, AS is generated and $|\Delta Z|$ initially jumps and returns to almost zero magnitude as shown in Fig. 11. Now, as per the proposed algorithm, the PCC voltage is compared with 0.88 PU and PCC voltage is found almost zero. Therefore, this event is detected as a fault event.

4.1.6 DG Output Variation

As discussed in Sect. 1.1, solar-based DGs are the fastest growing DGs. The output of this type of DG varies as per the intensity of sunlight. Therefore, the impact of DG output variation on the proposed scheme is studied. The DG output has been changed from 1 to 0.8 PU at 0.6 s (results are not included to save space). The presented scheme has not been affected by the DG output variation since $|\Delta Z|$ was found less than $|\Delta Z_{thr}|$ and PCC voltage was more than 0.88 PU, and therefore, neither islanding event nor fault event has been detected under this condition.

4.2 Validation Using RTDS

To validate the new algorithm in a real-time environment, RTDS is used and results are obtained for all the conditions which are included in Sect. 4.1 with identical data. However, only islanding conditions are included in this section. The minimum sampling interval in RTDS is 50 μs.

4.2.1 Islanding During Nearly Perfect Power Matching Condition

When islanding event occurs at 0.2 s during nearly perfect power match, the ROCONSV crosses the threshold as depicted in Fig. 12a and alert signal is generated, see Fig. 12e. The magnitude of SI ($|dZ|$) is found greater than its threshold (i.e., $|dZ_{thr}|$) for a duration of more than 0.3 s which is shown in Fig. 12f. Thus, islanding is detected and ID changes its state from '0' to '1' as shown in Fig. 12g. Further, it can also be seen in Fig. 12c, d that PCC voltage and frequency, respectively, are almost unchanged after islanding event.

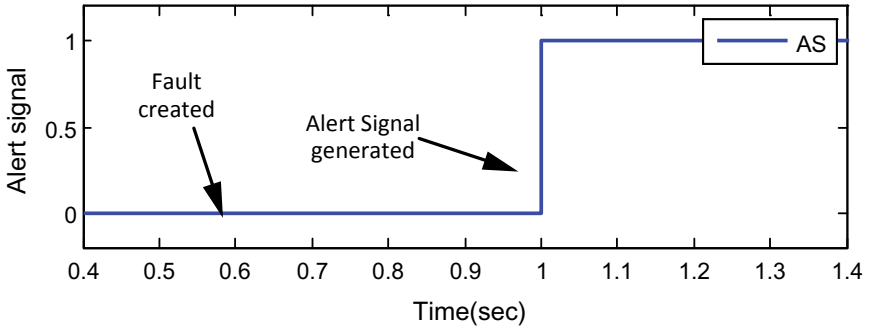

(a) Alert signal (AS)

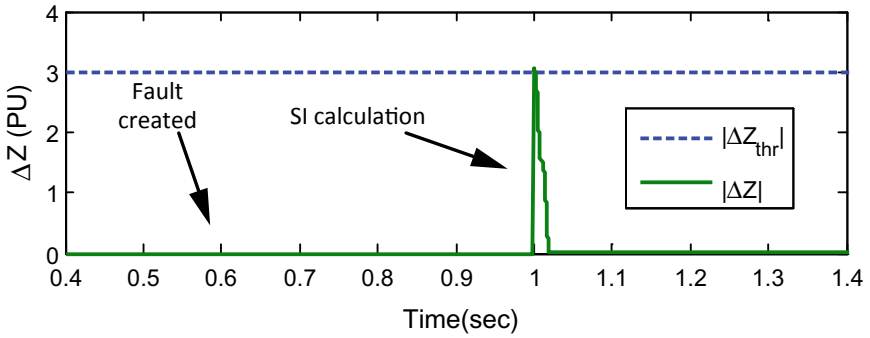

(b) Superimposed impedance (SI)

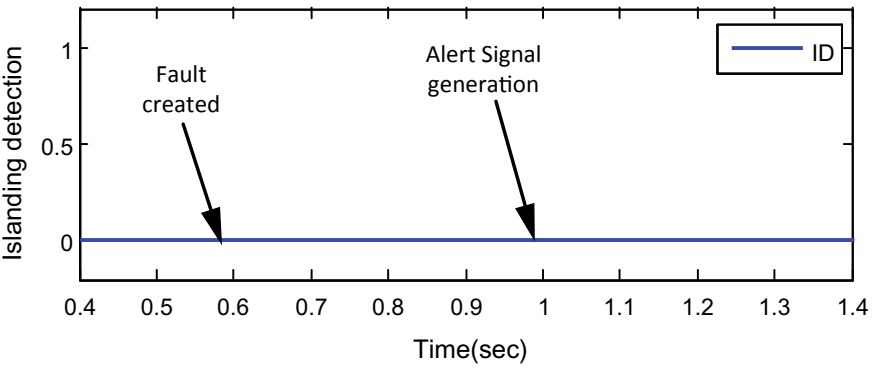

(c) Islanding detection indicator (ID)

Fig. 11 Different waveforms during fault at PCC

4.2.2 Islanding During Mismatch of Reactive Power

For the case of reactive power mismatch, islanding occurs at 0.2 s and features of Eqs. 3–5 such as ROCONSV, ROCOV, and ROCOF cross their respective thresholds. Therefore, an alert signal is generated by the algorithm and SI is obtained. The magnitude of SI is found more than its threshold value for more than 0.3 s which indicates the detection of an islanding event and the ID changes its value from 0 to 1 (see Fig. 13). Hence, RTDS result successfully validates the proposed scheme for islanding event during reactive power mismatch.

4.2.3 Islanding During Mismatch of Active Power

Similarly, for an islanding event with active power mismatch, the alert signal is generated since the features of Eqs. 3–5 cross the corresponding thresholds, and as

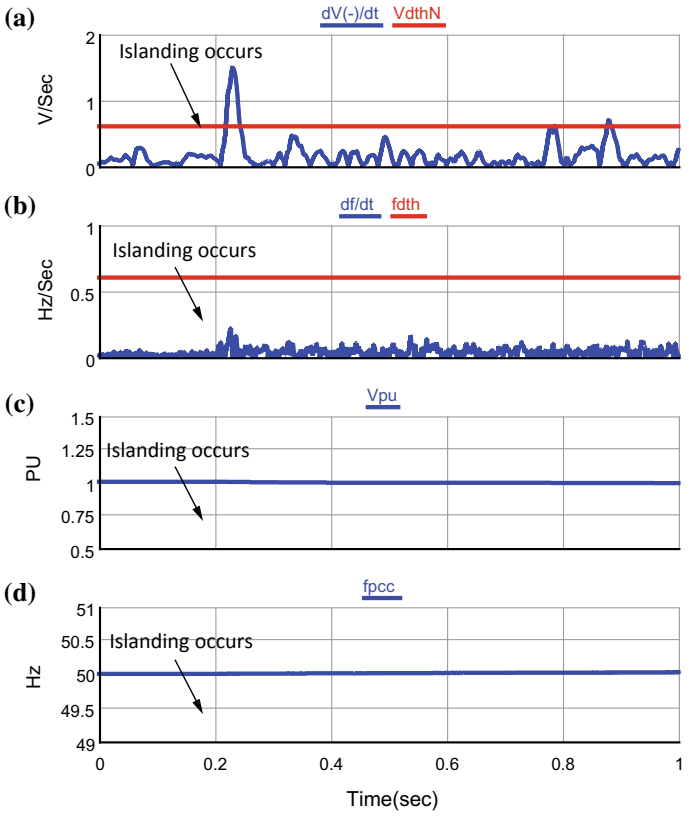

Fig. 12 RTDS results for islanding event during nearly perfect power match **a** ROCONSV, **b** ROCOF, **c** PCC voltage, **d** frequency, **e** alert signal, **f** SI (|dZ|), and **g** Islanding detection indicator

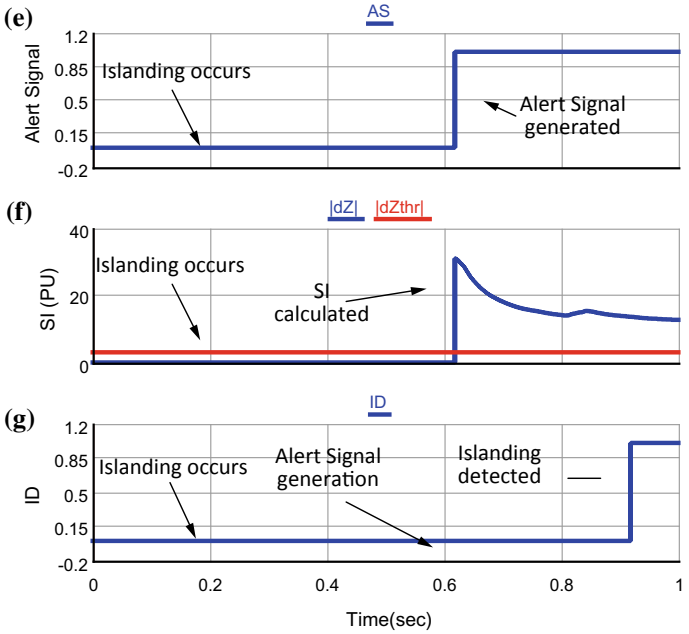

Fig. 12 (continued)

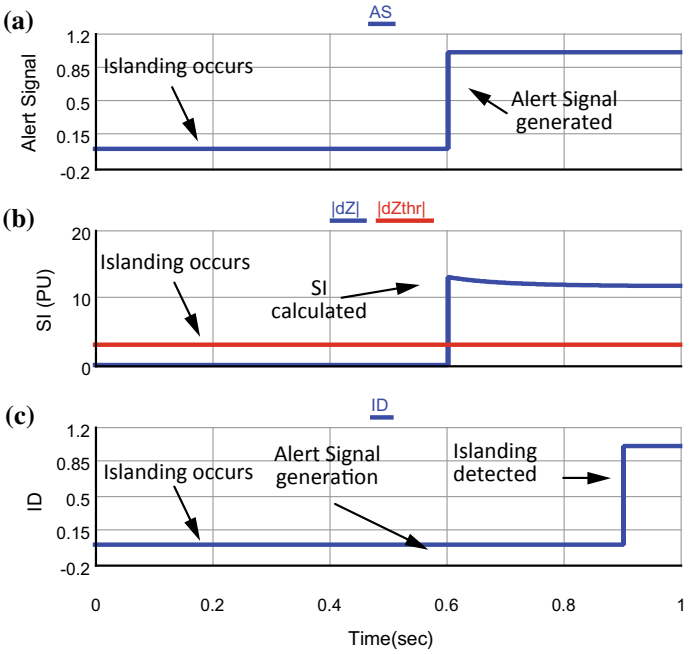

Fig. 13 Different waveforms for islanding event during reactive power mismatch

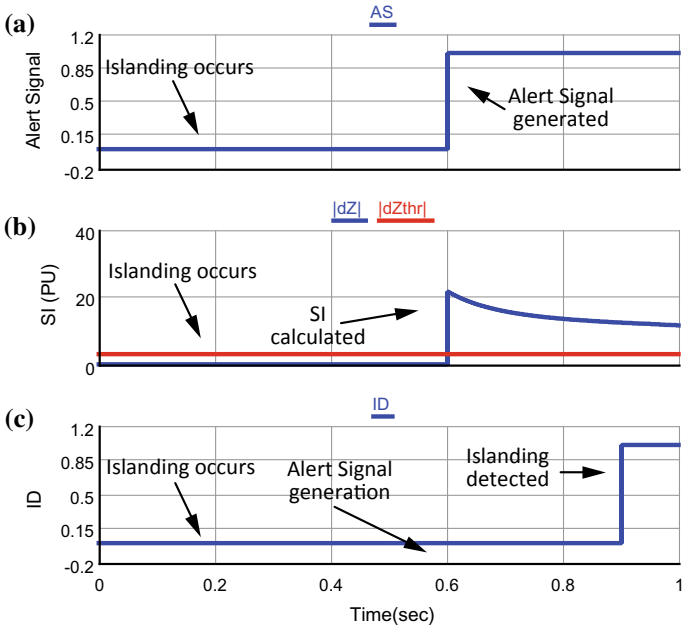

Fig. 14 Different waveforms for islanding event during active power mismatch

per the proposed algorithm, the magnitude of SI is greater than its threshold for the duration more than 0.3 s and ID becomes high as shown in Fig. 14. Hence, RTDS result successfully validates the proposed scheme for islanding event during active power mismatch.

4.3 Comparison Between Proposed and Existing Solutions

The scheme proposed in this chapter is compared with a passive islanding detection scheme reported in [26] which is based on rate-of-change-of-voltage-phase-angle (ROCOVPA). In the case of a dependent mode of operation (i.e., the converter is using PCC frequency as positive feedback), both the schemes detect islanding event as shown in Fig. 15.

In the case of independent mode, Fig. 16a illustrates very small variations in the magnitude of ROCOVPA which is not sufficient to detect an islanding event. On the contrary, in the proposed scheme, the $|\Delta Z|$ becomes high and crosses the $|\Delta Z_{\text{thr}}|$ following an islanding event as depicted in Fig. 16b. Therefore, the proposed scheme detects islanding event and scheme of [26] finds limitation as it fails to detect islanding event in the independent mode of operation of the converter.

Under fault inception at PCC, the ROCOVPA jumps to a very high value and remains more than the threshold of 10°/s for nearly 0.15 s as shown in Fig. 17a. On

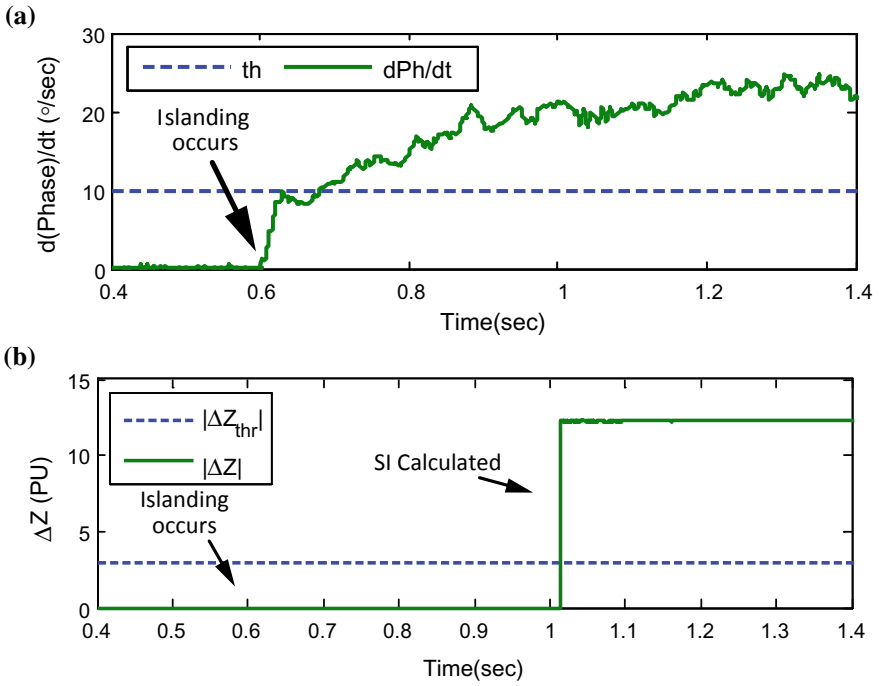

Fig. 15 Nearly perfect power match with a dependent mode of operation **a** ROCOVPA [26] and **b** magnitude of SI

the other hand, the $|\Delta Z|$ remains below the threshold value as shown in Fig. 17b. Therefore, ROCOVPA-based scheme [26] finds its limitation during fault while the proposed scheme is unaffected by a fault at PCC.

Overall, it is found that the scheme based on the ROCOVPA [26] is highly susceptible to the disturbances other than islanding and fails to detect islanding if the converter is independently controlled with nearly perfect power matching condition. While the proposed scheme works absolutely fine in all of the cases. Moreover, only a very small amount of perturbation is injected to detect islanding which hardly degrades the power quality. The proposed scheme takes more time to detect the islanding event as compared to the scheme of [26]. However, it is less than the time specified in IEEE STD 1547-2003 [2], i.e., 2 s. Furthermore, the proposed scheme is more robust than the scheme of [26].

5 Conclusion

The limitations of existing schemes are addressed in this chapter and a new SI-based event detection and classification scheme is proposed. The islanding and fault events

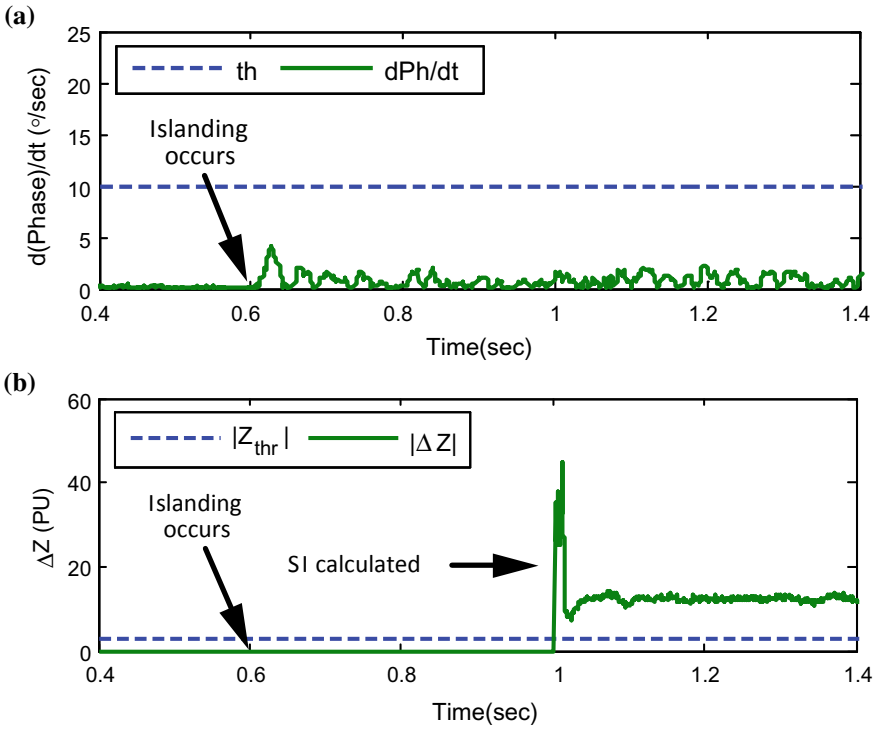

Fig. 16 Nearly perfect power match with independently controlled converter **a** ROCOVPA [26] and **b** magnitude of SI

are detected and classified based on the variations in the magnitude of SI and PCC voltage, respectively. If the SI is more than the threshold, the islanding event is detected. Else if SI and PCC voltage both are nearly zero, fault event is detected. To calculate the SI, a very small perturbation is injected that too only when a disturbance is detected at the PCC.

The proposed scheme was tested using MATLAB simulation for various events such as islanding event, fault event, load switching event, and DG output variation. The results proved the effectiveness of the proposed scheme. Further, the scheme is successfully validated using RTDS model and compared with the recent schemes [26] and [40] in respect of fault event, the effect of the operational mode of the converter, and power quality. The promising results demonstrate the superiority of the proposed method in the aspects listed below:

- The scheme has a negligibly small, nearly zero, NDZ.
- It does not degrade power quality.
- It does not confuse a fault event as an islanding event.
- It can be used to detect islanding when the inverter is independently controlled.

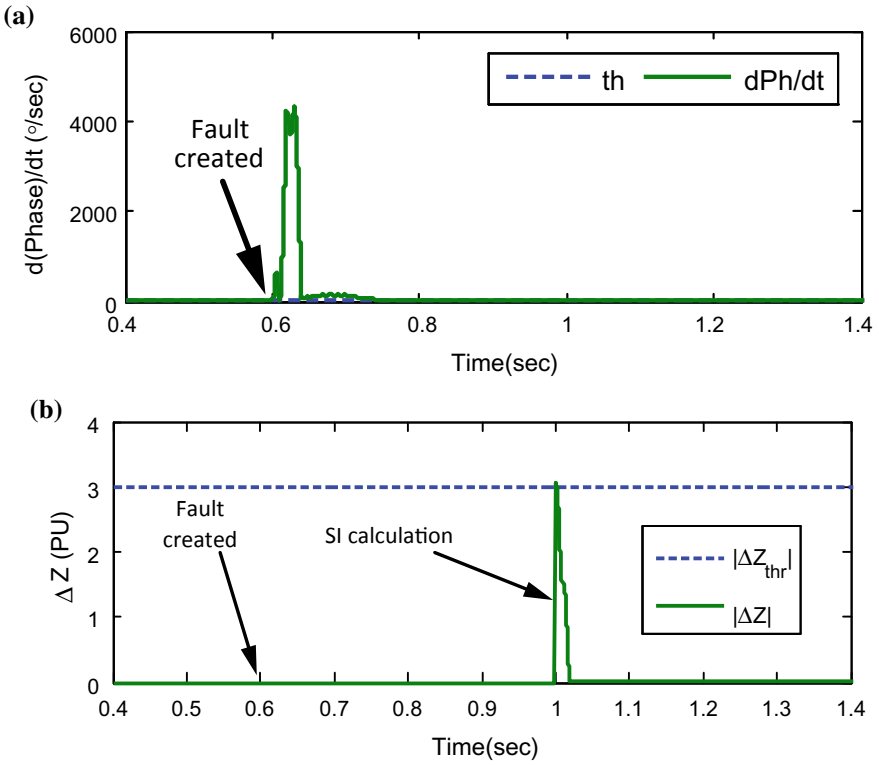

Fig. 17 Short-circuit fault at PCC **a** ROCOVPA [26] and **b** magnitude of SI

- All the aspects have been validated in off-line and real-time environments using MATLAB and RTDS, respectively.

In case of microgrid systems, the scheme is very helpful in regulating the operational mode of the converter-based DG if it is needed to change from constant power/current to constant voltage mode. It would be interesting to test this scheme for a multi-bus distribution feeder in the future.

Appendix

Data of microgrid [41]: PCC rated voltage, $V_{\text{PCC}} = 0.44$ kV, and rated frequency, $f = 50$ Hz, DG rated output power = 50 kW.

Grid data:

- Grid rated voltage = 0.44 kV

- $R_{IB} = 1$ mΩ
- $L_{IB} = 1$ mH.

Load data:

- Rated load power = 50 kW
- $R = 3.872\ \Omega$
- $L = 41.0832$ mH
- $C = 246.6244\ \mu$F.

Transformer data:

- $L_1 = L_2 = 0.04$ PU,
- Voltage = 0.1/0.44 kV (star-star),
- $R_1 = R_2 = 1 \times 10^{-4}$ PU,
- $R_m = 500$ PU,
- $L_m = 500$ PU.

References

1. Hossain MA, Pota HR, Hossain MJ, Blaabjerg F (2019) Evolution of microgrids with converter-interfaced generations: challenges and opportunities. Int J Electr Power Energy Syst 109:160–186. https://doi.org/10.1016/J.IJEPES.2019.01.038
2. IEEE Standard for Interconnecting Distributed Resources with Electric Power Systems (2003)
3. Katiraei F, Iravani MR, Lehn PW (2005) Micro-grid autonomous operation during and subsequent to islanding process. IEEE Trans Power Deliv 20:248–257. https://doi.org/10.1109/TPWRD.2004.835051
4. Lasseter RH, Paigi P (2004) Microgrid: a conceptual solution. In: 2004 IEEE 35th annual power electronics specialists conference (IEEE Cat. No.04CH37551). IEEE, pp 4285–4290
5. Hirodontis S, Li H (2009) An adaptive load shedding method for intentional islanding. In: 2009 international conference on clean electrical power. IEEE, pp 300–303
6. Mahat P, Bak-Jensen B (2008) Review of islanding detection methods for distributed generation. In: 2008 third international conference on electric utility deregulation and restructuring and power technologies. IEEE, pp 2743–2748
7. Chandorkar MC, Divan DM, Adapa R (1993) Control of parallel connected inverters in standalone AC supply systems. IEEE Trans Ind Appl 29:136–143. https://doi.org/10.1109/28.195899
8. Iravani MR (2008) A control strategy for a distributed generation unit in grid-connected and autonomous modes of operation. IEEE Trans Power Deliv 23:850–859. https://doi.org/10.1109/TPWRD.2007.915950
9. Najy WKA, Zeineldin HH, Alaboudy AHK, Woon WL (2011) A bayesian passive islanding detection method for inverter-based distributed generation using ESPRIT. IEEE Trans Power Deliv 26:2687–2696. https://doi.org/10.1109/TPWRD.2011.2159403
10. Samantaray SR, El AK, Joos G, Kamwa I (2010) A fuzzy rule-based approach for islanding detection in distributed generation. IEEE Trans Power Deliv 25:1427–1433. https://doi.org/10.1109/TPWRD.2010.2042625
11. Shooshtari BA, Golshan MEH, Sadeghkhani I (2014) A combined method to efficiently adjust frequency-based anti-islanding relays of synchronous distributed generation. Int Trans Electr Energy Syst 25:3042–3059. https://doi.org/10.1002/etep.2021

12. Pai Fu-Sheng, Huang Shyh-Jier, Pai FS, Huang SJ (2001) A detection algorithm for islanding-prevention of dispersed consumer-owned storage and generating units. IEEE Trans Energy Convers 16:346–351. https://doi.org/10.1109/60.969474
13. Padhee M, Dash PK, Krishnanand KR, Rout PK (2012) A fast gauss-newton algorithm for islanding detection in distributed generation. IEEE Trans Smart Grid 3:1181–1191. https://doi.org/10.1109/TSG.2012.2199140
14. Liu F, Kang Y, Zhang Y et al (2010) Improved SMS islanding detection method for grid-connected converters. IET Renew Power Gener 4:36. https://doi.org/10.1049/iet-rpg.2009.0019
15. Karimi H, Yazdani A, Iravani R (2008) Negative-sequence current injection for fast islanding detection of a distributed resource unit. IEEE Trans Power Electron 23:298–307. https://doi.org/10.1109/TPEL.2007.911774
16. Sul S-KK (2012) Anti-islanding detection method using negative sequence voltage. In: Proceedings of the 7th international power electronics and motion control conference. IEEE, pp 604–608
17. Hanif M, Basu M, Gaughan K (2011) A discussion of anti-islanding protection schemes incorporated in a inverter based DG. In: 2011 10th international conference on environment and electrical engineering. IEEE, pp 1–5
18. Hernandez-Gonzalez G, Iravani R (2006) Current Injection for active islanding detection of electronically-interfaced distributed resources. IEEE Trans Power Deliv 21:1698–1705. https://doi.org/10.1109/TPWRD.2006.876980
19. Chiang W-J, Jou H-L, Wu J-C (2012) Active islanding detection method for inverter-based distribution generation power system. Int J Electr Power Energy Syst 42:158–166. https://doi.org/10.1016/j.ijepes.2012.03.038
20. Jou HL, Chiang WJ, Wu JC (2007) Virtual inductor-based islanding detection method for grid-connected power inverter of distributed power generation system. IET Renew Power Gener 1:175. https://doi.org/10.1049/iet-rpg:20070018
21. Zeineldin HH, Conti S (2011) Sandia frequency shift parameter selection for multi-inverter systems to eliminate non-detection zone. IET Renew Power Gener 5:175–183. https://doi.org/10.1049/iet-rpg.2010.0096
22. Reigosa D, Briz F, Blanco C et al (2012) Active islanding detection for multiple parallel-connected inverter-based distributed generators using high frequency signal injection. In: 2012 IEEE energy conversion congress and exposition (ECCE). IEEE, pp 2719–2726
23. Stevens J, Bonn R, Ginn J et al (2000) Development and testing of an approach to anti-islanding in utility-interconnected photovoltaic systems. Sandia National Laboratories
24. Velasco D, Trujillo C, Garcera G, Figueres E (2011) An active anti-islanding method based on phase-PLL perturbation. IEEE Trans Power Electron 26:1056–1066. https://doi.org/10.1109/TPEL.2010.2089643
25. Pourbabak H, Kazemi A (2014) A new technique for islanding detection using voltage phase angle of inverter-based DGs. Int J Electr Power Energy Syst 57:198–205. https://doi.org/10.1016/j.ijepes.2013.12.008
26. Ghanbari T, Samet H, Hashemi F (2015) Islanding detection method for inverter-based distributed generation with negligible non-detection zone using energy of rate of change of voltage phase angle. IET Gener Transm Distrib 9:2337–2350. https://doi.org/10.1049/iet-gtd.2015.0638
27. Menon V, Nehrir MH (2007) A hybrid islanding detection technique using voltage unbalance and frequency set point. IEEE Trans Power Syst 22:442–448. https://doi.org/10.1109/TPWRS.2006.887892
28. Mahat P, Bak-Jensen B (2009) A hybrid islanding detection technique using average rate of voltage change and real power shift. IEEE Trans Power Deliv 24:764–771. https://doi.org/10.1109/TPWRD.2009.2013376
29. Freitas W, Xu W, Affonso CM, Huang Z (2005) Comparative analysis between ROCOF and vector surge relays for distributed generation applications. IEEE Trans Power Deliv 20:1315–1324. https://doi.org/10.1109/TPWRD.2004.834869

30. Sadeh J, Kamyab E (2013) Islanding detection method for photovoltaic distributed generation based on voltage drifting. IET Gener Transm Distrib 7:584–592. https://doi.org/10.1049/iet-gtd.2012.0507
31. Jang SI, Kim KH (2004) An islanding detection method for distributed generations using voltage unbalance and total harmonic distortion of current. IEEE Trans Power Deliv 19:745–752. https://doi.org/10.1109/TPWRD.2003.822964
32. Karegar HK, Sobhani B (2012) Wavelet transform method for islanding detection of wind turbines. Renew Energy 38:94–106. https://doi.org/10.1016/j.renene.2011.07.002
33. Ray PK, Kishor N, Mohanty SR et al (2012) Islanding and power quality disturbance detection in grid-connected hybrid power system using wavelet and s-transform. IEEE Trans Smart Grid 3:1082–1094. https://doi.org/10.1109/TSG.2012.2197642
34. ElNozahy MS, El-Saadany EF, Salama MMA (2011) A robust wavelet-ANN based technique for islanding detection. In: 2011 IEEE power and energy society general meeting. IEEE, pp 1–8
35. Balaguer IJ, Lei Q, Yang S et al (2011) Control for grid-connected and intentional islanding operations of distributed power generation. IEEE Trans Ind Electron 58:147–157. https://doi.org/10.1109/TIE.2010.2049709
36. Dash PK, Padhee M, Panigrahi TK (2012) A hybrid time–frequency approach based fuzzy logic system for power island detection in grid connected distributed generation. Int J Electr Power Energy Syst 42:453–464. https://doi.org/10.1016/j.ijepes.2012.04.003
37. Geng H, Xu D, Wu B, Yang G (2011) Active islanding detection for inverter-based distributed generation systems with power control interface. IEEE Trans Energy Convers 26:1063–1072. https://doi.org/10.1109/TEC.2011.2159720
38. Reigosa D, Briz F, Blanco C et al (2014) Active islanding detection for multiple parallel-connected inverter-based distributed generators using high-frequency signal injection. IEEE Trans Power Electron 29:1192–1199. https://doi.org/10.1109/TPEL.2013.2263845
39. Hou C-CC, Chen Y-CC (2013) Active anti-islanding detection based on pulse current injection for distributed generation systems. IET Power Electron 6:1658–1667. https://doi.org/10.1049/iet-pel.2012.0542
40. Yu BG, Matsui M, Yu GJ (2011) A correlation-based islanding-detection method using current-magnitude disturbance for PV system. IEEE Trans Ind Electron 58:2935–2943. https://doi.org/10.1109/TIE.2010.2080651
41. Skocil T, Gomis-Bellmunt O, Montesinos-Miracle D et al (2009) Passive and active methods of islanding for PV systems. In: 13th European conference on power electronics and applications, 2009, EPE '09. IEEE, pp 1–10

Intelligent Relay Coordination Method for Microgrid

Papia Ray

Abstract This chapter basically deals with the protection coordination of a typical microgrid with distributed energy sources. As we are aware that fault current changes its direction when microgrid switches from non-islanded condition to islanded condition, so the main challenge before the power engineer's is to have a proper protection coordination in dual configuration of microgrid (islanded and non-islanded condition). In this chapter, a smart grid-based fault current limiter (FCL) has been proposed which suppresses the fault currents to the level such that the proper protection coordination is possible. One of the unique characteristics of the FCL is that it is 'invisible' during normal condition but becomes active during faulted or islanding condition. The important component in FCL is the reactance which has a major contribution in reducing the fault current of the microgrid. So in this chapter, investigation with reactance FCLs is discussed for proper coordination of directional overcurrent relay (DOCR) settings during symmetrical three-phase faults. Here, the microgrid model with distributed generation (DG) is considered for the investigation. The DG taken for the study is the conventional synchronous generator connected to medium voltage network. The proposed protection scheme is validated on radial distribution system (the benchmark Canadian distribution system model) of 9-bus which is adequately connected to DGs within the microgrid. Further in the present work, three configurations of the microgrid are considered, i.e. grid connected, islanded and dual. From the simulation results, it is concluded that the optimized FCL is able to co-ordinate properly the protective devices for different configurations of microgrid.

Keywords Fault current limiter · Overcurrent relay · Distributed generation · Differential evolution · Teaching learning-based optimization · Microgrid

P. Ray (✉)
Department of Electrical Engineering, Veer Surendra Sai University of Technology, Burla, Sambalpur, Odisha, India
e-mail: papia_ray@yahoo.co.in

P. Ray and M. Biswal (eds.), *Microgrid: Operation, Control, Monitoring and Protection*, Lecture Notes in Electrical Engineering 625,
https://doi.org/10.1007/978-981-15-1781-5_8

Nomenclature

CTI	Coordination Time interval
DE	Differential Evolution
DG	Distributed Generation
DOCR	Directional Overcurrent Relay
FCL	Fault Current Limiter
PDS	Power Distribution System
PS	Plug Setting
pu	Per unit
s	Seconds
TDS	Time Dial Setting
TLBO	Teaching Learning-Based Optimization

1 Introduction

Electric power system is a complex system consisting of non-linear and interconnected devices. Continuous availability of the electric power system to the end user is possible by proper planning, design, installation, maintenance and function of each of the equipment in the grid. This grid is constantly subjected to failures like faults occurring at the generator, transmission or load end, load fluctuations, failure of protective devices, etc. Selection and adequate arrangement of protective devices to limit the effect of short circuit current for a small portion of power system are defined as protection coordination. Besides the disturbances faced by the grid, it uses to remain in a quasi-stable state due to quick response (in milliseconds) and proper coordination of protective devices (specially relays) [1]. So, proper coordination of relays plays an important role in maintaining stability of the power system. Further, quick and accurate backup protection is also a need in power system if the main protective system fails to operate. This section mainly focuses on the general overview of protection coordination, its need and the importance of FCL into it.

1.1 General Overview

Protection coordination is a need for power system where many protective devices are placed in series between the source and the fault [2]. Appropriate coordination means the protective device closest to the fault should respond first as compared to others. Coordination means to limit the service interrupted duration and to selectively isolate the fault. The technical meaning of relay coordination is to activate downstream devices like circuit breaker, fuse, etc., before upstream devices in order to prevent the system from fault or any other disturbance. Backup protection comes into picture only

if the primary protection fails to respond. Overcurrent relay plays a very important role in selective coordination and is set based on comparison of relay operating time with the fault current level. Improper coordination leads to maloperation of relays and other protective devices which further cause isolation of non-faulty parts of the power network, cascading trips and finally black out or total collapse of the system. Nowadays, power system networks consist of many elements and setting of protective devices are not possible traditionally. Earlier radial type of distribution systems with simple overcurrent relay settings was mostly used with the set value of the major downstream relay's plug setting (with the help of power engineer). Further, the relay's TMS settings are then set based on the observed values of the fault current by the relay and according to primary and backup relay, the value of upstream relays is placed. This was possible because of fault currents unidirectional characteristics and simple relay setting calculation. However, due to the advent of growing technology and the application of distributed generation in the distribution system, many constraints are imposed in the relay setting calculations making the distribution system meshed and complex.

Microgrid is the combination of small-scale micro sources and loads which operates independently during islanding and other conditions and provides power as a single entity. Importance of microgrid in power sector is that it meets the energy crisis, reduces losses in transmission network, provides reliable power supply to critical loads and separates itself from the grid seamlessly without disturbing the load within the network. The major problems faced by microgrid are control, interface and protection coordination of micro sources, stability, power flow control, load sharing during islanding condition, etc. There is always a need of smooth transition from islanding to the grid-connected state and overcurrent relay with proper coordination fulfills this requirement. During fault or islanding condition, the current flows bidirectional in the microgrid and becomes many times the rated current as a result of which the protection scheme gets disturbed. So in order to gain same protection scheme for both islanded and grid-connected mode of the microgrid, proper coordination is required. One of the advantages of microgrid is that it encourages penetration of renewable energy for better impact with environment and to reduce emission of carbon dioxide. So, for this purpose distributed generation (DG) is introduced in the microgrid which has the advantage of improving the power quality, better voltage support, reduction in losses and improved reliability of power flow for the supply grid. In this chapter, DG of conventional type has been introduced into the microgrid network for better power reliability.

Further, three-phase short circuit faults play a major role in fault analysis and protection coordination issue in microgrid. As we are aware that three-phase fault is the worst type of fault affecting the power network, so they are taken as a base case for protection coordination setting. Further from the investigation with three-phase fault current, the size of protective devices having the capability to withstand worst fault condition is determined. Minimum amount of short circuit current was used conventionally by researchers in the past for determining relay settings. In this chapter, sum of the operating times of the primary and backup relays are considered during faulted condition at various sections of the distribution network with the help

of optimization techniques. Also, the operating times are determined by mapping of three-phase short circuit fault current for each relay connected to the distribution network. Many optimization tools are available nowadays for solving problems related to constraints in power systems. Some of the optimization techniques are weighting objective method, stochastic, goal programming schemes, linear programming techniques, etc., with computational intelligence-based heuristic methods. The traditional optimization techniques have the disadvantage of falling into local minima, whereas global solution is provided by heuristic methods. So, to maintain stability and ensure security of the grid, proper coordination of overcurrent relay is required by developing real-time algorithms based on heuristic optimization techniques which can detect the fault current instantaneously and respond with adequate speed.

In this chapter, global optimization techniques like TLBO and DE have been implemented to optimize the DOCR settings and size of reactance FCL for proper relay coordination in order to reduce incidence of sympathetic tripping and avoid blackout or cascading during the occurrence of fault or any other disturbance. Further, the optimized values of relay and FCL have been implemented here for IEEE 9-bus radial distribution system.

1.2 Fault Current Limiter (FCL)

In normal operation, the power transmission and distribution network are designed in such a way that it possess low impedance and large short circuit capacity in order to have low voltage drop, good power quality, improved stability and low perturbation in the system, whereas in faulted condition, the situation reverses. So, to maintain and support properly the normal and faulted condition in power network, fault current limiter (FCL) is implemented [3]. Proper solution is given by FCL to reduce large short circuit current flowing in the grid. Requirement of FCL occurs due to rise in the level of short circuit current in the grid which happens because of renewable energy or DG penetration [4]. Advantages of FCL are reduction in utility and maintenance cost, minimization of black out and power disruption, reduction of voltage dip during faulted condition, improvement in stability, better safety and power delivery. In research, two types of FCL are in use [5]. One is high temperature conducting (HTS) or SFCL and the other one is solid-state FCL. Further SFCL is subcategorized into two types: resistive and inductive. The configuration of resistive type with the grid has series-connected HTS element and shunt resistance. Resistive-type SFCL is compact and has very quick limiting action. Inductive-type SFCL behaves like a current transformer by linking itself magnetically to the network. It has the capability to reduce short circuit current level during faulted condition in a microgrid with DG penetration. This chapter deals with optimized HTS-type FCL having the characteristics of low impedance in normal condition, adequate current limitation and quick restoration after the faulted condition.

2 Literature Review

Investigation has been carried out with genetic algorithm (GA) in [6] to obtain the capacity of FCL and relay settings so that protection coordination is possible for both grid and islanded mode during the occurrence of fault in the transmission line. In [7] a hybrid protection system based on FCL and microprocessor-based overcurrent relay is presented instead of relay coordination and impact of DG on distribution system is also discussed. Investigation has also been carried out in [7] with superconducting type FCL to minimize the operating time of overcurrent relays by obtaining time dial setting (TDS) and plug setting (PS). Research has been carried out in [8] to restore the original relay coordination and limit the fault current in looped power distribution system (PDS) by applying FCL. It was concluded from the simulation results in [8] that restoration of relay coordination is possible in PDS with DG during fault without disturbing the earlier relay setting. Optimal number and placement of FCL with smallest FCL parameters have been investigated in [9], in order to resist the circuit breaker short circuit current. Relay coordination based on TLBO is discussed in [10] for 3-, 4- and 6-bus system with weighing factor and CTI constraints. Also, differential evolutionary algorithm with information exchange scheme is presented in [10] which implements sub-populations instead of single one to raise the search power of the algorithm. An investigation for optimal coordination of directional overcurrent relays has been carried out in [11] with genetic algorithm for a 7-bus ring distribution system. In [12], impact of conventional synchronous generator (CSG) and inverter-based DGs on protection coordination has been discussed and it was concluded from [12] that CSG has more impact than inverter-based DG. Reference [13] proposes FCL to eliminate the impact of short circuit current in a microgrid. Investigation has been carried out in [14] to solve the problem of short circuit level difference in both grid and islanded mode of the microgrid using FCL. Further in [14], particle swarm optimization (PSO) technique and Cuckoo search algorithm have been implemented to obtain fault current limiter impedance and optimal relay coordination. Improvement of protection coordination using unidirectional FCL has been discussed in [15]. Also, scheme based on unidirectional FCL has been formulated in [15] to eliminate the cause due to which the existing CTI of overcurrent relay gets disturbed. An investigation has been carried out in [16] for optimal utilization of FCL to obtain proper coordinated operation of overcurrent relay in the presence of DG in a microgrid. Further, multi-objective PSO has been applied in [16] to obtain optimized location and size of FCL in DG based meshed and radial power system. A differential protection scheme based on non-linear signal transformation for a microgrid is discussed in [17]. Also, in [17], feature extraction is done by the non-linear signal transformation scheme and then fed to extreme learning machine for prediction of fault for primary and backup protection. Efficient schemes for protection coordination with overcurrent relays, directional overcurrent relays (DOCR) and differential relays of a microgrid are presented in [18]. Protection of AC microgrids with different characteristic curve for islanded and grid-connected mode is reported in [19]. In [19], three variables, i.e. TMS, PS and curve setting

which are associated with time scaling, characteristic curve selection and pick up value of DOCR have been applied to obtain correct operating times. Further, GA has been applied in [19] to solve the non-linear programming problem. A novel optimization method called hyper-sphere search algorithm has been presented in [20] to optimize the TMS and characteristics of overcurrent relay for adequate protection coordination of microgrid. Solid-state transformer with embedded phasor measurement unit has been used in [21] to improve the protection coordination of overcurrent relay in a microgrid. Protection coordination of microgrid using a novel approach based on time–time (TT) transform is presented in [22]. Further an index based on TT-transform is formulated in [22] and compared with a threshold value in order to detect fault for both grid-connected and islanded mode of operation of microgrid. Reference [23] presents superimposed reactive energy (SRE)-based protection scheme for microgrid which protects the radial and looped microgrids from solid and high impedance faults. Further, Hilbert transform is used in [23] to obtain SRE and the sequence components of SRE with a threshold is implemented in [23] to detect the fault. An adaptive protection scheme for microgrid is discussed in [24] which featured bidirectional communication. Differential protection of microgrid is presented in [25] which uses fuzzy and Hilbert schemes to evaluate the difference in power of sending and receiving end of the network in order to differentiate between normal and faulted condition. In [26], distance-based protection of microgrid with mid-voltage level is reported where impedance of the network is measured to detect the fault. Further in [26], simulation results showed that the variations in fault current observed by forward relays are large in magnitude as compared to observations made by backward relays. Also, it was depicted in [26] that there is no variation of fault current except with the presence of renewable energy. Reference [27] focuses on voltage-based microgrid protection which uses low voltage uni-ground configuration for microgrid. Six protection zones with uni-grounding feature were assigned in [27] for AC microgrid and further protection schemes were developed for each zone in order to explore by the operator which of the main and backup scheme gives optimal value.

It was concluded from literature review that special attention needs to be given for protection coordination of overcurrent relays when microgrid changes from grid-connected mode to islanding mode. During this state of microgrid, difference in current level happens and bidirectional current starts flowing as a result of which the CTI of overcurrent relay gets disturbed which finally leads to occurrence of fault. Also, by the presence of DG in the microgrid, the protection coordination of relays gets worsen. Earlier researchers have proposed unidirectional FCL to overcome the protection coordination problem of overcurrent relays in microgrid. Also, a large number of optimization tools like GA, PSO, Hilbert transform, etc., were used in the past to monitor the status of protection coordination of overcurrent relays. Also, it was observed from the literature survey that ample scope still remains to improve the strategy for adequate protection coordination of overcurrent relays in microgrid. It was also studied from the literature survey that many protection schemes are available

for microgrid like differential protection, distance protection, voltage-based protection, adaptive protection, etc., which mainly depends on microgrid configuration and the constraints.

2.1 Issues or Challenges

The greatest key challenge before the power engineers is to maintain proper protection coordination of overcurrent relays when the microgrid operates in both grid and islanded mode. When the microgrid operates in islanded mode with inverter-based generation sources, then the fault currents become less than the rated current [28] as a result of which conventional protection scheme fails to detect the fault with low value of fault current. Further due to penetration of DG in the microgrid, the difference of fault current levels becomes small which leads to maloperation of relays. The other challenges due to DG effect in a microgrid is rise of voltage which limits its capacity, power quality issues like variation of transient voltage and harmonic voltage distortion, islanding problem, issues related to network stability and security. Also, presence of DG in the microgrid leads to the variation in the magnitude and direction of short circuit current during normal and faulted condition which finally leads to loss of coordination of protective devices. In order to overcome this situation, coordination of protective devices is required to be redone to make sure that maloperation of relays does not occur and proper relays trip during faulted condition. However, this job of re-coordination of protective relays is quite tedious and time consuming and makes the task challenging for the grid engineers. Further reconfiguration of microgrid leads to overcurrent protection issues [29]. When a fault occurs in feeder or grid or bus, then short circuit current flows in the microgrid which changes its amplitude and direction frequently and leads to severe protection issues.

Another issue in a microgrid is when it relates to DG unit, then relay experiences under reach problem and does not trip when fault occurs [29]. Sympathetic tripping is also a severe issue in microgrid [29]. When sympathetic tripping occurs, the healthy feeders get disconnected and it happens when DG is connected to the microgrid and reverse power flow takes place [29]. Unsuccessful fault clearance and unintentional islanding are the other major issues in a microgrid when DG is interfaced with it [29].

2.2 Existing Solutions

Many existing solutions for issues in microgrid have been proposed by researchers in the past. Some of the solutions are inclusion of large capacity fault current inverters and energy storage devices in the microgrid network, proper ground connection of the microgrid system with adequate number of DG units, application of adaptive protection scheme, introduction of differential protection technique based on

symmetrical components, distance protection, coordinated schemes of protection, implementation of voltage-based protection and overcurrent protection scheme [29].

For different types of fault detection in microgrid, protection schemes were available in the past. For LLG fault detection, harmonic content-based protection scheme was available in which total harmonic distortion and frequency of the converter voltages were analyzed [29]. Protection scheme based on voltage measurement was used for analyzing LLL, LL and LG faults. In this scheme, Abc-dq0 transformation of DGs output voltages was done and communication between the relays was analyzed to detect the fault. For LG and LL fault detection, symmetrical fault and residual current-based protection scheme were available in the past. Adaptive protection schemes were used in the past for microgrid protection where it uses IEDs and high-speed communication link to accomplish its task.

3 Proposed Method

Overcurrent relay plays an important role to secure security of the power grid by quickly and accurately detecting the fault current keeping in view that the backup relays operate after the primary ones. TLBO and DE are the emerging optimization tools which are used in this work to accomplish the task. Here, in this chapter, investigation on fault detection has been carried out with radial and meshed type of microgrid. Further FCL in combination with TLBO or DE has been implemented in the proposed method to detect the fault in the microgrid network. In the present work, series-connected reactance FCL has been used to suppress the short circuit current due to the occurrence of fault in such a manner that the DOCR settings in microgrid make optimal protection for both modes (grid and islanded). A benchmark test case has been investigated to validate the proposed scheme which is IEEE 9-bus Canadian radial distribution network. The distribution network is penetrated by adequate number of DG units. Reactance FCL used in the present work has the exclusive feature that they appear only during faulted condition otherwise remains inactive. The reactance of the FCL is the main component which helps to lower the level of fault current flowing in the microgrid. Optimal setting of overcurrent relays is also investigated in this chapter to remove sympathetic tripping during fault condition. The detailed description of proposed FCL in this chapter is discussed in Sect. 3.1.

3.1 FCL for Microgrid Coordination

Nowadays, relay coordination problem deals with fixed network configuration for almost all research works. However, due to the existence of large operating conditions and contingencies, multiple topologies are created, and the protective system operates without the selectivity feature. So, implementation of all coordination constraints

(which are a set of non-linear inequality constraints for every network configuration) for solving the coordination problem is required. Generally, when fault occurs, primary relay becomes active and trips the faulted section. If the primary relay fails in its operation, then only backup relay comes into picture but sometimes it is observed that a small number of relays which are neither primary nor backup starts operating during faulted condition. Due to such unwanted trips, healthy operating circuits get isolated with faulted ones as a result of which the power system reliability reduces. In order to avoid such situation, optimized FCL has been used here to solve microgrid coordination problem.

Overcurrent relay's (OCR) operating time depends on fault current 'I_{sc}' and its TMS and I_p (Least value of current above which the operation of OCR takes place) these settings are independent of each other. Further directional parameter setting is needed in OCR to achieve selectivity in multiple transient configurations. Operating time 't' of inverse characteristic relay is given in Eq. (1).

$$t = \text{TDS}\frac{K_1}{\left(\frac{I_{sc}}{I_p}\right)^{K_2} - 1} \tag{1}$$

where TDS denotes time differential setting, K_1 and K_2 are constants which change for various characteristics of OCRs. For OCR having minimum time inverse characteristics, K_1 and K_2 values are 0.14 and 0.02, respectively. In this chapter, the objective function is minimization of operating time which is evaluated for each primary and backup relay during faulted condition for both modes of microgrid (grid-connected and islanded) and to explore optimal setting of FCL which is shown below in Eq. (2).

$$\text{Minimize } T = \sum_{L=1}^{l}\sum_{i=1}^{N}\sum_{j=1}^{R}\left(t^{p} + \sum_{k=1}^{K} t^{b_k}\right) \tag{2}$$

In Eq. (2), 'L' indicates two modes (Grid and Islanded), 'N' denotes the number of faulted nodes, 'R' indicates the total number of relays (primary and backup) active during faulted condition, 't^{p}' is primary relay operating time and 't^{b}' is backup relay operating time. The required constraints within which Eq. (2) will be satisfied are given in Eqs. (3) and (4).

$$I_{p_i-\min} \leq I_{p_i} \leq I_{p_i-\max}, \quad \forall i \tag{3}$$

$$\text{TDS}_{i-\min} \leq \text{TDS}_i \leq \text{TDS}_{i-\max}, \quad \forall i \tag{4}$$

Here, inductive FCL size to be placed at the grid end is defined by Eq. (5) below which is further taken for exploring the optimized value.

$$0 \leq X_{\text{FCL}} \leq X_{\text{FCL}\max} \tag{5}$$

For proper protection coordination of relays, it is very much required that backup relays will be active only when primary relay fails to operate. In order to ensure this condition, a minimum time interval (CTI) is assigned between the operating time of primary and backup relay as mentioned in Eq. (6). In this chapter, CTI is assumed to be 0.2 s.

$$t_{L_{i,j}}^{\mathrm{b}_k} - t_{L_{i,j}}^{\mathrm{p}} \geq \mathrm{CTI} \quad \forall L, i\{j,k\} \tag{6}$$

In this chapter due to the implementation of inductive FCL during faulted condition, admittance (Y_{bus}) and impedance (Z_{bus}) matrixes change and X_{FCL} merges with impedance matrix. Thereafter, global optimization schemes are required to find the solution. So, to accomplish the proposed task, global optimization methods have been implemented which consist of mathematical formula and optimization function with large number of variables and constraints. In this work, DE and TLBO have been implemented. The description of the proposed DE and TLBO is given below.

3.1.1 Differential Evolution (DE)

DE is an evolutionary search method which is based on population and is stochastic in nature. The main characteristics of DE are its simplicity, robustness and prompt operation. The main difference of DE with earlier conventional techniques like GA, PSO, etc., is that the optimization problem need not be differentiable and replaces crossover and mutation operation. The key benefit of this algorithm is that it has self-organizing ability and a smaller number of parameters to be tuned. Initially, DE explores NP D vector variables and discrete time step ($t = 0, 1, 2 \ldots$ etc.) is used to represent the succeeding generation. Further all the search variables have been assigned a certain range and investigation with the DE parameters within the defined range has been carried out to acquire optimized result. In each generation of DE, a donor vector is formed after its initialization at $t = 0$. Three vectors from the population are chosen randomly in DE and a scaling factor is determined from the difference of these chosen random numbers in order to create the vector. To diversify the algorithm, mutation and crossover are used. The proposed DE algorithm [30] is shown in Fig. 1.

3.1.2 Teacher Learner-Based Algorithm (TLBO)

TLBO is a nature-inspired heuristic population-based algorithm which is developed to achieve global optimal results. The main difference between TLBO and the conventional optimization techniques is that TLBO gives global minima as solution for the problem. Here, TLBO is implemented to investigate the optimal solution to the overcurrent relay coordination and optimal size of FCL to be used. TLBO algorithm constitutes two methods of learning in a classroom. One is teacher phase which is interaction between learner and teacher and the other one is interaction among

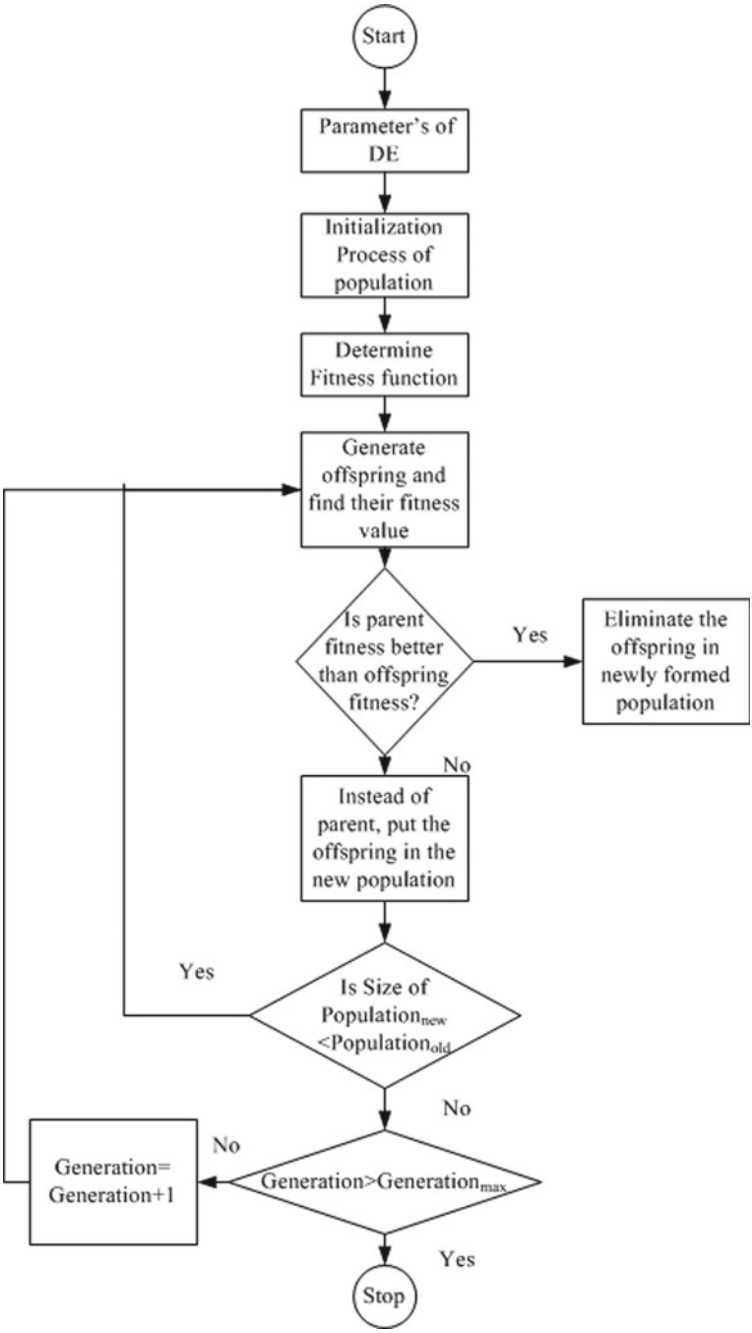

Fig. 1 Proposed DE algorithm

the learners—called the learner phase. The number of students (learners) in a class denotes the population in the TLBO algorithm and the various constraints indicate the different subjects taught. In this algorithm, teacher of the class is the learner with best performance which is measured by problem's fitness value. Therefore, Teacher in TLBO algorithm is a knowledgeable and learned person and plays an important role in improving learner's output (results or grades) and elevating the average level (which is based on learner's output) of the class. Improvement in grades of the learners is done by the combined process of random interaction between the learners and the teacher's input which takes place in the learner phase. Fitness is the learner's output in this algorithm. In the teacher phase, the existing solution is updated based on mean or average value and in the learner phase, the learner interacts either among themselves or with good knowledgeable learner to learn new things and to raise the level of their knowledge.

In this chapter, TLBO is implemented to obtain the solution of relay settings and FCL size in the test system. Further optimized value of time multiplier setting (TMS) and plug setting (I_p) of each relay in the test system must be investigated by this algorithm. So, if a test system has 'N' number of relays and 'M' FCLs, then TLBO's objective would be to evaluate $2N + M$ optimization values. Therefore, the population considered consists of number of individuals based on teacher's input where each individual is a array of suitable dimension. In this chapter, objective function of TLBO plays a role in finding out the summation of operating times of the primary and backup relays for every fault node of the system under study and also considers penalty values due to constraints like CTI. Here, the main objective of TLBO is to explore optimized value of overcurrent relays and FCL size in order to protect the microgrid in both configurations, i.e. grid connected and islanded mode. The proposed TLBO algorithm is shown by flowchart [31] in Fig. 2. In Fig. 2, 'T_F' indicates teaching factor which evaluates average value of a class to be changed according to performance (fitness) of learner and 'r' is a factor whose value lies between 0 and 1. Value of 'T_F' is randomly assigned according to the problem.

3.1.3 Performance Evaluation of TLBO and DE in Microgrid Coordination

TLBO and DE are used in this chapter to determine the optimized value of relay setting and FCL for the microgrid under study. Here, TMS and I_p are investigated for every relay. For 'N' number of relays and 'M' number of FCLs, the objective of the proposed program would be to investigate '$2N + M$' optimizer values. This gives 43 dimensions in the IEEE 9-bus radial distribution system under study. So, the population considered in the optimization scheme consists of a set of individuals determined by the input and every individual in the set is a string of proper dimension as described above. Operating conditions are used to modify the constraints and population's proper optimal generation is decided accurately so that the optimizer results are suitable. FCL values are also acquired from the optimizer and FCL is applied only in case of short circuit calculation for a feeder with grid connection. Implementation

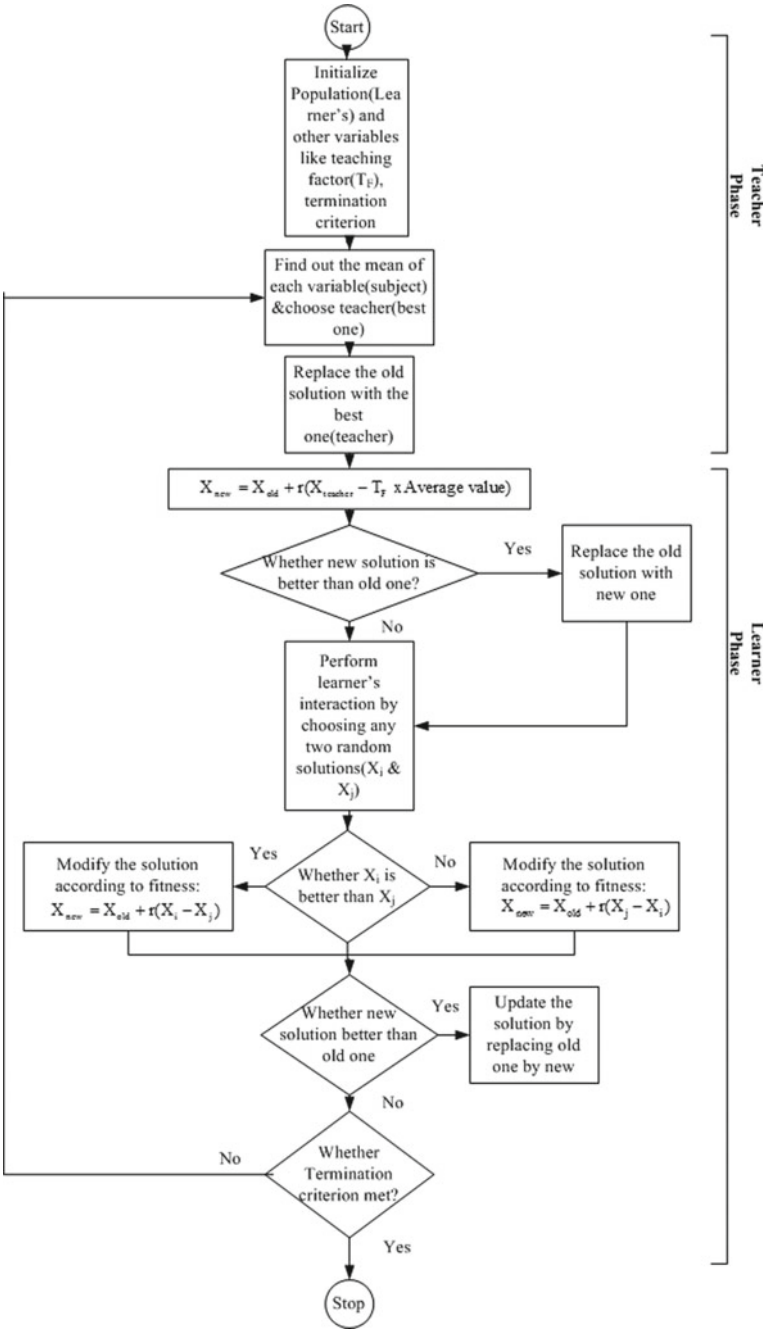

Fig. 2 Proposed TLBO scheme

of FCL in a grid-connected configuration of microgrid makes admittance bus (Y_{bus}) matrix totally different from that of islanding case matrix. For each fault location and relay, fault current is determined.

In this chapter, the optimizer's objective function explores at each fault point the summation of operating times of relays (primary and backup), i.e. 10–17 fault nodes in IEEE 9-bus test system. Penalty values which exist because of one or more constraints like CTI are also considered by the objective function. Here, the minimum difference in operating time of primary and its backup relay is taken as 0.2 s; so that unnecessary tripping of backup relay before its primary can be avoided. Further three-phase short circuit to ground fault is considered here at every fault node for analysis purpose to ensure FCL's capability during worst fault case. The overall proposed scheme is shown in the form of flowchart in Fig. 3.

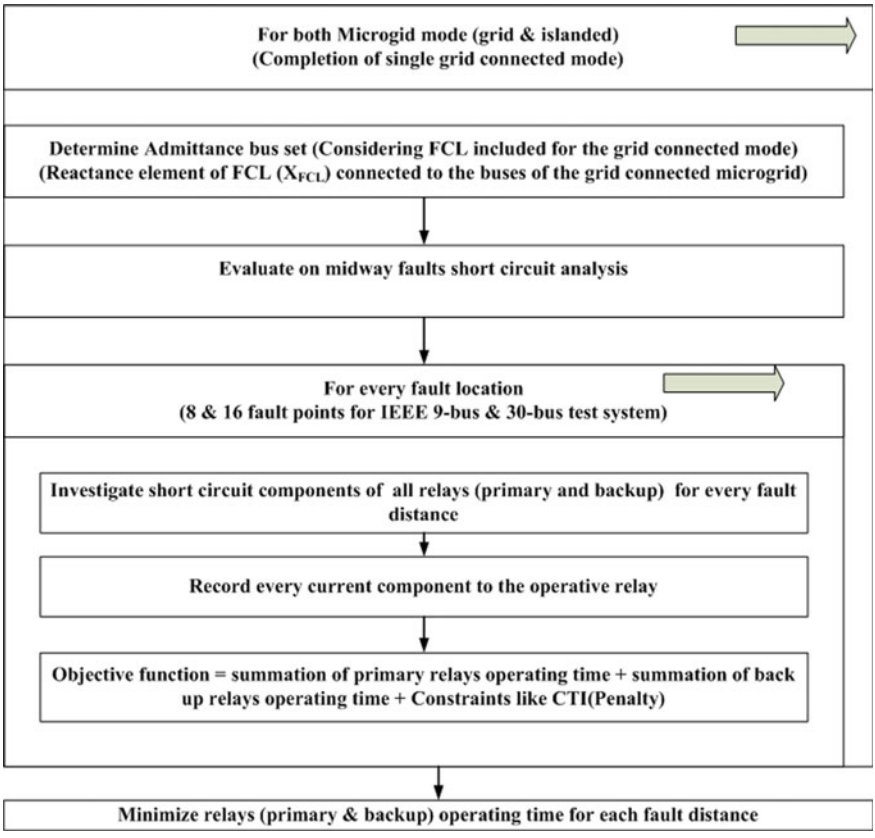

Fig. 3 Proposed scheme

4 Simulation Results with Various Test Cases

A peculiar test bench case has been considered for performance validation of the proposed scheme. The test system under study is IEEE 9-bus Canadian urban radial distribution network. The brief description of the test case is given below:

4.1 IEEE 9-Bus Canadian Urban Test System

This test system is shown in Fig. 4 where 02 numbers of feeder are connected with rating 8.7 MVA and $0.1529 + j0.1046\ \Omega$/km impedance. These feeders are connected to a utility of short circuit ratio 500 MVA and X/R is 6. Also, the test system consists of distribution transformer of 115/12.47 kV rating. For conversion of the above-mentioned radial distribution system into a microgrid, conventional DG (4 numbers) is connected to 4, 5, 6 and 9 no of buses through 12.47 kV/480 V, 5 MVA transformers with rated loads of 2 MVA, 0.9 power factor connected to all the buses from 2 to 9.

Further, 17 numbers of DOCR are connected at both the ends of the feeder which use to operate during occurrence of line faults for primary and backup relays. Faults are made to occur in the middle of the feeder and simultaneously mapping is done with primary and backup relays for each fault case. Further, short circuit analysis

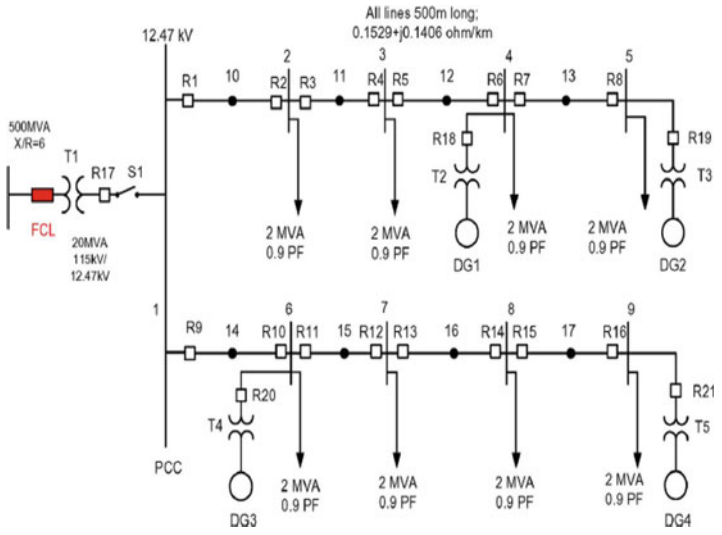

Legends: *PCC*-Point of Common Coupling, *R*- Relay, *PF*-Power Factor, *DG*-Distributed generator

Fig. 4 IEEE 9-bus radial distribution network [32]

Table 1 Relay data

Bus fault nodes	Primary	Backup 1	Backup 2
10	1	10	17
10	2	4	
11	3	1	
11	4	6	
12	5	3	
12	6	8	18
13	7	5	18
13	8	19	
14	9	2	17
14	10	12	20
15	11	9	20
15	12	14	
16	13	11	
16	14	16	
17	15	13	
17	16	21	

is done with the introduction of 08 additional fault nodes in the system. Because of multiple sources of the test system, fault current use to flow from both ends. Primary relays are assigned at both ends of the feeder for each mid-point fault and placement of backup relays is decided based on direction of flow of fault current. Here, 02 no of backup relay is assigned for each primary relay.

From Fig. 4, it can be observed that if a fault occurs at node 14, then the primary relays which will operate are R9 and R10 and backup relays which will operate if primary fails are R2 and R17 (for R9) and R12 and R20 (for R10). Faults are three-phase which is made to occur from node 10 to 17 of the system and simultaneously DOCRs are decided. The detail data of primary and backup relays for different bus nodes are given in Table 1.

From Table 1, it has been observed that for each bus fault nodes, one primary and one or two backup relays have been assigned. Further, it was also noticed from Table 1 that for 16 numbers of bus fault nodes, 16 numbers of primary relays, 16 numbers of backup relays and 6 numbers of additional backup relays (for node 10, 12, 13, 14, 15) have been assigned. Investigation has been carried out to find optimal relay settings and FCL value for seamless operation of microgrid in both modes (Grid connected and islanded) under the effect of three-phase faults.

Table 2 Optimized value of relay setting

Relay	TDS (s)	I_p (pu)	Relay	TDS (s)	I_p (pu)
1	0.230	0.650	12	0.351	0.178
2	0.204	0.650	13	0.297	0.001
3	0.224	0.209	14	0.292	0.396
4	0.258	0.650	15	0.010	0.001
5	0.132	0.112	16	0.302	0.489
6	0.283	0.650	17	0.500	0.078
7	0.010	0.001	18	0.397	0.239
8	0.392	0.240	19	0.316	0.495
9	0.229	0.650	20	0.198	0.560
10	0.300	0.290	21	0.367	0.451
11	0.166	0.650			
			T_{ops}	28.9	

4.1.1 Grid-Connected Mode

In this mode, the 9-bus radial distribution system does not consists of FCL and has grid and DG connection only. Standard MATLAB programme from [32] are used to determine the fault currents which use to flow from both ends of the feeder. Optimization programmes were executed to get optimal settings of primary and backup relays which is given in Table 2.

In Table 2, T_{ops} indicates optimal setting of time. From Table 2, time and current setting of 21 numbers of relays can be found in the 9-bus system with grid-connected mode under study. It can be noticed from Table 2 that T_{ops} is quite high (28.9 s) in grid mode.

4.1.2 Islanded Mode

Here, the microgrid is connected to DG and disconnected from the utility. Optimal relay setting in this mode provides adequate protection coordination during occurrence of fault which is enumerated in Table 3.

From Table 3, it can be noticed that optimized time setting (T_{ops}) for islanded mode is less (27.855 s) than that of grid mode (28.9 s), so can be concluded that proper protection coordination comes into picture during islanded mode.

4.1.3 Dual Mode

Here, both the modes, i.e. grid and islanding are considered. The main objective is to obtain optimal setting of relay and FCL so that same values can be implemented in

Table 3 Optimized set value of the relay

Relay	TDS (s)	I_p (pu)	Relay	TDS (s)	I_p (pu)
1	0.262	0.210	12	0.307	0.136
2	0.261	0.498	13	0.135	0.109
3	0.145	0.340	14	0.338	0.199
4	0.338	0.453	15	0.011	0.334
5	0.160	0.024	16	0.313	0.355
6	0.466	0.320	17	0.398	0.396
7	0.010	0.001	18	0.332	0.461
8	0.327	0.461	19	0.375	0.463
9	0.192	0.530	20	0.235	0.384
10	0.196	0.650	21	0.292	0.529
11	0.306	0.050			
			T_{ops}	27.855	

both configurations (grid and islanding) in order to protect the microgrid. Optimized relay value with FCL is shown in Table 4.

It can be observed from Table 4 that optimal time setting of relays in dual mode with the presence of FCL gives larger value (65.36) as compared to grid mode (28.9) and islanded mode (27.855). So, it can be said that FCL values give significant results which are almost same as the results given by earlier researchers and has the capability to reduce the level of short circuit current. There is also a variation in DOCRs setting. Constraints like CTI have been analyzed in the present chapter in

Table 4 Optimized value of relay setting with FCL

Relay	TDS (s)	I_p (pu)	Relay	TDS (s)	I_p (pu)
1	0.320	0.255	12.000	0.481	0.072
2	0.290	0.355	13.000	0.068	0.041
3	0.160	0.309	14.000	0.291	0.474
4	0.279	0.386	15.000	0.012	0.051
5	0.155	0.033	16.000	0.482	0.045
6	0.463	0.390	17.000	0.160	0.092
7	0.012	0.273	18.000	0.498	0.139
8	0.357	0.274	19.000	0.432	0.137
9	0.219	0.429	20.000	0.366	0.282
10	0.246	0.362	21.000	0.448	0.390
11	0.138	0.155			
X_{FCL}			1.952		
Total T_{ops}			65.36		

order to evaluate optimal setting of relays for grid and islanded mode which is as shown in Tables 5 and 6, respectively.

It can be noticed from Table 5 that CTI value for some of the relays is more than the assigned value, i.e. **0.2** s. Table 5 shows that for fault point 4, 5 and 6 and for 2nd backup relay, CTI violates the referred value (0.2 s).

It can be depicted from Table 6 that 04 numbers of relays violate with assumed CTI constraints, i.e. 0.2 s, whereas 03 numbers of relays are greater than 0.2 s in case of grid mode as noticed from Table 5.

In order to validate the proposed scheme, behavior of the test system is monitored with wrong value of relay setting. The setting value of grid mode is implemented in islanded mode for fault case to observe the effect. The results are given in Table 7.

In Table 7, highlighted (in yellow) portion (for relay 10, 0.74 and for relay 2, 0.74) indicates random relays having operating time less than that of primary relay for particular fault point, thus concluded that relay coordination failed.

5 Conclusion

This chapter presents an accurate technique for adequate protection coordination in microgrid with conventional-type DG and inductive-type SFCL. In the proposed technique, global optimization schemes like TLBO and DE are implemented in order to obtain optimized relay (primary and its backup) setting and value (size) of FCL during faulted condition. Further, in this chapter, to enhance the power delivery, inverse-type DOCR is considered. It was observed from the simulation results that introduction of optimized reactive FCL in both grid and islanded mode leads to variation in admittance bus matrix which finally reduces short circuit current level to an optimum value such that protection coordination is possible. Further, it was observed that the optimal setting of relay operation time (T_{ops}) gets raised due to the presence of FCL into the network. Also concluded that the capability of FCL depends on its size and network complexity. For avoiding maloperation of relays in feeders, a constraint called CTI (difference in operating time of primary and its backup) of 0.2 s has been assigned here for improved relay coordination. Further CTI for grid and islanded mode is investigated and it was noticed that a higher number of relays in islanded mode violate assigned CTI (0.2 s) than grid mode. In order to explore the importance of CTI, behavior of the test system is monitored with wrong value of relay setting and without implementation of CTI. Also, the setting value of grid mode is implemented in islanded mode for fault case to observe the effect. It was observed that during this situation some of the random relays maloperate due to large operating time compared to the operating time of primary relays. The proposed scheme is validated on IEEE 9-bus Canadian benchmark radial distribution system. Simulation results show that operating time of grid and islanded mode becomes same when optimal settings are done for the relay and FCL which further depicts that short circuit current level has been reduced and made same for both the modes due to FCL for improved protection coordination.

Table 5 Analysis of CTI for optimal relay settings in grid mode

Fault point	P_Primary	Primary_T_{ops}	Backup1_Primary	Backup1_T_{ops}	Backup2_Primary	Backup2_T_{ops}	CTI1	CTI2
1	1	0.601	10	0.827	17	0.807	0.2	0.2
1	2	0.786	4	0.990		0.000	0.2	0.0
2	3	0.409	1	0.610		0.000	0.2	0.0
2	4	0.965	6	1.166		0.000	0.2	0.0
3	5	0.217	3	0.417		0.000	0.2	0.0
3	6	1.146	8	1.347	18	1.348	0.2	0.2
4	7	0.012	5	0.220	18	1.366	0.2	**1.4**
4	8	1.321	19	1.526		0.000	0.2	0.0
5	9	0.577	2	0.803	17	0.813	0.2	0.2
5	10	0.806	12	1.035	20	1.543	0.2	**0.7**
6	11	0.391	9	0.592	20	1.562	0.2	**1.2**
6	12	1.023	14	1.337		0.000	0.3	0.0
7	13	0.202	11	0.404		0.000	0.2	0.0
7	14	1.315	16	1.517		0.000	0.2	0.0
8	15	0.008	13	0.209		0.000	0.2	0.0
8	16	1.500	21	1.711		0.000	0.2	0.0

Bold values violates the assigned CTI value (0.2 s)

Table 6 Analysis of CTI for optimal relay settings in islanded mode

Fault Location	P_Primary	Primary_T_{ops}	Backup1_Primary	Backup1_T_{ops}	Backup2_Primary	Backup2_T_{ops}	CTI1	CTI2
1	1	0.617	10	0.824	17	0.000	0.2	0.0
1	2	0.786	4	0.990		0.000	0.2	0.0
2	3	0.423	1	0.626		0.000	0.2	0.0
2	4	0.965	6	1.166		0.000	0.2	0.0
3	5	0.221	3	0.431		0.000	0.2	0.0
3	6	1.146	8	1.347	18	1.348	0.2	0.2
4	7	0.012	5	0.224	18	1.365	0.2	**1.4**
4	8	1.321	19	1.526		0.000	0.2	0.0
5	9	0.601	2	0.802	17	0.000	0.2	0.0
5	10	0.805	12	1.035	20	1.535	0.2	**0.7**
6	11	0.401	9	0.615	20	1.553	0.2	**1.2**
6	12	1.023	14	1.337		0.000	**0.3**	0.0
7	13	0.207	11	0.414		0.000	0.2	0.0
7	14	1.315	16	1.517		0.000	0.2	0.0
8	15	0.008	13	0.214		0.000	0.2	0.0
8	16	1.500	21	1.711		0.000	0.2	0.0

Bold values violates the assigned CTI value (0.2 s)

Table 7 Relay maloperation chart relays

Fault point	1	2	3	4	5	6	7	8	9	10	11	12	13	14	15	16	17	18	19	20	21
1	0.81	0.72	0.00	0.92	0.00	0.00	0.00	0.00	0.00	0.74	0.00	0.00	0.00	0.00	0.00	0.00	0.00	0.00	0.00	0.00	0.00
2	0.83	0.00	0.50	0.90	0.00	0.99	0.00	0.00	0.00	0.00	0.00	0.00	0.00	0.00	0.00	0.00	0.00	0.00	0.00	0.00	0.00
3	0.00	0.00	0.51	0.00	0.24	0.96	0.00	1.16	0.00	0.00	0.00	0.00	0.00	0.00	0.00	0.00	0.00	1.16	0.00	0.00	0.00
4	0.00	0.00	0.00	0.00	0.25	0.00	0.01	1.15	0.00	0.00	0.00	0.00	0.00	0.00	0.00	0.00	0.00	1.18	1.35	0.00	0.00
5	0.00	0.74	0.00	0.00	0.00	0.00	0.00	0.00	0.83	0.73	0.00	0.93	0.00	0.00	0.00	0.00	0.00	0.00	0.00	0.92	0.00
6	0.00	0.00	0.00	0.00	0.00	0.00	0.00	0.00	0.86	0.00	0.49	0.91	0.00	1.11	0.00	0.00	0.00	0.00	0.00	0.93	0.00
7	0.00	0.00	0.00	0.00	0.00	0.00	0.00	0.00	0.00	0.00	0.51	0.00	0.22	1.10	0.00	1.30	0.00	0.00	0.00	0.00	0.00
8	0.00	0.00	0.00	0.00	0.00	0.00	0.00	0.00	0.00	0.00	0.00	0.00	0.22	0.00	0.01	1.28	0.00	0.00	0.00	0.00	1.48

References

1. Stanley H, Horowitz AG (eds) (2013) Power system relaying. Wiley
2. Department of US Army (1991) Coordinated power systems protection. Technical manual, TM 5-811-14 [online]. Retrieved from http://www.usace.army.mil/publications/armytm/tm5-811-14/
3. Noe M, Steurer M (2006) R&D status of fault current limiters for utility applications. In: IEEE PES general meeting, Montreal, Canada
4. Office of Electricity Delivery and Energy Reliability (2009) Plugging America into the future of power. US Department of Energy, Washington, DC. Retrieved from https://energy.gov/sites/prod/files/oeprod/DocumentsandMedia/hts_fcl_110609.pdf
5. EPRI (2005) Survey of fault current limiter (FCL) technologies. Palo Alto, CA
6. Najy W, Zeineldin H, Woon W (2013) Optimal protection coordination for microgrids with grid-connected and islanded capability. IEEE Trans Ind Electron 60:1668–1677. https://doi.org/10.1109/tie.2012.2192893
7. Singh M, Panigrahi B, Abhyankar A (2013) A hybrid protection scheme to mitigate the effect of distributed generation on relay coordination in distribution system. In: IEEE power and energy society general meeting (PES), pp 1–5. https://doi.org/10.1109/PESMG.2013.6672159
8. El-Khattam W, Sidhu T (2008) Restoration of directional overcurrent relay coordination in distributed generation systems utilizing fault current limiter. IEEE Trans Power Delivery 23:576–585. https://doi.org/10.1109/tpwrd.2008.915778
9. Teng JH, Lu CN (2007) Optimum fault current limiter placement. In: International conference on intelligent systems applications to power systems ISAP, pp 1–6. https://doi.org/10.1109/ISAP.2007.4441611
10. Singh M, Panigrahi B, Abhyankar A (2013) Optimal coordination of directional over-current relays using Teaching Learning-Based Optimization (TLBO) algorithm. Int J Electr Power Energy Syst 50:33–41. https://doi.org/10.1016/j.ijepes.2013.02.011
11. Chen C, Lee C, Chang C (2013) Optimal overcurrent relay coordination in power distribution system using a new approach. Int J Electr Power Energy Syst 45:217–222. https://doi.org/10.1016/j.ijepes.2012.08.057
12. Barker P, de Mello R (2000) Determining the impact of distributed generation on power systems. I. Radial distribution systems. In: IEEE power engineering society summer meeting 3, pp 1645–1656
13. Girgis A, Brahma S (2001) Effect of distributed generation on protective device coordination in distribution system. In: Large engineering systems conference on power engineering (LESCOPE), pp 115–119

14. Ahmarinejad A, Hasanpour S, Babaei M, Tabrizian M (2016) Optimal overcurrent relays coordination in microgrid using cuckoo algorithm. Energy Procedia 100:280–286. https://doi.org/10.1016/j.egypro.2016.10.178
15. Abdel-Salam M, Abdallah A, Kamel R, Hashem M (2017) Improvement of protection coordination for a distribution system connected to a microgrid using unidirectional fault current limiter. Ain Shams Eng J 8:405–414. https://doi.org/10.1016/j.asej.2015.08.008
16. Elmitwally A, Gouda E, Eladawy S (2015) Optimal allocation of fault current limiters for sustaining overcurrent relays coordination in a power system with distributed generation. Alex Eng J 54:1077–1089. https://doi.org/10.1016/j.aej.2015.06.009
17. Mishra M, Panigrahi R, Rout P (2019) A combined mathematical morphology and extreme learning machine techniques based approach to micro-grid protection. Ain Shams Eng J 10:307–318. https://doi.org/10.1016/j.asej.2019.03.011
18. Haron A, Mohamed A, Shareef H (2013) Coordination of overcurrent, directional and differential relays for the protection of microgrid system. Procedia Technol 11:366–373. https://doi.org/10.1016/j.protcy.2013.12.204
19. Aghdam TS, Karegar HK (2017) Relay curve selection approach for microgrid optimal protection. Int J Renew Energy Res 7(2):636–642
20. Ahmadi S, Karami H, Sanjari M et al (2016) Application of hyper-spherical search algorithm for optimal coordination of overcurrent relays considering different relay characteristics. Int J Electr Power Energy Syst 83:443–449. https://doi.org/10.1016/j.ijepes.2016.04.042
21. Hooshyar H, Baran M, Firouzi S, Vanfretti L (2017) PMU-assisted overcurrent protection for distribution feeders employing solid state transformers. Sustain Energy Grids Netw 10:26–34. https://doi.org/10.1016/j.segan.2017.02.003
22. Gashteroodkhani O, Majidi M, Fadali M et al (2019) A protection scheme for microgrids using time-time matrix z-score vector. Int J Electr Power Energy Syst 110:400–410. https://doi.org/10.1016/j.ijepes.2019.03.040
23. Bukhari S, Saeed Uz Zaman M, Haider R et al (2017) A protection scheme for microgrid with multiple distributed generations using superimposed reactive energy. Int J Electr Power Energy Syst 92:156–166. https://doi.org/10.1016/j.ijepes.2017.05.003
24. Ustun TS, Khan RH, Hadbah A (2013) An adaptive microgrid protection scheme based on a wide-area smart communications network. In: Proceedings of IEEE Latin America on communications, Santiago, Chile
25. Abdulwahid AH, Wang S (2016) A new differential protection for microgrid using Hilbert space based power setting and fuzzy decision processes. In: IEEE 11th conference on industrial electronics and applications, Hefei, China, pp 6–11
26. Lin H, Liu C, Guerrero JM (2015) Distance protection for microgrids in distribution system. In: Proceedings of the 41st annual conference of the IEEE industrial electronics society, Yokohama, Japan, pp 731–736
27. Bui DM, Chen SL, Lien KY (2015) A generalized fault protection structure for uni-grounded low-voltage AC microgrids. In: Proceedings of innovative smart grid technologies-Asia, Bangkok, Thailand, pp 1–6
28. Kang X, Nuworklo C, Tekpeti B, Kheshti M (2017) Protection of micro-grid systems: a comprehensive survey. J Eng 2017:1515–1518. https://doi.org/10.1049/joe.2017.0584
29. Swathika OVG, Hemamalini S (2016) Review on microgrid and its protection strategies. Int J Renew Energy Res 6(4):1574–1587
30. Subhashini K, Kumar A (2014) Comparative analysis of linear and nonlinear pattern synthesis of hemispherical antenna array using adaptive evolutionary techniques. Int J Antennas Propag 2014:1–10. https://doi.org/10.1155/2014/987140
31. Akin A, Aydogdu I (2015) Optimum design of steel space frames by hybrid teaching-learning based optimization and harmony search algorithms. In: Proceedings of 17th international conference on structural engineering, Paris, France, vol 17, pp 1486–1493
32. Sadat H (ed) (2014) Power system analysis. Tata McGraw Hill (TMH) Pub

Energy Management System of a Microgrid Using Particle Swarm Optimization (PSO) and Communication System

Vijay K. Sood, Mohammad Y. Ali and Faizan Khan

Abstract This chapter focuses on the energy management system (EMS) for a microgrid. The hierarchy of the various controllers utilized in the EMS consists of three levels. Various programming methods can be used for optimizing the behavior of the EMS such that the MG can operate in a safe and reliable manner to match the demanded load with the available energy sources. A test case with a particle swarm optimization technique is provided. The requirements for a communication system within the MG are briefly discussed.

Keywords Energy management system · Particle swarm optimization · Grid integration · Distributed energy sources

Nomenclature

ACL	Agent communication language
ADP	Approximate dynamic programming
BESS	Battery energy storage system
CHP	Combine heat and power
DE	Differential evolution
DERs	Distributed energy resources
DGs	Distribution generations
DR	Demand response
DSO	Distribution system operator

V. K. Sood (✉) · M. Y. Ali · F. Khan
University of Ontario Institute of Technology (UOIT), 2000 Simcoe Street North, Oshawa, ON L1H 7K4, Canada
e-mail: Vijay.sood@uoit.ca

M. Y. Ali
e-mail: Mohammad.ali2@uoit.net

F. Khan
e-mail: Faizan.khan@uoit.net

P. Ray and M. Biswal (eds.), *Microgrid: Operation, Control, Monitoring and Protection*, Lecture Notes in Electrical Engineering 625,
https://doi.org/10.1007/978-981-15-1781-5_9

ED	Economical dispatch
EMS	Energy management system
ESSs	Energy storage systems
EVs	Electric vehicles
FANs	Field area networks
F/V	Frequency/voltage
GA	Genetic algorithm
HANs	Home area networks
HMI	Human–machine interfaces
IEC	International Electrotechnical Commission
MAS	Multi-agent system
MGs	Microgrids
MGMS	Microgrid management system
MILP	Mix-integer linear programming
NN	Neural network
O&M	Operation and maintenance
P2P	Point-to-point
PCC	Point of common coupling
P/Q	Active/reactive
PSO	Particle swarm optimization
PV	Photovoltaic
QoS	Quality of service
RESs	Renewable energy sources
SCADA	Supervisory control and data acquisition
SOC	State of charge
UC	Unit commitment
VPP	Virtual power plant
VSIs	Voltage source inverters
WANs	Wide area networks

1 Introduction

Microgrids (MGs) are the new paradigm for the evolution of the distribution system. MGs are composed of distributed energy resources (DERs), such as generators, renewable energy sources (RESs), energy storage systems (ESSs) and a cluster of critical and non-critical loads. They provide stability to the main grid and offer optimal integration of these subsystems into the distribution system. MGs operate in one of two modes: grid-connected or islanded mode [1–5]. In grid-connected mode, a microgrid draws/supplies power from/to the main grid, depending on the generation and load requirements, and respecting certain suitable market policies to maximize the efficiency/cost, etc. Likewise, it can separate itself from the main grid whenever a fault occurs in the main grid and continues to supply power to connected

critical loads. Furthermore, to ensure that the MG operates in an economical and reliable manner, it is equipped with a suitable supervisory control and data acquisition (SCADA) system. The control system is responsible for scheduling and controlling of all DERs to warrant the stability, reliability and economical operation of the MG.

In this book chapter, the microgrid control system is presented. The MG control system functions at three levels: primary, secondary and tertiary. Section 2 describes the two different types of energy management systems (EMS) used in a MG (i.e., either centralized or decentralized) and gives the advantages and disadvantages of both. Section 3 reviews various methods to assist the MG EMS to achieve optimal operation while minimizing operational costs. Section 4 deals with the different methods, i.e., using either linear, nonlinear, dynamic, rule-based, metaheuristic, artificial intelligent or multi-agent methods for establishing the EMS. Section 5 describes the role of communication systems in the area of MGs. In Sect. 6, a test case of a particle swarm optimization technique for a MG model is presented. Section 7 provides the conclusions for this chapter.

2 Microgrid Management System

A crucial unit that controls the operation of the microgrid is the microgrid management system (MGMS), which operates the system autonomously, connecting it to the utility grid appropriately for the bi-directional exchange of power and providing support to components within the microgrid. It enables the interplay of components and different controllers to operate the EMS in a safe and controlled manner. This approach will allow customization of the system to enhance optimization to improve the overall efficiency without sacrificing the plug-and-play functionality. MGMS is broken down into three different subsystems, i.e., primary, secondary and tertiary control layers that manage the entire microgrid operation as shown in Fig. 1.

The MGMS controls the DGs to maintain the balance between generation and load demand during islanded mode, grid-connected mode or the transition period between the two modes. The three control layers are described next [6].

2.1 Primary Control Layer

This is the base layer that has the fastest response time (typically, in the region of milliseconds to minutes) and is responsible for the control of devices that respond to system dynamics and transients. It is also known as the local or internal controller. This control is based exclusively on local measurements and requires no communications. The function of this control includes islanding detection, converter output control, frequency regulation, voltage regulation and power-sharing control. In the microgrid, the voltage source inverters (VSIs) are the common interface between the DERs and the microgrid. VSI controller requires a specially designed control to

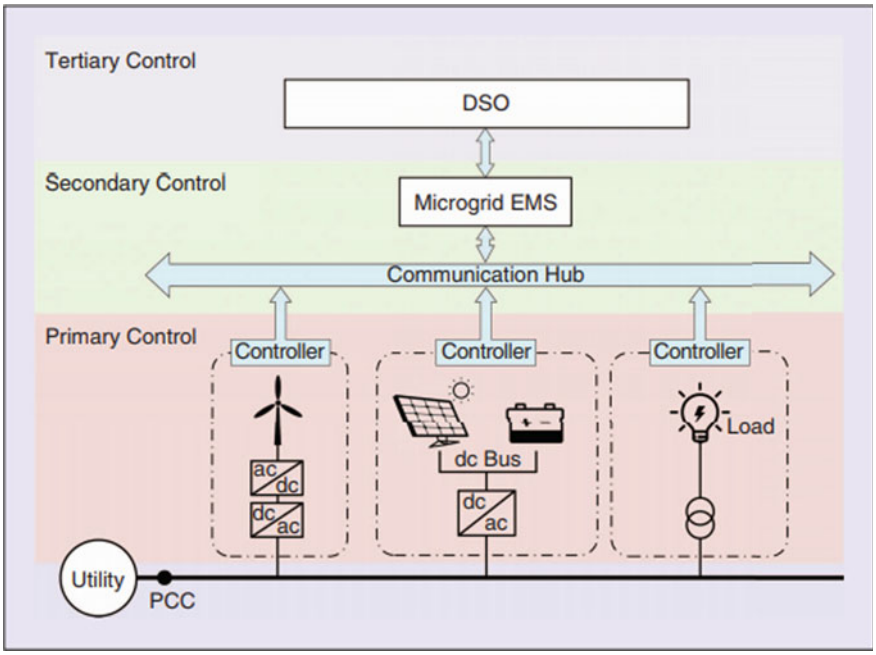

Fig. 1 Microgrid management system (MGMS) [9]

simulate the inertia characteristic of synchronous generators and provide appropriate frequency regulation. The VSI has two stages of control: inverter output control and power-sharing control. The inverter typically consists of an outer control loop for voltage control and an inner loop for current regulation. The power-sharing control is used for the sharing of the active and reactive power in the system.

2.2 Secondary Control Layer

This is the central layer (Fig. 2) and is responsible for the reliable and economical operation of the microgrid. Its main function includes an EMS and automatic generation control system. The secondary control also helps reset the frequency and voltage deviations of the droop-controlled VSIs and generators, then assigns to them new optimal long-term set points calculated from the microgrid EMS. The EMS minimizes the microgrid's operation cost and maximizes its reliability in grid-connected or islanded modes of operation. The objective of the EMS consists of finding the optimal unit commitment (UC) and economic dispatch (ED) of the available DER units to achieve load and power balance in the system. The cost function is designed in terms of economic tolls, such as fuel cost, power bill, maintenance cost, shutdown and start-up cost, emissions, and social welfare and battery degradation cost and the

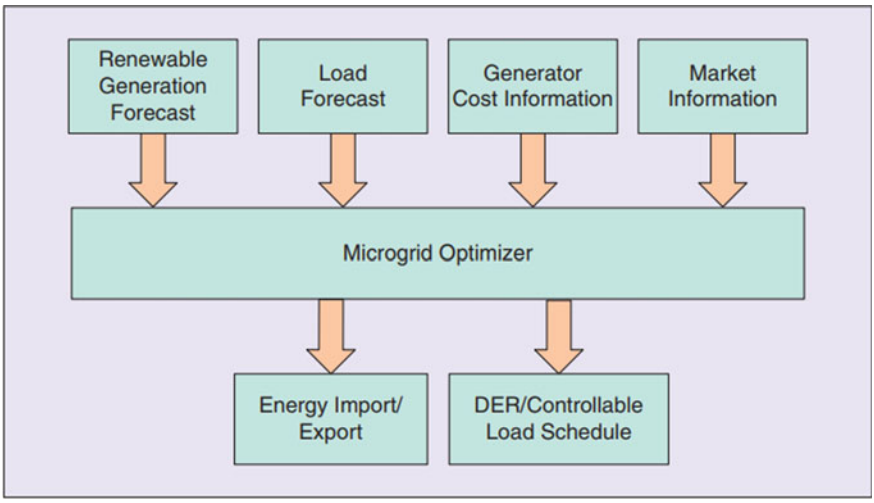

Fig. 2 Secondary control layer [9]

cost of loss of load. The reliability indices are formulated as constraints, such as load forecast, forecasted power availability of RESs, the generation and demand balance, energy storage capacity limits and power limits for all controllable generations. The EMS resolves a multi-objective optimization problem with complex constraints and falls under mixed-integer linear/nonlinear programing. The output of the optimizer is the scheduled energy import/export and DGs power output.

2.3 Tertiary Control Layer

This is the highest control layer and provides intelligence for the whole system. It is responsible for buying and selling of energy between consumers and grid system, as well as providing active and reactive power support for the whole distribution system. Tertiary control layer is not a part of MGMS as it is recognized as a sub-system of the utility distribution system operator (DSO). But, due to the increase of microgrids within the distribution system, the tertiary control layer is evolving into a concept called virtual power plant (VPP). The objective of a VPP is to coordinate the operation of multiple microgrids interacting with one another within the system and communicate needs and requirements from the main grid. The VPP can provide transmission system primary frequency support, reactive power support and energy market participation. The control layer response time is typically of the order of several minutes to hours, providing signals to secondary controls at microgrids and other subsystems that form the full grid. Figure 3 shows the time-scales of the three MGMS control layers where the lower (primary) layer controls devices with fastest

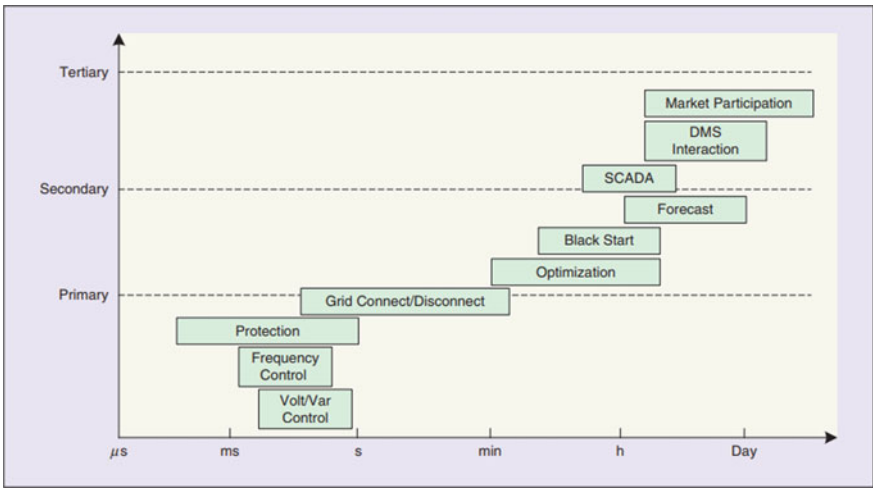

Fig. 3 Response times of various layers in MGMS [9]

response times, and whereas the higher (secondary and tertiary) layers controls tend to have slower response times.

3 Microgrid Energy Management Systems

The International Electrotechnical Commission in the standard IEC 61970, defines an EMS as "a computer system comprising a software platform providing basic support services and a set of applications providing the functionality needed for the effective operation of electrical generation and transmission facilities so as to assure adequate security of energy supply at minimum cost" [7]. Hence, the microgrid EMS is a product of these features. It is usually equipped with decision-making algorithms, load and power forecasting, human–machine interfaces (HMI) and SCADA system. These functions help the EMS in optimizing microgrid operation, while satisfying the technical constraints.

MG EMS supervisory control can be sub-divided into two types, namely, centralized and decentralized EMSs. This section will be going into more depth about the two different types of control methods, and also into their advantages and disadvantages.

3.1 Centralized Energy Management

In the centralized EMS system, data information and collection are usually required from the tertiary and primary control layers such as operating cost, weather forecast, load demand, voltage and current readings from each component, etc. Based on the gathered information, an appropriate unit commitment and dispatch optimization algorithm are executed to achieve efficient, economical operation, and maintain power quality as well as match generation with load demand. The microgrid relies on the secondary layer, where a Master Controller with a high computing performance and a dedicated communication network is utilized for the operation. Usually, the Master Controller supports EMS and SCADA functions with an HMI which allows the system operator to control and monitor the microgrid. A centralized configuration is shown in Fig. 4.

In Fig. 4, the centralized configuration requires a two-way communication channel between the primary control (local controllers) and secondary control (EMS) for the exchange of information. This configuration is called a star connection topology and a master/slave technique is established. The communication channels can be either wired or wireless depending on its requirements. Some of the available technologies are based on power line carriers, telephone lines or a wireless medium.

In centralized EMS, operation is in real-time where the secondary controller frequently observes the entire system and samples the critical generation/demand information from each component. This frequent communication may cause a computational burden; therefore, a high-performance computing unit is required where

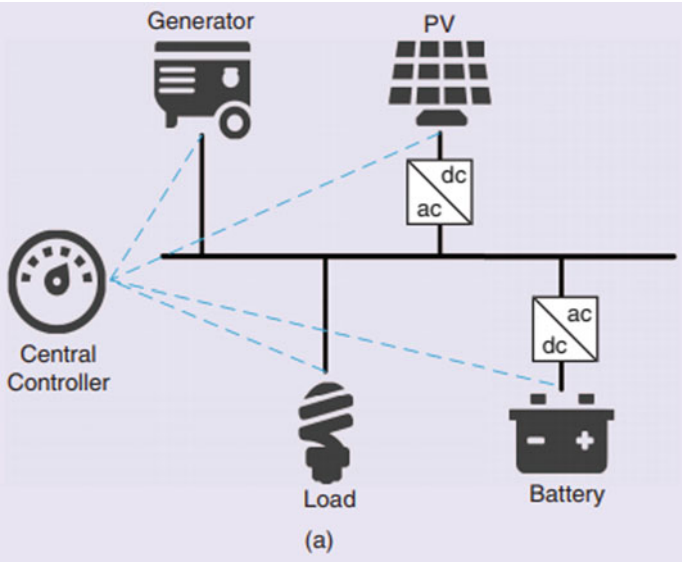

Fig. 4 Centralized EMS configuration [9]

the EMS can execute accurate decisions by processing the data read through the communication channel. Moreover, a high-bandwidth communication is required to meet the growing demands of EMSs.

Centralized EMS is a comparatively straightforward implementation but can also endanger the overall performance as any single-point failure or any fault at a unit can cause the entire system to breakdown. Therefore, it is considered to have a low expandability and flexibility. Considering its structure and functionality, the following options can be more desirable for the microgrid cases [8]:

- A small-scale microgrid, with low communication and computational cost where centralized information can be processed
- Unity between the components is required which can operate the microgrid with a common goal for generation/demand balances
- Must operate with a high security that keeps the data information secure.

The EMS optimizes the microgrids power flow distribution, resulting in maximizing the DG's production depending on the various parameters, constraints, variables and market prices provided as an input to the EMS controller. Some of the most commonly used data provided as input information to the controller to process and provide the reference values to the primary control layer, may include:

- Forecasting of the grid electricity prices
- Status of interconnection of utility grid
- Reliability and security constraints of the microgrid
- Operational limits of DG to be discharged
- State of charge (SOC) of the battery energy storage system (BESS)
- Load day-ahead forecast values
- RESs generation forecasted power output.

Centralized EMS enables all the relevant information to be gathered at a single point for the controller to perform its function. The following steps are involved in a centralized framework for the EMS to perform its tasks [9] (Fig. 5):

1. Performing a RES generation and day-ahead load forecast
2. Performing a day-ahead energy scheduling calculation by collecting information from all the components

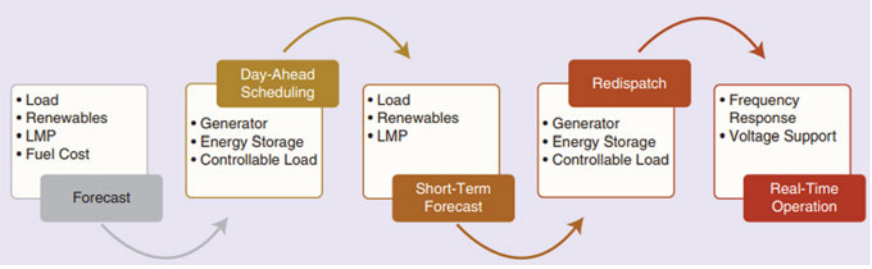

Fig. 5 Centralized framework for the EMS [9]

3. Executing an optimization algorithm to calculate the optimal day-ahead schedules
4. Assigning optimal day-ahead schedules to the corresponding components
5. Acquiring real-time system information, as there might be unexpected events or forecast errors
6. Generating short-term forecasts during the operation
7. Re-executing the optimization algorithm and rescheduling the dispatch of RESs (15 min)
8. Finally, sending the EMS the most updated and optimal set points to the primary control.

When the EMS is executed, a set of information is dispatched to the local controllers at the primary control level to operate the DG's in a cost-effective manner and simultaneously maximize the reliability of the microgrid. The set of information dispatched are [10]:

- Set points for DG's to dispatch the production of power
- Set points for local loads to be shed or to be served
- Market prices to serve as the input for EMS.

3.2 Decentralized Energy Management

In the decentralized EMS scheme (Fig. 6), local controllers are interfaced with each DG unit to communicate among each other through a communication channel within the microgrid. Each unit is controlled by its local controller where data for each of the DG controllers is exchanged. Local controllers communicate with each other to request/offer a service, exchange information, communicate expectations and share knowledge which is relevant to the microgrid operation. These controllers have advanced algorithms to make their own decisions or to process information and execute commands from the upper level. This EMS scheme is known for its intelligence as it is not fully aware of the decision made by controllers or the system-wide variables.

In Fig. 6, the decentralized configuration illustrates a two-way communication channel between the local controllers for the exchange of information. This configuration is called a peer-to-peer (P2P) communication topology and is established within the primary control layer. The EMS is implemented locally in each of its local controllers connected to either DGs or the loads within the microgrid to allow the interaction of each unit to enable a decision-making process to optimally solve the energy management problem while providing flexibility within the microgrid to provide autonomy for all DG's and loads.

In a decentralized EMS operation, the need for the secondary control layer is eliminated since the collaboration at the primary control layer between the local controllers, which work jointly to achieve local goals to meet generation and demand

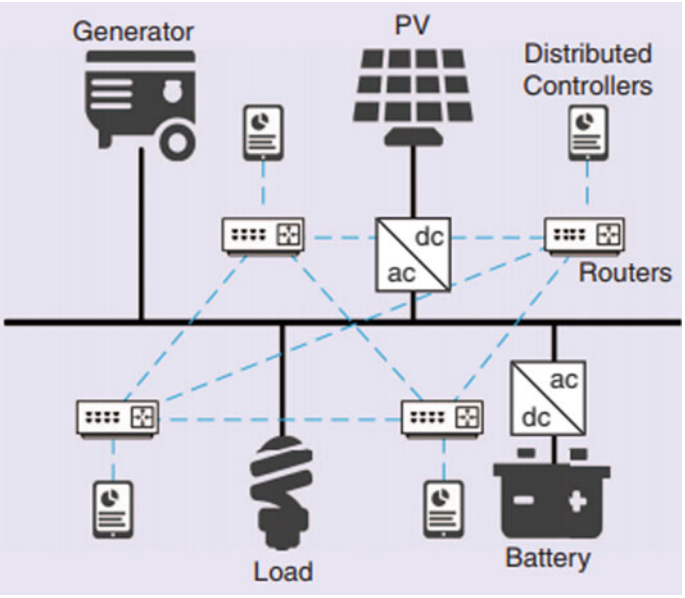

Fig. 6 Decentralized EMS configuration [9]

of the entire microgrid, overrides it. This can reduce the computational burden to some degree, as the customers no longer need to report their current or historical generation and demand data to EMS at the secondary control layer. Processing of information such as weather forecast, operating cost, load demand, etc., can be optimized by the local controllers, which reduces the use of hierarchical levels in the microgrid.

Implementation of an EMS in decentralized control architecture can increase the overall complexity of the entire microgrid. Although this can be overcome when looking at other perspectives in terms of its flexible operation and avoidance of single-point failure, which can still maintain the normal operation of the EMS. Another advantage is that it can allow interaction of various other DG units, like a plug-and-play functionality, without the need to make continuous changes to the local controller settings. Considering its structure and functionality, the following options can be more desirable for the microgrid cases [8]:

- Large-scale microgrids, or the consumption, storage and generation are widely isolated which can make data acquisition costly or difficult when using centralized EMS
- Requirement of local decision-making, when the resources are owned by multiple owners
- Adding or removing of DGs.

When modeling the microgrid using the decentralized approach, the concept of multi-agent system (MAS) has been primarily addressed in the literature. MAS has evolved from a classical distribution control system which is specially designed for

automated control systems with capabilities to control large and complex entities or groups of entities by dedicated controllers. Distributed control and MAS have a similar structure but what distinguishes them is the level of intelligence which the agents are embedded with. The MAS relies on a framework to achieve multiple local and global objectives autonomously, where two or more agents or intelligent agents are provided with local information. The characteristics of the local information, responsibilities and functionalities assigned to each agent and information shared by the agents between each other play a vital role in the overall performance of the system for the enhanced robustness, reliability and flexibility of microgrid. An intelligent agent is distinguished from a hardware or a software automated system and can be described as an agent which possess the characteristics such as [6]:

- **Reactivity**: the ability to show reaction and reach to the changes in the environment in a timely manner
- **Pro-activeness**: seeking initiatives to achieve goals
- **Social-ability**: interaction with other agents through a communication channel.

These characteristics in local controllers work toward improving the performance of the system and not have the main objective to maximize the revenue of the corresponding unit. This means that the intelligent agents can interact with other intelligent agents to react to the environmental changes and establish a goal-oriented behavior.

Overall operation of MAS is to control objectives such as: economy, reliability, energy market participation and microgrid operation. Although this is an overall global goal for the microgrid to operate in a reliable manner, in MAS only local goals are defined and not global goals. When intelligent agents cooperate among themselves and work toward local goals, the targeted global goal may be achieved with local goals responding to sub-parts of the global goal. The design of MAS algorithms is a complex process that requires a great deal of expertise to decompose global goal task by modeling the agent's interactions and classifying agents. Intelligent agents working together to achieve various local goals is a multi-objective problem, where the complexity of the MAS algorithm is structured in a rigorous manner for the agents to communicate autonomously.

An agent communication language (ACL) is an environment for knowledge and information exchange and is required within the microgrid to enable agents to process only allowable or necessary knowledge for the agents to communicate among each other and eventually agree upon to determine the power mismatch between the demand and generation, as well as the estimated incremental cost. In decentralized EMS, MAS algorithms rely on a modern communication infrastructure which supports P2P communication between the agents for the exchange of data. IEC 61850 standards are utilized which support P2P data exchange. Communication can be either wired or wireless depending on requirements.

The general architecture of a microgrid EMS based on MAS is described in [11] and shown in Fig. 7. Several different types of agents are defined in MG secondary and local controllers including:

- Database gateway agent for storing and retrieving information with databases

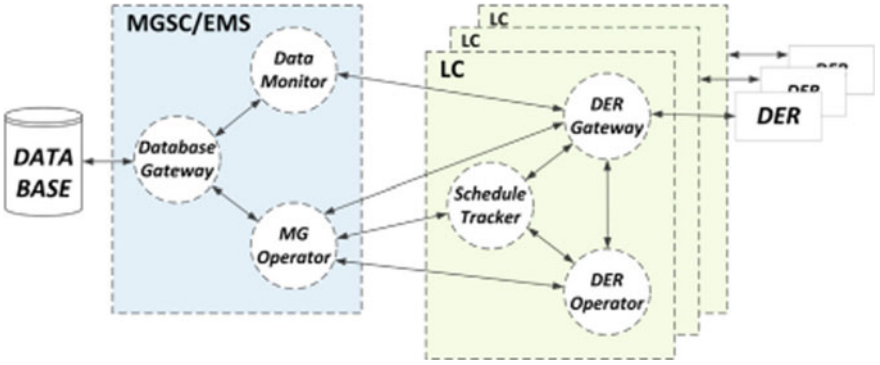

Fig. 7 A general architecture of MAS-based MG EMS [8]

- Data monitor agent for obtaining real-time operation data from DER and feeding essential information to databases
- MG operator agent for optimizing the operation of the whole system
- DER gateway agent for interfacing other agents and control system with DER devices
- Schedule tracker agent for following the schedule from MG operator agent and sending set-point to DER
- DER operator agent for locally optimizing the operation of DER and response with MG operator agent. Based on this scheme, a secondary control is implemented for regulating MG frequency and power flow in islanded and grid-connected modes.

3.3 Comparison Between Centralized and Decentralized EMS

In addition to the comparison shown in Table 1, the decentralized framework has the following benefits:

- Decentralized controllers require less computing power, which is more cost effective
- Decentralized control systems have greater controller redundancy and are robust to a single point of failure. Controller failures will not cause system blackout
- Local decision-making reduces network use, relaxing the communication bandwidth requirement
- System maintenance and upgrades can be done without shutting down the entire system.

The decentralized control framework is more flexible and scalable for future modifications and expansions.

Table 1 Comparison of centralized and decentralized

Controls	Advantages	Disadvantages
Centralized	• Simple to implement • Easy to maintain • Relatively low cost • Widely used and operated • Wide control over the entire system	• Computational burden • Requires high-bandwidth links • Single point of failure • Not easy to expand • Weak plug-and-play functionality
Decentralized	• Easier plug-and-play (easy to expand) • Low computational cost • Avoid single point of failure • Suitable for large-scale complex, heterogeneous systems	• Need synchronization • May be time-consuming for local agents to reach consensus • Convergence rates may be affected by the communication network topology • Upgrading cost on the existing control and communication facility • Needs new communication structure

4 MG EMS Solution

Many researchers have used different approaches to achieve optimal and efficient operation of MGs. This section outlines some popular methods used by researchers to solve the EMS.

4.1 EMS Based on Linear and Nonlinear Programming Methods

In [12], the authors present an optimal energy management of a residential MG to help minimize the operation cost. The cost function consists of: energy trading cost, penalty cost on adjustable load shedding, electric vehicles (EVs) batteries wearing out cost, the range anxiety term for EVs. Three test cases have been defined using three different range anxiety levels and have been studied to analyze the trade-off between operational cost of MG and average SOC of EVs battery. As well, three different types of load are considered, namely: critical, adjustable and shiftable loads. This optimal EMS is formulated using mix-integer linear programing (MILP). Similarly, in [13], the authors proposed MILP optimization model for an optimal MG EMS to maximize daily revenue with main grid peak shaving application by introducing demand-responsive loads. For the system, it was assumed that the load demand of the MG will always be more than generation. Two different systems were used to test and analyze the performance of the algorithm: first, a one-bus MG, and second a 14-bus MG system.

The authors in [14] proposed a centralized architecture for EMS of a grid-connected MG using sequential quadratic programing method. The EMS aims to

optimize the operation of the MG during interconnected operation, i.e., maximize its value by optimizing production of the local DGs and power exchanges with the main distribution grid. Two policies are used: first policy is operational cost minimization, while second policy aims to maximize its profit considering energy transactions with the main grid. Likewise, [15] introduced strategic EMS of a grid-connected MG, constrained by an operation window of transformer nominal operation and voltage security. The developed model minimizes MG operational cost using modified gradient descent solution method. The forward–backward sweep algorithm determines power flow solution of MG. Three scenarios are considered in the objective function with respect to customer benefits, network losses and load leveling.

4.2 EMS Based on Dynamic Programming and Rule-Based Methods

Another solution of MG EMS is presented in [16]. An approximate dynamic programming (ADP) approach is to overcome the curse of dimensionality in the proposed EMS model of a grid-connected MG. The cost function is computed using receptive field weight regression and lookup table. Various scenarios of wind speed, load demand and ambient temperature are generated to consider their uncertainty in the proposed model, which uses economic dispatch and unit commitment operations to optimize the energy scheduling of MG. The proposed system is compared to myopic optimization and dynamic programming methods. In comparison with myopic optimization, the proposed system had lower operation cost, but higher computational time. But, with dynamic programming, the system had faster computational time and higher operation cost for MG.

4.3 EMS Based on Metaheuristic Approaches

Various authors have used metaheuristic approaches to solve the MG EMS. In [17], the authors proposed a genetic algorithm (GA) and rule-based approach to solve an economic load dispatch and battery degradation cost-based multi-objective EMS for a remote MG. The system both day-ahead and real-time operations considers diesel generator supply, battery supply and load shedding options in a sequential order to maintain load generation balance. An optimal EMS for grid-connected MG that considers uncertainties of renewable energy sources (RESs), load demand and electricity price using particle swarm optimization (PSO) [18]. The efficiency of PSO in finding the best solution is better in comparison with GA, combinatorial PSO, fuzzy self-adaptive PSO and adaptive modified PSO. Similarly, a differential evaluation (DE) based EMS for a grid-connected MG is presented in [19]. The objectives of the proposed EMS are minimization of operational and emission costs

of the MG. Operational cost of MG includes bidding cost of DERs, demand response (DR) incentives and energy trading cost with the main grid. The results obtained using DE algorithm are compared with the PSO-based results. On comparison, the proposed DE algorithm was found to be superior in terms of solution quality and convergence speed. In [20], an ant colony optimization-based multi-layer EMS model for an islanded MG is proposed to minimize its operational cost. The objective function is comprised of bidding cost of RESs, DGs and battery, penalty cost on load shedding, and DR incentives in both day-ahead scheduling and 5 min interval real-time scheduling layers. Three case studies were used to analyze the system: operation, sudden high requirement of load demand and plug-and-play ability. The proposed approach reduces operational cost of MG by almost 20% and 5% more than the modified conventional EMS and PSO-based EMS, respectively.

4.4 EMS Based on Artificial Intelligent Methods

In [21], the authors presented a fuzzy-based MG EMS. The algorithm utilized two GAs to optimize its day-ahead MG scheduling and built a fuzzy expert system to control the power output of the storage system. The first GA determined MG energy scheduling and fuzzy rules, while the second GA tuned fuzzy membership functions. Reference [22] proposed an intelligent adaptive dynamic EMS for a grid-connected MG. It maximized the utilization of RESs and minimized carbon emissions to achieve a reliable and self-sustainable system. It also improved battery lifetime. The proposed EMS was modeled using evolutionary adaptive dynamic programming and reinforcement learning concepts and solved by use of two neural networks (NNs). An active NN is used to solve the proposed EMS strategy, while a critical NN checks its performance with respect to optimality. The newly defined performance index evaluates the performance of dynamic EMS in terms of battery lifetime, utilization of renewable energy and minimum curtailment of controllable load. The performance of the proposed approach is better as compared to decision tree approach-based dynamic EMS.

4.5 EMS Based on Multi-agents Systems (MAS)

A decentralized MAS-based MG EMS for a grid-connected MG is presented in [23]. For optimal operation of MG all the consumers, storage units, generation units and grid are considered as agents. Also, the consumer consumption preference has been considered as an important factor for decision-making. The algorithm helps reduce the power imbalance cost while considering consumer consumption preference as an important factor in the decision-making process. In [24], multi-objective hierarchical MAS-based EMS for a grid-connected MG system is presented to minimize its operational cost, emission cost and line losses. The hierarchical MAS is divided into

three levels: The upper level agent in a centralized control responsible for energy management of the whole system to maximize economical and environmental benefits, the middle level agent is responsible for operational mode switching of this region to maintain secure voltages and the lower level agent responsible of f/V and PQ-based control strategies for unit agents to manage real-time operation of DERs.

5 MG EMS Wireless Communication

Traditional power grids which only supported one-way communication are now evolving into smart grids with two-way communication infrastructure to support intelligent mechanisms for predicting failures and monitoring the condition of the network. Communication will play a vital role to transform the smart grids into a set of microgrids. One important aspect of concern in microgrid is the security, load sharing and the variability of DG's. The variability of power generation by the DG's influences two aspects which are a matter of concern, i.e., power flow management and voltage control in the microgrid. Therefore, effective communication combined with advanced control techniques is needed to maintain the stability and safe operation during islanded mode operation of the microgrid [25].

The communication network can be treated as the spinal cord of a MG. It connects the power generating sources, transmission, distribution and consumption systems to the management block in order to evaluate the real-time data that reflects the stability of the entire grid [26]. Information is exchanged bi-directionally among operators, energy generating sources and consumers. Microgrid communication networks can be divided into the following categories:

1. **Home Area Networks (HANs)**: Provides low bandwidth, two-way communication between the home appliances and equipment such as smart meters to collect the real-time data
2. **Field Area Networks (FANs)**: Provides low bandwidth, two-way communication between the microgrid control station and customer premises
3. **Wide Area Networks (WANs)**: Provides high bandwidth, two-way communication between the microgrid and utility grid.

To establish a reliable, secure and effective two-way communication for the information exchange, a communication subsystem in a microgrid must consist of the following requirements:

- Must support the quality of service (QoS) of data. This is because the critical data must be delivered promptly
- Must be highly reliable since large number of devices will be connected and will be communicating with different devices
- Must have a high coverage, so it can respond to any event in the microgrid
- Must guarantee security and privacy.

Communication technologies can be wired or wireless. Wireless technologies offer significant benefits over wired technologies such as rapid deployment, low installation cost, mobility, etc. Most commonly used wireless technologies are: Wireless mesh network, Cellular communications, Cognitive Radio, IEEE 802.15, Satellite communications and Microwave communications. Whereas, some of the most commonly used wired technologies are: Fiber-optic communications and power line communications.

6 MG EMS Test Case

As a case study, a MG EMS based on PSO is presented for grid-connected and islanded modes of operation, while considering a full-day load demand profile. The proposed EMS is required to verify load demand during 24 h operation with the lowest operating cost for the DGs, while taking into account the grid tariff and various system constraints [27].

6.1 Modeling of the Microgrid

The schematic diagram of the MG model used for the EMS is shown in Fig. 8.

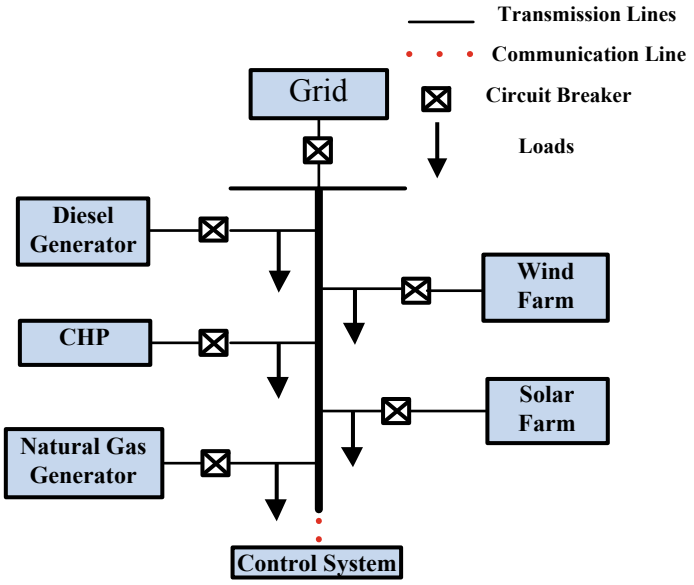

Fig. 8 Overall system [27]

Table 2 Rating of all the DGs in the system

Distribution generations	Minimum power (MW)	Maximum power (MW)
Combined heat and power	0.0	1.5
Diesel generation	0.0	1.0
Natural gas generation	0.0	1.0
Solar farm	0.0	0.5
Wind farm	0.0	0.5
Grid	−1.0	1.0

For this study, a typical MG model is used which includes different DGs such as: Combined heat and power (CHP) plant, diesel generator, natural gas-fired generator, photovoltaic (PV) generator, wind generator and energy storage system (ESS). The DGs are connected and integrated at the point of common coupling (PCC) to provide power to a cluster of loads. The rated power for DGs is shown in Table 2. The MG is capable to operate in two different modes:

- **Grid-connected mode** where the MG is able to buy power from the grid if demand exceeds available power or sell power back to the grid if production exceeds demand. The load demand in this mode is 4.35 MW.
- **Islanded mode** where it supplies power to only the critical loads. The load demand in this mode is 2.50 MW.

6.2 Mathematical Model of System

In this section, the mathematical modeling of the system is presented.

6.2.1 Generator Cost Function

The fuel cost function for the CHP, diesel generator and natural gas generator are typically approximated by a quadratic function, as stated in Eq. (1):

$$F_j(P_j) = \alpha_j + \beta_j P_j + \gamma_j P_j^2 \tag{1}$$

where j = generating source; P_j = power output of a source j; F_j = operation cost of source j in \$/h; α, β, γ are the cost coefficients in \$/h (shown in Table 3) [28].

Table 3 Cost figures for various generators

	CHP	Diesel generator	Natural gas
α ($/h)	15.30	14.88	9.00
β ($/h)	0.210	0.300	0.306
γ ($/h)	0.000240	0.000435	0.000315

6.2.2 Solar Generation Cost Function

The solar generation cost function is given by:

$$F(P_s) = a * I_p * P_s + G^e * P_s \tag{2}$$

$$a = \frac{r}{\left[1 - (1+r)^{-N}\right]} \tag{3}$$

where

P_s Solar generation (kW)
a Annuitization coefficient (dimensionless)
r Interest rate
N Investment lifetime (taken as $N = 20$ years)
I_p Investment costs, per unit installed power ($/kW)
G^e Operation and maintenance (O&M) costs, per unit generated energy ($/kW).

Equations (2) and (3) are used to calculate the total generating cost of the solar energy considering the depreciation of all the equipment for generation. In this system, the values for the investment **costs** per unit of installed power (I_p) and O&M costs per unit of generated energy (G^e) are assumed to be equal to $5000 and 1.6 cents per kW, respectively. Therefore, the final cost function can be derived, represented in Eq. (4) [29].

$$F(P_s) = 545.016 P_s \tag{4}$$

Figure 9 depicts the forecasted power for the solar farm for this study over an aggregated 24-h period. This data is not based on any one particular season or geographical area; however, it is a typical curve and is used here for discussion purposes. The seasonality over the year of particular geographical regions can also be accommodated, if desired.

6.2.3 Wind Generation Cost Function

The cost function for wind generation by Eqs. (2), and (3) is similar to solar generation. But, the investment costs per unit installed power (I_p) and O&M costs per unit generated energy (G^e) are assumed to be equal to $1400 and 1.6 cents per kW.

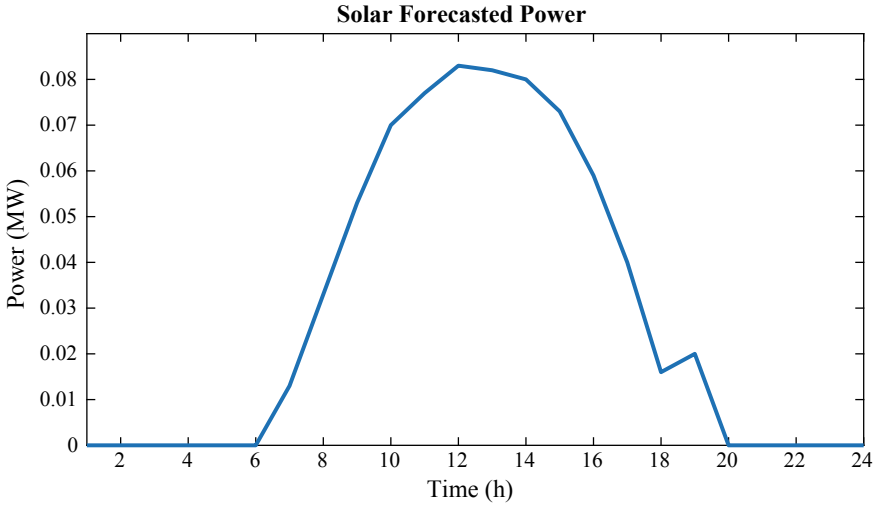

Fig. 9 Forecasted power for solar farm [27]

Therefore, the final cost function can be derived and is represented in Eq. (5) [29].

$$F(P_{\mathrm{w}}) = 152.616 P_{\mathrm{w}} \tag{5}$$

Figure 10 depicts the forecasted aggregated power for the wind farm for this study over a 24-h period. Again, this data is not based on any particular season or geographical area; however, it is typical, and it is just assumed here for test purposes.

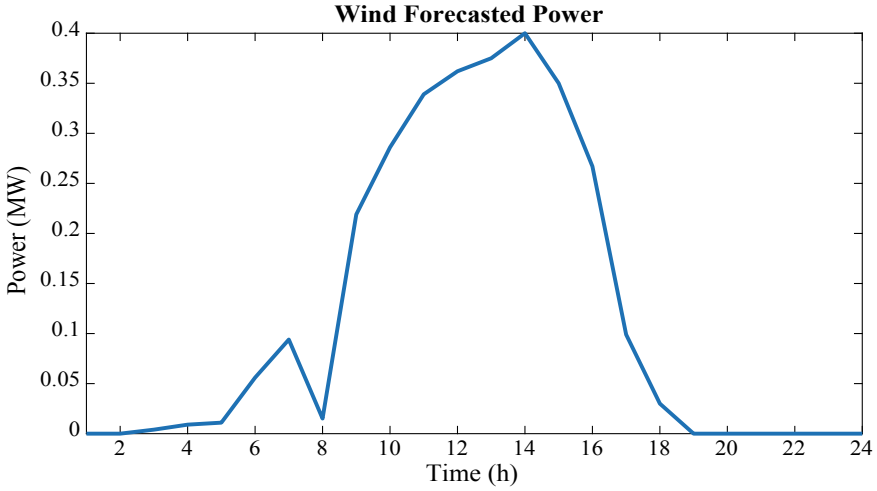

Fig. 10 Forecasted power for wind farm [27]

6.2.4 Constraints Function

The constraints functions are used to help guide the system to achieve the desired results.

A. *Grid-Connected Mode*

In grid-connected mode, the MG is able to buy/sell power from/to the main grid depending on the load demand. Hence,

$$P_{\text{generated}} \neq P_{\text{Load}} \tag{6}$$

If Eq. (6) is true then

$$P_{\text{grid}} = P_{\text{generated}} - P_{\text{Load}} \tag{7}$$

Therefore, if P_{grid} is positive, then microgrid is purchasing power from the grid and if P_{grid} is negative then microgrid is selling power to the grid.

B. *Islanded Mode*

Since, in islanded mode, the MG is disconnected from the main grid, there cannot be any buying/selling of power. Hence,

$$P_{\text{generated}} = P_{\text{Load}} \tag{8}$$

Thus, Eq. (8) must always be true.

C. *Power Generation Limits*

Each DG has a power rating as shown in Table 1.

$$P_j^{\min} \leq P_j \leq P_j^{\max} \tag{9}$$

6.3 Results of PSO

The load demand for a 24-h period, as used for both case studies, is presented in Fig. 11. It can be seen in Fig. 11 that load demand for the islanded mode is significantly lower than load demand during grid-connected mode. That is because when the system goes into islanded condition, then load shedding takes place and the system only supplies power to the critical loads.

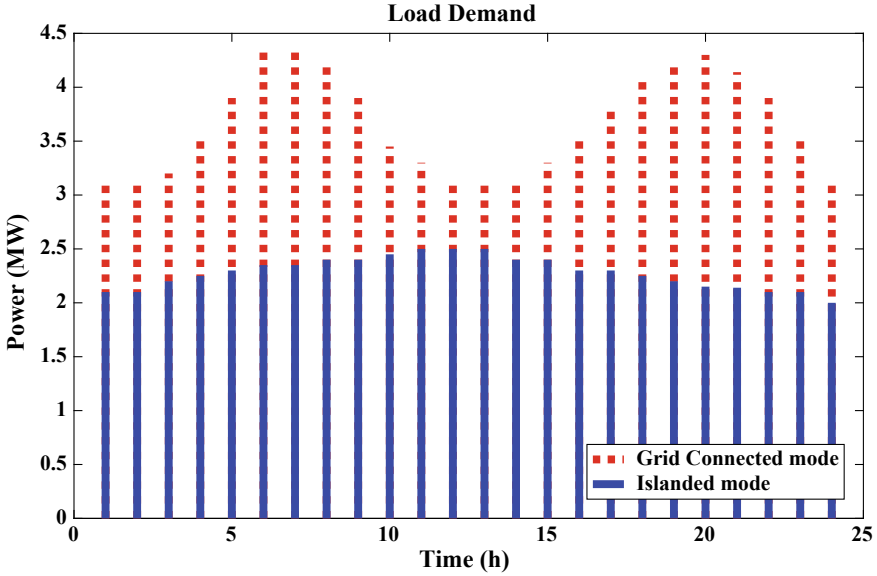

Fig. 11 Load demand [27]

6.3.1 First Case Study: Grid-Connected Mode

Figure 12 depicts the best output achieved from the EMS for grid-connected mode. The algorithm was able to find the optimal solution to dispatch DGs to satisfy the given load demand for the time period. It can be observed that the system is able to buy and sell power from the grid during off-peak and peak hours. The total cost of operation during the 24-h period achieved is $2297.96.

6.3.2 Second Case Study: Islanded Mode

Figure 13 depicts the best output achieved from the EMS for islanded mode of operation. The algorithm was able to find the optimal solution to dispatch every generator to satisfy the given load demand for each time interval. As can be observed, the three generators CHP (Gen1), diesel generator (Gen2) and natural gas generator (Gen3) are being rapidly ramped up and down to help for each time interval to help reduce or increase the generation to help satisfy the load. This ramping in the system has to be controlled by adding a ramp rate constraint in the algorithm, but for this study, the ramp rate has been ignored due to the use of a one-hour time step. The total operation cost achieved during the 24-h period for case is $2277.92.

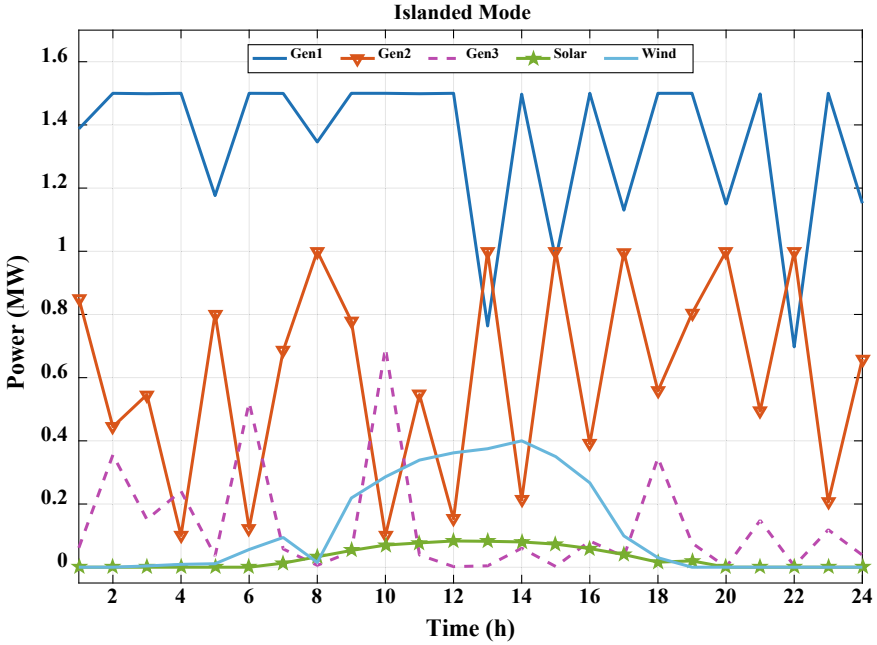

Fig. 12 Output of PSO (first case study) [27]

7 Conclusion

Microgrid management system (MGMS) operates the system autonomously connecting it to the utility grid appropriately for the bi-directional exchange of power and providing support to components within the microgrid. It enables the interplay of components and different controllers to operate the EMS in a safe and controlled manner. MGMS is broken down into three different subsystems, i.e., primary, secondary and tertiary control layers. Furthermore, the MGMS supervisory control can be subdivided into two types, namely, centralized and decentralized. Many researchers have used different approaches to achieve optimal and efficient operation of MGs. This chapter outlines some popular methods used by researchers to solve the EMS. A test case with a particle swarm optimization technique is provided. Also, the requirements for a communication system within the MG are briefly discussed.

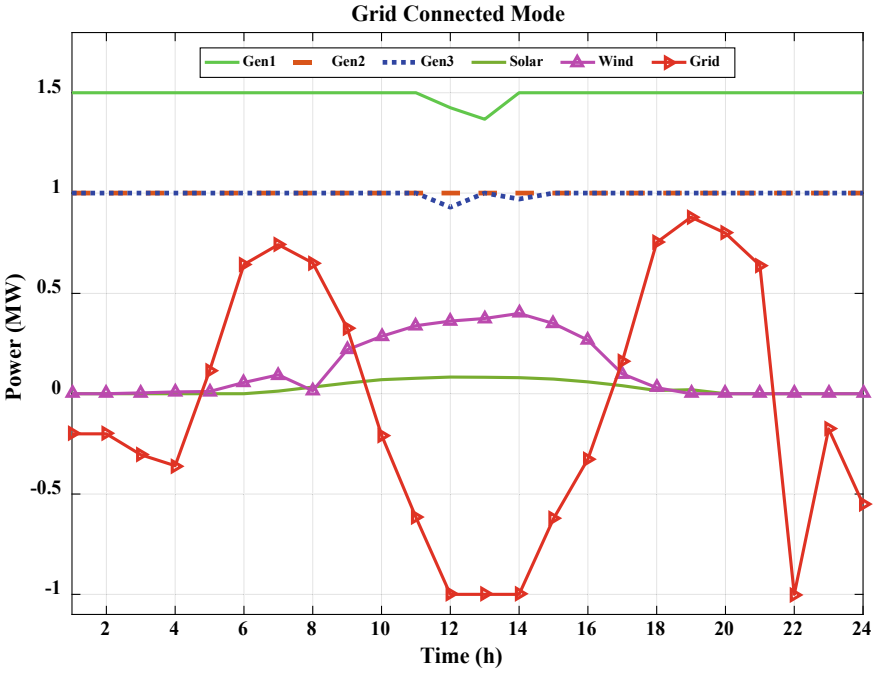

Fig. 13 Output of PSO (second case study) [27]

References

1. Nwulu N, Xia X (2017) Optimal dispatch for a microgrid incorporating renewables and demand response. Renew Energy 101:16–28. https://doi.org/10.1016/j.renene.2016.08.026
2. Basak P, Chowdhury S, Halder nee Dey S, Chowdhury S (2012) A literature review on integration of distributed energy resources in the perspective of control, protection and stability of microgrid. Renew Sustain Energy Rev 16:5545–5556. https://doi.org/10.1016/j.rser.2012.05.043
3. Ezhilarasan S, Palanivel P, Sambath S (2015) Design and development of energy management system for DG source allocation in a micro grid with energy storage system. Indian J Sci Technol. https://doi.org/10.17485/ijst/2015/v8i13/58252
4. Bhavsar YS, Joshi PV, Akolkar SM (2015) Simulation of microgrid with energy management system. In: International conference on energy systems and applications, ICESA 2015, pp 592–596
5. Monesha S, Kumar SG, Rivera M (2016) Microgrid energy management and control: technical review. In: IEEE international conference on automatica, pp 1–7
6. Olivares D, Mehrizi-Sani A, Etemadi A et al (2014) Trends in microgrid control. IEEE Trans Smart Grid 5:1905–1919. https://doi.org/10.1109/tsg.2013.2295514
7. Zia M, Elbouchikhi E, Benbouzid M (2018) Microgrids energy management systems: a critical review on methods, solutions, and prospects. Appl Energy 222:1033–1055. https://doi.org/10.1016/j.apenergy.2018.04.103
8. Meng L, Sanseverino E, Luna A et al (2016) Microgrid supervisory controllers and energy management systems: a literature review. Renew Sustain Energy Rev 60:1263–1273. https://doi.org/10.1016/j.rser.2016.03.003

9. Cheng Z, Duan J, Chow M (2018) To centralize or to distribute: that is the question: a comparison of advanced microgrid management systems. IEEE Ind Electron Mag 12:6–24. https://doi.org/10.1109/mie.2018.2789926
10. Katiraei F, Iravani R, Hatziargyriou N, Dimeas A (2008) Microgrids management. IEEE Power Energ Mag 6:54–65. https://doi.org/10.1109/mpe.2008.918702
11. Jimeno J, Anduaga J, Oyarzabal J, de Muro A (2011) Architecture of a microgrid energy management system. Eur Trans Electr Power 21:1142–1158. https://doi.org/10.1002/etep.443
12. Igualada L, Corchero C, Cruz-Zambrano M, Heredia F (2014) Optimal energy management for a residential microgrid including a vehicle-to-grid system. IEEE Trans Smart Grid 5:2163–2172. https://doi.org/10.1109/tsg.2014.2318836
13. Shen J, Jiang C, Liu Y, Qian J (2016) A microgrid energy management system with demand response for providing grid peak shaving. Electr Power Compon Syst 44:843–852. https://doi.org/10.1080/15325008.2016.1138344
14. Tsikalakis AG, Hatziargyriou ND (2011) Centralized control for optimizing microgrids operation. In: 2011 IEEE power and energy society general meeting, pp 1–8
15. Panwar L, Konda S, Verma A et al (2017) Operation window constrained strategic energy management of microgrid with electric vehicle and distributed resources. IET Gener Transm Distrib 11:615–626. https://doi.org/10.1049/iet-gtd.2016.0654
16. Strelec M, Berka J (2013) Microgrid energy management based on approximate dynamic programming. In: 2013 4th IEEE/PES innovative smart grid technologies Europe (ISGT EUROPE), pp 1–5
17. Chalise S, Sternhagen J, Hansen T, Tonkoski R (2016) Energy management of remote microgrids considering battery lifetime. Electr J 29:1–10. https://doi.org/10.1016/j.tej.2016.07.003
18. Radosavljević J, Jevtić M, Klimenta D (2015) Energy and operation management of a microgrid using particle swarm optimization. Eng Optim 48:811–830. https://doi.org/10.1080/0305215x.2015.1057135
19. Tiwari N, Srivastava L (2016) Generation scheduling and micro-grid energy management using differential evolution algorithm. In: 2016 IEEE international conference on circuit, power and computing technologies (ICCPCT), pp 1–7
20. Marzband M, Yousefnejad E, Sumper A, Domínguez-García J (2016) Real time experimental implementation of optimum energy management system in standalone microgrid by using multi-layer ant colony optimization. Int J Electr Power Energy Syst 75:265–274. https://doi.org/10.1016/j.ijepes.2015.09.010
21. Fossati J, Galarza A, Martín-Villate A et al (2015) Optimal scheduling of a microgrid with a fuzzy logic controlled storage system. Int J Electr Power Energy Syst 68:61–70. https://doi.org/10.1016/j.ijepes.2014.12.032
22. Venayagamoorthy G, Sharma R, Gautam P, Ahmadi A (2016) Dynamic energy management system for a smart microgrid. IEEE Trans Neural Netw Learn Syst 27:1643–1656. https://doi.org/10.1109/tnnls.2016.2514358
23. Ghorbani S, Rahmani R, Unland R (2017) Multi-agent autonomous decision making in smart micro-grids energy management: a decentralized approach. In: German conference on multiagent system technologies. Springer, pp 223–237
24. Dou C, Liu B (2013) Multi-agent based hierarchical hybrid control for smart microgrid. IEEE Trans Smart Grid 4:771–778. https://doi.org/10.1109/tsg.2012.2230197
25. Safdar S, Hamdaoui B, Cotilla Sanchez E, Guizani M (2013) A survey on communication infrastructure for micro-grids. In: 2013 9th international wireless communications and mobile computing conference (IWCMC), Sardinia, pp 545–550
26. Fang X, Misra S, Xue G, Yang D (2012) Smart grid—the new and improved power grid: a survey. IEEE Commun Surv Tutor 14:944–980. https://doi.org/10.1109/surv.2011.101911.00087
27. Ali Mohammad Y, Khan F, Sood VK (2018) Energy management system of a microgrid using particle swarm optimization and wireless communication system. In: 2018 IEEE electrical power and energy conference (EPEC), Toronto, ON, pp 1–7

28. Gaing Z (2003) Particle swarm optimization to solving the economic dispatch considering the generator constraints. IEEE Trans Power Syst 18:1187–1195. https://doi.org/10.1109/tpwrs.2003.814889
29. Augustine N, Suresh S, Moghe P, Sheikh K (2012) Economic dispatch for a microgrid considering renewable energy cost functions. In: 2012 IEEE PES innovative smart grid technologies, pp 1–7

Uninterrupted Power Supply to Microgrid

Shubham Ghore and Monalisa Biswal

Abstract This chapter provides a detailed review report on various methods used to provide uninterruptible power supply to the microgrid. The methods majorly deal with the energy storage system (ESS) and its application in the microgrid to reduce the power interruptions. This chapter also signifies the use of line adaptive reclosing scheme which optimizes the use of ESS providing improved efficiency and savings in cost. Finally, a backup line-based UPS system is introduced to enhance the resilience and reliability of microgrid.

Keywords Microgrid · Energy storage system · Line adaptive reclosing · Uninterruptible power supply · Distributed energy resources

Nomenclature

BESS	Battery Energy Storage System
CAES	Compressed Air Energy Storage
CB	Circuit Breaker
DER	Distributed Energy Resource
DG	Distributed Generation
ESS	Energy Storage System
FESS	Flywheel Energy Storage
HESS	Hybrid Energy Storage System
HSS	Hydrogen Energy Storage System
LVRT	Low Voltage Ride Through
PCC	Point of Common Coupling
PHS	Pumped Hydro Energy Storage

S. Ghore (✉) · M. Biswal
Department of Electrical Engineering, National Institute of Technology Raipur, Raipur, Chhattisgarh 492010, India
e-mail: shubhamghore@gmail.com

M. Biswal
e-mail: monalisabiswal22@gmail.com

P. Ray and M. Biswal (eds.), *Microgrid: Operation, Control, Monitoring and Protection*, Lecture Notes in Electrical Engineering 625,
https://doi.org/10.1007/978-981-15-1781-5_10

PV Photovoltaic
PWM Pulse Width Modulation
SC/UC Supercapacitor/Ultracapacitor
SMES Superconducting Magnetic Energy Storage
SODT Second-Order Difference of THD
TES Thermal Energy Storage System
THD Total Harmonic Distortion
UPS Uninterruptible Power Supply

1 Introduction

A microgrid is a localized group of interconnected distributed energy resources (DERs) and loads, which is normally connected to the electrical grid to draw or supply power, but it can also function autonomously by disconnecting itself from the main grid and operate in isolated or islanding mode when required. The structure of a typical microgrid is shown in Fig. 1.

Use of microgrid improves power quality, reliability, resilience, and financial performance. Since it has localized generations, the microgrid system is highly reliable and efficient. It promotes clean energy by integrating renewable sources. It also strengthens the central grid by providing ancillary and bulk energy services and by participating in demand response programs. During outages in the utility supply, it can locally feed the critical loads. However, the protection and resynchronization to the utility grid are challenging issues. As the renewable distributed generators are highly affected by weather and climatic changes, its fluctuations and intermittency may cause instability in the grid, especially in islanding mode.

Different research works are being accomplished on to reduce the grid interruption. Firstly, various energy storage techniques and backup generators are employed for this purpose. The battery storage system is one of them but its use is limited primarily due to its cost. Then, the attention was drawn towards flywheel and other

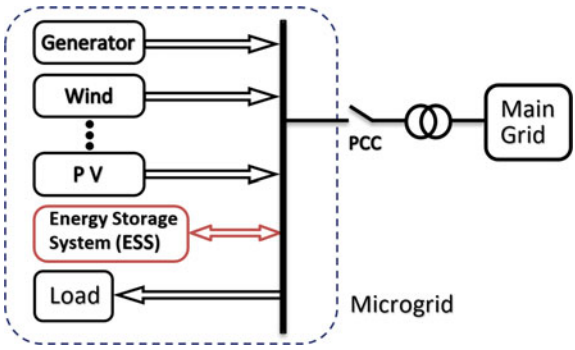

Fig. 1 Typical structure of microgrid

energy storage systems, but due to its low energy density and high initial cost, its use is also limited. Then, for getting faster response and better efficiency, the use of supercapacitor energy storage has been encouraged. Although, with the advancement in battery technologies, battery energy storage system (BESS) is achieving higher efficiency and higher power density at a lower cost. Research and development are being carried out to minimize the power interruptions at a reduced cost. Secondly, the adaptive reclosing scheme is used to make the reclosers smart enough to reclose the breaker as soon as the transient fault gets cleared. Thirdly, the microgrid network can be made robust by using interconnecting tie lines and a different source connected through a backup line. The detailed survey report is discussed in the next section.

2 Literature Survey

In the literature, several research works are reported which encourage the use of ESS in power grid. A practical implementation of grid-interactive PV UPS system has been presented by Ref. [1] which uses BESS and a backup diesel generator. Two such systems are working satisfactorily in two Indian cities since May 1997. Reference [2] highlights the key factors, issues, and challenges with possible recommendations for the further development of ESS in future microgrid applications. It also reviewed various ESS technologies and their configurations with their advantages and disadvantages.

Various adaptive reclosing schemes have been proposed to reduce the dead time by detecting the instant fault clearance in the transmission system [3–13]. But due to several reasons like short length and dissimilar configurations of distribution network, the same adaptive reclosing technique cannot be applied in the distribution system. Therefore, very few studies have been performed for implementing the adaptive reclosing scheme in the distribution system. Reference [14] uses wavelet transform and THD calculation to detect the instant of fault clearance. The method proposed for adaptive reclosing in [15] uses SODT (second-order difference of THD). In [16] an adaptive reclosing method for unbalanced distribution system is presented. Methods presented in [14–16] are successfully implemented in EMTP/ATPDraw software. Details of these methods are discussed in Sect. 4.2.

In the last segment of this chapter, a backup and tie line-based UPS system is briefly introduced which can greatly enhance the resilience of the microgrid.

3 Energy Storage System (ESS)

Energy storage system (ESS) is an essential part of power distribution system and renewable interconnected grid which ensures the uninterruptible supply of power. ESS used in a microgrid provides benefits for power quality, voltage regulation, reactive power support, and operating reserves. In the event of failure of utility supply,

start-up of backup generators (diesel gensets) may take some time. Therefore, there have to be some arrangements for supplying critical loads like the hospitals and the banks for some time while the diesel engines are started. This is where the ESS has its another application, as in the uninterruptible power supply (UPS) system which uses stored energy of ESS to bridge the time between the utility failure and the availability of generator power and maintain uninterrupted power supply. Since the microgrid is in islanding mode, we do not have to worry about synchronization and frequency issues as it is handled by the UPS, and the backup power can be restored much faster than it would be otherwise. The challenge here is to minimize the unnecessary usage of ESS as there is considerable wastage of energy during its charging and discharging process. We also have to consider the cost, life cycle, reliability, size, safety, and overall management.

3.1 Types of Energy Storage Systems

The energy storage system uses energy storing devices such as batteries, flywheels, super/ultracapacitors, etc., to store the surplus energy and provide it when needed. It can perform different tasks depending on its application in a microgrid. When it is combined with DGs, it suppresses the fluctuations and complements the DGs.

There are many techniques used for energy storage out of which most commonly used are:

- Pumped Hydro Energy Storage (PHS)
- Compressed Air Energy Storage (CAES)
- Battery Energy Storage System (BESS)
- Superconducting Magnetic Energy Storage (SMES)
- Super/UltraCapacitor Energy Storage (SC/UC)
- Flywheel Energy Storage (FESS)
- Thermal Energy Storage System (TES)
- Hydrogen Energy Storage System (HSS)
- Hybrid Energy Storage System (HESS).

The advantages and disadvantages of the above mentioned ESS technologies are summarized in Table 1. The comparison of discharge duration and power rating of these technologies is also shown in Fig. 2. The hybrid energy storage system (HESS) uses the advantages of two or more technologies but it becomes costly. HESS has been recommended by many researchers who aim at improving the life expectancy of batteries. The typical structure of HESS is shown in Fig. 3.

Table 1 Comparison of different ESS technologies

ESS technology	Advantage	Disadvantage
PHS	Large capacity	High investment, large geographical area
CAES	High capacity, long continuous discharge time	Limited locations, high response time
BESS	High energy density, efficient	Power density, poor life cycle
SMES and SC/UC	High power density, quick response, high cycling times	Low energy density, expensive
FESS	High power density, quick response	Low energy density
TES	High energy density, low cost	Low life expectancy
HSS	High energy density, eco-friendly	Costly, low efficiency

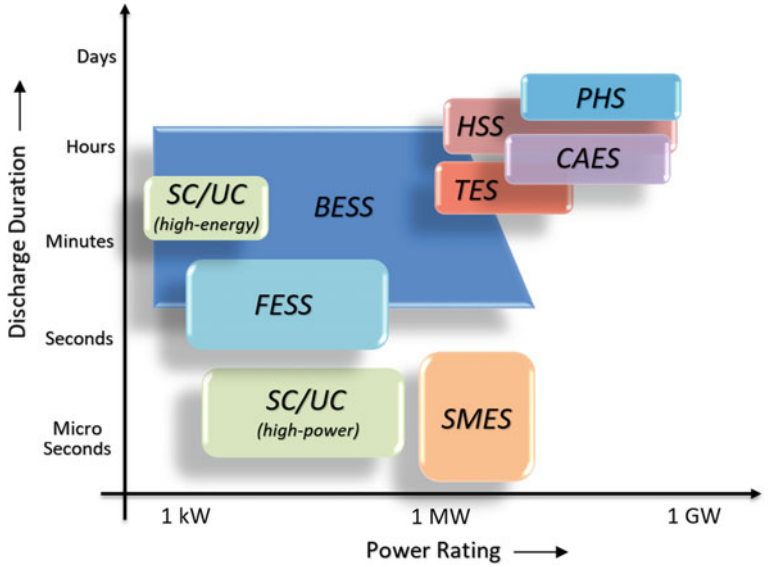

Fig. 2 Comparison of sizing and discharge duration of ESS technologies

3.2 Configurations of ESS

The ESS is typically configured in either aggregated manner or in a distributed manner. In aggregated configuration (shown in Fig. 4a), a single ESS of large capacity is connected to the PCC of the microgrid via a suitable VSC. It consists of a large number of storage units which can store a huge amount of energy. The amount of power flow from DGs to PCC bus remains almost constant. It can supply critical loads during the failure of utility supply until the backup generator starts. It can complement PV microgrid by storing energy in the daytime and supplying in the

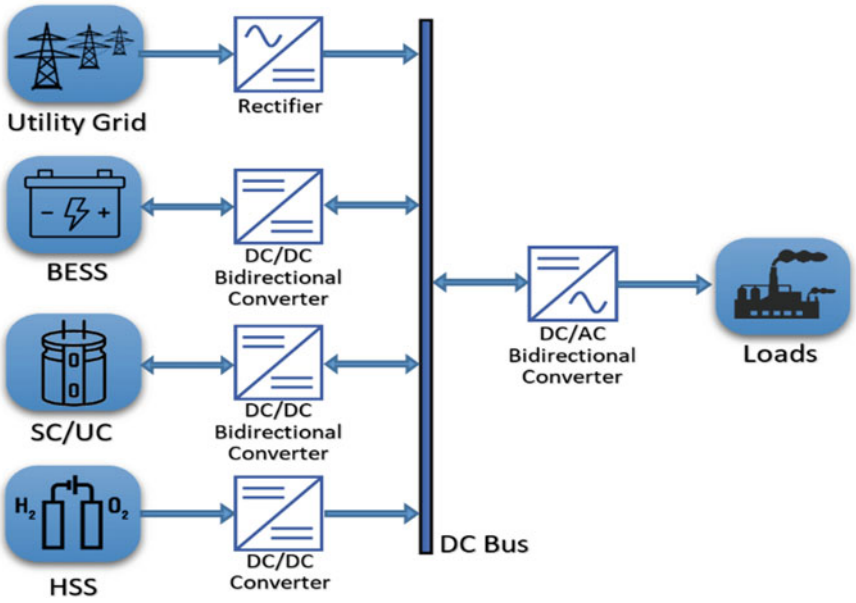

Fig. 3 Hybrid energy storage system

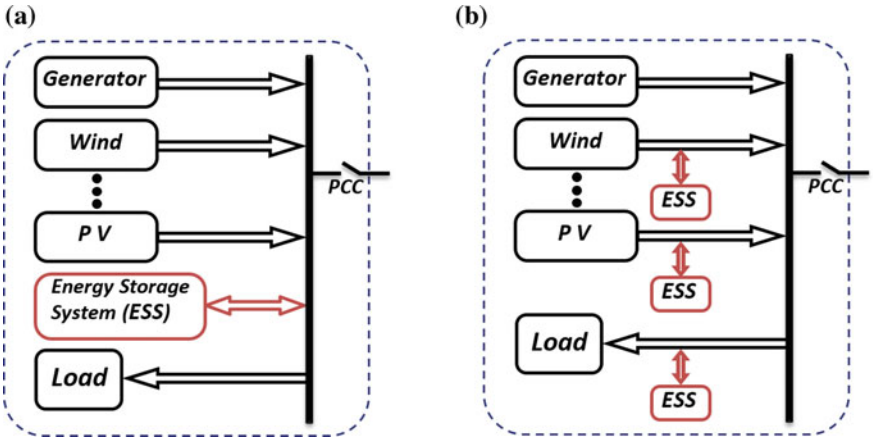

Fig. 4 **a** Aggregated ESS configuration; **b** distributed ESS configuration

night time. With an increase in capacity, it becomes more costly, and it is difficult to manufacture and control. As it can use its full capacity to mitigate fluctuations, it is more effective than the distributed type.

The distributed ESS as shown in Fig. 4b is of much smaller capacity than the aggregated ESS. The distributed ESS type is easier in handling and controlling than the aggregated type. The generator side distributed ESS is installed on-site with each

DGs for suppressing the fluctuations. It is connected directly to the DC link of specific DGs with suitable interfaces. It enhances the low voltage ride through (LVRT) ability for solar and wind power generation. Load side distributed ESS is connected to the local loads. Its main objective is to supply the rapidly changing local load demands, thus reducing the stress on DGs.

3.3 Applications of ESS

There are vast applications of ESS in a microgrid. Apart from fluctuation suppression, ESS can be used for energy management functions like load leveling and peak shifting resulting in significant cost savings. Figure 5 shows the implementation of peak-shifting technique by charging the ESS at off-peak hours (at lower electricity price) and discharging at peak hours (at higher electricity price). Load leveling is also similar to peak shifting but it used for a short time period.

Other major applications of ESS include enhancing LVRT ability of wind generators, in the uninterrupted power supply system, power quality improvement, voltage regulation, reactive power support, and operating reserves.

The use of ESS as uninterruptible supply system is limited due to its high cost. However, with constant improvements in battery storage technologies, the energy density is getting better at a reduced cost.

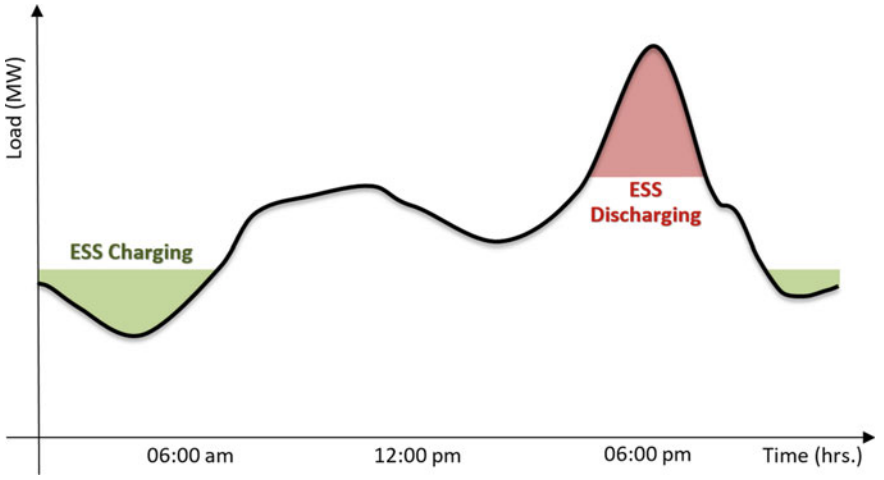

Fig. 5 Using ESS for peak shifting

3.4 Advantages of ESS

The various advantages of ESS are:

3.4.1 Transmission Congestion Relief

Transmission congestion occurs when the energy demand will be high but the available transmission facility is inadequate to carry it efficiently and economically. The presence of ESS in the downstream side can help in reducing the peak demand and relief congestion (similar to peak shifting as shown in Fig. 5).

3.4.2 Improved Power Quality

Poor power quality can be due to voltage variations (spikes, surges, and sags), frequency variation, low power factor, presence of harmonics, or due to interruptions in service. All these issues can be reduced significantly by using ESS.

3.4.3 Better Power Reliability

ESS used in microgrids can supply loads during outages in islanding mode for a short time. ESS supplemented by diesel gensets further increases the power reliability for longer outages.

3.5 ESS-Based UPS System

Uninterruptible power supply (UPS) system is an important application of ESS in a microgrid. In islanding mode, as the power is solely supplied by renewable energy DGs, there are chances that the output of RES may suddenly fall due to wind stoppage in case of wind generation and cloudy weather in case of PV generations or due to some other faults in the system. Even in grid-connected mode, in the event of faults in the utility grid, the external breaker trips. This can cause outages in the microgrid. Therefore, there is a need for an intelligent arrangement that senses this condition and connects some other power source to the grid. Generally, a diesel generator is employed for this purpose, but the problem is that it cannot be started instantly. It takes around 10 s for starting and developing full power [17]. So, to bridge this time gap, the stored energy of ESS is used. Now in order to coordinate these power sources (DGs/utility grid, diesel gensets, and ESS), an intelligent set-up known as uninterruptible power supply (UPS) is used. It has transfer switches that are normally

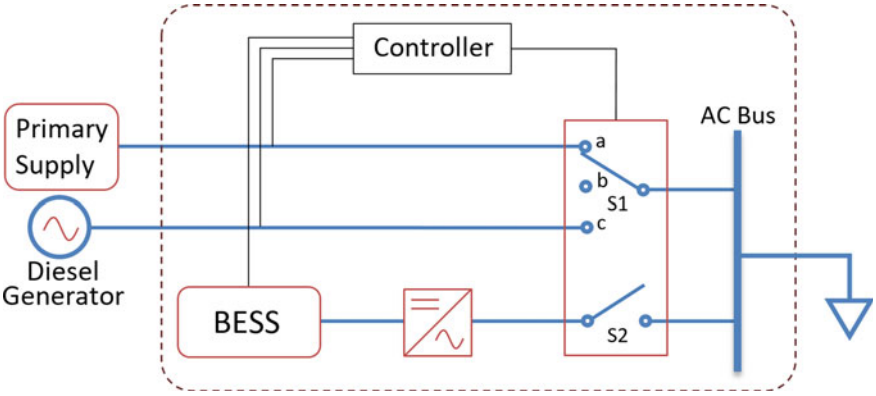

Fig. 6 Schematics diagram of UPS system in a microgrid

connected to the primary supply (DGs in islanded mode and utility supply in grid-connected mode), and in the event of failure of primary supply, it instantly switches to the ESS and waits for the backup diesel gensets to start. It switches to the diesel generator once it is fully operational and waits for the primary supply to get restored. In case the primary supply is restored before the diesel gensets starts, the transfer switch is directly switched from ESS to primary supply. Once the primary supply is restored, the ESS is again charged. Figure 6 shows a schematic diagram of a simple UPS configuration for a microgrid.

In the scheme, the controller continuously monitors the voltages of the power sources. If there is voltage sag in primary supply, S1 opens and S2 closes connecting BESS to AC bus via a bidirectional converter. If the voltage gets normal in short time (before diesel generator starts), then S1 is switched back to 'a', and once BESS gets fully charged, S2 opens. If voltage sag persists, then controller waits for diesel generator voltage buildup and then switches to 'c' and S2 opens. As primary supply gets restored, S1 comes back to 'a' and S2 is closed till BESS gets charged and then opens. Here, the BESS can also be charged by the diesel generator, but generally, it is not preferred as it is not economical.

3.5.1 Bidirectional Converter Topology

The utility grid, diesel generator, and the BESS (via converter) are connected in parallel to the supply to the load as shown in Fig. 7 [1]. The AC bus terminals are connected to the output terminals of the converter, and the converter is synchronized with the grid. When the primary supply is available within the specified tolerances of voltage and frequency, it will deliver the active power demanded by load and the converter will supply the required reactive power minimizing the cycling power flowing through the BESS. The converter keeps the load voltage constant.

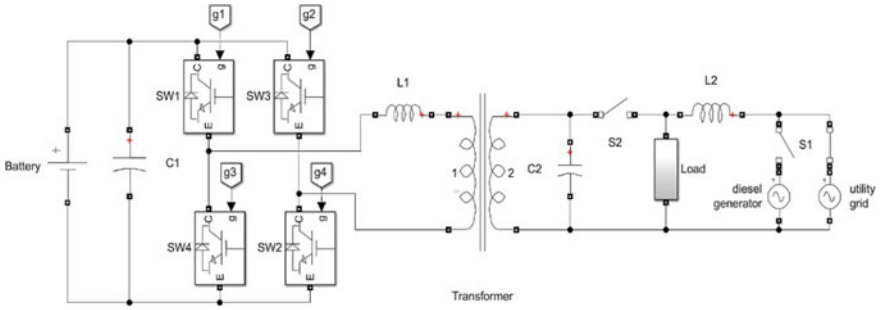

Fig. 7 Bidirectional converter topology

If any irregularities in the grid supply like under/over voltage or frequency conditions, power interruptions are detected by the controller, the utility grid is isolated from the microgrid, and the converter works as a stand-alone inverter. If this irregularity persists for a long time, then the diesel generator is started and synchronized with a converter. The switch S1 is generally an electromechanical switch which permits either utility grid or diesel generator to be connected to the microgrid.

The converter allows bidirectional power flow for charging and discharging of BESS. The converter is controlled by the PWM technique. When utility grid supply is available, no active power flows from the battery, but it should remain connected to compensate reactive power demanded.

3.5.2 Battery Energy Storage System (BESS)

A battery energy storage system uses a large number of batteries to store electrical energy in the form of chemical energy in stacked cells. This stored energy can be utilized at a later time. The comparison of various battery technologies is summarized in Table 2 [18].

Table 2 Comparison of different battery technologies

Battery type	Energy density (kW/kg)	Life span (years)	Efficiency (%)
Li-ion	150–250	10–15	95
NaS	125–150	10–15	75–85
Flow	60–80	20–25	70–75
Ni-Cd	40–60	5–10	60–80
Lead acid	30–50	3–6	60–70

3.5.3 Calculation of Battery Capacity

The capacity of BESS can be calculated as:

$$\text{BESS Capacity [MWh]} = \frac{\text{power required [MW]} * \text{duration required [h]}}{\text{depth of discharge [\%]} * \text{battery efficiency [\%]}}$$

3.5.4 Fault Current Contribution from BESS

When battery energy storage system (BESS) is used as UPS, the BESS is interfaced with distribution system via power electronic devices (i.e. inverters) which inherently do not have any inertia as in the case with conventional synchronous generators and induction machines. Consequently, in an inverter-based distributed generation (DG), the fault current does not increase beyond 1.5–2 times of the inverter full load rated current for one cycle or less. The inverter-based distributed generation could produce 1.2 p.u. peak current for a period of approximately seven cycles. Since the discharge characteristic of BESS is very similar to that of inverter-based DG, the studies show that the fault current contribution from BESS is less than 1.2 p.u. which is marginally more than its rated current, and hence, overcurrent relay cannot work with BESS, and it will continue to supply the fault.

4 Auto-Reclosing Scheme

As BESS is of limited capacity and has associated losses in charging and discharging, it should not be used unnecessarily. More than 80% of faults on overhead distribution circuits are temporary (transient) in nature which may be caused by tree limb contact, animal interference, wind bringing bare conductors in contact, or by lightning. But due to the fixed dead times of conventional reclosers, the BESS often gets unnecessarily used even when fault gets cleared, waiting for reclosers to close the breaker, and a significant amount of energy is wasted. This can be avoided by using line adaptive reclosing scheme.

4.1 Conventional Reclosing Scheme

Auto-reclosers are basically a type of circuit breakers that are equipped with mechanisms to automatically perform a pre-programmed sequence of opening and closing operations after it has been opened due to a fault. The operating sequence of a typical two-shot reclosing scheme is given as O–t_1–C O–t_2–C O. The first dead time (t_1) is programmed to be around 0.5 s which is sufficient for any transient fault to clear

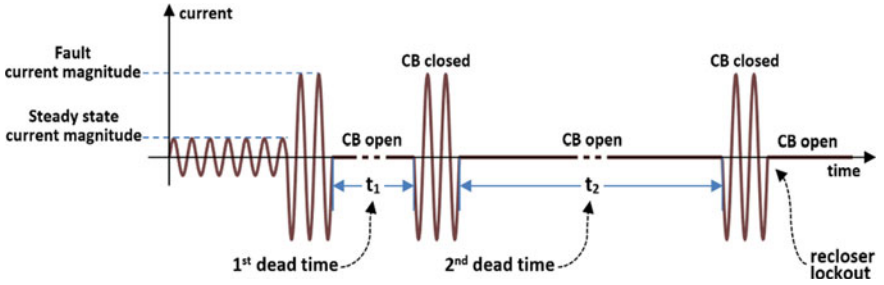

Fig. 8 Operating sequence of a typical 2-shot auto-recloser

and then a reclosing is attempted. If the fault persists, the CB opens and waits for the second dead time (t_2), which is programmed to be around 10–15 s. This dead time (t_2) gives sufficient time to a sectionalizer or a CB to isolate any downstream fault or any semi-permanent fault to clear. Then again, a reclosing is attempted. If the fault still persists, then the recloser opens and locks out to avoid any further automated reclosing attempt. Figure 8 [19] shows the operating sequence of a typical auto-recloser.

4.2 Line Adaptive Reclosing Scheme

The conventional reclosing scheme does not know when exactly the fault gets cleared and waits for the predefined dead time for reclosing, causing increased outage time. As discussed previously, the microgrid initially uses ESS to supply the grid in case of a fault in utility supply. So, if the conventional reclosing scheme is implemented, ESS is used unnecessarily from the instant of fault clearing to reclosing of recloser (or the start of diesel gensets). On the contrary, line adaptive reclosing scheme can sense the exact instant of fault getting cleared and recloses the breaker which avoids the unnecessary losses. By using this method, not only a significant amount of stored energy can be saved but also the energy that would have been used to recharge ESS, and the energy lost in conversion cycle can be saved. Apart from this, the conventional reclosing scheme cannot be used in applications where there is the presence of different power sources at either end of the recloser. In an islanded microgrid, one end of recloser is connected to utility supply and the other end is connected to the ESS or generator supply of microgrid. Additionally, the line adaptive reclosing scheme has provision for synchronizing the two supplies before reclosing.

For implementing line adaptive reclosing, the conventional recloser needs to be replaced with a CB and a protective relay, and a suitable communication method is required. In Ref. [15] an adaptive reclosing technique is introduced to overcome the limitations of the conventional reclosing scheme. During a fault, the healthy phase is fed by BESS reducing the outage time significantly. In this method of fault clearance detection, THD of BESS current at fault condition is used to provide adaptive dead

time. The protective relay receives the current $i_1(t)$ and voltage $v_1(t)$ from the system and the current $i_2(t)$ and voltage $v_2(t)$ from the BESS as the input. Then, the voltage phasors and the frequency of both the system and BESS are calculated. The RMS values of the system current ($I_{1\text{RMS}}$) and the THD value of BESS current ($I_{2\text{THD}}$) are calculated. When a fault occurs, the system circuit breaker is opened. For the detection of the faulty phase, the following conditions are checked,

$$I_{1\text{RMS\_A}} \text{ or } I_{1\text{RMS\_B}} \text{ or } I_{1\text{RMS\_C}} > \alpha \tag{1}$$

where α is the relay pickup current value and $I_{1\text{RMS\_A}}$, $I_{1\text{RMS\_B}}$, and $I_{1\text{RMS\_C}}$ are RMS values of system currents for A, B, and C phase, respectively.

Then, using a moving window, the second-order differences of THD (SODT) of the faulted phase current are calculated. The SODT for k^{th} sample is calculated as:

$$\text{SODT}\,[k] = I_{2\text{THD}}\,[k] - I_{2\text{THD}}\,[k-2] \tag{2}$$

At the instant of fault clearance, the value of $I_{2\text{THD}}$ is suddenly increased, and

$$\text{SODT} > \beta_{\text{THD}} \tag{3}$$

where β_{THD} is a threshold value for THD.

If this condition persists for a certain predefined duration, fault clearance is judged, and reclosing is attempted after a synchronism check. For a successful synchronization of the two segments of the grid on either side of the breaker, the following conditions should satisfy:

$$|f_1 - f_2| < \gamma_{\text{frequency}} \tag{4}$$

$$|(|V_1| - |V_2|)/|V_2|| < \gamma_{\text{voltage}} \tag{5}$$

$$|\theta_1 - \theta_2| < \gamma_{\text{angle}} \tag{6}$$

where f_1, V_1, and θ_1 are the frequency, voltage, and phase angle corresponding to segment-1, and f_2, V_2, and θ_2 are the frequency, voltage, and phase angle corresponding to segment-2, respectively, during synchronization. The terms $\gamma_{\text{frequency}}$, γ_{voltage}, and γ_{angle} denote the maximum allowed deviations in frequency, p.u. voltage, and phase angle for a smooth synchronization of the two segments of the grid.

The method proposed by Ref. [14] has a similar approach. Here, instead of calculating the SODT of BESS current at fault condition, wavelet transform followed by THD calculation is used to classify whether the fault is of transient or permanent nature.

In the method presented in [14], the phase and neutral currents are taken as input. The phase current is used for overcurrent relaying logic (same as Eq. 1). A level-2 Haar MW wavelet transform is performed on neutral current. For the detailed

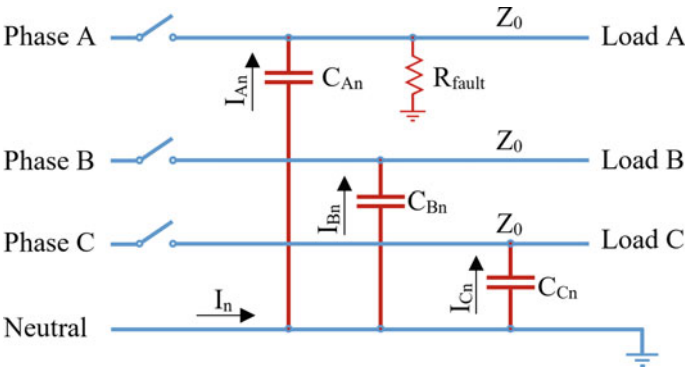

Fig. 9 Equivalent circuit of the isolated faulty section

coefficient obtained by wavelet transform, the THD is calculated. Then, this THD value is used to distinguish the transient and permanent fault.

For a transient fault,

$$\mathrm{THD}_{\mathrm{calculated}} > \varepsilon_{\mathrm{THD}} \tag{7}$$

where $\varepsilon_{\mathrm{THD}}$ is a threshold value for THD.

If the THD (or SODT) calculated by these logics does not satisfy the transient fault condition in 15 s after the first unsuccessful reclosing attempt, the logic is terminated and the recloser locks out.

Reference [16] presented an adaptive reclosing algorithm for the unbalanced distribution system. From Fig. 9, the technique works on the principle of electrostatic induction between the three-phase lines and the neutral line of the distribution system.

Due to the unbalanced state of the upstream healthy section, neutral current exists even if the faulty section is isolated. The current flowing in the neutral conductor is divided into the three-phase currents.

$$I_{\mathrm{n}} = I_{\mathrm{An}} + I_{\mathrm{Bn}} + I_{\mathrm{Cn}} \tag{8}$$

The current flowing in the faulty phase due to electrostatic induction can be written as,

$$I_{\mathrm{An}} = \frac{V_{\mathrm{n}}}{\frac{1}{\mathrm{j}\omega C_{\mathrm{An}}} + Z_0 \| R_{\mathrm{fault}}} \tag{9}$$

whereas the current flowing in other phases can be written as,

$$I_{\mathrm{Bn}} = \frac{V_{\mathrm{n}}}{\frac{1}{\mathrm{j}\omega C_{\mathrm{Bn}}} + Z_0} \tag{10}$$

$$I_{\mathrm{Cn}} = \frac{V_{\mathrm{n}}}{\frac{1}{\mathrm{j}\omega C_{\mathrm{Cn}}} + Z_0} \tag{11}$$

where V_{n} is neutral voltage.

The values of mutual capacitances (C_{An}, C_{Bn}, and C_{Cn}) are very small and similar. The value of fault resistance (R_{fault}) is generally much smaller than the characteristic impedance (Z_0) of line. Therefore, the current flowing in the faulty phase will be greater than that of healthy phases. As soon as the fault gets cleared, all the three currents get similar. This change in current can be used to detect the instant of fault clearance.

Reference [19] proposed a method to avoid the flow of large fault current during the unsuccessful reclosing attempt of reclosers by using two CBs at either end of the distribution line. During a fault, both the CBs are opened simultaneously. But when reclosing is attempted, only the load side CB is closed first to reduce the fault current in case the fault persists. If the reclosing attempt by load side CB is successful, the source side CB is closed after the synchronization check. In this scheme, instead of detecting the fault by large fault current, the magnitude of load current supplied by BESS is observed. When load side CB is opened, the steady-state three-phase load current is supplied. If during reclosing, the fault persists, the load current of the faulty phase will be diverted to the fault. This change in load current can be used to judge the status of fault. This method significantly reduces the fault current as the fault current through BESS is limited by the bidirectional converter (as discussed in Sect. 3.5.4). This avoids the damage caused by large fault current supplied by source if unsuccessful reclosing is attempted by source side CB.

5 Backup Line-Based UPS System

In backup line-based UPS system, an additional bypass line is installed which is connected between the main bus and dead end of the microgrid system through a reserve bus. This arrangement provides an easy solution to temporarily reroute the power flow from the main line to the backup line during maintenance or failure of the main bus. The application of this UPS system is illustrated on an IEEE standard 33-bus system as shown in Fig. 10. Here, with the help of a backup line, tie lines, communication link, and a reserve bus connected to a different feeder, a highly resilient microgrid network can be formed.

In case the main bus or feeder is faulty or under maintenance, the main CB is opened and bypass CB is communicated to connect the second feeder via a reserve bus and backup line. Additionally, the tie lines provide multiple redundant paths to extend the line and minimize the power interruptions in the healthy section of the microgrid.

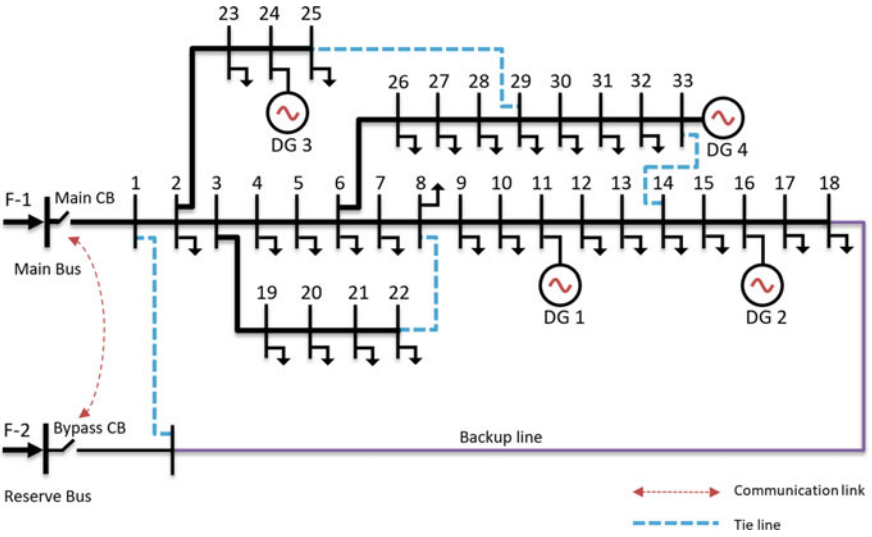

Fig. 10 Backup line-based UPS system

6 Conclusion

In this chapter, various techniques to provide uninterruptible power supply to the microgrid have been reviewed along with the comparison of different ESS technologies used for this purpose. The use of line adaptive reclosing scheme instead of conventional reclosing scheme is justified as it minimizes the usage of BESS during a transient fault condition, avoiding unnecessary losses. Various schemes have been discussed to provide the adaptive dead time to the auto-recloser by detecting the exact time of fault clearance. Additionally, the use of backup line-based UPS system results in a more robust and resilient microgrid structure.

References

1. Nayar CV, Ashari M, Keerthipala WWL (2000) A grid-interactive photovoltaic uninterruptible power supply system using battery storage and a back up diesel generator. IEEE Trans Energy Convers 15(3):348–353. https://doi.org/10.1109/60.875502
2. Faisal M, Hannan MA, Ker PJ, Hussain A, Mansor MB, Blaabjerg F (2018) Review of energy storage system technologies in microgrid applications: issues and challenges. IEEE Access 6:35143–35164. https://doi.org/10.1109/access.2018.2841407
3. Cho GJ, Park JK, Sohn SH, Chung SJ, Gwon GH, Oh YS, Kim CH (2017) Development of a leader-end reclosing algorithm considering turbine-generator shaft torque. Energies 10(5):622. https://doi.org/10.3390/en10050622
4. Keyvani B, Zadeh MK, Lesani H (2014) Stability enhancement of multi-machine systems using adaptive reclosing of transmission lines. Int J Electr Power Energy Syst 62:391–397. https://doi.org/10.1016/j.ijepes.2014.04.013

5. Sadi MAH, Ali MH (2014) Combined operation of SVC and optimal reclosing of circuit breakers for power system transient stability enhancement. Electr Power Syst Res 106:241–248. https://doi.org/10.1016/j.epsr.2013.09.001
6. Heo JY, Oh YS, Seo HC, Kim CH (2015) An adaptive autoreclosure scheme with reference to transient stability for transmission lines. J Electr Eng Technol 10(3):795–803. https://doi.org/10.5370/jeet.2015.10.3.795
7. Luo X, Huang C, Jiang Y (2016) Improved digital algorithm for adaptive reclosing for transmission lines with shunt reactors. IET Gener Transm Distrib 10(9):2066–2070. https://doi.org/10.1049/iet-gtd.2015.1078
8. Park J, Kim CH, Cho G, Sohn SH, Chung S (2017) A novel reclosing algorithm considering turbine-generator shaft torque. IEEE Trans Power Delivery 32(2):703–712. https://doi.org/10.1109/tpwrd.2016.2569607
9. Wang X, Yang J, Liu P et al (2016) Online calculation for the optimal reclosing time of transmission lines. Electr Power Compon Syst 44(17):1904–1916. https://doi.org/10.1080/15325008.2016.1199071
10. Terzija VV, Radojevic ZM (2004) Numerical algorithm for adaptive autoreclosure and protection of medium-voltage overhead lines. IEEE Trans Power Delivery 19(2):554–559. https://doi.org/10.1109/tpwrd.2003.823184
11. Ahn SP, Kim CH, Aggarwal RK, Johns AT (2001) An alternative approach to adaptive single pole auto-reclosing in high voltage transmission systems based on variable dead time control. IEEE Trans Power Delivery 16(4):676–686. https://doi.org/10.1109/61.956756
12. Vogelsang J, Romeis C, Jaeger J (2016) Real-time adaption of dead time for single-phase autoreclosing. IEEE Trans Power Delivery 31(4):1882–1890. https://doi.org/10.1109/tpwrd.2015.2511660
13. Zhalefar F, Zadeh MRD, Sidhu TS (2017) A high-speed adaptive single-phase reclosing technique based on local voltage phasors. IEEE Trans Power Delivery 32(3):1203–1211. https://doi.org/10.1109/tpwrd.2015.2388474
14. Park JH, Seo HC, Kim CH, Rhee SB (2016) Development of adaptive reclosing scheme using wavelet transform of neutral line current in distribution system. Electr Power Compon Syst 44(4):426–433. https://doi.org/10.1080/15325008.2015.1117165
15. Seo HC (2017) New adaptive reclosing technique using second-order difference of THD in distribution system with BESS used as uninterruptible power supply. Int J Electr Power Energy Syst 90:315–322. https://doi.org/10.1016/j.ijepes.2017.02.012
16. Seo HC (2017) New adaptive reclosing technique in unbalanced distribution system. Energies 10(7):1004. https://doi.org/10.3390/en10071004
17. Sechilariu M, Locment F (2016) Urban DC microgrid. Elsevier, Amsterdam
18. Asian Development Bank (2018) Handbook on battery energy storage system. Asian Development Bank, Philippines
19. Seo HC (2017) New configuration and novel reclosing procedure of distribution system for utilization of BESS as UPS in smart grid. Sustainability 9(4):507. https://doi.org/10.3390/su9040507

Mitigation of Power System Blackout with Microgrid System

Kasimala Venkatanagaraju and Monalisa Biswal

Abstract To meet the ever-increasing electricity demand, the traditional power system needs to be expanded with more rigid economic and environmental limitations. The increasing power demand causes the electrical utilities to push the power system to operate at its maximum allowable limit. Consequently, the system gets stressed and vulnerable to widespread disturbances which may lead to power outages or blackout. Therefore, the scope for the occurrence of blackouts in such power system is more and their prevention is inevitable. From the reported blackout studies, it is disclosed that most of the blackouts are occurred only due to voltage instability and frequency deviations in the system. The reason behind these two phenomena is due to the mismatch between growing demand and generation. To make the system free from blackouts and to obtain a perfect load match situation, an intelligent load-shedding and adaptive defence plan for islanding for integrated power system are introduced in this book chapter. This proposal reduces carbonic emissions by the integration of renewable sources with the utility grid, allows more business markets to reduce the cost of energy, improves the utilization of electricity particularly at remote areas and provides continuity of supply through auxiliary tie-lines during power outages.

Keywords Blackout · System architecture · Renewable energy sources · Microgrid · Load-shedding · Distributed generation · Islanding

Nomenclature

DER	Distributed energy resource
DG	Distributed generation
DSM	Demand-side management
NERC	North American Electric Reliability Corporation

K. Venkatanagaraju (✉) · M. Biswal
Department of Electrical Engineering, National Institute of Technology Raipur, Raipur, Chhattisgarh 492010, India
e-mail: nagaraju048@gmail.com

M. Biswal
e-mail: monalisabiswal22@gmail.com

P. Ray and M. Biswal (eds.), *Microgrid: Operation, Control, Monitoring and Protection*, Lecture Notes in Electrical Engineering 625,
https://doi.org/10.1007/978-981-15-1781-5_11

1 Introduction

1.1 General Overview

The three main parts of power system are generation, transmission and distribution. For the conventional way of power generation, thermal, hydro and nuclear power plants are used. Next, transmission lines are reinforced to transport power from generating stations to primary- and secondary-level transmission grids. The operating voltage level of the transmission system is ranging from 33 to 765 kV. The distribution system is the system which feeds power to the domestic, commercial, agricultural and industrial loads. The operating voltage levels of the distribution system are ranging in between 11 kV and 230 V. In the power system, the power is flowing only from generation system to the loads through transmission and distribution system as shown in Fig. 1 [1]. The characteristics of conventional power system are listed as

- Unidirectional power flow.
- All the generating plants are centrally controlled.
- Most of the equipped infrastructure is electromechanical.
- Step up or step down the voltage levels by using a transformer.
- Power plant operates on alternating current.

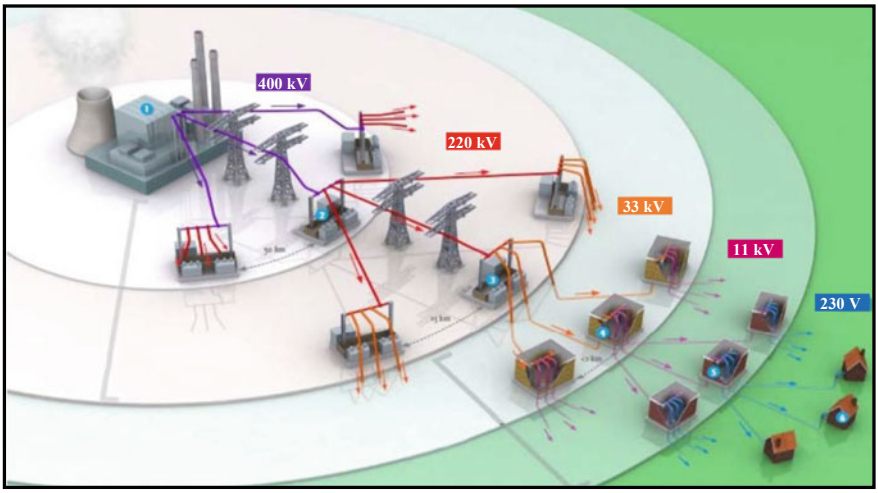

Fig. 1 Traditional power system

1.2 Issues with the traditional power system

- Emission of greenhouse gasses is more due to the combustion of fossil fuel.
- It does not have the ability to store bulk amount of energy.
- It does not allow bidirectional power flow.
- Sudden shutdown of power plant causes loss of large load.
- Quick restoration of power plants is not possible.
- More prone to system instabilities due to rapid variations in load demand.
- Difficult to maintain stability of power flow during emergency conditions and thus reliability and security issues develop in power system.
- Sustainability during emergency is less due to type of power sources.
- Transmission line losses are more.
- Difficult to manage unscheduled power flow.
- Lack of effective communication between inter-regional grids leads to unintended power outages.
- Less flexibility to interface with the advanced system components.
- Requirement of manual monitoring and intervention.
- Power transmission capacity is inadequate due to limited expansion of the transmission system.
- Insufficient dynamic reactive reserves.
- Power system operators unable to predict and respond to the system disturbances timely due to lack of wide area monitoring and knowledge over the system disturbances.
- Right of way issues are noteworthy during system expansion.
- Large power mismatch leading more power interruption.
- Protection system maloperation due to stressed condition, hidden failure and lack of proper equipment maintenance.
- Future scarcity of resources for power generation.
- A lot of interconnections can create transmission congestion.
- Poor control and management of the distribution system.
- Exposed to more electrical thefts.
- Manual replacement or renovation of damaged system components creates longer power interruption.
- Load forecasting issues.
- Low voltage profile at remote distribution locations.

The above-mentioned issues lie with the traditional power system and using advanced technology, power system upgradation can be done to achieve reliability, stability and security in power system. In this way, power outage rate can also be reduced by making a perfect balance between generation and load demand. After the past severe worldwide blackouts [2], the engineers and researchers put their best efforts to increase system reliability, but with new developments also the reduction percentage of power system failure rate is very less and the reasons are not limited to only geographical disasters and cascading failures.

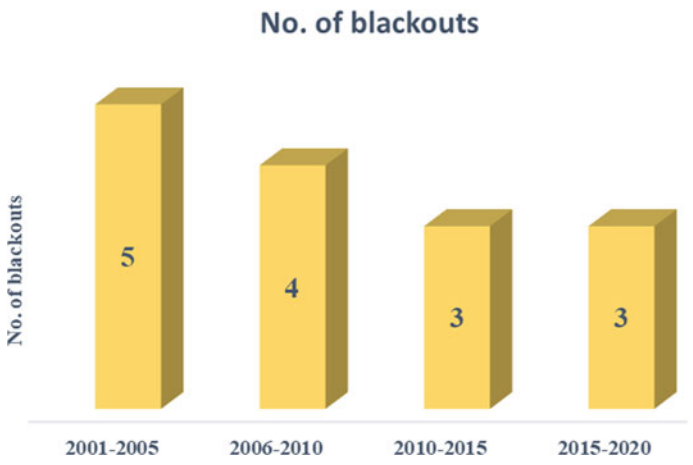

Fig. 2 Analysis of power system blackouts

The well-known definition of power system blackout is 'loss of loads in a large area for a considerable duration'. Generally, blackout is caused by cascading failures, but all such failures do not necessarily cause blackout. As per North American Electric Reliability Corporation (NERC) report as shown in Fig. 2, the number of blackouts occurred during 2001–2005 is more as and the statistics gradually reduces in the recent years.

Even though the power system blackout is an unavoidable event, there is a provision for reducing the propagation of cascading failures leading to a blackout. One of many solutions can be the large development of microgrid, so that intra-regional power demand can be balanced with the help of renewable sources. The basic definition for microgrid is 'a microgrid is a group of interconnected loads and distributed energy resources (DERs) within clearly defined electrical boundaries that acts as a single controllable entity with respect to the grid. A microgrid can be operated both in grid-connected and island mode' [3]. It provides both efficient and clean energy at low cost, enhances local resiliency and improves the operation and stability of the regional electric grid. It can also provide dynamic responsiveness unprecedented for an energy resource. The schematic diagram of a microgrid is shown in Fig. 3. The DERs include both renewable energy sources and electricity storage systems. The renewable energy is generated from sources that naturally replenish themselves and never run out. The solar, wind and geothermal are the most common renewable energy sources for power generation.

Over 80% of the total energy consumed by human is derived from fossil fuel. However, renewable is the fastest growing source of energy in the world. They had many benefits.

- First, it can combat climate change because it creates no direct greenhouse gas emissions.

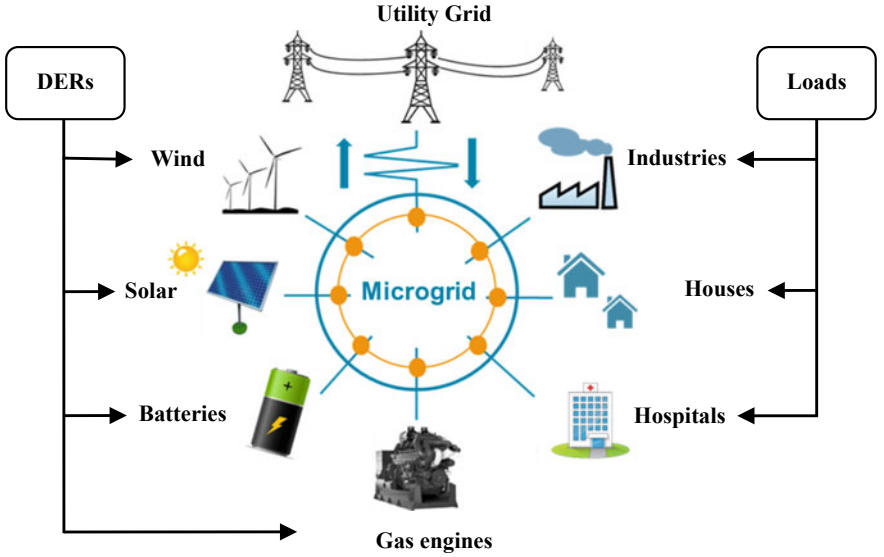

Fig. 3 Microgrid

- Second, it can decrease pollution and therefore reduce threats to our health. Wind, solar and hydroelectric systems create no air pollution and the emissions from geothermal and biomass energy systems are much lower than non-renewable energy sources.
- Third, it is a reliable source of power generation and the cost of operation and fuel cost are too less. It can also be mentioned that per unit cost of energy from renewable source is almost stable all the time.

While renewable energy has many advantages, it is not without downsides.

- It is difficult for renewable energy sources to generate power on the same large scale as fossil fuels.
- Building wind farms and dams can disrupt wildlife and migration patterns and lead to ecological destruction.
- Both solar and wind energy are intermittent that means they only generate power while the sun is shining or while the wind is blowing.
- Batteries can store excess energy for later use. However, they are often costly.

While renewable energy presents some challenges, it also offers an environmentally friendly alternative to greenhouse gas emissions and pollution of fossil fuels. As advances in technology make renewable energy more accessible, affordable and efficient, an end to climate change could be within our reach.

From future smart grid point-of-view, microgrids are best suited for maintaining electricity provision during or after a failure of large block of supply through tie-lines. In an interconnected network, bulk power transfer is generally transported through tie-lines. But the concept of microgrid can reduce a high percentage of future

tie-lines. Integration of microgrids as shown in Fig. 4 can dramatically improve the reliability of power systems. The first instance of such reliability improvement occurs at the local site of the microgrid. It can be noticed from Fig. 4 that the power flow direction is bidirectional. This is possible when power demand will be less than total generation. During blackout, an islanded microgrid can continue operation, maintaining local power supply autonomously. Microgrids can also improve the reliability of supply more broadly than their immediate vicinity. If the utility grid is operational but strained, a microgrid can assist by reducing the load on the utility grid, or even exporting power from the microgrid to a broader area. As well as power management, microgrids can also help with voltage and frequency control in such situations. In case of utility grid failure, power restoration facility can be provided through microgrid to neighbouring stations. In this way, the propagation of cascading outage rate can be checked. Such scenarios need particularly careful management to ensure electrical safety and maintain the reliable operation of the microgrid itself.

The reliability of transmission system is ensured based on NERC system operating and planning standards [4]. The key principles behind these standards are as follows:

- Always balance the electricity generation and demand.
- Maintain scheduled voltage levels by balancing the reactive power demand and supply.
- Continuously monitor power flows through transmission lines for knowing their thermal limits.
- Maintain stable and reliable operation even under single contingency.
- Plan and design the system in such a way that it operates reliably.
- Prepare for power transfer under emergency conditions.

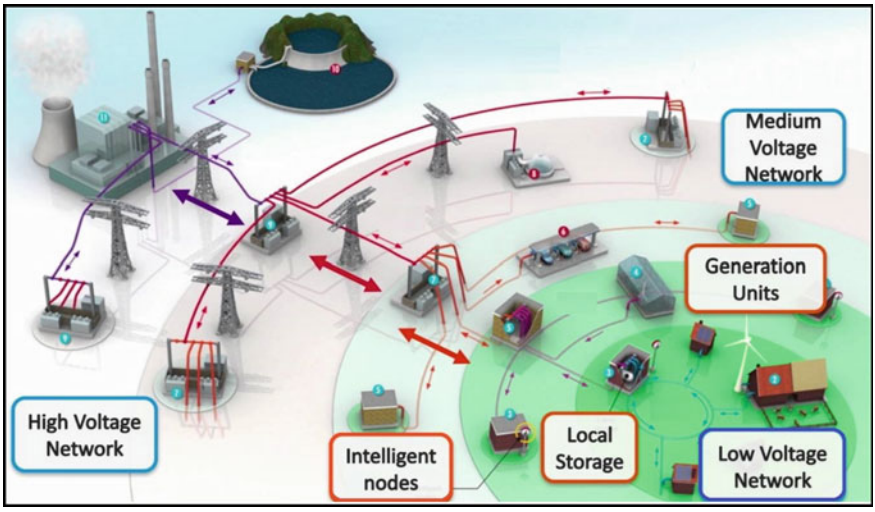

Fig. 4 Integration of microgrid with the utility grid

Although these standards are executed by the integrated system, blackouts are still unavoidable due to:

- Growing demand for electricity
- Insufficient upgradation of the transmission system
- Grid interconnections
- Absence of effective cost recovery mechanisms for transmission investments.

Therefore, to avoid large power interruption, it is essential to integrate more renewable sources, desired upgradation of grid architecture, adoption of advanced control, monitoring and protection schemes. Again, in addition to the load management, intelligent load-shedding and adaptive defence plan for islanding situation is essential for the stable, reliable and secure operation of the modernized electric grid. All these concepts are discussed in the subsequent sections.

2 Modification of Architecture

2.1 Need for Architecture Modification

Historically, the electric grid was built with a lot of components that are having service lives of more than fifty years and actively involved in unidirectional power flow, i.e. from generating stations to loads. But, now the operation of the electric grid is complex and power flow in certain portions of the grid becomes bidirectional. The reasons for such changes in the grid are penetration of variable energy resources like renewables, distributed energy resources, replacing foundational aging infrastructure and adoption of information and communication technology with small life cycles. To perfectly manage all the system changes, it is necessary to focus on grid architecture. In practice, every grid has a specific architecture. It describes the way the grid is structured and how all the components are equipped and coordinated with each other. The grid structure determines its size and properties, which include its resiliency and capability to do simply and cost-effectively.

2.2 Architectural Principles

The modification of grid architecture follows the basic grid architectural principles as listed below:

- **Standardization**—The components of the infrastructure and the ways of interconnections between them are well-defined with specified ratings, advantageous, open and stable over time.

- **Openness**—The infrastructure should be technology dependent. So, it will provide an open chance to all the investors who are willing to provide technology with a proper plan.
- **Interoperability**—The standardization of interface within the infrastructure is structured as the system has ability to adapt for a specific application. But adaption does not affect the actual communications between components.
- **Security**—The infrastructure is interface with the generalized performances and protected from illegal access through the security strategies.
- **Extensibility**—The design of infrastructure can facilitate extending feasibility for the latest applications.
- **Scalability**—The infrastructure does not have restrictions on the system geographical area and they can be extended all over the power system.
- **Manageability**—The components of the infrastructure and their configuration can be easily evaluated and managed. They are capable of faults identification and isolation of faulty section.
- **Upgradeability**—The infrastructure software, operational procedures, configuration and secure authentications can be upgraded securely.
- **Shareability**—The infrastructure deals with the economies of scale, increases actual efforts and encourages new solutions for challenging issues because they use shared resources.
- **Ubiquity**—Authorized grid users can only deal with the infrastructure and assess what they actually provide irrespective of geographical limitations.
- **Integrity**—The infrastructure works at a high level of availability, performance and reliability. At the time of power outages, it automatically redirects the communications, operate and save the outage data for recovery and future reference.
- **Ease of use**—Expanding the information of grid upgradation and its facilities to the public and reducing the rules and regulations for increasing a greater number of users for easy access of electricity.

With the consideration of all the above principles and the use of advanced infrastructure, modification of the traditional grid architecture will become easy. In the research application, the modified IEEE 39 bus test system as shown in Fig. 5 is used for simulation study [5]. During blackout condition, microgrid can operate as an isolate entity to supply power to the local loads continuously. Sometimes the microgrid does not have enough generation to fulfil local load demand. Under such a situation, only the emergency loads can be powered and other loads can be disconnected from that of the microgrid.

In order to supply power to all the local loads under such a situation, tie-line concept between microgrids can be introduced. In this concept, all the microgrids will be interconnected with auxiliary tie-lines as shown in Fig. 6. These tie-lines provide a path for power exchanging between the microgrids if required. Thus, prevents the local loads from unintentional power outages and maintains continuity of supply. Based on this concept, IEEE 39 bus test system can be further modified and is depicted in Fig. 7.

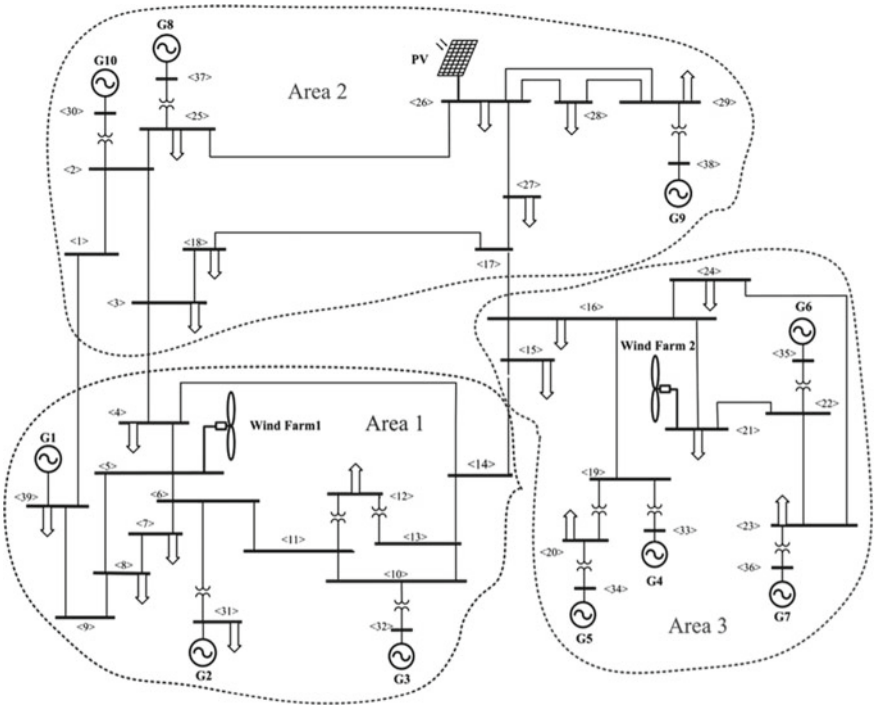

Fig. 5 Modified IEEE 39 bus New England test system

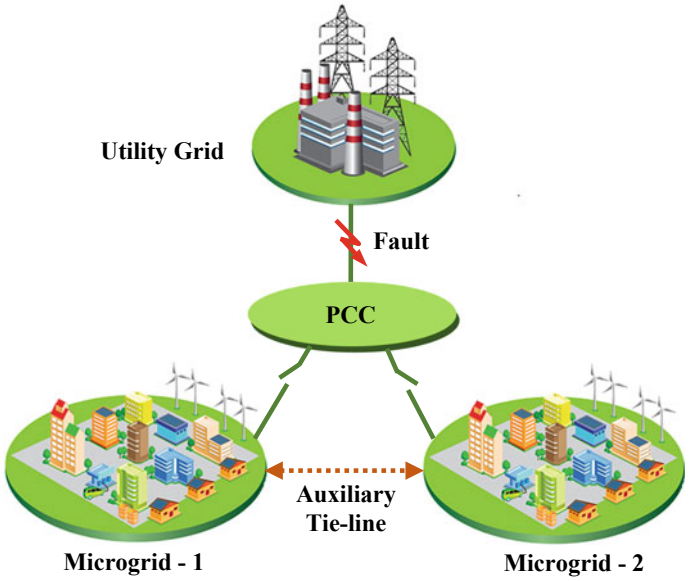

Fig. 6 Concept of tie-lines between microgrids

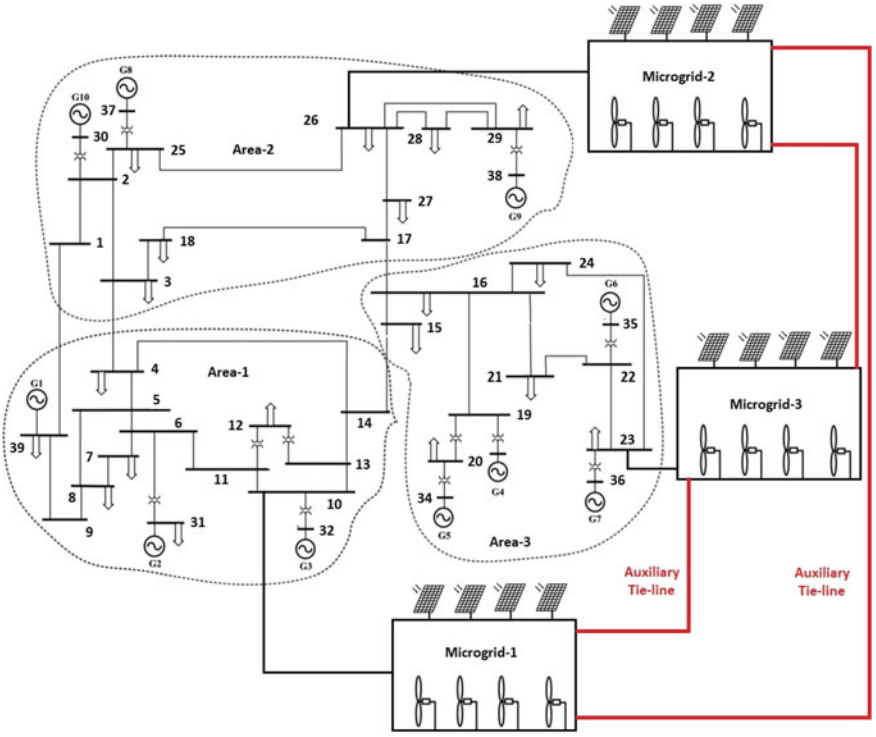

Fig. 7 Proposed architecture of IEEE 39 bus New England test system

2.3 Advantages of Modified Grid Architecture

- Reduction in transmission and distribution losses.
- Avoid complex interconnections.
- Reroute the power flow through auxiliary tie-line during fault.
- During blackout situation, a microgrid can maintain continuity of power supply through islanding mode of operation.
- Increase grid visibility.
- Self-healing grid.
- Allow more penetration of renewable energy.
- Provide decentralized power control.
- Easy to manage peak load demand.
- Increased choices to consumers for easy access of electricity.
- Improve environmental conditions.
- Improve grid resiliency, security and reliability.

3 Enhanced Load Management

3.1 Introduction

The load management is also called demand-side management (DSM). It is the way of maintaining a perfect balance between generation and load demand by managing the load and not by altering the power plant outcome [6]. In practice, this can be accomplished by the direct involvement of the utility. During peak load situation, it allows utilities to decrease electricity demand. Instead of allowing the power plants to run at peak load condition, DSM applies enhanced load management technique to provide most economical electricity. As a result, harmful emissions can be reduced. The advanced technologies needed by the DSM are still under development due to inability to store bulk amount of electrical energy. When the load connected to a system goes on increasing and reaches to the maximum generation point, the system operator must find alternative ways either to allow other energy supplies or to limit the connected load. However, if the operator fails to provide remedial actions, then the system becomes unbalance and provision for the occurrence of blackout is more.

In long-term load management planning, the physical belongings such as configuration, capacity, characteristics of connected loads and lines of distributed system are described by building sophisticated models. The analysis of load management comprises of weather forecast, the impact on the expected loads to be shedding and estimated time for offline components renovation. In practice, the capacity factor of a generating power plant can be improved by proper generation and load scheduling. Generally, the capacity factor is expressed as the ratio of actual energy generated by the plant to the maximum energy that could be generated. If the value of capacity factor is high, then the performance of the power plant is effective. Similarly, a higher load factor can also improve the performance of power plant.

3.2 Load Management Steps

The load management involves in following steps to manage the loads under peak demands:

- Analyze changes in load.
- Identify manageable loads.
- Select proper control option.
- Implement the exact strategy.

3.3 Load Management Options

In load management, all loads are controlled based on nature of control options.

- Direct load control (DLC): In DLC, utility has the right to directly switch off the consumer loads when required. Most of the domestic and agricultural loads are controlled by DLC.
- Interruptible load control (ILC): In ILC, utility forecasts the electricity shortages and provides advance notice to industrial consumer to switch off the loads. Based on productivity, all the industrial consumers prefer ILC instead of DLC.
- Time of use (TOU) tariffs: The utility provides flexibility to the industrial consumers for selecting suitable tariff plan. Thus influences the industrial consumers to shift their loads from peak to off-peak situation.

4 Intelligent Load-Shedding (ILS)

4.1 Need of Load-Shedding

The power system is susceptible to large-scale disturbances such as false generator tripping [7, 8], islanding and more. The longer the load-shedding system ways to react to a disturbance, more load is required to be shed. The generator controllers such as exciters and governors can act fast during desired situations. The load-shedding system needs to act faster even than protection schemes as they may lead to cascaded events. Without a protective load-shedding scheme, the system will be susceptible to loss of production and blackout. A proactive system will also look at type and location of the disturbance. The system should respond to any disturbance depending on the location. The power requirements from the generators should be graded when the fault will occur. Again, the load-shedding system should be dependent on fault location. Another important factor is the type of disturbance, for example, sudden drop in the level of steam pressure. This may cause partial decrease of power generation and demands a desired load-shedding to save the tripping of other running generators. Under such a situation, a non-proactive system will not be able to differentiate between the type and location of a disturbance.

A proactive system will also take system operating conditions variants into account before taking action. Every system is unique, but the way of loading is different. Sometimes, it can be cyclic or it could be random depending on how much load is there in the system at the time of the disturbance. The load-shedding system needs to report and respond accordingly. If the operating load is closer to the capacity of the system, then the system is more susceptible to a stability loss. Low variation of feeder load must be taken into account when a breaker will be selected for tripping. It makes a big difference to drop a feeder operating at light load compared to when it is operating at heavy load. This is very common in industrial networks such as mines

where loss constantly moved from location to location and can operate at random times.

In utility systems, although a load can be roughly predicted in a given day, it can suddenly change to unforeseen condition. At present, this kind of issues is raised with the introduction of renewables and microgrids. Sudden change in weather condition can change load quickly. The system topology is also important to know when performing load-shedding and initiating control actions. Breaker operations also affect the behaviour of the power flow as they change the impedance into the generation as well as the capacity of transferring power from one point to another point.

Monitoring the operation of switching devices is a crucial factor in deciding which control actions to initiate. As they could be in a separate network if islanding has occurred. At the time of performing load-shedding, it is required to analyse how much generation we have available. This has a direct impact on the available generators to respond to certain changes. A reliable and intelligent load-shedding system can help in cost reduction by reducing required peaking backup generation. The change in governor settings has also impact on the system response and it must be taken into account when transient conditions occur.

At the time of disturbance, it is also essential to consider the operator's law. If the network connected to the grid is islanded, then the system operator can assess the local power generation and demand. With an interconnected system, the load-shedding scheme needs to consider maximum and minimum import or export power contracts. Violations of such limits can cause large penalties. After islanding or operating during islanded mode, most of the time the system operates with limited generation capacity. A reliable load-shedding system is even more critical as any imbalance of load and generation can develop an unstable system condition. With different operating conditions, different responses can be observed a proactive system would look at existing conditions and ready for the disturbance events so that for future initiation of critical event, it can take immediate action. In order to perform proper load-shedding, it is required to account the following parameters at the time of any disturbance:

- System topology
- Configuration
- Operating status
- Generation levels
- Power exchange
- Operating load
- Spinning reserve
- Disturbance type and location
- Transient response to disturbances.

But it is impossible for any proactive system to account all of the above-mentioned parameters and respond in milliseconds.

4.2 Conventional Load-Shedding Methods

- **Static load-shedding**: In this method, a fixed block of the load is curtailed at each stage. Based on the rate of change of frequency (ROCOF) and overloading of the system, the time to shed the load is generally calculated. It facilitates a greater number of stages to restrict over-shedding and allows a very less amount of load for each stage. Such a method has significant impact on weak system whose total demand is very less. Again, such a scheme requires more time to recover and restore the system frequency.
- **Dynamic load-shedding**: In this method, dynamic amount of load is curtailed at each stage. It is achieved only by considering the voltage and frequency response of the system and magnitude of disturbance at each stage. If a large imbalance exists in the system, then it allows to shed large block of load and vice versa. As compared with the static load-shedding, dynamic load-shedding is dependent on dynamic nature of the system parameters, and the amount of load to be shed is also not fixed.

4.3 Issues with the Traditional and Existing Load-Shedding Schemes

The reports of the recent power system blackouts disclosed that the power system instability issues such as voltage instability and frequency instability are the significant causes behind the occurrence of outages. In order to prevent the system from such instability issues, different protection schemes have been introduced and implemented individually in the real-time power system. In this context, the under-frequency load-shedding (UFLS) [9] and the under-voltage load-shedding (UVLS) [10] schemes are proposed. Both frequency and voltage instability conditions can occur simultaneously during severe system stressed conditions [11]. However, the UFLS and UVLS schemes are designed for specific conditions only and may not be suitable for other cases due to their design aspects. A centralized two-level UFLS is proposed in [12]. However, the information of individual bus is required to be communicated to the central control centre to determine the system imbalance. In addition, the central control requires faster communication link which is not cost-effective and scalable. In [13], an optimization technique is proposed for the restructured power system to reduce the total cost. However, it requires more computational time due to large network size. An event-driven-based optimal load-shedding technique is introduced to avoid voltage instability issue [14]. However, determination of load-shedding location requires high-speed wide area monitoring device. In [15], a method is proposed to recover the system stability from contingency conditions based on modified settings of relays and load-shedding system. However, the modification of relay setting involves mathematical manipulations. A fast load-shedding scheme with comprehensive features is proposed in [16]. An online load-shedding strategy

is proposed to predict and access fault-induced delayed voltage recovery (FIDVR) severity based on slope-based method and voltage recovery time [17]. However, it gives a high prediction error with the use of a linear approximation method. A UFLS scheme is proposed based on the frequency of centre of India (COI) [18]. However, it may fail under too much deficit in generation. A synchrophasor-based load-shedding scheme is proposed for self-healing of the system under critical contingencies [19]. However, the reactive power impact on the voltage stability issue is considered improperly.

In [20], an adaptive combinational load-shedding scheme is introduced to improve the system stability. However, it neglects motor dynamics. In [21], genetic algorithm is applied to curtail sheddable load and to increase the lowest swing frequency at all the stages of UFLS relays. However, it will face over-shedding issue due to violation of frequency limit. An auto-load-shedding scheme is proposed in [22]. But such a technique may fail to provide optimal result due to the unavailability of proper wide area information. A new approach using mixed-integer programming is proposed to set the UFLS relays [23]. However, the impact of generator governing system is neglected for the estimation of inertia constant. An adaptive and centralized UVLS scheme is proposed in [24], to mitigate the short-term voltage instabilities. But the impact of frequency deviation is not considered for predetermination of load margin. Similarly, another technique based on synchrophasor measurements is proposed in [25]. However, it suffers from the latency issue. In [26], a priority-based load-shedding scheme is introduced to get power balancing between generation and load. But with such a method, it is difficult to review the type of consumers that are connected to the distribution system. A sensitivity-based UFLS scheme is proposed to find optimal locations and amount of load to be shed [27]. The technique in [27] is not adaptive to the changes in system configuration. An adaptive load-shedding scheme is proposed based on local end measurements of frequency and voltage along with their decreasing rate to enhance the conventional UFLS relays [28]. However, the estimated location and the amount of load to be shed are not optimal. In [29], a centralized and adaptive scheme is proposed by using communication channels between central control and remote-end relays to enhance the under-frequency relay. But it is heavily exposed to single or multiple disturbances in the complex power system. In addition, the central control unit requires a bulk amount of time-synchronized system data. A decentralized UFLS scheme based on a two-layered consensus algorithm is proposed for enhancing islanded microgrids [30]. However, it requires high reliable communication system. In [31], a real-time centralized adaptive UFLS scheme is implemented to estimate the amount of load to be shed based on rate of frequency deviation and voltage dip. But it is very sensitive to small disturbances and lower rate of inertia causes unintended shedding of non-critical loads.

An adaptive UFLS scheme using rate of change of frequency is proposed to evaluate the amount of generation outage and its inertia constant [32]. Evaluation and updating of inertia constant at each stage of load-shedding is a challenging task for the technique proposed in [32]. A priority-based adaptive UFLS scheme [33] used to enhance the frequency response from overshoots meets challenges in determining inertia constant under more penetration of renewable energy. The WAMS-based

UFLS approach [34] is proposed to predict the system frequency which is highly dependent on the placement of PMU. A synchrophasor-based adaptive UFLS scheme is developed to estimate the amount of load to be rejected and its location [35]. But due to the oscillatory nature of frequency derivatives, the measurement error will be high. In [36], a combined intelligent load-shedding technique is proposed based on the active participation of smart appliances. However, the delay setting for smart appliances is not viable.

4.4 Need of ILS

An ILS system is essential to address the aforementioned limitations of conventional and proposed load-shedding methods. Besides, it increases response time, precisely forecasts deviation in system frequency and enables load-shedding by taking the right decision at the right time. The capabilities of the ILS system are listed as follows:

- It is capable of mapping a nonlinear and complex power system to a simpler system with lesser data collection points with reduced storage space.
- It can remember system configuration automatically and respond to all types of disturbances pertaining to the system configurations.
- It can identify various system configurations under various disturbances to forecast the system outcome.
- It is adaptive in nature.
- It applies knowledge base scheme for a specific disturbance.
- Based on the status of the connected load, it is capable of taking quick and accurate decision for shedding the prioritized load.
- From stability perspective, it minimizes the curtailed load.
- Based on complete information about the system dependencies, it can optimally shed the load breakers with possible combinations.

According to different system disturbances, the ILS system must identify the significant parameters to collect the required information for effective dynamic knowledge. Again, few parameters are there in the system that directly influence the system frequency response are:

- The total amount of power to be shared during and after the disturbance
- The total generation available at the time of pre- and post-disturbance
- Dynamics of the generator
- Dynamic nature of load
- Actual loading and status of each load to be shedded.

4.5 Requirements for ILS System

The essential requirements for the designing and tuning of the ILS scheme are:

- Selection of knowledge base case and proper arrangement.
- Capability to include user-defined functions and system dependencies.
- Ability to assure that knowledge base of the system is complete, accurate and verified.
- Ability to obtain the information from various locations of the system by using online monitoring system.
- Ability to train the system for generating several cases for the system knowledge base to assure precision and completeness.
- Ability to operate the system in different modes such as protective and predictive.
- Ability to generate dynamic load-shedding data with respect to dynamic changes in the system configuration.
- Ability to supervise the centralized and locally distributed control system for the stable operation of the power system.

4.6 Functional Block Diagram of the ILS

The functional block diagram of the ILS system is shown in Fig. 8. It consists of disturbance database, advanced monitoring system, network models, knowledge base, computation engine and centralized distributed local controls.

- **Disturbance database**: It has a list of pre-defined disturbance data generated from the offline system simulation studies. It will send the input data to the knowledge base when a disturbance occurs.
- **Advanced monitoring system**: It visualizes all the operating situations of the power system and sends the status of the system to the knowledge base.
- **Network models**: It gives information about the actual configuration of the system under pre- and post-disturbance condition.
- **Knowledge base**: Based on the input data acquired from the disturbance database, system response and its configuration, the knowledge base gives an intermittent interrupt to computation engine.
- **Computation engine**: Based on the interruption given by the knowledge base, it will update the tables corresponding to load-shedding.
- **Distributed controls**: These are equipped very nearer to every sheddable load. Based on the updated load-shedding tables, distributed controls will shed the loads immediately.

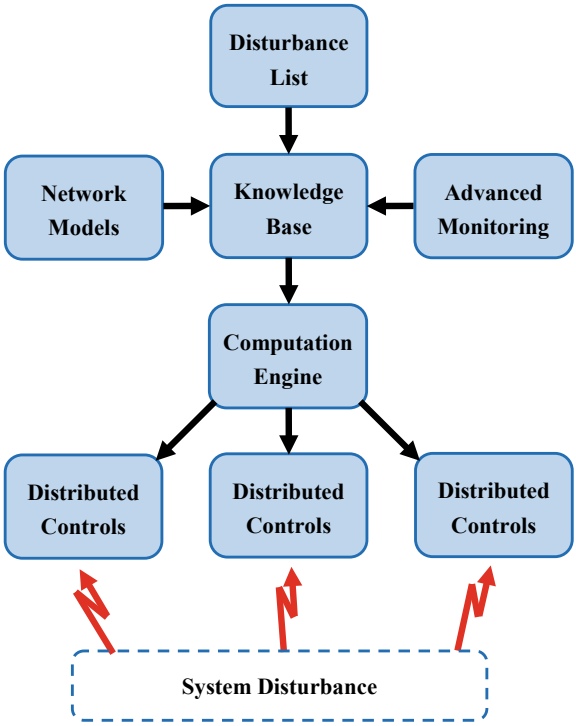

Fig. 8 Functional block diagram of the ILS scheme

4.7 Implementation of ILS

The implementation of ILS is shown in Fig. 9 [37]. Basically, the ILS server inherently consists of both computation engine and knowledge base. The server frequently acquires the system data, i.e. the status of real-time monitoring system. Based on computation engine outcome, the load-shedding tables are updated dynamically. These tables are downloaded for the distributed programmable logic control (PLC). If any of the PLC detects a disturbance in the system, then it will initiate a load-shedding signal to the associated load circuit breaker (LCB). Based on the generated load-shedding tables, these breakers will trip.

5 Adaptive Defence Plan During Islanding of Microgrid

5.1 Introduction

Islanding is a condition in which a part of the power system is electrically isolated from rest of the power system and during that period, power supply to the isolated

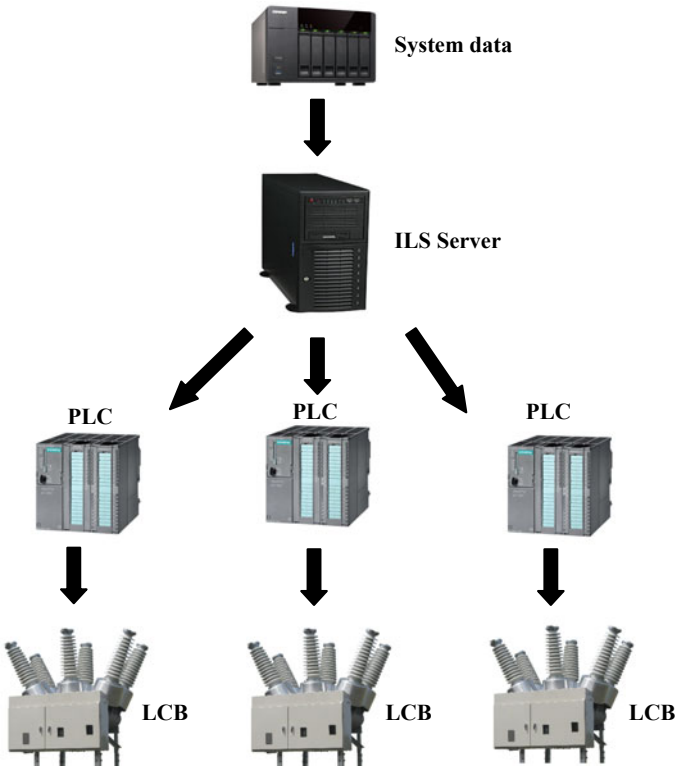

Fig. 9 Implementation of the ILS scheme

area can be provided through local supply [38]. In practice, there are two types of islanding: one is intentional and the other is unintentional. Intentional islanding condition executed with proper planning. Therefore, during such islanding situation, the microgrid has:

- Sufficient DERs with balanced load points
- Measures to maintain the isolated system in a stable manner and parallel to main grid even after disconnection
- Facility to collaborate with other local electric power supply system
- Emergency planned architecture.

5.2 Issues with Unintentional Islands

The exiting issues associated with unintentional islanding system are:

- **Personnel safety**: At the time of restoration of supply system, the utility workers assume that there is no power flowing in the lines. But it may not be true always and can cause harmful threats to them.
- **Over-voltages**: Any sudden loss of load resulting in transient over-voltage. With inadequate ground supply during islanding, a ground fault will persist and this results in increasing the faulty phase voltage as 173% from the healthy phase.
- **Reconnection out of phase**: Reconnection of the islanded system to the main grid during out-of-phase condition may produce heavy transient torque. Under such a condition, the motors and the mechanical systems connected to the islanded section will be highly affected. This may cause damage to the electrical and mechanical equipment.
- **Power quality**: It is difficult to supply quality power to the loads from the distributed generators during unplanned islanding.
- **Protection**: An unintentional island may not provide sufficient fault current to the protective devices such as over current relays or fuses. So, the protection system requires proper setting adjustment during unplanned islanding, which is very difficult.

5.3 Essential Requirements for an Unintentional Islanding

- The non-islanding inverter should be able to cease the electrical energization of utility line within two seconds when the real power mismatch is within 50% and the power factor is less than 0.95.
- The aggregate capacity of DER should be less than the local load, i.e. one-third of the minimum load.
- The DER must contain minimum or reverse power flow protection.
- The DER should be certified for non-islanding situation.
- The DER must hold other non-islanding needs such as transfer trip, forced voltage shifting, forced frequency shifting, excitation control and governor control which keeps the power mismatch and frequency within the limits.

5.4 Islanding Detection Methods

The islanding detection methods are broadly classified as local and remote techniques as shown in Fig. 10. The local methods work based on the microgrid side parameters and remote methods work on the communication-based signals collected from utility grid [39].

- **Passive anti-islanding**: The change in system parameters like voltage, current, frequency and harmonic distortion are directly monitored and play a vital role in

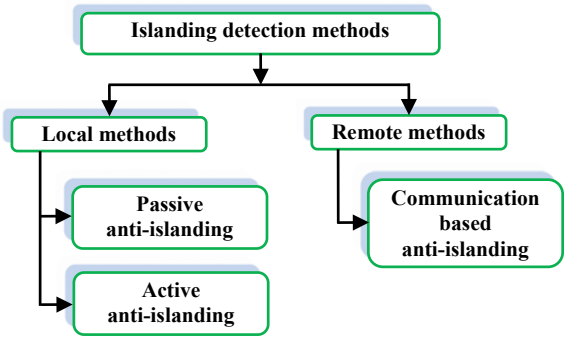

Fig. 10 Islanding detection methods

islanding detection process. During islanding, the deviation obtained in the above stated parameters will be significant. In order to determine whether the system is being operated either in grid-connected or islanding mode, proper thresholds are set based on change in parameters. The procedures used to set the threshold must be systematic, so that it can properly discriminate the system disturbance from islanding [40]. Passive anti-islanding methods are fast and do not create any disturbances in the system. However, such techniques fail to detect islanding condition due to large non-detectable zone (NDZ) and are restricted to single DG system with a specific power imbalance [41].

- **Active anti-islanding**: The active anti-islanding methods directly introduce a disturbance into the system for detecting significant change in voltage, frequency, current, power and impedance of the system. The change in system parameters is noteworthy during islanding mode rather than grid-connected mode. As compared with passive anti-islanding methods, the active anti-islanding methods have the ability to detect islanding even under zero power mismatch situation. In addition to that such methods have small NDZ and reduced error detection ratio. However, active anti-islanding methods are inevitable to deteriorate power quality and their application in multiple DG systems need to be improved.
- **Communication-based anti-islanding**: Basically, remote islanding detection methods work on the actual communication existing between DGs and utilities. As compared with local anti-islanding methods, such methods have negligible NDZ, ability to maintain quality of power, effective and reliable. However, implementation of these methods is expensive for small systems. Few of the communication assisted remote anti-islanding methods are as follows:

Direct transfer trip (DTT)—The basic theme behind this method is to know the exact status of reclosers and circuit breakers that could island a DG system. It is achieved only by monitoring such devises through the supervisory control and data acquisition (SCADA) systems. However, it needs high-level interfacing systems to provide better communication between DGs and utilities.

Power line carrier (PLC)—The basic idea of this method is that the continuous broadcasting of a signal from transmission system to distribution feeders through the power lines. The signal transmitters and receivers are equipped on utility side

and DGs side. The PLC-based methods detect the island condition only when the receiver fails to receive a signal from the transmitter. The reason for occurrence of such failures is the opening of breakers. These methods are widely used in multiple DG systems.

5.5 *Proposal for Adaptive Defence Plan During Islanding*

The industry-based microgrid as shown in Fig. 11 consists of renewable energy sources, energy storage systems, thermal generator, critical loads and sheddable loads. The significant role of such a microgrid for industrial application is not only to provide reliable power supply in islanded and grid-connected mode of operations but also for transition modes [42].

For the coordinated, economic and optimal operation of microgrid during transition mode, a new scheme is proposed in this chapter and the flow diagram of proposed methodology is shown in Fig. 12. The proposed framework involves in the following steps:

Step 1. In the grid-connected mode of operation, the microgrid operates in 'economy mode'. It means that the microgrid can get the profits from ancillary service and energy market.

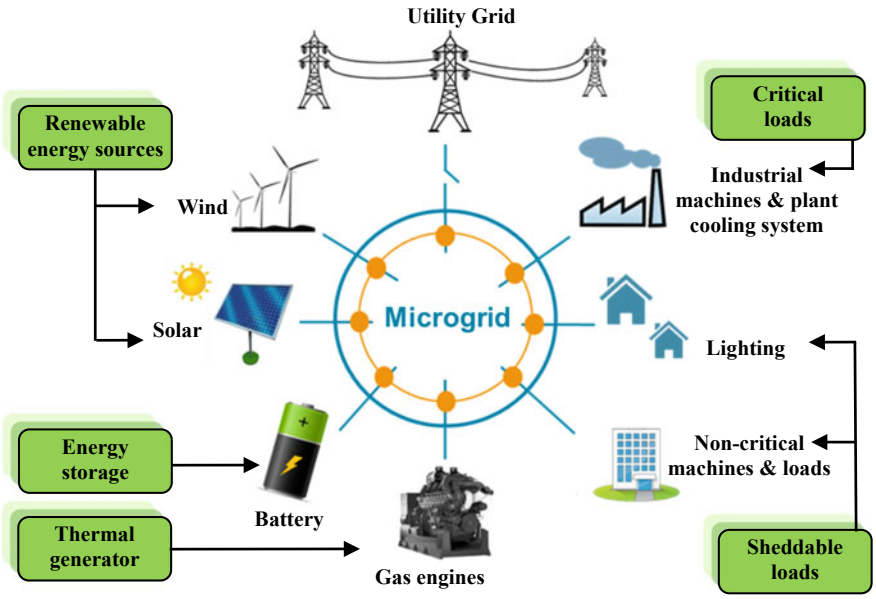

Fig. 11 Configuration of typical microgrid in an industrial facility

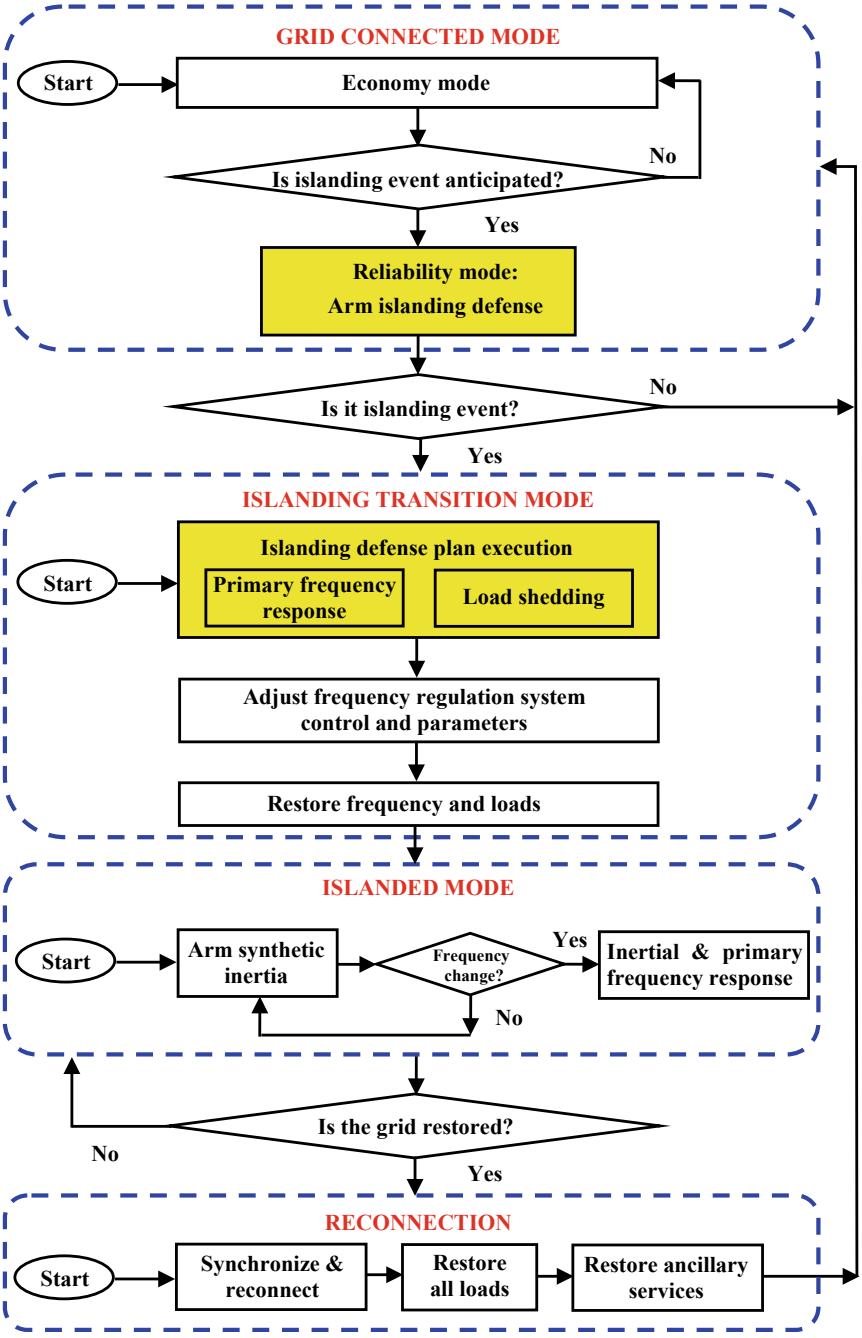

Fig. 12 Framework for adaptive islanding

Step 2. Check whether the islanding event is expected or not. If it is not expected, then the microgrid should operate in economy mode. Otherwise, go to Step 3.
Step 3. If an islanding event is expected, then the microgrid will shift to 'reliability mode'. In this mode, an islanding defence plan is armed and lost its economy to confirm the optimal islanding transition.
Step 4. Check whether islanding event is occurred or not. If it is not occurred, then the microgrid should operate in grid-connected mode. Otherwise, go to Step 5.
Step 5. If an islanding event happened, then the defence plan will execute in such a way that minimum load can be shedded. Later, by the adjustment of auxiliary controls, the frequency and loads can be restored in a secure and reliable manner.
Step 6. If the microgrid is operating in islanded mode, then the deployed energy storage systems will enhance its frequency response. Consequently, frequency of the local generators also recovered and restored.
Step 7. Check whether the grid is restored or not. If it is not restored, then go to Step 6. Otherwise, go to Step 8.
Step 8. If the grid is restored, synchronize and reconnect the microgrid to the main grid.

6 Conclusion

To mitigate the power system blackouts caused by several disturbances in the traditional grid and to achieve a new equilibrium state between generation and load, a new proposal has been introduced in this chapter based on the scope for the integration of microgrids, modified grid architecture and load management strategy. First, the ILS approach is broadly discussed along with its requirements, block diagram and procedure for practical implementations. The ILS approach dynamically shed the minimum amount of load in proportion to the dynamic changes in generation. The load-shedding tables prepared by the ILS server can enhance the system decision-making and prevent over-shedding problems. In addition, ILS approach can improve the system frequency response. Later, an adaptive defence plan during islanding of microgrid is discussed by considering real-time industrial application as an example. During islanding transition mode, the minimum amount of load can be shedded and restored the system frequency by adjusting auxiliary controls. Based on discussions presented in this chapter, it is confirmed that the new proposed scheme can make a perfect balance between the demand and generation, and also it will help the power system to maintain the operating stability. In this way, the power system blackouts can be mitigated successfully.

References

1. Aljahani ME (2014) An enhanced self-healing protection system in smart grid: using advanced and intelligent devices and applying hierarchical routing in sensor network technique. Master's theses, Western Michigan University, pp 1–39
2. Venkatanagaraju K, Biswal M (2019) Synchrophasor based wide area protection scheme for system stressed conditions to avoid power system blackout. In: Handbook of research on smart power system operation and control. IGI Global, pp 1–34
3. Ton DT, Smith MA (2012) The U.S. department of energy's microgrid initiative. Electr J 25(8):84–94
4. U.S.-Canada Power System Outage Task Force (2003) Causes of the August 14th blackout
5. Bevranil H, Ghosh A, Ledwich G (2010) Renewable energy sources and frequency regulation: survey and new perspectives. IET Renew Power Gener 4(5):438–457
6. Banerjee R (1998) Load management in the Indian power sector using US experience. Energy 23(11):961–972
7. Jose T, Biswal M, Venkatanagaraju K et al (2018) Integrated approach based third zone protection during stressed system conditions. Electr Power Syst Res 161:199–211
8. Venkatanagaraju K, Jose T, Biswal M et al (2019) Third zone protection to discriminate symmetrical fault and stressed system conditions. Int Trans Electr Energy Syst. https://doi.org/10.1002/2050-7038.12121
9. Concordia C, Fink LH, Poullikkas G (1995) Load shedding on an isolated system. IEEE Trans Power Syst 10(3):1467–1472
10. Taylor CW (1992) Concepts of undervoltage load shedding for voltage stability. IEEE Trans Power Delivery 7(2):480–488
11. IEEE/CIGRE JTF STD (2004) Definition and classification of power system stability. IEEE Trans Power Syst 19(2):1387–1401
12. Seyedi H, Sanaye-Pasand M (2008) New centralized adaptive load shedding algorithms to mitigate power system blackouts. IET Gener Transm Distrib 3(1):99–114
13. Wang P, Ding Y, Goel L (2009) Reliability assessment of restructured power systems using optimal load shedding technique. IET Gener Transm Distrib 3(7):628–640
14. Wang Y, Pordanjani IR, Li W et al (2011) Strategy to minimize the load shedding amount for voltage collapse prevention. IET Gener Transm Distrib 5(3):307–313
15. Chen CS, Hsu CT, Lee YD (2010) Protective relay settings of tie line tripping and load shedding for an integrated steelmaking cogeneration system. IEEE Trans Ind Appl 46(1):38–45
16. Jethwa UK, Bansal RK, Date N et al (2010) Comprehensive load-shedding system. IEEE Trans Ind Appl 46(2):740–749
17. Hua B, Ajjarapu V (2011) A novel online load shedding strategy for mitigating fault-induced delayed voltage recovery. IEEE Trans Power Syst 26(1):294–304
18. Rudez U, Mihalic R (2011) Monitoring the first frequency derivative to improve adaptive underfrequency load-shedding schemes. IEEE Trans Power Syst 26(2):839–846
19. Seethalekshmi K, Singh SN, Srivastava SC (2011) A synchrophasor assisted frequency and voltage stability based load shedding scheme for self-healing of power system. IEEE Trans Smart Grid 2(2):221–230
20. Saffarian A, Sanaye-Pasand M (2011) Enhancement of power system stability using adaptive combinational load shedding methods. IEEE Trans Power Syst 26(3):1010–1020
21. Hong YY, Chen PH (2012) Genetic-based underfrequency load shedding in a stand-alone power system considering fuzzy loads. IEEE Trans Power Delivery 27(1):87–95
22. Ahsan MQ, Chowdhury AH, Ahmed SS et al (2012) Technique to develop auto load shedding and islanding scheme to prevent power system blackout. IEEE Trans Power Syst 27(1):198–205
23. Ceja-Gomez F, Qadri SS, Galiana FD (2012) Under-frequency load shedding via integer programming. IEEE Trans Power Syst 27(3):1387–1394
24. Modarresi J, Gholipour E, Khodabakhshian A (2018) New adaptive and centralised undervoltage load shedding to prevent short-term voltage instability. IET Gener Transm Distrib 12(11):2530–2538

25. Tang J, Liu J, Ponci F, Monti A (2013) Adaptive load shedding based on combined frequency and voltage stability assessment using synchrophasor measurements. IEEE Trans Power Syst 28(2):2035–2047
26. Adamiak M, Schiefen M, Schauerman G (2014) Design of a priority-based load shed scheme and operation tests. IEEE Trans Ind Appl 50(1):182–187
27. Reddy C, Chakrabarti S, Srivastava S (2014) A sensitivity-based method for under-frequency load-shedding. IEEE Trans Power Syst 29(2):984–985
28. Abedini M, Sanaye-Pasand M, Azizi S (2014) Adaptive load shedding scheme to preserve the power system stability following large disturbances. IET Gener Transm Distrib 8(12):2124–2133
29. Manson S, Zweigle G, Yedidi V (2014) Case study: an adaptive underfrequency load-shedding system. IEEE Trans Ind Appl 3(50):1659–1667
30. Gu W, Liu W, Zhu J et al (2014) Adaptive decentralized under-frequency load shedding for islanded smart distribution networks. IEEE Trans Sustain Energy 5(3):886–895
31. AbdElwahid S, Babiker A, Eltom A et al (2014) Hardware implementation of an automatic adaptive centralized underfrequency load shedding scheme. IEEE Trans Power Delivery 29(6):2664–2673
32. Ketabi A, Fini MH (2015) An underfrequency load shedding scheme for hybrid and multiarea power systems. IEEE Trans Smart Grid 6(1):82–91
33. Laghari JA, Mokhlis H, Karimi M et al (2015) A new under-frequency load shedding technique based on combination of fixed and random priority of loads for smart grid applications. IEEE Trans Power Syst 30(5):2507–2515
34. Rudez U, Mihalic R (2016) WAMS-based underfrequency load shedding with short-term frequency prediction. IEEE Trans Power Delivery 31(4):1912–1920
35. Shekari T, Aminifar F, Sanaye-Pasand M (2016) An analytical adaptive load shedding scheme against severe combinational disturbances. IEEE Trans Power Syst 31(5):4135–4143
36. Wang J, Zhang H, Zhou Y (2017) Intelligent under frequency and under voltage load shedding method based on the active participation of smart appliances. IEEE Trans Smart Grid 8(1):353–361
37. Shokooh F, Dai J, Shokooh S et al (2005) An intelligent load shedding (ILS) system application in a large industrial facility. In: 40th IAS annual meeting, 2005, pp 417–425
38. Nale R, Biswal M, Kishor N (2019) A transient component-based approach for islanding detection in distributed generation. IEEE Trans Sustain Energy 10(3):1129–1139
39. Nale R, Biswal M, Almoataz YA (2019) Protection schemes for sustainable microgrids. In: Sustainable interdependent networks: from theory to application. Springer. https://doi.org/10.1007/978-3-319-98923-5_14
40. Nale R, Venkatanagaraju K, Biswal S et al (2019) Islanding detection in distributed generation system using intrinsic time decomposition. IET Gener Transm Distrib 13(5):626–633
41. Nale R, Biswal M (2017) Comparative assessment of passive islanding detection techniques for microgrid. In: IEEE international conference on innovations in information embedded and communication systems, 2017
42. Mohammed Manaz MA, Lu C-N (2019) Adaptive defense plan against anticipated islanding of microgrid. IEEE Trans Smart Grid 10(3):3071–3080

Author Index

P. Ray and M. Biswal (eds.), *Microgrid: Operation, Control, Monitoring and Protection*,
Lecture Notes in Electrical Engineering 625,
https://doi.org/10.1007/978-981-15-1781-5

Subject Index

P. Ray and M. Biswal (eds.), *Microgrid: Operation, Control, Monitoring and Protection*,
Lecture Notes in Electrical Engineering 625,
https://doi.org/10.1007/978-981-15-1781-5

P

R

S